

**REMOVAL OF NITRATE NITROGEN AND
AMMONIA NITROGEN FROM AQUEOUS MEDIA
USING NANO BIOSORBENTS**

A THESIS

Submitted by

HASEENA P.V.

*for the award of the degree
of*

DOCTOR OF PHILOSOPHY

Under the Faculty of Engineering



**SCHOOL OF ENGINEERING
COCHIN UNIVERSITY OF SCIENCE AND TECHNOLOGY, KOCHI
NOVEMBER 2019**

THESIS CERTIFICATE

This is to certify that the thesis entitled “**REMOVAL OF NITRATE NITROGEN AND AMMONIA NITROGEN FROM AQUEOUS MEDIA USING NANO BIOSORBENTS**” submitted by **Haseena P.V.** to the Cochin University of Science and Technology, Kochi for the award of the degree of Doctor of Philosophy is a bonafide record of research work carried out by her under our supervision and guidance at School of Engineering, Cochin University of Science and Technology. The contents of this thesis, in full or in parts, have not been submitted to any other University or Institute for the award of any degree or diploma.

We further certify that the corrections and modifications suggested by the audience during the pre-synopsis seminar and recommended by the doctoral committee are incorporated in the thesis.

Prof. (Dr.) G. Madhu (*Research Guide*)
Head
Division of Chemical Engineering
School of Engineering
Cochin University of Science and Technology
Kochi-682 022, Kerala, India

Prof. (Dr.) Dipak Kumar Sahoo (*Co-Guide*)
Head
Division of Safety and Fire Engineering
School of Engineering
Cochin University of Science and Technology
Kochi-682 022, Kerala, India

Place: Kochi-22
Date: 22-11-2019

DECLARATION

I hereby declare that the work presented in the thesis entitled “**REMOVAL OF NITRATE NITROGEN AND AMMONIA NITROGEN FROM AQUEOUS MEDIA USING NANO BIOSORBENTS**” is based on the original research work carried out by me under the supervision and guidance of Prof. (Dr.) G. Madhu, Division of Chemical Engineering and Prof. (Dr.) Dipak Kumar Sahoo, Division of Safety and Fire Engineering, School of Engineering, Cochin University of Science and Technology for the award of degree of Doctor of Philosophy with Cochin University of Science and Technology. I further declare that the contents of this thesis in full or in parts have not been submitted to any other University or Institute for the award of any degree or diploma.

Place: Kochi -22

Haseena P.V.

Date: 22-11-2019

Dedicated to My Parents & Teachers

ACKNOWLEDEMENTS

I thank God **Almighty** for giving me the strength and courage to reach this milestone in my life.

It is a great pleasure for me to put on record my deep sense of gratitude to Prof. (Dr.) G.Madhu, my guide for his steadfast support, constant encouragement, and inspiration. I am immensely thankful to him for all the technical and moral support he has given me throughout this work. Without his suggestions and timely guidance, this work will not have been progressed further. The patience in listening to me in various stages and advice given by him is gratefully acknowledged.

I am incredibly thankful to Prof. (Dr.) Dipak Kumar Sahoo, my Co-Guide for the valuable suggestions and advises given to me in the course of my work. I express my immense thanks to him for the timely help he rendered to me in various stages of this research work.

I wish to express my sincere thanks to all the teaching staff, non-teaching staff, and students of the Department of Chemical Engineering, Government Engineering College, Thrissur, for helping and supporting me during this research work. I thank Dr.Padmavathy K S., Associate. Professor in Chemical Engineering, Government Engineering College, Kozhikode for her admirable and wholehearted willingness to clarify all doubts during my research work. I sincerely acknowledge the services rendered by Dr.Anjana R., Associate Professor, Dr.SubinPoulose, Associate Professor, and Mrs.Renjana R, Assistant Professor in the Department of Chemical Engineering Government Engineering College, Thrissur. I thank Dr.Rejini

V.O., our former Head of Department of Chemical Engineering, now Principal, Government Engineering College, Kannur, for her understanding and encouragement. I am thankful to Dr.Ushakumary E. R Head of Department of Chemical Engineering, Government Engineering College, Kozhikode for supporting me. I thank all the teaching staff and office staff of School of Engineering, Cochin University of Science and Technology for the cooperation they extended to me during my research work.

The financial support (SEED money) for conducting the experimental work received from CERD (Centre for Engineering Research and Development), Government of Kerala, is greatly acknowledged.

The love, care, suggestions and prayers of my loving parents, Mr. P V Veeravu and Mrs.Fathima V is always a source of constant inspiration to me throughout my life. I express my sincere gratitude and dedicate this work to them. I thank my brothers and sisters for their unconditional love and support given to me in my whole life. I would also like to thank my mother in law, Haseena M, for sharing my household tasks during the writing of this thesis. Last but not least, I thank my beloved husband, Dr.Anshad M.H, sons Asif and Adil, who gave me every reason to complete this Ph.D. through all hardships with a happy and smiley face.

Haseena P. V.

ABSTRACT

Inorganic nitrogen pollution in recent years has left their impression on the environment and ecological system. Extensive use of nitrogen fertilizers, wastewater from livestock and poultry breeding industries, municipal sewage treatment plants contribute to highly aggressive nitrogen contamination. They cause negative impacts on water quality through eutrophication and soil erosion. The high concentration of nitrates and ammonia in drinking water causes serious health issues in human beings. Adsorption is found as the most efficient process to remove harmful nitrogencontaining compounds effectively in a wastewater treatment system.

In the present work, the removal of nitrate nitrogen ($\text{NO}_3\text{-N}$) from aqueous solution by adsorption using nano-bio sorbents, namely Fe-CH-NSP (Iron loaded Chitosan Nutmeg shell powder) and Chitosan-Bentonite Nanocomposite films (CH-B-NCF) has been studied. The adsorption efficiency of CH-B-NCF onto ammonia nitrogen ($\text{NH}_4^+\text{-N}$) has also been investigated. The nanobiosorbents used in the study were synthesized in the laboratory using standard methods, and they were characterized by SEM, TEM, FTIR and TGA. Batch adsorption studies were conducted to assess the effect of various parameters on adsorption. The maximum nitrate nitrogen removal efficiency for Fe-CH-NSP was found to be 83.33 mg/g, and that of CH-B-NCF was 76.92 mg/g. From the batch study of nitrate removal with CH-B-NCF, a pH of 4 was obtained as the optimum. The pH identified for maximum nitrate removal using Fe-CH-NSP was 8. Further studies to find the effect of initial concentration, time and temperature were conducted at the optimum pH. The adsorption equilibrium data were analyzed with Freundlich, Langmuir, Tempkin, and Dubinin Radushkevich isotherms. The adsorption

equilibrium data of nitrate removal with Fe-CH-NSP and CH-B-NCF was best fitted to Langmuir isotherm. Kinetic studies for nitrate removal using both the adsorbents showed that the adsorption data fitted to the pseudo-second-order kinetic model. Thermodynamic studies on nitrate removal were carried out with Fe-CH-NSP and chitosan bentonitenanocomposite films. The optimization of batch adsorption of nitrate-nitrogen uptake onto CH-B-NCF using response surface method was carried out. On considering the ease of handling and economic loss due to small particle size, chitosan bentonite films were selected for column operation. The regeneration of chitosan bentonitenanocomposite films loaded with nitrate was done with 1 M NaCl.

The acidic or alkaline conditions were not conducive in the adsorption of ammonia nitrogen with CH-B-NCF. So further adsorption studies were conducted at pH value of pH= 6. The equilibrium adsorption data gave a better prediction with the Freundlich model. The kinetic studies suggested the pseudo-second-order mechanism for adsorption. The values of thermodynamic parameters proposed that the adsorption is a spontaneous and exothermic process. RSM has been employed to evaluate and optimize the effects of initial ammonia concentration, pH, contact time, and temperature on NH_4^+ -N removal. The desorption study of nanocomposite films laden with NH_4^+ -N was conducted using 0.5 M NaOH.

Continuous fixed-bed studies for nitrate removal using chitosan bentonitenanocomposite films showed that with an increase in bed height, the breakthrough curve shifted to the right, and more volume of effluent could be treated. As the flow rate of nitrate solution increased, the saturation of the bed occurred faster. Modeling of the packed bed column was performed using the Thomas model, Yoon Nelson model, and Adam Bohart model. The correlation between experimental and theoretical data of column operation

was compared for the three models by plotting (C_t/C_0) experimental versus (C_t/C_0) theoretical. From the values of the correlation coefficient, the Thomas model and the Yoon Nelson model were found to fit well to the experimental data. Adam Bohart correlation was proved best for the initial part of the adsorption process. Results revealed that packed bed adsorption column using nanocomposite films could be used in water treatment systems to eliminate nitrogenous contaminants effectively

Keywords: Adsorption, Nano biosorbents, Chitosan, Bentonitenanoclay, Nutmeg shell powder, Packed bed column.

CONTENTS

ACKNOWLEDGEMENTS	i
ABSTRACT.....	iii
TABLE OF CONTENTS	vii
LIST OF TABLES	xiii
LIST OF FIGURES	xv
ABBREVIATIONS	xxi
CHAPTER 1 INTRODUCTION.....	1
1.1 Background of the Research	1
1.2 Sources of Nitrate Nitrogen and Ammonia Nitrogen	2
1.3 Adverse Effects of Nitrogenous Wastes	2
1.4 Methods for Technological Removal of Nitrate Nitrogen and Ammonia Nitrogen.....	5
1.5 Adsorption and Adsorbents.....	5
1.6 Scope of the Study	8
1.7 Objectives of the Present Work	10
1.8 Outline of the Thesis	12
CHAPTER 2 LITERATURE REVIEW.....	15
2.1 Introduction.....	15
2.2 Sources of Nitrogen Contaminants	15
2.3 Impacts of Nitrogen	17
2.4 Methods of Nitrogen Removal.....	19
2.4.1 Denitrification	20
2.4.2 Ion Exchange.....	22
2.4.3 Reverse Osmosis	24
2.4.4 Electrodialysis	24
2.4.5 Adsorption.....	25
2.5 Literature Review on Adsorption and Adsorbents.....	28
2.5.1. Chitosan-Based Adsorbents	29

2.5.2	Clay-Based Adsorbents	32
2.5.3	Biosorbents.....	34
2.5.4	Nano AdsorbentsandNanocomposite Adsorbents.....	38
2.6	Mechanism of Adsorption.....	41
2.7	Factors Affecting Batch Adsorption	42
2.7.1	Effect of pH on Adsorption.....	42
2.7.2	Effect of Contact Time.....	44
2.7.3	Effect of Initial Concentration on Adsorption	46
2.7.4	Effect of Temperature and Pressure.....	47
2.7.5	Effect of Agitation Speed and Adsorbent Dosage	48
2.8	Adsorption Isotherm	47
2.9	Adsorption Kinetics	50
2.10	Adsorption Thermodynamics.....	52
2.11	Response Surface Methodology.....	54
2.12	Desorption.....	57
2.13	Characterization of Adsorbents.....	59
2.14	Analytical Method.....	61
2.15	Continuous Removal in Packed Bed Adsorption Column.....	63
2.16	Summary	68
CHAPTER 3 MATERIALS AND METHODS		71
3.1	Introduction.....	71
3.2	Preparation of Nitrate and Ammonium Stock Solutions	71
3.3	Preparation of Adsorbents.....	72
3.3.1	Preparation of Fe-loaded Chitosan Nutmeg Shell Powder	72
3.3.2	Preparation of Chitosan-BentoniteNanocomposite Films.....	74
3.4	Analytical Method for Nitrate Nitrogen and Ammonia Nitrogen Determination	76
3.5	Characterization of Adsorbents.....	77

3.6	Batch Experiments	78
3.6.1	Batch Experiments for Nitrate Removal using Fe- CH-NSP and CH-B-NCF	79
3.6.2	Effect of Various Parameters on Adsorption of Nitrate Nitrogen by Fe-CH-NSP and Chitosan- Bentonite Nanocomposite Films	80
3.6.3	Equilibrium Studies for Nitrate Removal Using Fe-CH- NSP and Chitosan-Bentonite Nanocomposite Films	81
3.6.4	Kinetic Studies for Nitrate Removal Using Fe-CH-NSP and Chitosan-Bentonite Nanocomposite Films.....	83
3.6.5	Thermodynamic Studies for Nitrate Removal Using Fe- CH-NSP and Chitosan-Bentonite Nanocomposite Films	84
3.6.6	Response Surface Methodology for Nitrate Nitrogen Removal Using Nanocomposite Films.....	85
3.6.7	Desorption Studies of Nitrate Nitrogen with CH-B-NCF	87
3.6.8	Adsorption Using Nanocomposite Films for Ammonia Nitrogen	88
3.6.9	Design of Experiments for Ammonia Nitrogen Adsorption Using Chitosan-Bentonite Nanocomposite Films	90
3.7	Removal of Nitrate Nitrogen in Continuous Fixed Bed Adsorption Column Using Chitosan- Bentonite Nanocomposite Film as Adsorbent	90
3.7.1	Thomas Model	94
3.7.2	Yoon Nelson Model	95
3.7.3	Adam Bohart Model.....	96
3.8	Summary of the Chapter	97

CHAPTER 4	RESULTS AND DISCUSSION	99
4.1	Introduction.....	99
4.2	Batch Adsorption Study for Nitrate Nitrogen Removal Using Fe-CH-NSP.....	100
4.2.1	Effect of pH and Temperature on Nitrate Removal by Fe- CH-NSP.....	100
4.2.2	Adsorption Isotherms of Nitrate Nitrogen Removal onto Fe-CH-NSP.....	103
4.2.3	Kinetics of Adsorption of NO ₃ -N onto Fe-CH-NSP.....	108
4.2.4	Effect of Temperature on Adsorption of Nitrate Nitrogen Using Fe-CH-NSP.....	112
4.2.5	Characterisation of Fe-CH-NSP.....	114
4.2.6	Morphological Behavior by SEM and TEM Analysis.....	114
4.2.7	FT-IR Analysis of Nitrate Nitrogen Removal by Fe-CH- NSP	117
4.2.8	X-ray Diffraction Pattern of Fe-CH-NSP	120
4.3	Batch Adsorption of Nitrate by Chitosan- Bentonite Nanocomposite Films.....	122
4.3.1	Effect of pH on Nitrate Nitrogen Uptake by Chitosan Bentonite Films.....	122
4.3.2	Adsorption Kinetics	124
4.3.3	Equilibrium Adsorption Isotherm.....	129
4.3.4	Thermodynamics of Nitrate Nitrogen Adsorption.....	134
4.3.5	Desorption Studies of Nitrate Nitrogen	136
4.3.6	Response Surface Methodology for Analysis of Nitrate Nitrogen Removal Using Chitosan-Bentonite Nanocomposite Films	138
4.3.7	Combined Effect of Variables on Nitrate Nitrogen Removal	141

4.3.8	Characterisation of Chitosan Bentonite Nanocomposite Films.....	143
4.3.9	Surface Morphology Analysis by Scanning Electron Microscopy.....	143
4.3.10	X-ray Diffraction.....	144
4.3.11	Thermogravimetric Analysis.....	146
4.4	Continuous Removal of Nitrate Nitrogen in Packed Column Using Nanocomposite Films.....	148
4.4.1	Effect of Bed Height on Breakthrough Curves.....	148
4.4.2	Effect of Flow Rate on the Performance of Packed Column.....	151
4.5	Modeling of Packed Bed Adsorption Column.....	154
4.5.1	Thomas model.....	154
4.5.2	Yoon Nelson model.....	158
4.5.3	Adam Bohart model.....	161
4.5.4	Comparison of Thomas Model, Yoon Nelson Model and Adam Bohart Model.....	165
4.6	Batch Adsorption Study of Ammonia-Nitrogen Removal Using Chitosan-Bentonite Nanocomposite Films.....	170
4.6.1	Effect of pH on Ammonia Nitrogen Removal by CH-B- NCF.....	170
4.6.2	Adsorption Isotherms of Ammonia Nitrogen Uptake Onto Chitosan Bentonite Nanocomposite Films.....	172
4.6.3	Kinetics of Adsorption of Ammonia Nitrogen onto CH- B-NCF.....	175
4.6.4	Thermodynamics of Adsorption of Ammonia Nitrogen onto CH-B-NCF.....	179
4.6.5	Characterisation of Nanocomposite Films.....	181
4.6.6	Scanning Electron Microscopy Equipped with Energy Dispersive X-ray Spectroscopy.....	183

4.6.7	FT-IR Studies on Ammonia Nitrogen Removal by CH-B-NCF.....	183
4.6.8	Application of Response Surface Methodology for NH ₄ ⁺ - N Removal Using Nanocomposite Films.....	185
4.6.9	Optimization of Ammonia Removal Using Response Surface Methodology	191
4.6.10	Combined Effect of Variables on Adsorption of Ammonia Nitrogen Using CH-B-NCF	192
4.6.11	Desorption Studies of Ammonia Nitrogen.....	195
4.7	Summary	196
CHAPTER 5 SUMMARY AND CONCLUSIONS		199
5.1	Summary	199
5.2	Conclusions of Batch Study	201
5.3	Conclusions of Fixed Bed Study.....	203
5.4	Limitations of the Study	203
5.5	Scope for Future Research	204
REFERENCES.....		205
ANNEXURES.....		225

LIST OF PAPERS SUBMITTED ON THE BASIS OF THIS THESIS

CURRICULUM VITAE

LIST OF TABLES

Table No	Title	Page No
Table 1.1	Physicochemical properties of nitrogen and its compounds -----	4
Table 2.1	Advantages and disadvantages of common technologies for nitrate removal from waste water sources -----	27
Table 4.1	Equilibrium parameters for adsorption of NO ₃ -N on Fe-CH-NSP-----	104
Table 4.2	The kinetic constants and correlation coefficients for adsorption of NO ₃ -N onto Fe-CH-NSP -----	110
Table 4.3	The intraparticle diffusion and film diffusion constants and correlation coefficients for adsorption of NO ₃ -N onto Fe-CH-NSP-----	112
Table 4.4	Thermodynamic parameters of adsorption of NO ₃ -N onto Fe-CH-NSP-----	114
Table 4.5	The kinetic constants and correlation coefficients for adsorption of nitrate on to chitosan bentonitenanocomposite films-----	127
Table 4.6	The intraparticle diffusion and film diffusion constants and correlation coefficients for adsorption of NO ₃ -N onto CH-B-NCF-----	129
Table 4.7	Equilibrium parameters for adsorption of NO ₃ -N on to chitosan bentonitenanocomposite films-----	133
Table 4.8	The nitrate adsorption capacities of the chitosan derivative adsorbents-----	134
Table 4.9	Thermodynamic parameters of adsorption of nitrate onto nanocomposite film-----	136
Table 4.10	Coded levels of independent variables in Box-Behnken design for NO ₃ -N using nanocomposite films-----	138
Table 4.11	Design of experiments for nitrate removal using chitosan bentonite nanocomposite films-----	139
Table 4.12	The characteristic peaks and intergallery spacing of chitosan bentonitenanocomposite film.-----	145
Table 4.13	Mathematical description of fixed bed nitrate column parameters (C ₀ =70 mg/L)-----	153

Table 4.14	The Thomas model parameters at different flow rates and bed heights (initial concentration = 70 mg NO ₃ -N/L)-----	157
Table 4.15	The Yoon Nelson model parameters at different flow rates and bed heights (initial concentration = 70 mg NO ₃ -N/L) -----	160
Table 4.16	Parameters predicted by Adam Bohart model for varying initial concentration, pH, bed height and flow rate -----	163
Table 4.17	Correlation coefficients for Thomas model, Yoon Nelson model and Adam Bohart model for various experimental conditions -----	169
Table 4.18	Correlation coefficients for Thomas model, Yoon Nelson model and Adam Bohart model for different flow rates -----	169
Table 4.19	Equilibrium parameters for adsorption of NH ₄ ⁺ -N on to chitosan bentonite nanocomposite films -----	173
Table 4.20	Ammonia nitrogen adsorption capacities of various adsorbents -----	173
Table 4.21	The kinetic constants and correlation coefficients for adsorption of ammonia nitrogen on to chitosan bentonitenanocomposite films. -----	179
Table 4.22	Distribution coefficients and thermodynamic parameters for ammonia nitrogen adsorption onto CH-B-NCF -----	180
Table 4.23	Coded levels of independent variables in Box-Behnken design for NH ₄ ⁺ -N using chitosan bentonitenanocomposite films -----	185
Table 4.24	Experimental design for removal of ammonia nitrogen using chitosan-bentonitenanocomposite films. -----	186
Table 4.25	Coefficients of the model equation and t, p, (1-p) values for ammonia nitrogen removal by nanocomposite films -----	187
Table 4.26	Analysis of variance for adsorption of ammonia nitrogen onto chitosan bentonitenanocomposite films -----	190

LIST OF FIGURES

Figure	Title	Page No
Fig. 2.1	Structure of Chitosan -----	30
Fig. 2.2	Physical & Chemical Structure of Montmorillonite C lay-----	33
Fig. 3.1	Nutmeg and nutmeg shell-----	73
Fig. 3.2	Synthesized Fe-loaded chitosan nutmeg shell powder-----	73
Fig. 3.3	Synthesized chitosan-bentonite nanocomposite films-----	74
Fig. 3.4	Synthesis of chitosan betonies nanocomposite films in the lab-----	75
Fig. 3.5	Ammonium solution with Nessler's reagent for analyzing in UV vis spectrophotometer -----	77
Fig. 3.6	Schematic of the experimental packed bed column with proper dimensions-----	91
Fig. 3.7	Nitrate fixed bed column using CH-B-NCF -----	92
Fig. 4.1	Effect of pH and adsorbent dosage on adsorption efficiency and adsorption capacity of nanokaolinite clay -----	102
Fig. 4.2	Langmuir, Freundlich, Tempkin and Dubinin- Radushkevich isotherm of NO ₃ -N adsorption using Fe- CH-NSP -----	106
Fig. 4.3	Equilibrium isotherms for NO ₃ -N removal from aqueous solution onto Fe-CH-NSP-----	107
Fig. 4.4	Kinetics of adsorption of nitrate nitrogen onto Fe-CH- NSP-pseudo first order, second order, and pseudo second order models. -----	110
Fig. 4.5	Kinetics of adsorption diffusion model of NO ₃ -N onto Fe-CH-NSP, Weber-Morris intraparticle diffusion model and Dunwald-Wagner film diffusion model.-----	112
Fig. 4.6	Thermodynamic plot for the adsorption of NO ₃ -N onto Fe-CH-NSP -----	113
Fig. 4.7	SEM images of Fe-CH-NSP at different magnifications before nitrate adsorption -----	115
Fig. 4.8	SEM images of Fe-CH-NSP after nitrate adsorption -----	116

Fig. 4.9	TEM image of Fe-CH-NSP-----	117
Fig. 4.10	FTIR of raw nutmeg shell powder-----	118
Fig. 4.11	FTIR of Fe-loaded chitosan nutmeg shell powder. -----	119
Fig. 4.12	FTIR of Fe-CH-NSP after nitrate adsorption -----	119
Fig. 4.13	XRD spectra of Fe-CH-NSP-----	121
Fig. 4.14	XRD spectra of Fe-CH-NSP after adsorption of NO ₃ -N. -----	121
Fig. 4.15	Influence of pH on nitrate adsorption (initial nitrate concentration 50 mg N/L and nanocomposite film dose 0.1 g/100 mL). -----	124
Fig. 4.16	Kinetics of adsorption of nitrate nitrogen onto CH-B-NCF, pseudo first order, second order, and pseudo second order models -----	127
Fig. 4.17	Kinetics of adsorption diffusion model of nitrate nitrogen onto chitosan bentonite nanocomposite films, Weber-Morris intraparticle diffusion model and Dunwald-Wagner film diffusion model.-----	128
Fig. 4.18	Langmuir, Freundlich Tempkin and Dubinin-Radushkevich isotherm of NO ₃ -N adsorption using CH-B-NCF. -----	132
Fig. 4.19	Equilibrium isotherms for NO ₃ -N removal from aqueous solution onto CH-B-NCF-----	133
Fig. 4.20	Free energy change of adsorption of nitrate ions using chitosan bentonite nanoclay adsorbent versus temperature-----	135
Fig. 4.21	Desorption of nanocomposite films loaded with nitrate by 1 M NaCl -----	137
Fig. 4.22	Experimental versus predicted efficiency for adsorption of nitrate onto nanocomposite films-----	140
Fig. 4.23	Optimizer plot of for adsorption of nitrate onto nanocomposite films-----	141
Fig. 4.24	Contour and surface plots for combined effect of variables for nitrate removal by nanocomposite films -----	142

Fig. 4.25	SEM of chitosan-bentonite nanocomposite films at different magnifications -----	143
Fig. 4.26	XRD of chitosan bentonite nanoclay film -----	145
Fig. 4.27	XRD of chitosan bentonite nanoclay film after nitrate adsorption -----	146
Fig 4.28	TGA of chitosan bentonite nanocomposite films-----	147
Fig 4.29	Effect of bed height on breakthrough curves -----	150
Fig. 4.30	Effect of bed height on adsorbed concentration in continuous packed bed nitrate column -----	150
Fig. 4.31	Effect of flow rate on breakthrough curves -----	152
Fig. 4.32	Effect of flow rate on adsorbed concentration -----	152
Fig. 4.33	Plot for determining Thomas kinetic coefficient k_{Th} (mL/min mg) and maximum solid phase concentration q_0 (mg/g) for varying bed height -----	154
Fig. 4.34	Plot for determining Thomas kinetic coefficient k_{Th} (mL/min mg) and maximum solid phase concentration q_0 (mg/g) for varying flow rate -----	155
Fig. 4.35	Comparison of experimental and theoretical breakthrough curves predicted by Thomas model for varying bed height -----	156
Fig 4.36	Comparison of experimental and theoretical breakthrough curves predicted by Thomas model for varying flow rate-----	156
Fig. 4.37	Yoon Nelson parameters determination for varying bed height-----	158
Fig. 4.38	Determination of coefficients in the Yoon Nelson model for varying flow rate-----	159
Fig. 4.39	Comparison of experimental and theoretical breakthrough curves by Yoon Nelson model for varying bed height -----	160
Fig 4.40	Comparison of experimental and theoretical breakthrough curves by Yoon Nelson model for different flow rates -----	161
Fig. 4.41	Determination of Adam Bohart model parameters for bed height = 10 cm, 15 cm and 20 cm -----	162

Fig. 4.42	Determination of Adam Bohart model parameters for different flow rate -----	162
Fig. 4.43	Breakthrough curves by Adam Bohart Model and experimental for bed height=10 cm, 15 cm and 20 cm -----	164
Fig. 4.44	Breakthrough curves by Adam Bohart Model and experimental for varying flow rate Q=6mL/min,10mL/min and 15 mL/min. -----	164
Fig. 4.45	Comparison of $(C_f/C_0)_{\text{experimental}}$ and $(C_f/C_0)_{\text{theoretical}}$ by Thomas model for varying bed height -----	166
Fig. 4.46	Comparison of $(C_f/C_0)_{\text{experimental}}$ and $(C_f/C_0)_{\text{theoretical}}$ by Thomas model for varying flow rate -----	166
Fig. 4.47	Comparison of $(C_f/C_0)_{\text{experimental}}$ and $(C_f/C_0)_{\text{theoretical}}$ by Yoon Nelson model for varying bed height -----	167
Fig. 4.48	Comparison of $(C_f/C_0)_{\text{experimental}}$ and $(C_f/C_0)_{\text{theoretical}}$ by Yoon Nelson model for varying flow rate -----	167
Fig. 4.49	Comparison of $(C_f/C_0)_{\text{experimental}}$ and $(C_f/C_0)_{\text{theoretical}}$ by Adam Bohart model for varying bed height -----	168
Fig. 4.50	Comparison of $(C_f/C_0)_{\text{experimental}}$ and $(C_f/C_0)_{\text{theoretical}}$ by Adam Bohart model for varying flow rate. -----	168
Fig. 4.51	Effect of pH on percentage removal and adsorption efficiency of ammonia nitrogen using CH-B-NCF -----	171
Fig. 4.52	Langmuir and Freundlich isotherm plots for ammonia nitrogen adsorption onto CH-B-NCF -----	174
Fig.4.53	Equilibrium data of ammonia removal from aqueous solution fitted to Langmuir and Freundlich isotherms -----	175
Fig. 4.54	Kinetic plots for ammonia nitrogen adsorption onto CH-B-NCF -----	177
Fig. 4.55	Kinetics of adsorption diffusion model of ammonia nitrogen onto chitosan bentonite nanocomposite films. -----	178
Fig. 4.56	Free energy change of adsorption of ammonium ions using chitosan bentonite nanoclay adsorbent versus temperature -----	180
Fig. 4.57	SEM Image of Nano composite film after ammonia nitrogen adsorption at different magnifications -----	181

Fig. 4.58	EDX of chitosan bentonite film composite before ammonium adsorption-----	182
Fig. 4.59	EDX of chitosan bentonite film composite after ammonium adsorption-----	183
Fig. 4.60	FTIR of raw chitosan bentonite nanocomposite film -----	184
Fig. 4.61	FTIR of chitosan bentonite nanocomposite film after ammonium adsorption. -----	184
Fig. 4.62	Fitted line plot for ammonia nitrogen removal by CH-B-NCF -----	189
Fig. 4.63	Optimization plot for NH_4^+ -N removal -----	191
Fig. 4.64	Surface and contour plots of combined effect of temperature and pH -----	193
Fig. 4.65	Surface and contour plots of combined effect of temperature and time -----	193
Fig. 4.66	Contour and Surface Plots of combined effect of Time and pH -----	194
Fig. 4.67	Contour and surface plots of combined effect of concentration and temperature -----	194
Fig. 4.68	Comparison of removal performance of virgin and regenerated Nano composite films for varying pH and Temperature -----	194

ABBREVIATIONS

A-B model	Adam Bohart model
BBD	Box Behnken Design
BDST	Bed Depth Service Time
COD	Chemical Oxygen Demand
D-R	DubininRadushkevich
DTA	Differential Thermal Analysis
ED	Electrodialysis
EDX	Energy Dispersive X-ray Spectroscopy
EPA	Environmental Protection Agency
FTIR	Fourier Transform Infrared Spectroscopy
FWHM	Full Width at Half Maximum
IR	Infrared
MCL	Maximum Contaminant Level
MMT	Montmorillonite
NH ₄ ⁺ -N	Ammonia Nitrogen
NO ₃ -N	Nitrate Nitrogen
RO	Reverse Osmosis
RPM	Revolutions per minute
RSM	Response Surface Methodology
SAED	Selected Area Electron Diffraction
SEM	Scanning Electron Microscope
TEM	Transmission Electron Microscope
TGA	Thermogravimetric Analysis
USEPA	United States Environmental Protection Agency
UV vis	Ultraviolet Visible
WHO	World Health Organisation
XRD	X-ray Diffraction

CHAPTER 1

INTRODUCTION

1.1 BACKGROUND OF THE RESEARCH

Advanced wastewater treatment is attracting an international spotlight for effective shielding of environmental degradation due to the discharge of detrimental chemicals. The rapid growth of industries and agriculture causes water pollution. The presence of contaminants deteriorates the quality of water which undergoes a distinct shift in its capability to support human life and biotic communities. The World Health Organization (WHO) reported that half of the world's inhabitants will be living in water stressed areas by 2025. To find innovative solutions to this global issue is therefore an emergent research need.

Nutrient compounds such as ammonia nitrogen ($\text{NH}_4^+\text{-N}$), nitrite (NO_2^-) and nitrate (NO_3^-) are often present in surface and ground water. Due to their high solubility, they can quickly end up in all water resources. High nutrient concentration in water can lead to an imminent risk to animal and human health. (Yian *et al.*, 2012). Also, nutrients contribute extensively to eutrophication in the aquatic environment. Nutrients at a desirable level are essential for plant growth and development. The recovered nutrients detached from the wastewater can be used as fertilizers (Zuohao *et al.*, 2011). So recovery of the nutrients has relevance. Therefore, new research strategies for the removal of nitrogenous contaminants are indispensable.

1.2 SOURCES OF NITRATE NITROGEN AND AMMONIA NITROGEN

The primary cause of nitrogen contamination is the extensive use of nitrogenous fertilizers and the increasing escalation of farming practices. Nitrogen fertilizers are used in agriculture to increase yield and quality. Nitrogen is a precious limiting nutrient in plant growth and is a constituent of chlorophyll. It is a fundamental building block of plant and animal proteins and many other molecules. Usually, proteins hold nearly 16% nitrogen. About 40–70% of the nitrogen available in standard fertilizers escapes to the surroundings and cannot be absorbed by plants, especially in autumn and winter, when vegetation uptake is decreased, and precipitation exceeds evapotranspiration (Raheleh Malekian *et al.*, 2011). Sewage and organic solid wastes provide nitrogen pollution largely next to agriculture. The human and animal excreta contain nitrogen in the form of organic molecules, such as urea and urine. The microbial action on urea causes the ammonia release, propping up the growth of algae in water bodies. Beyond water and soil pollution, the air pollution through nitrous oxides which is a green house gas also contributes to the offensive effect of nitrogen. The reactive nitrogen enters into the flora and fauna by vehicular pollution, fossil-fuel burning and exhausts of air pollution control devices. Nitrous oxide is a fast-growing sponsor to global climate change. The petrochemical, pharmaceutical and explosive industries are the major industrial activities that result in the release of nitrogenous wastes.

1.3 ADVERSE EFFECTS OF NITROGENOUS WASTES

Extreme nitrogen inputs can initiate adverse ecological effects, ranging from eutrophication to global acidification. Reduced water clarity and

excessive growth of weeds and algae are typical signs of eutrophication. The high levels of organic matter after the decomposition of algae deplete the dissolved oxygen, leading to the death of fish and other aquatic species. Soil acidification, plant biodiversity reduction, phytoplankton blooms and production of the greenhouse gas nitrous oxide (N₂O) are the other crucial environmental issues associated with nitrogen contaminants.

Nitrite ions transformed from nitrate ions is a precursor of carcinogenic nitrosamines (Amit and Mika, 2011). Typically three types of cancers are reported due to nitrates, viz., gastric cancer, non-Hodgkin's lymphoma, and cancer of alimentary canal. Under the acidic conditions in the human stomach the nitrate forms nitrous acid. The protonation of nitrous acid forms nitrosonium cation and water. The reaction of the nitrosonium cation with amine produces carcinogenic nitrosamines and water. It is given in equation 1.1



Hemoglobin is a blood protein that helps to carry blood throughout the body. The hemoglobin, in the presence of nitrates gets converted to methemoglobin. The conversion of the ferrous state of iron in the heme group to the ferric state in methemoglobin decreases the ability of blood to carry oxygen, which becomes lethal in infants. Blue baby syndrome (Methemoglobinemia) and cyanosis have been widely reported due to nitrates in drinking water (Costas *et al.*, 2010). The nitrates also impose a negative effect on human health through congenital disabilities, spontaneous abortion, changes in the immune system, diarrhoea, diabetes, respiratory tract infections, and hypertension (Kassae *et al.*, 2011). The increased usage of groundwater for drinking and irrigation purposes in India resulted the presence

of nitrates in drinking water recently. The maximum permissible concentration limit of nitrate nitrogen ($\text{NO}_3\text{-N}$) fixed by the World Health Organization (WHO) is 10 mg/L (Anni *et al.*, 2015). Ammonia has an indispensable role in the biosynthesis of purines, pyrimidines, and non-essential amino acids. Ammonia induces toxic effect on healthy humans if the concentration of intake exceeds the detoxification capacity (Haiming *et al.*, 2010). The influences in metabolism, decreasing the tissue sensitivity to insulin, lung edema, nervous system dysfunction, kidney damage, acidosis, and upsetting the glucose tolerance are the health issues associated with ammonia nitrogen. The ammonia nitrogen ($\text{NH}_4^+\text{-N}$) concentration in a range of 0.2-0.5 mg/L is lethal to fish and other aquatic animals (Aref. *et al.* 2018). In India, CPCB has set a stringent restriction for the discharge standard of ammonia nitrogen as 1.2 mg/L or less for class D water in the propagation of wildlife and fisheries. These facts pinpoint the necessity of the development of an efficient method for removing nitrogen contaminants from wastewater. Physico chemical properties of nitrogen and its compounds has given in Table 1.1(www.google.com)

Table 1.1 Physico chemical properties of nitrogen and its compounds

Property	Nitrogen	KNO_2	KNO_3	NH_4Cl	HNO_3
Melting Point ($^\circ\text{C}$)	-210	440	334	338	-42
Boiling Point ($^\circ\text{C}$)	-196	537	440	520	83
Solubility in water(g/L)	soluble	soluble	soluble	soluble	soluble
Density (g/cm^3)	1.25(0°C)	1.915	2.109	1.52	1.51
Heat Capacity, J/mol K	30	107.4	95.06	84.1	146

1.4 METHODS FOR TECHNOLOGICAL REMOVAL OF NITRATE NITROGEN AND AMMONIA NITROGEN

Researchers have developed a number of methods for the remediation of nitrogen contaminants such as electro dialysis, ion exchange, biological denitrification, ozonation, reverse osmosis, membrane separation, coagulation, flocculation, and adsorption (David *et al.*, 2011; Shady *et al.*, 2012). Of the various methods, adsorption is found to be a promising process because of its simplicity and low operational cost. The adsorption process exploits the ability of certain solids to take up specific substances from solution onto their surface (Amit *et al.*, 2011). Minimum sludge production reduces the disposal effort. Adsorption is found more suitable in water treatment systems. The simple handling of the system and effective contaminant removal are the peculiarities attributed to adsorption. The easy restoration of adsorbents could reduce operational costs. The property of selectivity in the presence of other ions could be utilized in the adsorption process. The impurities from wastewater get adhered on the surface of the material by van der Waals force (physisorption) or chemical bonds (chemisorption). Adsorbents are the critical factors in adsorption operation.

1.5 ADSORPTION AND ADSORBENTS

Adsorption is a surface phenomenon in which specific components of a gaseous or liquid phase are selectively transferred to the surface of a solid material. The particular element from the aqueous medium will form bonds with the solid and become attached to its surface. The ions or molecules which get deposited are called the adsorbate. The material whose surface receives adsorbate molecules is known as adsorbent. Adsorption is also known as a separation process because we are separating the desired or undesired (contaminants) particles into the adsorbent surface. The high temperatures

rarely support the adsorption process. So generally, adsorption is an exothermic process. The enthalpy change is negative for exothermic processes. Generally, with gas molecules adsorbed in the surface of the solid, the entropy goes down. However in solid–liquid adsorption system, solute adsorption process and solvent desorbing process works simultaneously. So there is a chance of occurrence of positive entropy change. The positive value of entropy change is due to the increase in the degree of randomness of the molecules near the adsorbent surface during adsorption (Arshadi, *et al.*, 2015). The endothermic adsorption is sometimes seen in chemisorption. The change in enthalpy value is positive in an endothermic reaction. An increase in temperature might be favoring the chemical bonding in such a case. At constant pressure, the adsorption is a spontaneous process, and free energy decreases during adsorption. The negative value of change in free energy is attributed to a favorable adsorption process. The method of detaching the adsorbed molecules from the surface of the adsorbent is called desorption.

The parameters which influence the batch adsorption process are the changes in the solution pH, initial solution concentration, time of contact, agitation speed, adsorbent dosage, temperature, and pressure. The optimum values of the variables for obtaining maximum elimination of the desired constituent are estimated in the batch study. The optimization of the batch process can be carried with the appropriate software. In the present work, Minitab software has been used for this purpose. Box Behnken design of response surface methodology (RSM) has been used for the optimization of the batch adsorption process. Response surface methodology is a statistical method that helps to enumerate the significance of the effects of different variables on the response of interest of the particular process (Soumasree *et al.*, 2012). In RSM, firstly, the batch adsorption experiments are carried out

according to the design of experiments assigned by Box Behnken design. The advantage of BBD is that it does not contain combinations which all factors are simultaneously at their highest or lowest levels. The model equation is developed, and the estimation of coefficients is done. Finally, the response prediction and checking the sufficiency of the model are made.

The elementary information of the adsorption process is obtained from the batch study. The long duration of time consumed, the requirement of high adsorbent dosage, and the small capacity are the main limitations of the batch study. Continuous processes are preferred for large scale operations. The extended operating period and capacity for handling of a high volume of aqueous solution can be achieved only in continuous packed column operation. The continuous column operation is cost-effective, and proper control of the adsorption process is possible compared to the batch adsorption (Emine and Yasar , 2006). The adsorbent material is packed in an appropriate column, and the wastewater to be treated is passed through the column either in up-flow or down flow mode. The solutes get adsorbed onto the adsorbent packing during the operation. The solution leaving the column is analysed for the residual ions. The bed heights of the adsorbent and flow rate of the solution through the column are the two crucial packed column parameters. A plot of the output solute concentration against time is called the breakthrough curve. The shape of the breakthrough curve is an essential factor that determines the time of operation of the fixed bed column. The column can be modelled by fitting the experimental data to empirical models like Thomas model, Yoon Nelson model, and Adam Bohart model. The regeneration of the bed is done by passing a suitable desorbing solution through the column.

Adsorbents are the determining factors in the adsorption process. Previous researchers have used several adsorbents like activated carbon (Azhar *et al.*, 2010), ion exchange resins (Chabani *et al.*, 2009), clays (Deepesh *et al.*, 2012), metal oxides (Diana *et al.*, 2015), nanomaterials (Yu-Hoon *et al.*, 2011; Bekhradinassab and Sabbaghi *et al.*, 2014), agricultural wastes (Ari *et al.*, 2012; Xing Xu *et al.*, 2012), industrial wastes (Asim *et al.*, 2013; Zukhra. *et al.*, 2015), biosorbents (Bing *et al.*, 2015; Zuohao *et al.*, 2011; Haiwei *et al.*, 2010) and modified chitosan (Yian *et al.*, 2012; Sudipta *et al.*, 2009) for the removal of nitrate nitrogen and ammonia nitrogen. Recently the synthesis of environmentally benign bio nanocomposite adsorbents is gaining attention. The higher adsorption capacity of nanomaterials as adsorbents is attributed to their large surface area and pore size distribution.

1.6 SCOPE OF THE STUDY

The proper treatment and reuse of wastewater are the primary objectives of wastewater engineering. The treatment objective in the removal of nutrients, such as nitrogen and phosphorous began to be addressed from the early 1970s to 1980s. Water quality issues arise when higher amounts of untreated wastewater are discharged to streams that are ultimately used as sources of drinking water. The wastewater management system is carefully assessing the health and environment effects due to improper treatment and discharge into water bodies. The essential steps in the wastewater treatment system include preliminary treatment, primary treatment, advanced primary treatment, secondary treatment, secondary treatment with nutrient removal, tertiary treatment and advanced treatment. Preliminary treatment involves the removal of coarse and suspended solids like rags, sticks, floatables, grit and

grease by screening. This is done by passing the wastewater through grit chambers and equalization chambers. Primary treatment consists of the use of primary clarifiers for the removal of suspended solids and organic matter that are not removed during the preliminary treatment. The advanced primary treatment uses chemical addition or filtration for the enhanced removal of suspended solids and organic matters from water. Secondary treatment involves unit processes and is meant for the treatment of water by either aerobic or anaerobic methods in the presence of microorganisms. During the secondary treatment, removal of organic matters, suspended solids and disinfection are done. The elimination of the nutrient is carried out both in the secondary treatment with the nutrient removal process and in the tertiary treatment (Arcadio and Gregoria, 2011). The uptake of dissolved and suspended materials remaining after biological treatment is removed in advanced wastewater treatment systems.

The adsorption process is usually installed in a tertiary treatment system in a wastewater treatment plant. Tertiary treatment is meant for the final treatment of wastewater, which contains traces of impurities that are not removed during the secondary treatment and disinfection of water (Tchobanoglous *et al.*, 2003). The nutrients in trace amounts could be treated during tertiary treatment by adsorption onto suitable materials. The quality of water needs to be ensured before recycling and reuse. Compared to other conventional tertiary treatment methods, adsorption is more commonly used these days due to its efficacy and low cost. The environmental friendly adsorbent material with high removal capacity adds proficiency to the adsorption process.

Adsorption using nano biosorbents is a relevant technology since the concept of sustainable green technology is achieved (Abdolali, *et al.*, 2014). The utilization of waste materials and the immense potential of nanomaterials have been used together in forming nano biosorbents. Nanoadsorbents are highly efficient when compared to conventional adsorbents due to their small size, high surface area, and pore size distribution. The problem encountered with nanoscale iron particles is corrosion and deposition on reactor wall. This drawback can be reduced if we can support them on insoluble solid supports with chemical and thermal stability. In this study, the biomaterial nutmeg (*Myristicafragrans*) shell powder is used to prepare chitosan supported nanoscale iron particles (Fe-CH-NSP). The antioxidant, tannic acid present in nutmeg, which is a polyphenol derivative acts as a reducing and stabilizing agent (Henam and Thiyam , 2016). The performance of synthesized Fe-CH-NSP on nitrate removal has been investigated. Chitosan is a biopolymer with highly reactive hydroxyl and amino groups (Appunni and Sankaran, 2013). A composite (CH-B-NCF) in the form of films was synthesized with chitosan and bentonite nanoclay. The synthesis of films requires only acetic acid as the dissolving agent. No other harsh chemicals were used for preparing nanocomposite films. The difficulty and economic loss in the handling of very small size nanoparticles were overcome in film forms. This nanocomposite film was used in the batch study for the removal of both nitrate nitrogen and ammonia nitrogen from the aqueous medium. The fixed-bed column adsorption performance for nitrate-nitrogen with chitosan bentonite nanocomposite films has also been investigated in this study.

1.7 OBJECTIVES OF THE CURRENT WORK

The main objective of the present work is to develop an appropriate nano biosorbent for the removal of nitrate nitrogen and ammonia nitrogen

from aqueous solution. Batch experiments are proposed to be performed using Fe loaded chitosan nutmeg shell powder (Fe-CH-NSP) and chitosan-bentonite nanocomposite films (CH-B-NCF) to analyze the effect of various parameters on adsorption. An appropriate continuous fixed bed column has to be developed in order to overcome the limitations of batch study. Suitable solvent for desorption of the adsorbent is also to be determined. A detailed review of the relevant literature has been carried out and presented in Chapter 2. The objective and methodology of the current work were finalized based on the gaps and led recognized from the literature review. The main objectives of the present study are

- To synthesize chitosan-bentonite nanoclay film composite
- To synthesize Fe-loaded chitosan nutmeg shell powder by the activation of nutmeg shell powder using chitosan, FeCl_2 , FeCl_3 , and NaOH solutions
- To assess the efficiency of adsorbents by performing batch adsorption experiments.
- To estimate the isotherm parameters of Fe-CH-NSP and chitosan bentonite nanocomposite films
- To model the batch equilibrium adsorption data using Langmuir, Freundlich, Tempkin and Dubinin- Radushkevich (D-R) isotherm models.
- To determine the adsorption kinetics of Fe-CH-NSP and CH-B-NCF.
- To model batch adsorption kinetic data using pseudo-first-order, second order, pseudo-second-order, Weber Morris intraparticle diffusion model and Dunwald-Wagner film diffusion model.
- To study the thermodynamics of Fe-CH-NSP and chitosan-bentonite nanocomposite films as adsorbents.

- To develop a suitable method to recover and reuse the nanocomposite films so that the adsorbent becomes cost-effective.
- To design and fabricate a fixed-bed adsorption column for NO₃-N removal using chitosan-bentonite nanocomposite films
- To investigate the effects of bed height and flow rate on the breakthrough performance of the NO₃-N column using chitosan-bentonite nanocomposite films
- To model the NO₃-N column adsorption data using the pragmatic models of Thomas, Yoon Nelson and Adam Bohart.

1.8 OUTLINE OF THE THESIS

This work mainly investigates the adsorption of nitrate nitrogen and ammonia nitrogen onto nano biosorbents. The synthesis and characterization of two novel adsorbents, Fe-CH-NSP and chitosan-bentonite nanocomposite films have been carried out. The removal efficiency of Fe-CH-NSP concerning nitrate nitrogen has been analyzed. A detailed study on removal and adsorption capacity of chitosan-bentonite nanocomposite films on nitrate-nitrogen and ammonia nitrogen has been carried out. Considering the risk of exiting the adsorbent with the flow, chitosan-bentonite nanocomposites films were selected in the continuous packed bed adsorption column for NO₃-N removal. This thesis is organized into five chapters.

In Chapter 1, the introduction to the sources of various nitrogen contaminants in water has been explained. The adverse effects of nitrogen contamination and its treatment methods are clearly stated. The advantages of adsorption when compared to the other methods and the use of nano biosorbents in adsorptive removal of nitrate-nitrogen and ammonia nitrogen

are highlighted in this chapter. The scope and objectives of the study have been set out.

In Chapter 2, a detailed literature survey on adsorption, various adsorbents for nitrate nitrogen and ammonia nitrogen removal, factors affecting adsorption, kinetics, thermodynamics, isotherm, and desorption study for adsorbent reuse are included. Literature review on a continuous packed bed adsorption column for the removal of nitrate-nitrogen in aqueous solution is also described in this chapter. Literature review on laboratory synthesis of nano biosorbents is also included.

Chapter 3 describes the different materials used and the methodology adopted in the present study for the removal of nitrate nitrogen and ammonia nitrogen from aqueous solution by adsorption. Methods for the synthesis of nano biosorbents, batch adsorption tests performed in this work, continuous packed bed column fabrication and operation for $\text{NO}_3\text{-N}$ removal, models used for batch and continuous experiments, equipment used for analysis, and characterization of the synthesized adsorbents are explained in this chapter. The results obtained from the batch and continuous adsorption tests for $\text{NO}_3\text{-N}$ and $\text{NH}_4^+\text{-N}$ removal are presented in Chapter 4. Characterization of adsorbents, optimization, modeling, validation of batch results by RSM and modeling of $\text{NO}_3\text{-N}$ column are presented in this chapter.

The summary and conclusions of the present study are included in Chapter 5 of the thesis. This is followed by the scope for future work and the limitations of the work. The references cited in the thesis are listed in the next section. An annexure containing calibration curves and experimental results of batch and continuous studies is added after the references.

.....❁.....

CHAPTER 2

LITERATURE REVIEW

2.1 INTRODUCTION

The quality improvement and preservation of water and water resources need the utmost importance in the present world. The water resources in the world are facing the severe threat of contamination problems due to human-made industrial and agricultural activities. Environmental engineers are developing methods to protect the environment by developing technical methods. The awareness about the constituents in water and maximum concentration level to be present is needed. Know-how of the environmental and health impacts with the toxic components is essential. Manufacturing is a crucial requirement for the augmentation of human society. The intensive expansion of agriculture and the application of chemicals led to the contamination of many natural water reservoirs and groundwater with nitrogen compounds. The high solubility of nitrogenous compounds caused its natural leaching. Finally, they end up in water resources like rivers, lakes, wells, and groundwater. Eutrophication of water bodies, depletion of much of dissolved oxygen affects the aquatic life. The nitrogen contaminants induce various health issues for both human beings and animals. In the current scenario, the development of innovative technologies for the remediation of water contamination by nitrogen contaminants is necessary.

2.2 SOURCES OF NITROGEN CONTAMINANTS

Nitrogen is the lightest member of the 15th group in the periodic table. Nitrogen is present in the amino acids, nucleic acids, and adenosine triphosphate in all organisms. About 3% nitrogen by mass is seen in the

human body. Nitrogen got its name due to the reason that it is present in nitric acid and nitrates. The industrially significant compounds like ammonia, nitric acid, nitrates, and cyanides contain nitrogen. Nitrate is a stable, highly soluble ion that belongs to the class of inorganic chemicals. It is termed as oxo-anions, which include arsenate, bromate, chlorate, perchlorate, selenate, tungstate, and phosphate (Gruber and Galloway 2008) .

Nitrogen is a necessary element for all living organisms, but high concentrations of the nitrogen-containing compounds, including ammonia, nitrate, and nitrite, are often found in drinking water and various types of wastewater and become detrimental to all creatures (Camargo and Alonso, 2006). Sources of these compounds can be attributed to the improper treatment of industrial wastewater and the extensive use of nitrogen fertilizers (Wen *et al.*, 2016). The propellants and explosive industry uses nitrates and contribute to nitrogen contamination. Xing *et al.*, 2012 reported that atmospheric deposition from nitrogen oxide emission causes an increase in nitrogen pollution. Yanhui *et al.*, 2011, reported that nitrogen pollution is the consequence of the use of nitrogen-containing fertilizers. Animal wastes, septic system irrigation, and storm runoffs from farmlands are the sources of nitrogen contaminants (Yinghua *et al.*, 2011). The use of explosives in mining results in nitrate emissions. Changes in land-use patterns from field to arable crops and increased recycling of domestic wastewater in plain rivers causes' nutrient containing water (Hualin *et al.*, 2013). The nitrogen is a significant constituent in a pharmacological drug class, including antibiotics, and hence wastewater from the pharmaceutical industry also contributes to nitrogenous wastes.

Ammonia is used in both fertilizer and animal feed production. It is used in the production of fibres, plastics, explosives, paper, and rubber. In metal processing, ammonia is used as a coolant. It is used as a starting product for many nitrogen-containing compounds. Ammonia and ammonium salts are widely used in cleansing agents. It is also used as food additives and as a diuretic (Hazardous Substances Data Bank, 1990). Ammonia is an essential metabolite in mammals. Ammonia has a vital function in the biosynthesis of purines, pyrimidines, and non-essential amino acids. The role of acid-base regulation is made by ammonium. The ammonia is formed in the body by the deamination of amino acids in the liver and as a metabolite in nerve excitation and muscular activities. The enzymatic breakdown of food components in the gastrointestinal tract with the help of bacterial flora also produces ammonia. Municipal sewage treatment plants, use of fertilizers in agriculture, livestock & poultry farms, petrochemical industries, and landfills generate high-strength ammonia nitrogen ($\text{NH}_4^+\text{-N}$) wastewaters (Aref *et al.*, 2018). The effluent from aquaculture activities also a source of ammonia nitrogen (Kairan *et al.*, 2012). Ammonia-nitrogen end up to the water stream from industries like steel, refining, fertilizer, inorganic chemicals, ferroalloy, glass, meat processing, and feed production.

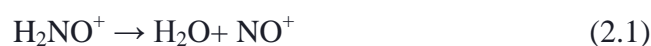
2.3 IMPACTS OF NITROGEN

Nitrogen contamination causes an increasingly ubiquitous issue worldwide, affecting the quality of drinking water, the ecology, and the value of the aquatic ecosystems. The nitrate leaching in the surface water is commonly considered as the cause of water quality deterioration. (Dongjin *et al.*, 2009). Because of the interaction between surface and groundwater, high loads of nitrogen compounds in surface water caused groundwater pollution (Bekhradinassab and Sabbaghi, 2014). Eutrophication of water bodies is

attributed to the increased amounts of nutrients like ammonia, nitrates, and phosphates in water resources. Eutrophication is otherwise also known as hypertrophication. The excessive growth of algae happens when a water body is overly enriched with nutrients and minerals. The oxygen depletion of the water body affects all lives which benefit from water. The increase of phytoplankton in water bodies due to the high amount of nutrients is termed as an algal bloom. The severe environmental problem is a consequence of the excessive release of both organic and inorganic nitrogen species (Engracia *et al.*, 2011).

The epidemiological researchers have found a prominent risk of cancer, undesirable birth outcomes, and other health impact associated with the presence of nitrate in drinking water. The risk of non-Hodgkin's lymphoma due to nitrates was reported by Ward *et al.*, 1996. Other health risks due to nitrate pollution are methemoglobinemia (Dong-Wan *et al.*, 2011) and bladder, ovarian, or gastric cancers to humans (Weyer *et al.*, 2001). The formation of carcinogenic nitrosamines is taken place when nitrates or nitrites enter into the human body. Strongly acidic medium and high temperature are the favorable conditions for the formation of nitrosamines from nitrates and secondary amines. Under acidic conditions in the human stomach, the nitrites form nitrous acid (HNO₂). It is protonated and splits into NO⁺, the nitrosonium cation.

The reaction is as follows:



The nitrosonium ion reacts with an amine form nitrosamines. Frying of food items at high temperatures causes the formation of nitrosamines. Three

hundred nitrosamine compounds were tested, and 90 % of them were deemed to be carcinogenic in experimental animals.

The ingestion of high nitrate through drinking water or plants may result in acute poisoning in cattle within 0.5 h to 4 h. The cattle found regular one day and found dead the next day. The symptom of salivation followed by recurrent urination is first seen. Then the animals exhibit respiratory problems and chocolate brown colored blood and mucous membrane are seen. The immediate abortion could be seen in pregnant cattle with an intake of higher levels of nitrates (Amit and Mika, 2011).

These health effects are often found at drinking water nitrate concentrations significantly lower than the level associated with methemoglobinemia. The methemoglobinemia or blue-baby syndrome is a life-threatening condition due to oxygen deprivation. The U.S. drinking water standard for nitrate of 10 mg/ L nitrate (as nitrogen) was first set in 1962 to protect against methemoglobinemia. The Canadian legal limit for nitrate in drinking water is equivalent to the U.S. standard, and the European standard is comparable, allowing up to 50 mg/L of nitrate as nitrate, which is equivalent to 11.3 mg/L nitrate as nitrogen. The World Health Organization (WHO) has set the maximum contaminant level (MCL) in drinking water for nitrate as 10 mg N /L (Antonio *et al.*, 2010). The US environmental protection agency (USEPA) has set maximum contaminant levels of 10 mg/L and 1mg/L for nitrate-nitrogen($\text{NO}_3\text{-N}$) and nitrite nitrogen ($\text{NO}_2\text{-N}$), respectively (USEPA, 2016).

2.4 METHODS OF NITROGEN REMOVAL

Nitrogen compounds at high concentrations cause both water pollution and air pollution, and they affect all forms of life. These pollutants should be

removed from effluent water before discharging into the water bodies to protect the people and environment. There are various methods for the removal of these pollutants so that they can be maintained within the permissible limits prescribed by legislation. Several methods for removal of nitrate nitrogen and ammonia nitrogen have been reported. The advantages and disadvantages of various methods for nitrates and ammonium removal have been discussed in detail in the following section.

2.4.1 Denitrification

The microbial reduction of nitrates to molecular nitrogen through a series of intermediate gaseous nitrogen oxide products is called biological denitrification (Malgorzata et al., 2006). The gaseous product is primarily nitrogen gas, but it may also be the nitrous oxide or nitric oxide. *Pseudomonas*, *Micrococcus*, *Archromobacter*, *Thiobacillus*, and *Bacillus* are the different kinds of bacteria usually used for biological denitrification. In water treatment processes, organic compounds methanol, methane, glucose are used as carbon sources. Chemical denitrification includes the use of metals for the reduction of nitrates to dinitrogen. The challenge in chemical denitrification is the difficulty in stopping the reduction at molecular nitrogen. The metals used are zinc, iron, chromium, tin, aluminium, cadmium, and lead.

The treatment of groundwater contaminated with nitrate was done in two stages biological and coagulation systems (Pudukadu *et al.*, 2007). The biological treatment was performed with the nitrate-degrading bacteria *Pseudomonas* sp. R-7. The effect of carbon sources on nitrate removal was studied, and starch at 1% was found to be most effective. Chemical coagulants like alum, lime, and poly aluminium chloride were tested for the further removal of nitrate. Lime at 150 mg/L exhibited the highest nitrate

removal efficiency among the coagulants, with complete disappearance for the mineral salt medium solutions.

The use of biodegradable polymers as carbon source and biofilm carrier for denitrifying microorganisms has been reviewed by Jianlong and Libing (2016). Woodchips, sawdust, straw, cotton, maize cobs, seaweed, polyhydroxy alkanolate, polylactic acid, are the materials usually used for denitrification. The excellent performance, low cost and abundant availability make them selective. It is also reported that the denitrifiers used in solid-phase denitrification are commonly from the family Comamonadaceae, Diaphorobacter, and Simplicispira. The future perspectives of the simultaneous removal of nitrate and toxic organic contaminants by solid-phase denitrification have also been explained.

The feasibility of zero-valent magnesium for removal of nitrate from aqueous solution, was carried out by Kumar and Chakrabarty (2006). They found that 84 % denitrification efficiency was achieved at Mg to nitrate molar ratio of 5:8. Optimum pH was 2, and the reactions were first order. The activation energy of the chemical denitrification process over the temperature range of 10-50⁰C was observed as 17.7 kJ/mol.

Huang and Zhang (2004) investigated the effect of pH on nitrate reduction by iron powder. The low pH of 2 to 4.5 was found favorable. The main two impacts of pH on the kinetics of nitrate reduction are found as H⁺ ions participation in the redox reaction of nitrate reduction following first-order kinetics, and H⁺ ions affect the nitrate adsorption onto reactive sites.

Shahin *et al.*, 2009 used palm shell activated carbon for nitrate remediation in a novel upflow bio-electrochemical reactor (UBER). This study

investigated the biological denitrification method, which is a treatment method able to reduce inorganic nitrate compounds to harmless nitrogen gas. The upflow bio-electrochemical reactor was used to lodge the hydrogenotrophic denitrifying bacteria. The palm shell granular activated carbon was used as the bio carrier and cathode material. Results showed that nitrate could be entirely reduced with the application of a wide operational range of electric current (10–16 mA) as well as HRT (13.5–30 h). However, an increase of pH at cathode zone up to 10.5 inhibited nitrite reductions, and it was not reduced to the satisfactory level.

Yuansheng *et al.*, 2010, investigated the nitrate removal by microbial enhancement in a riparian wetland. The effect of the addition of *Bacillus subtilis* FY99-01 for nitrate removal in riparian wetland built in a river bend was studied. The removal efficiency was found significant in the summer than in the winter owing to integrated hydraulic, microbial, and environmental effects. The maximal nitrate removal and the mean nitrate loss rate in the riparian wetland were 36.1% and 50.5 g/m²/yr, respectively.

2.4.2 Ion Exchange

Ion exchangers have high treatment capacity, high removal efficiency, and fast kinetics. Ion exchangers are classified as cationic and anionic exchangers which contain synthetic resins for the exchange of specific ions. Synthetic resins are commonly used for the removal of inorganic contaminants from wastewater. The resins are eluted to recover the ions and reused. The ion exchange method possesses high nitrates ammonia nitrogen removal rate, but post-treatment is required due to the corrosiveness of product water. Also, the ion exchange process involves waste brine disposal.

Adsorption kinetics of nitrate ions on a macroporous anion exchange resin, IND NSSR resin, was investigated by Hekmatzadeh *et al.*, 2013. It was observed in kinetic modeling that the pseudo-first and second-order models describe the experimental kinetic data adequately. The performance of the ion-exchange column was evaluated using the particle diffusion model in conjunction with a mass balance equation. It was found that mathematical equations reproduced the experimental breakthrough data very well.

Zhongmin and Ting (2015) studied the removal of ammonium ions with a novel hybrid polymeric sorbent loaded with copper oxide microparticles within the cation exchanger. The adsorption data agreed well with the pseudo-second-order model and the Langmuir model. Removal of low-concentration ammonium (1.0–10 mg/ L) was investigated in fixed-bed column runs, and dynamic breakthrough data were found to follow the Thomas model. It is also observed that the exhausted cation exchanger can be repeatedly utilized after regeneration by NaOH solution.

Novel anion exchangers were prepared from different plant parts, pine sawdust and bark, spruce, bark, birch for the removal of nitrate nitrogen by Anni Kerranen *et al.*, 2013. Epichlorohydrin, ethylenediamine, and triethylamine in the presence of N, N-dimethyl formamide was used for chemical modification. Modified pine sawdust exhibited the best nitrate removal efficiency. Nitrate nitrogen of 80% was removed at doses of 43 g/L with a nitrate concentration of 30 mg/L. The column test with modified pine sawdust was performed, where it maintained its ion exchangeability for five ion-exchange cycles, with successful desorption cycles.

2.4.3 Reverse Osmosis

The application of reverse osmosis for water denitrification and desalination was investigated by Schoeman and Steyn (2003). The concentration of nitrate-nitrogen in the RO feed was 42.5 mg/L. The reduction of NO₃-N to 0.9 mg/L was obtained in the RO product water. Also, the total dissolved solids were found to reduce from 1292 mg/L to 24 mg/L in the reverse osmosis permeate.

Antonio *et al.*, 2005 studied the behavior of cellulose acetate membranes in the treatment of ammonia nitrogen from aqueous solution by reverse osmosis. Ammonium concentrations between 0.055 kg/m³ and 9.545 kg/m³ were treated. A simulation model described for a semi-batch, and the unsteady-state system was applied, and the solution diffusion approach was used by the model to depict the mass transfer through the membrane.

2.4.4 Electrodialysis

Electrodialysis is a membrane process. The transportation of ions from one solution to another solution through a semipermeable membrane in the presence of an electric field is taking place. Two electrodes are present in the electrodialysis unit in which an electric field is applied. The membranes are ion exchange resins that are selective in transporting positive or negative ions. High removal of nitrates and ammonium ions are accomplished in this process, but it requires high capital and operating cost. Another drawback of electrodialysis is that membranes are fouled frequently.

Xiaolin *et al.*, 2015 developed an integrated process of electrodialysis with struvite reactor for the simultaneous removal and phosphate from wastewater. They found that during the single electrodialysis process efficient

to remove the ammonium ions. The X-ray diffractogram confirmed the formation of struvite from the wastes.

The removal of inorganic trace contaminants from real brackish groundwater using electrodialysis was investigated by Cristina *et al.*, 2017. It is found that the removal of bromide, chloride, fluoride, and nitrate was pH-independent. The results of the study showed that although electrodialysis is useful in the removal of contaminants from real waters, membrane scaling is a problem in considering its long-term practical applicability.

2.4.5 Adsorption

The predictable consideration of the adsorption process in recent periods is due to its higher efficiency, economical consumption, and simplicity. Adsorption technology has been found successful in removing various types of contaminants, including nitrate nitrogen and ammonia nitrogen (Amit and Mika 2011). Surface energy is responsible for adsorption. In the interior surface of an adsorbent, all the bonding requirements of the atoms are filled by other atoms. But, on the surface, the atoms are not fully surrounded by other atoms, and therefore, adsorbates can be bonded on the surface of adsorbents. Physical adsorption is a reversible process. The adsorbed contaminant can be desorbed, and the application of proper solvents can reuse the adsorbent. Adsorption can be carried out for higher capacity operations in a continuous column. In water treatment operations, adsorption is widely used due to its simplicity and ease of operation, less initial investment, free from or less generation of toxic substances, and less production of sludge.

Low-cost adsorbents for the removal of organic pollutants from wastewater were studied by Imran *et al.*, 2012. The adsorption of organic pollutants on a number of low-cost adsorbents have been carried out. Fruit wastes, coconut shells, tannin-rich materials, sawdust, rice husk, and other wood type materials are some examples. Plant bark, fruit wastes and agricultural wastes are tannin rich. Petroleum wastes, fertilizer wastes, fly ash, scrap tyres, sugar industry wastes and blast furnace slag are examples for industrial waste used as adsorbents. The use of chitosan, and seafood processing wastes, seaweed, and algae, peat moss, clays, red mud, zeolites, sediment and soil, ore minerals as adsorbents is also found out. The results of adsorption proved that these adsorbents after proper activation could remove 80-99.9% organic pollutants. The discussion on the conversion of waste products into effective adsorbents and their application for water treatment have described in detail. The future perspectives of low-cost adsorbents in water treatment are also represented.

The micro-particles of dried *Withania frutescens* plant was developed as an adsorbent for nitrates, phosphate and metallic elements by Mohamed *et al.*, 2012. The adsorption was done in two real wastewaters, municipal and industrial wastewaters and found that adsorption increased with increasing contact time.

Rangabhashiyam *et al.*, 2014 studied the use of biosorbents in the adsorption technology. The biosorbents are naturally occurring, abundant, renewable, biodegradable and has economic features. It is reported that adsorption isotherm equations used to describe the experimental data and the thermodynamic assumptions of the models often provide a few insights into the sorption mechanism, the surface properties and affinity of the biosorbents

towards the pollutants. Table 2.1 depicts advantages and disadvantages of different methods for nitrate removal.

Table 2.1 Advantages and disadvantages of common technologies for nitrate removal from wastewater sources (Reproduced from Amit and Mika, 2011).

Process	Advantages	Disadvantages
Adsorption	Medium operational cost Efficiency depends on adsorbents Post treatment is not often required	Saturated spent adsorbent disposal pH and temperature influence are important.
Reverse Osmosis	pH and temperature influence are not significant Efficiency of >95% can be achieved	Requires high TDS disposal Post-treatment is required due to corrosivity of product water High operational cost
Chemical methods	No waste disposal is required	Post-treatment is required for by-products pH and temperature influence are important High operational cost Max reported efficiency 60-70 %

Table 2.1 Continued...

Ion Exchange	pH and temperature influence are not important Medium operational cost Approximately 90% can be achieved	Requires waste brine disposal. Post-treatment is required due to corrosivity of product water
Biological methods	Medium operational cost >99% efficiency can be achieved	Requires biomass waste disposal. Temperature influence are important. Post-treatment is required due to microorganisms
Electrodialysis	High removal of nitrate and ammonia nitrogen	High capital cost Frequent fouling of membranes in considering long term practical applicability

2.5 LITERATURE REVIEW ON ADSORPTION AND ADSORBENTS

Adsorption is a separation process in which specific components of a gaseous or liquid phase are selectively transferred to the surface of a solid adsorbent. Surface energy is responsible for adsorption. In the interior surface of an adsorbent, all the bonding requirements of the atoms are filled by other atoms. But, on the surface, the atoms are not fully surrounded by other atoms, and therefore adsorbates can be bonded on the surface of adsorbents. There are two types of adsorption, physical and chemical. Physical adsorption takes

place due to the action of van der Waals forces. There is no reaction between adsorbent and adsorbate in physical adsorption, and forces present in this type are weak. The change in the chemical form of the adsorbate takes place due to a reaction between the adsorbate and adsorbent in chemical adsorption. (Haiwei *et al.*, 2010 c). The forces of attraction between adsorbate and adsorbent are strong, and they cannot be reversed.

When the porous surface of a specific solid is exposed to a liquid, the specific component from the liquid will form bonds with the solid and become attached to the solid surface. Adsorption is a cheap and effective method for wastewater treatment. Adsorption is extremely useful for low concentrations of contaminants. Adsorption also possesses advantages like availability, profitability, ease of operation, and efficiency. Adsorption is also a reversible process. Adsorption can be carried out for higher capacity operations in a continuous column. In water treatment operations, adsorption is widely used due to its simplicity and ease of operation, less initial investment, free from or less generation of toxic substances, and less production of sludge.

2.5.1. Chitosan-Based Adsorbents

Chitosan is a naturally occurring polysaccharide material next to cellulose. Several studies have been conducted using chitosan and chitosan composites for wastewater treatment. The product of the deacetylation of chitin results in the formation of chitosan. Chitosan is primarily composed of $\beta(1 \rightarrow 4)$ linked 2-amino 2-deoxy D-gluco pyranose units. Chitosan possesses excellent adsorption capacity. It also possesses high hydrophilicity, a large number of surface hydroxyl and amino groups. Chitosan is biocompatible, biodegradable, and less toxic. Chitosan has received more attention due to its high adsorption efficiency, bi-functionality, ease of handling, and low cost. It

is found suitable for the removal of dyes, heavy metal ions, organic and inorganic pollutants due to the presence of high content of amino (-NH₂) and hydroxyl (-OH) groups present. Fig 2.1 represents the structure of chitosan.

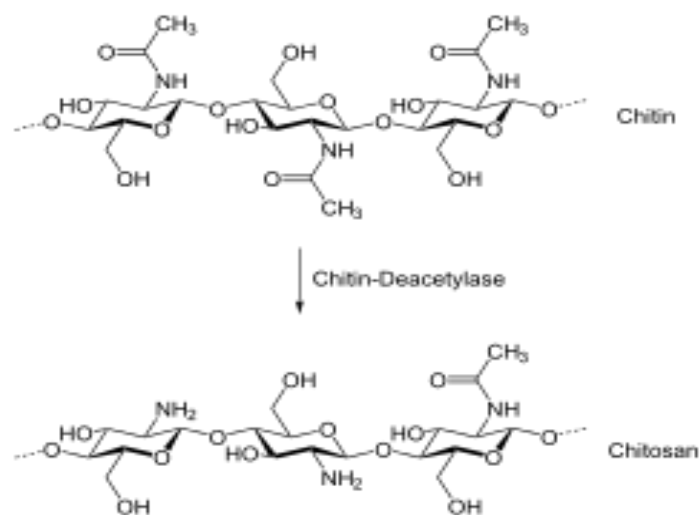


Fig. 2.1 Structure of chitosan

Amit and Mika (2009) reported the applications of chitin and chitosan derivatives for the removal of metal cations and anions, radionuclides, dyes, phenolic compounds, different types of anions and different pollutants from wastewater. Batch studies were analyzed for studying the various adsorption mechanisms. The study showed that chitosan-based adsorbent possesses high potential for detoxifying water and wastewater.

The raw chitosan has shown reduced adsorption capacity towards the removal of phosphate and nitrate due to the absence of positive sites. So several chemical modification methods, such as functionalization, grafting, cross-linking, composite blend forms, metal loading, etc., have been performed to get better adsorption capacity.

A three-dimensional cross-linked polymeric network based on chitosan and attapulgite was synthesized by Yian *et al.*, 2009 *b*. The process was a copolymerization reaction in aqueous solution. It was found that at natural pH, the composite adsorbent with 20 weight % attapulgite can adsorb 21.0 mg ammonia nitrogen per gram. It is also found that adsorbed ammonia nitrogen can be entirely desorbed by 0.1 mol/L NaOH within 10 min.

The adsorption efficiency of quaternary amine-modified chitosan beads for the removal of nitrate and phosphate anions was done by Appunni and Sankaran, 2013. The composite adsorbent was prepared by reacting cross-linked chitosan beads and glycidyl tri-methyl ammonium chloride. The cross-linked chitosan beads were treated with 20% glycidyl trimethyl ammonium chloride at 60°C for 24 h and then washed with water to remove excess glycidyl trimethyl ammonium chloride, then dried and used.

Cross-linked chitosan beads conditioned with sodium bisulfate was used for nitrate removal by Sudipta *et al.*, 2009 *b*. The cross-linked chitosan was contacted with NaOH and epichlorohydrin, and the cross-linking reaction was done at 60°C for 6 hours. It was then conditioned with a 500mL sodium bisulfate (NaHSO₄) solution at 50°C for 3 hours by agitation.

Qili *et al.*, 2015 prepared a spherical epigranular chitosan-Fe³⁺ complex with a particle size range of 1.04–1.16 mm and found useful for nitrate adsorption from aqueous solution. Three hundred mL of 0.2 M FeCl₃ aqueous solution and ammonia solution (12.5% v/v) are the reagents used.

Synthesis of novel nanocomposite Fe₃O₄/ZrO₂/chitosan was done by Hualin Jiang *et al.*, 2013 for nitrate removal. The reagents used were ZrOCl₂·8H₂O, nano Fe₃O₄ NH₃ solution, cetyltrimethylammonium bromide,

sodium dodecyl benzene sulfonate and methanol. The adsorption of nitrate from aqueous solutions by chitosan hydrogel beads was carried out by Sudipta and Seung (2009 *a*). The hydrogel beads with chitosan were prepared by the drop wise addition of chitosan solution into a chemical coagulating mixture. The average diameter of the spherically shaped beads was 2.5 mm. It was then kept in water for 30 minutes with pH adjustment.

Chitosan-g-poly (acrylic acid)/rectorite hydrogel composite was synthesized by Yian and Aiqin (2009 *a*), for ammonium adsorption. The composite was prepared by in situ copolymerization with the reagents acetic acid, rectorite, acrylic acid, ammonium persulfate, and methylene-bisacrylamide.

2.5.2 Clay-Based Adsorbents

Clays can be intercalated into the polymeric network. Polymer/clay composite possesses remarkable properties for being used as an adsorbent for wastewater treatment. The features of the composite include swelling properties, gel strength, low synthesis cost (Moumita and Anil, 2015)

Bentonite clay is naturally occurring aluminium phyllosilicate clay consisting mostly of montmorillonite. There are mainly four different types of bentonite-based on the respective element present in them. They are potassium, sodium, calcium, and aluminium. The physical and chemical structure of montmorillonite clay mineral is shown in Fig. 2.2

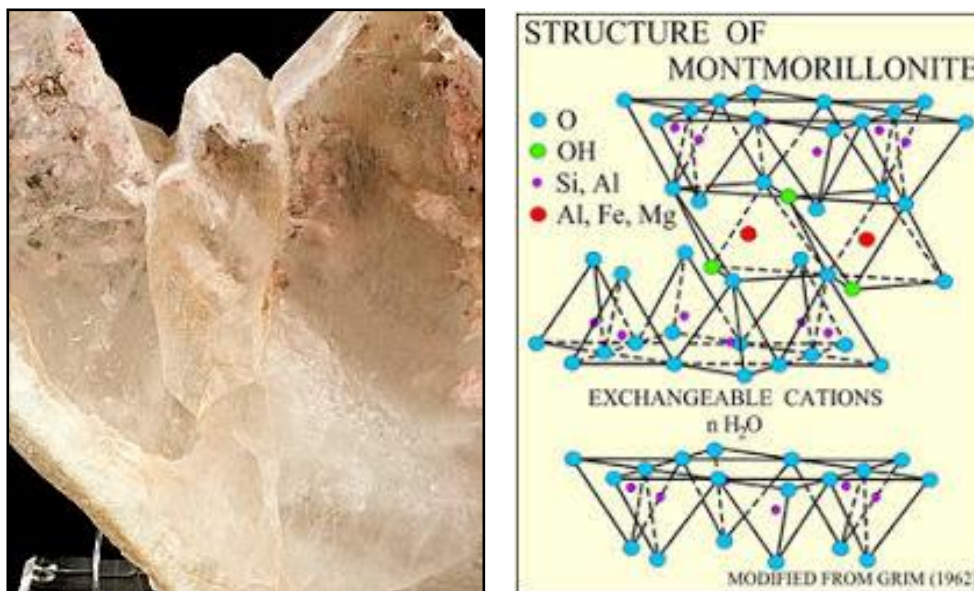


Fig 2.2 Physical and Chemical Structure of Montmorillonite clay

Moumita and 2015 conducted a study on the use of modified natural and synthetic clays for designing polymer nanocomposites. The commonly used natural clays for composite preparation are montmorillonite, hectorite, sepiolite, rectorite, bentonite, vermiculite, kaolinite, and chlorite. Various layered double hydroxides, synthetic montmorillonite, hectorite are the synthetic clays used. The preparation, structure, and properties of polymer nanocomposites using the modified clays are discussed. It is found that even at low loading, these composites are capable with remarkably superior mechanical, thermal, dynamic mechanical, adhesion and barrier properties.

Hanxin *et al.*, 2012 investigated ammonia-nitrogen and phosphates sorption from simulated reclaimed wastewater by modified clinoptilolite. The modification was done with 2% NaCl solution, 0.4 % FeCl₃ solution. Then it was calcinated at 200⁰C in a muffle furnce. Then cooled in a closed container.

The modified clinoptilolite has a high sorption efficiency and removal performance. It was observed that 98.46% of ammonia-nitrogen and 99.80% phosphates removal could be achieved with modified clinoptilolite. The surface of the modified clinoptilolite became loose, and some pores appeared, which enlarged specific surface area. It was found that the contents of Na and Fe increased, while the contents of Ca and Mg decreased after modification. The maximum adsorption efficiency obtained were 2.08 mg/g for ammonia nitrogen and 1.56 mg/g for phosphorous with modified clinoptilolite.

The synthetic organosilica and organoclay were used for the removal of nitrate by Moaaz. *et al.*, 2013. The reagent octadecyl trimethyl ammonium (ODTMA) chloride was used to prepare organosilica at room temperature. At the same time, cetyltrimethylammonium (CTMA) bromide was used to synthesize organoclay and layered organosilica material under hydrothermal conditions. A commercially available organoclay Cloisite 10A was also tested for nitrate removal.

2.5.3 Biosorbents

Mohamed Ali *et al.*, 2010, investigated the effects of temperature and pH on ammonium biosorption onto *Posidonia oceanica* fibers. They found that the adsorption capacity increased with temperature increase under a wide pH range. The film diffusion process governed the ammonium biosorption at various temperatures. The mono-layer coverage was confirmed as the equilibrium data was found well fitted to Langmuir isotherm. The *P. oceanica* fibers could be used as an effective biosorbent for the removal of ammonium, and waste can be recycled as a fertilizer and compost.

Hui-mei *et al.*, 2015 prepared adsorbent by loading Al/Fe oxides onto tea waste to remove fluoride from drinking water. It is observed that the biosorbent combinations Tea–Al or Tea–Al–Fe could effectively lower the fluoride concentration to below 1.5 mg/L in the drinking water. The residual strength of Al and Fe in the drinking water after Tea–Al–Fe treatment was below the standards set by WHO (pH range 5-10). The maximum fluoride adsorption capacities for the original tea, Tea–Fe, Tea–Al and Tea–Al–Fe biosorbents were obtained as 3.83, 10.47, 13.79 and 18.52 mg/g, respectively

Anni *et al.*, 2015 synthesized a resin by reacting pine sawdust with epichlorohydrin, ethylenediamine, and triethylamine in the presence of N, N-dimethyl formamide. The sorption data were fitted to the Langmuir, Freundlich, and Redliche Peterson isotherm models. Nitrate removal was successful at 5 to 70°C. Higher temperatures caused nitrate removal to decrease reasonably, and a sorption capacity of 22.2 to 32.8 mg/g for nitrate nitrogen was achieved. The removal of nitrate in the presence of sulfate and phosphate was studied at concentrations of 30 mg N/L, 10 to 500 mg S/L, and 1 to 50 mg P/L. A significant decrease in nitrate reduction was observed at sulfate and phosphate concentrations of 100 mg S/L and 50 mg P/L, respectively.

Hakan *et al.*, 2010 prepared activated carbons from sugar beet bagasse by chemical activation and the prepared activated carbons were used to remove nitrate from aqueous solutions. In chemical activation, ZnCl₂ was used as chemical agent. The maximum specific surface area of the activated carbon was about 1826 m² /g at 700 C and at an impregnation ratio of 3:1. The resulting activated carbon was used for removal of nitrate from aqueous solution. The effects of pH, temperature and contact time were investigated.

Isotherm studies were carried out and the data were analyzed by Langmuir, Freundlich and Tempkin equations.

Adsorption efficiency of nitrate from aqueous solutions onto modified wheat residue was studied by Yu Wang *et al.*, 2007. The wheat residue was modified by epichlorohydrin in the presence of pyridine and the adsorption kinetics was investigated in batch experiment. The results showed that modified wheat residue had great anion adsorbing capacity. The zeta potentials of raw wheat residue and modified wheat residue were -35 mV and $+40$ mV while the maximum adsorption capacity of raw wheat residue and modified wheat residue were obtained as 0.02 mmol g^{-1} and 2.08 mmol g^{-1} , respectively. And also, the adsorption can reached equilibrium in 20 min, the adsorption data fit to Freundlich isotherm model. With the increasing initial concentration, the rate constant of pseudo-second-order equation decreased and rate constant of intra-particle diffusion model increased. The adsorption kinetic analysis with the activated wheat residue could be of a great practical value for the technological applications of nitrate removal from aqueous solutions.

The adsorption of ammonium by boston ivy leaf powder (Haiwei *et al* 2010 *a*) and strawberry leaf powder was performed by Haiwei *et al* 2010 *b*. The maximum adsorption capacity of strawberry leaf powder were 3.93, 6.05 and 7.66 mg/g at 15, 25 and 35 °C, respectively while that of boston ivy leaf powder was 3.37, 5.28 and 6.59 mg N/g at 15, 25 and 35°C, respectively.

The sorption and desorption capacity of non-activated and chemically activated biochars from microwave pyrolysis using corn stover, ponderosa pine wood chips, and switch grass was done by Rajesh *et al.*, 2013. It was

found that chemical activation with concentrated HCl improved the surface characteristics of biochars and enhanced the nitrate sorption capacity.

The use of biosolids is a beneficial mean of recycling the by-products of wastewater treatment in agriculture. Hernandez Apaolaza and Guerrero, (2008) compared between pine bark and coconut husk sorption capacity of metals and nitrate when mixed with sewage sludge. It was found that mixing the sludge with pine bark is more effective than mixing with coconut husk. Pine bark columns leached lower amount of nitrate than the coconut fibres.

Yan Li *et al.*, 2012 developed *Paracoccus* species immobilized on bamboo carbon for denitrification. The results show that denitrification was significantly improved using immobilized cells compared to that of free cells. It was observed that the denitrification time decreased from 24 h (free cells) to 15 h (immobilized cells). The immobilized cells exhibited more nitrate removal at various conditions compared to free cells since bamboo carbon act as a carrier protects cells against changes in environmental conditions. Denitrification using the YF1 immobilized in bamboo carbon was also maintained 99.8% after the tenth cycle reuse.

Adsorbent from the carpobrotus edulis plant was used for the removal of nitrate, H_2PO_4^- , Pb^{2+} and Cd^{2+} ions from single, binary, and multi-component systems. (Mohamed Chibana *et al.*, 2011). The effect of parameters like pH, initial concentration, and contact time were studied through batch adsorption experiments. The dried carpobrotus edulis showed the highest affinity for Pb^{2+} , followed by NO_3^- , Cd^{2+} and H_2PO_4^- in single-component systems. The adsorption capacities of Pb^{2+} , Cd^{2+} , NO_3^- and

$\text{H}_2\text{PO}_4^{4-}$ were obtained as 175 mg/g, 28 mg/g, 125 mg/g,, and 26 mg/g, respectively.

The sorption and desorption of phosphate, ammonia nitrogen and nitrate nitrogen in cacao shell and corn cob biochars was done by Hale et al., 2013. It was found that ammonia nitrogen could bind via an electrostatic exchange with other cationic species on the surface of the biochar.

2.5.4 Nanoadsorbents and Nanocomposite Adsorbents

Wen Song *et al.*, 2016 synthesised a novel adsorbent of magnetic amine-crosslinked biopolymer-based corn stalk (MAB-CS) and used for nitrate removal from aqueous solution. It is found that the saturated magnetization of MAB-CS reached 6.25 emu/g. A pH range of 6.0-9.0 was found suitable. It was also found that the presence of PO_4^{3-} and SO_4^{2-} markedly decrease the nitrate removal efficiency. The calculated nitrate adsorption capacity of MAB-CS was found to be 102.04 mg/g by the Langmuir model at 45 °C. The thermodynamic study showed that nitrate adsorption is a spontaneous endothermic process and found that the removal of nitrate was mainly via electrostatic attraction and ion exchange.

Ting Wang *et al.*, 2014 used iron nanoparticles (Fe NPs) synthesized by green tea (GT-Fe) and eucalyptus leaves (EL-Fe) extracts, which regarded as cleaner production and that can be used for the efficient removal of nitrate. Batch experiment showed that 59.7% and 41.4% of nitrate was removed by GT-Fe and EL-Fe NPs. The nitrate removal efficiency with nanozero valent iron and Fe_3O_4 nanoparticles gave 87.6% and 11.7% of nitrate ions respectively.

Ahmed *et al.*, 2016 proposed methods to nitrate reduction kinetics by nanoscale zero-valent iron in water via copper salt addition. The nano zerovalent iron was synthesized under optimum conditions and characterized using TEM, surface area analyzer, XRD, and particle size analyzer. The effect of pH, presence or absence of oxygen and initial nitrate concentration (50, 100, 200, 300, and 500 mg/L) was analyzed. A comparison of nitrate removal by nano-Fe⁰ with and without copper salt addition was performed. It is reported that the presence of copper ions during nitrate reduction imposes two electrochemical reactions. First one was the stimulation of iron corrosion and another was hydrogen-electrocatalytic reduction of nitrate. Kinetics studies revealed that nitrate removal time was reduced from one hour to 20 min.

Bekhradinassab and Sabbaghi, 2014 studied removal of nitrate from drinking water using nano SiO₂-FeOOH-Fe core-shell. SiO₂-FeOOH-Fe core-shell was synthesized in order to overcome the common problems of the application of nanoscale zerovalent iron in nitrate removal from drinking water. The effects of parameters like pH, contact time, initial concentration, amount of NZVI loading, amount of nano SiO₂-FeOOH-Fe core-shell, and sonication time were studied. It was observed that by doubling NZVI loading, removal of nitrate increases from 69% to 86%.

The synthesis and characterization of a new adsorbent containing nanoscale zerovalent iron particles (NZVI) supported on sinoguelas waste (S-NaOH-NZVI) from agriculture biomass were developed by Soleymanzadeh *et al.*, 2015. The new nano-bio adsorbent was used for the adsorption of Cd(II) ions. The combination of ZVI particles on the surface of sinoguelas waste will help to prevent of agglomeration of ultra-fine powders. The agglomeration harms both active surface area and performance of the catalyst.

Batool Shahrooie *et al.*, 2015 developed a starch-based hydrogel nanocomposite prepared from starch and polyvinyl alcohol (PVA) blend as a polymeric matrix and fumarate-alumoxane (Fum-A) and maleic anhydride (MA) as cross-linking agents. The synthesized adsorbent was analyzed for its use in ammonia nitrogen removal from aqueous solutions. The boehmite nanoparticles were synthesized by the sol-gel method with Al (NO₃)₃ and NaOH solution. Fum A nanoparticles were synthesized from boehmite nanoparticles with fumaric acid as the precursor. The hydrogel nanocomposite was prepared by adding Fum-A, PVA, and MA to the gelatinized starch solution.

A novel palygorskite nanocomposite adsorbent was prepared by Xinggang *et al.*, 2014, with the aim of minimizing the negative impact of nitrogen pollution. The removal and recovery of ammonium ions from ammonium wastewater was done. The high removal efficiency for ammonium in a wide pH range of 4.0–8.0 was exhibited. The composite material had preferable water-absorbing and water-retention capacity so that it can be used for improving soil moisture content and reduce soil moisture evaporation rate. Nanoscale zerovalent iron has considerable potential in remediation of Cr(VI) and Pb(II) ions from aqueous solution (Ponder *et al.*, 2000). Fe₃O₄, Mn₃O₄ and MnFe₂O₄ nanoadsorbents were synthesised by microwave assisted hydrothermal synthesis technique and used for adsorption of arsenic III and V from wastewater (Parsons *et al.*, 2009). A pH range of 2-6 was selected for conducting adsorption experiments. Results of the above work indicated that the adsorption was largely pH independent for MnFe₂O₄. For Mn₃O₄, the maximum adsorption capacity was between pH 4-5. For Fe₃O₄ the dependence of adsorption on pH was highest and removal increased from pH 2-6.

Zhou *et al.*, 2009 used chitosan coated magnetic nanoparticles modified with α -ketoglutaric acid for removal of Cu^{2+} from water. The effect of pH, contact time, initial Cu^{2+} concentration and adsorbent dose were analysed, and the results proved that nanoadsorbents possessed considerable potential for removal of Cu^{2+} from aqueous solution.

The synthesis and the effect of rapid mixing devices on the properties of magnetite nanoparticles were reported by Li *et al.* (2012).

The synthesis of maghemite nanoparticles by coprecipitation method from an iron solution was done by Wenjun *et al.*, 2013. The efficiency of developed nanoparticles for Cr(VI) adsorption from aqueous solutions was done. In the study, it was reported that the adsorption followed pseudo-second-order kinetics. The equilibrium adsorption data were fitted to Langmuir and Freundlich models. pH affected the adsorption and optimum pH was observed to be 4.0 corresponding to maximum Cr(VI) removal.

2.6 MECHANISM OF ADSORPTION

The adsorption process is classified as physical adsorption and chemical adsorption. Physical adsorption is due to the presence of van der Waals force of attraction. In physical adsorption, the uniqueness of adsorbent and adsorbate are conserved. Physical adsorption occurs at low temperatures, and adsorption decreases with an increase in the temperature. It possesses low heat of adsorption and is reversible. In a physical adsorption multimolecular layer is formed on the surface of the adsorbent.

The chemisorption involves chemical bonding, and it takes place at relatively high temperatures. Chemisorption is an irreversible process. Chemical bond forces hold the adsorbent and the adsorbate. Here sharing of

electrons takes place, or the adsorbate molecules are broken to atoms or radicals during the adsorption process. Unlike physical adsorption, this is highly specific. This type of adsorption requires activation energy. Commonly the surface of adsorbent holds a monomolecular layer of adsorbate in chemisorption. Menkouchi Sahli *et al.*, 2008 conducted nitrate uptake from brackish underground water by chemical adsorption and by electro dialysis. The chitosan extracted from the waste of shrimps was used as the adsorbent. It is observed that the chemisorption requires a high reactional surface.

2.7 FACTORS AFFECTING BATCH ADSORPTION

The factors that affect the batch adsorption are pH, contact time, initial concentration, adsorbent dosage, agitation speed, temperature, and pressure. The nature of the adsorbent is also an essential factor that determines the adsorption efficiency and capacity. A lot of works has been done to study the effect of these parameters on the ability of the adsorption. Batch experiments are conducted commonly in the laboratory in a temperature-controlled incubated shaker. The shaker contains an oscillating board, and there are provisions for placing the beakers with the solution containing adsorbent and adsorbate. Batch tests have been conducted to study the influence of the factors affecting the adsorption.

2.7.1 Effect of pH on Adsorption

The pH of the aqueous solution is a significant controlling parameter in the ion adsorption processes. The functional groups on the surface of the adsorbent are an important parameter that governs the adsorption of materials on to the adsorbent. The solution pH influences the adsorption capacity of the functional groups. This parameter changes the charge on the adsorbent surface. The extent of dissociation of functional groups on the active sites of

the adsorbent, degree of ionization, structural changes, and conversion of the adsorbate are governed by the pH of the solution (Auta and Hameed, 2014).

Sudipta *et al.* (2013) reported the removal of nitrate using cross-linked chitosan beads conditioned with sodium bisulfate. Batch experiments were conducted to study the effect of pH, cross-linking, and effect of conditioning. The results indicated that nitrate adsorption was highly dependent on the pH of the solution. It is found that changes in pH affect the surface charge on chitosan beads. At a pH range of 3 to 6, more protons were available to protonate the amine groups of chitosan. Maximum nitrate removal was observed at pH three because of the increasing electrostatic interactions between the negatively charged nitrate and positively charged amine groups of chitosan. The increased concentration of hydroxide ions in the solution resulted in a repulsive effect between the deprotonated amine groups and the negatively charged nitrate. Hence, the adsorption capacity was significantly reduced at higher pH.

Appunni and Meenakshi, 2013 found that the pH of the aqueous solution is an essential controlling parameter in nitrate removal by quaternary amine-modified chitosan beads. The pH range of 3 to 9 was found favourable for nitrate sorption. At higher acidic medium, the restriction in the movement of nitrate ions due to excess H^+ ions in the solution lowers the adsorption capacity. They also reported that above pH 9, there were more OH^- ions enough to compete with the nitrate ions and, therefore, the decrease in the adsorption capacity.

Hualin *et al.*, 2013 conducted studies on the effects of pH on the adsorption of nitrate and phosphate on composite Fe_3O_4/ZrO_2 /chitosan. They

observed significant removal at the acidic condition. At pH below 6, the amino groups in chitosan and hydroxy group in ZrO_2 are protonated. The high adsorption capacity at low pH is obtained due to the strong electrostatic interaction between the positively charged sites of composite and the anions. In alkaline conditions, even though the electrostatic interaction between the anions and the adsorbent becomes so weak, there is still a considerable amount of nitrate and phosphate being adsorbed on the composite. It is inferred that there could be physical forces such as ion diffusion affecting the behavior of adsorbates in the vicinity of the adsorbent.

Yian and Aiqin, 2009, evaluated the ammonium removal using chitosan-g-poly (acrylic acid)/ rectorite hydrogel composite. It is observed that the adsorption capacity of hydrogel adsorbent remains constant within the pH range of 4.0–9.0. When pH is lower than 4.0 or above than 9.0, the adsorption capacity shows a slight decrease, and hence the composite can be used in a wide pH range.

2.7.2 Effect of Contact Time

The contact time between the adsorbent and the adsorbate solution is an essential parameter in adsorption processes. Equilibrium time of adsorption is very much useful for the economics of the process. The adsorption efficiency first increases in most cases, with an increase in contact time. After a specific time, there will be no change in the adsorption efficiency. This means that adsorption has reached equilibrium. The amount of adsorbent at equilibrium is the maximum adsorption capacity.

Aref *et al.*, 2014 investigated the effect of stirring time on the removal efficiency of ammonia nitrogen with modified zeolite. It was found that

ammonium ion adsorption increased with increasing stirring time. 92% of NH_4^+ -N removal was completed within 10 min. After 40 minutes, the removal efficiency plateau was observed. It is inferred that the utilization of the most readily available adsorption sites of the zeolite leads to a fast diffusion and rapid equilibrium attainment.

The maximum phosphate and ammonium adsorption capacities were 26.5 mg/g and 20.1 mg/g respectively. The change in free energy for phosphate removal was obtained as -1.92 to -3.2 at temperature ranging from 5 to 35°C. The values of delta G for ammonia nitrogen removal was obtained as -3, -0.9, -1.4 and -2.0 for temperatures 5 to 35°C.

Anni *et al.*, 2013 tested the effect of anion exchangers prepared from tree barks on nitrate adsorption. The effect of contact time was studied by shaking bottles containing 50 mL of nitrate solution with initial concentration 30mg/L. The varying periods was 2 min, 5min, 10min, 20min, 30min, 1h, 2h, 4h, and 7h. The amount of resin used was 0.2 g/50 mL. They found that variations in contact time had little effect on nitrate uptake. 70% of removal was reached within 2 minutes. The sorption was rapid, and a contact time of 5-10 minutes was enough to reach the equilibrium.

Ranjan *et al.*, 2015 reported that the removal of fluoride on neem leaf powder first increased steeply up to 60 minutes, after that it was reduced and reached a constant value. At equilibrium, the rate of adsorption and desorption were equal. Further increase in contact time did not show any increase in adsorption rate.

2.7.3 Effect of Initial Concentration on Adsorption

Initial concentration is an important parameter affecting the adsorption efficiency. With an increase in initial concentration, the driving force for adsorption increases. The active sites are fixed, even though there is a change in initial concentration. The driving force and fixed active sites act as opposing factors that determine the removal efficiency.

Aref *et al.*, 2014 conducted ammonium adsorption onto salt activated Chinese natural zeolite and found that the increment of removal efficiency was in the ranges of 10–50 mg/L of NH_4^+ -N concentrations, indicating that the initial NH_4^+ -N concentration plays a vital role in the adsorption of ammonium onto zeolites. The study inferred that an increase in the initial ammonia nitrogen concentration would increase the mass transfer driving force and, therefore, the rate at which ammonium ions pass from the bulk solution to the zeolite surface. The equilibrium was reached when all the exchangeable ammonium and cation on the external and internal surfaces of the zeolite were reached.

The physically activated carbon residue was used as an adsorbent for the removal of nitrates and phosphates from aqueous solution by Sari Kilpimaa *et al.*, 2015. Besides, raw carbon residue and activated carbon were also tested for nitrate uptake. The effect of initial phosphate or nitrate concentration on the removal efficiency of anions between the concentration levels of 10-140 mg/L was studied. The carbon residue, activated carbon residue and activated carbon gave an optimum initial phosphate concentration for phosphate removal as 80mg/ L, 20mg/L, and 10mg/L, respectively. It is because optimal adsorption sites are occupied at low concentrations while some driving forces exist when the concentration increases.

Auta and Hameed (2014) showed a rise in methylene blue (MB) uptake for an increase in initial concentration when modified ball clay-chitosan (MBC-CH) was used as the adsorbent.

2.7.4 Effect of Temperature and Pressure

Adsorption decreases with an increase in temperature generally, and pressure has a marked influence on the adsorption of gases. For gases, adsorption increases with pressure, and a decrease in pressure causes desorption.

The temperature dependence of nitrate sorption onto chemically modified pine sawdust was studied by Anni *et al.*, 2015. The batch shaking experiments were performed at different temperatures, 50, 60, and 70⁰C. The sorption capacities at an initial nitrate concentration of 250 mg N/L at temperatures 50, 60, and 70 were 24.9, 24.7 and 22.2 mg/g, respectively, for NO₃-N. The minor decrease in sorption capacities was found with temperature rise.

Miltiadis *et al.*, 2013 investigated the efficiency of bentonite-humic acid composite material BephosTM for the removal of phosphate and ammonium from eutrophic waters. The effect of temperature on phosphate and ammonium adsorption onto BephosTM was studied at temperatures ranging from 5⁰C to 35⁰C. The thermodynamic equilibrium constants (K_d) of the adsorption process were calculated from the fit of the adsorption isotherms. The change in Gibbs free energies (ΔG) was then calculated and found that the reaction is feasible.

2.7.5 Effect of Agitation Speed and Adsorbent Dosage

The removal of nitrates from brackish underground water by chitosan produced from some marine animal wastes was studied by Menkouchi Sahli *et al.*, 2008. The effect of the agitation on the adsorption capacity showed that the nitrate removal increases linearly with the agitation speed from 100 rpm to 600 rpm. After 600 rpm, an equilibrium level is reached.

The effect of adsorption on the dosage of a nano bio composite named nanoscale zero-valent iron supported on sineguelas waste was carried out by Arshadi *et al.*, 2014. Lead ions was the adsorbate. It was observed that the removal percentage of Pb (II) increased with increasing the adsorbent dosage from 0.05 to 0.15 g due to the increase in the number of adsorption sites.

Paunka and Dimitrinka (2009) investigated the adsorption of ammonium ions from aqueous solutions by natural and pre-treated Bulgarian clinoptilolite. It is observed that the adsorbed amount of ammonia nitrogen decreases with the increasing clinoptilolite doses from 2.5 to 30 g/L. The decrease in adsorption capacity is due to the increase in interface area when the suspension is diluted. The reduction in adsorption capacity continues to 10 g/L clinoptilolite concentration, and a further increase in adsorbent dosage had no significant effect on adsorbed ammonium ions.

2.8 ADSORPTION ISOTHERM

Adsorption equilibrium is defined as the ratio of the amount of adsorbate in the adsorbent to that in the bulk solution. Mathematical correlations are used to model adsorption isotherm of a system. The retention or release of a substance from an aqueous solution to a solid phase at constant temperature and pH is described best by adsorption isotherm. When the

concentration of adsorbate in the bulk solution is in a dynamic balance with the interface concentration between solution and adsorbent, then it is called adsorption equilibrium. A study on modeling of adsorption isotherm systems was reported in Foo and Hameed (2010). By conducting the isotherm study of a system, the mechanism of adsorption can be explained. Isotherm study gives an insight into the surface properties and the degree of affinity of the adsorbents. Langmuir model, Freundlich model, and D-R model and Tempkin model are commonly used to describe the adsorption of solids from aqueous solution to the specific adsorbent.

Numerous studies have been conducted previously for fitting the data of adsorption to the Langmuir model. The binding of ammonium ions on the surface of strawberry leaf powder was done by Haiwei Liu *et al.*, 2010. The equilibrium data were found to provide well to both the Langmuir Model and Freundlich Model, and the maximum adsorption capacities were obtained as 3.93, 6.05 and 7.66 mg/g at temperatures 15, 25 and 35 °C, respectively.

The ability of a nanocomposite Fe₃O₄/ZrO₂/chitosan for adsorbing nitrate and phosphate was done by Hualin *et al.*, 2013. It is found that the reaction follows the Langmuir isotherm model, and the maximum adsorption amount of nitrate and phosphate is 89.3 mg N/g and 26.5 mg P/g, respectively.

Bing *et al.*, 2015 conducted the ammonium adsorption by maple wood biochar. The adsorption characteristics of ammonium are well described by the Freundlich equation.

Yian *et al.*, 2009 performed the fit of D-R isotherm data on the removal of ammonium ions by chitosan-g-poly(acrylic acid)/attapulgit

composite. The mean free energy was calculated from D-R constant and obtained as -2.0×10^5 kJ/mol.

Ari *et al.*, 2012 modified powder of green coconut shell with 2-hydroxy propyl trimethyl ammonium chloride and used for nitrate uptake from aqueous solution through the batch process. The results showed that the experimental data fit well to Langmuir, SIPS, and Redlich–Peterson equations. The isotherm study of the adsorption of ammonium onto palygorskite nanocomposite elucidated that the Freundlich model provided the best fit for the equilibrium data. The adsorption equilibrium is achieved within 12 min, with the adsorption capacity of 237.6 mg /g (Xinggang *et al.*, 2014).

Mulan *et al.*, 2011 investigated removal of ammonia from aqueous solution by zeolite synthesized from fly ash by a fusion method. The fitting of equilibrium isotherm data was done with Langmuir, Freundlich, Koble-Corregan, Tempkin, and Dubinin-Radushkeich isotherm model. It is found that the Koble-Corregan model gives the best fit.

The equilibrium data of nitrate removal by sugar beet bagasse was analyzed with Tempkin isotherm (Hakan and Gul, 2010). The equilibrium binding constant A (L/mg) was obtained as 0.287 at temperature 298 K. The constant B is related to the heat of adsorption and is obtained as 3.118.

2.9 ADSORPTION KINETICS

The rates and controlling mechanism of the chemical process and the factors that govern the attainment of equilibrium in a specified time is given by the chemical kinetics. For testing the controlling mechanism of adsorption, three reaction models are commonly used, namely, Lagergren pseudo-first-order, second-order, pseudo-second-order model. Two diffusion models

commonly used the intraparticle diffusion model and the Dungwald Wagner diffusion model. The pseudo-first-order kinetics is mostly applicable for the initial stage of the adsorption process. In the final stages, this may not apply to most of the adsorption processes. If the adsorption follows pseudo-second-order kinetics, then the mechanism also involves chemisorption. Chemisorption consists of the exchange of electrons between the adsorbent and the adsorbate. While using pseudo-second-order kinetics, the errors generated from experiments are minimized. In literature, it is reported that most of the adsorption technique for contaminant removal follows pseudo-second-order kinetic models (Hakan and Gul, 2010). When the intraparticle diffusion controls the overall rate, then the kinetics can be expressed in terms of the intraparticle diffusion model. Adsorption of a solute on the surface of an adsorbent is divided into the following steps. In the first step, called the external diffusion, the solute is transferred from the bulk solution to the boundary film surrounding the adsorbent. Then the solute is transported through the film to the surface of the adsorbent. This is termed as film diffusion. In the third step called pore diffusion, the solute from the adsorbent surface diffuses to the active sites of the adsorbent. In the fourth step, the adsorbent interacts with the active site of the adsorbent. The slowest step determines the overall rate of the process.

The use of nanoscale zero-valent iron (NZVI) supported on sinesguelas waste for Pb(II) removal from aqueous solution was conducted by Arshadi *et al.*, 2014. The kinetic studies were carried out in terms of pseudo-first-order kinetics and pseudo-second-order kinetics. It was found that the lead adsorption kinetics follows the pseudo-second-order kinetic model with kinetic constant 0.0292 g/mg min.

The study on the controlling mechanisms of the adsorption of nitrate ions on sugar beet baggage was conducted by Hakan and Gul (2010). It is found that adsorption kinetic could well be approximated more favorably by the second-order kinetic model for nitrate. The intraparticle diffusion analysis showed that the lenier plot has an initial curved portion followed by an intermediate linear portion. The first portion is the external surface adsorption or instantaneous adsorption of nitrate ions, and the second portion is the gradual adsorption stage, where the intra-particle diffusion rate is controlling the mechanism. Sari Kilpimaa *et al.*, 2015 found that the kinetics of adsorption data of nitrate removal by physically activated carbon followed pseudo-second-order kinetics.

Haiwei Liu *et al.*, 2010 conducted adsorption of ammonium ions from aqueous solutions by strawberry leaf powder. Kinetics study suggested that the intraparticle diffusion was the rate-controlling step of ammonium adsorption by strawberry leaf powder. The optimum pH for ammonium adsorption was in the range of 5–8. Individual presence of the K^+ , Na^+ , Ca^{2+} , Mg^{2+} , Cl^- , NO_3^- or SO_4^{2-} had no significant effect on ammonium adsorption, indicating the selectivity of ammonium adsorption by strawberry leaf powder.

Haiming *et al.*, 2010 studied the removal of ammonium ion from aqueous solutions using natural Chinese (Chende) zeolite and found the reaction mechanism follows pseudo-second-order kinetics.

2.10 ADSORPTION THERMODYNAMICS

The thermodynamic analysis is used to determine the mechanism of adsorption. It helps to determine the adsorption equilibrium constant (K), Gibbs free energy change (ΔG), enthalpy change (ΔH), and entropy change (ΔS). The positive values of ΔG indicate that the reaction is not

thermodynamically feasible. The negative values of ΔG indicate the thermodynamic spontaneity and favourability of the process. The positive values of ΔH are a representation of the endothermic process and vice versa. Positive values of ΔS indicate increased disorder at the adsorbent-adsorbate solution interface during the fixation of adsorbate to the active site of the adsorbent (Anni *et al.*, 2015).

The thermodynamic study on the adsorption of nitrate by magnetic amine-cross linked biopolymer-based corn stalk (MAB-CS) was performed by Wen Song *et al.*, 2015 by varying the temperature from 298 to 318 K. It was observed that more nitrate ions were removed from the solution with an increase in temperature. The positive values of ΔH exposed the nitrate adsorption is an endothermic process, and the negative values of ΔG implied the feasibility and spontaneous nature of the process. Also, change in entropy was positive showed an increase in disorder and randomness during the adsorption of nitrate by MAB-CS.

The adsorption of ammonia nitrogen into natural and pretreated Bulgarian clinoptilolite as a function of temperature was studied by varying the mixing temperature from 293 K to 333 K (Paunka and Dimitrinka 2009). The removal efficiency was found to be decreasing with increasing temperature. It is inferred that the decrease in ammonia removal with temperature is due to the increasing tendency to desorb from the interface to the solution. The value of ΔH was -12.94 kJ/mol, and that of ΔS was 7.21 J/mol K.

2.11 RESPONSE SURFACE METHODOLOGY

Response surface methodology is a collection of statistical and mathematical models that help model any engineering problems. For the optimization of three or more variables, RSM is an efficient tool. The first step in RSM is to design a set of experiments by specifying the process parameters that affect the system. Tests are performed according to the experimental runs suggested by RSM. Then the model equation is developed by RSM. Then optimum values of process parameters that maximize or minimize the response are determined in the third and final step.

Box-Behnken design demands only a limited number of experimental runs for the optimization of a process. The model equation is developed in the Box-Behnken design, which relates the variable of interest, which is to be optimized with the various parameters that affect the process. Response surface methodology gives the interaction between multiple variables that affect a process and gives the shape of the response surface. Contour and surface plots of RSM give the pictorial representation of the interaction between various parameters that affect a process.

Peijing *et al.*, 2018 developed an electrochemical/adsorption system with iron particles and zeolites for remediating nitrates and its byproducts. The effect of the amount of iron particles, zeolite, and current density was investigated. A high nitrate removal efficiency of 95 % was achieved with 19.74 g of iron particles, 28.19 g zeolites and current density of 18.72 mA/cm².

Response surface methodology with Box–Behnken design was applied to investigate the effects of alkali treatment with NaOH on oil palm frond

towards the adsorption of heavy metals. The weaker effect of contact time and the stronger effect of base concentration was given by the quadratic models of RSM. The results obtained were found to be significant at a 99% confidence interval. The removal efficiency of 61.5 % for Zinc and 64 % for Copper was obtained by treating the oil palm frond with 1.0 M NaOH for a time duration of 45 minutes.

Uttam *et al.*, 2018 studied the application of BBD in response surface methodology for the elimination of arsenic with CeO₂/Fe₃O₂/grapheme nanocomposite. The analysis of regression showed the best fit of experimental results to a quadratic polynomial model with R²=0.99. ANOVA and lack of fit tests were also carried out to confirm the accuracy of the model. The removal efficiency of 98.53 % for As(III) was obtained at the optimum condition of C₀=10.52 ppm, adsorbent dose=0.198 g/L and pH=7.84.

The optimization of the effects of pH, adsorbent dose, contact time, temperature, and initial concentration by zeolite towards ammonia removal was carried out by Yuanhao and Majid, 2015. They used factorial design and response surface methodology. Findings of factorial design and response surface showed an optimum pH of 6, and the effect of temperature was not significant. The experimental data and model prediction was in good agreement with R² = 0.969.

Soumasree *et al.*, 2011 employed RSM to optimize the carbonizing condition, the weight ratio of activating agent to the development of an adsorbent from the biomaterial, parthenium. The effect of temperature and time of carbonization on the removal of methylene blue was studied. The optimum values obtained were 1.05:1.0 weight ratio of zinc chloride to

parthenium, carbonization temperature 5500C, and time one h. The MB adsorption efficiency was also statically investigated, and 93.4% removal with initial Methylene Blue concentration of 25 mg/L, the weight of charred parthenium 0.22 g at pH seven and temperature 35⁰C has been obtained.

The efficiency of synthetic cation ion exchange resin INDION 225 Na for ammoniacal nitrogen removal from semi-aerobic landfill leachate was investigated by Mohammed *et al.*, 2009. The effects and interaction of process variables like cationic dosage, speed of shaking, and contact time were analyzed with central composite design with RSM. They got a significant model with a low probability value. The effect of contact time was least significant compared to dosage and shaking speed.

Optimization of fast removal of ammoniacal nitrogen by a hydrogel consisting of polyvinyl alcohol, acrylic acid, and tourmaline was done using Box Behnken design of RSM (Yian *et al.*, 2011). Seventeen experimental runs were performed by varying three variables, namely, neutralization degree (ND) of acrylic acid (AA), the ratio of polyvinyl alcohol (PVA) to acrylic acid, and the ratio of tourmaline (Tm) to acrylic acid. The second-order polynomial equation was developed by RSM to fit the experimental data at work. The high adsorption of ammonium was achieved by the hydrogel prepared according to the predicted appropriate preparation condition of ND of AA 70%, the ratio of PVA to AA as 0.0833, and the ratio of Tm to AA of 0.5.

Box-Behnken design of RSM was used to optimize the processing parameters for maximum biodegradability of pulp and paper industry wastewater by electrochemical pre-treatment method by Solomon *et al.*, 2009.

The statistical investigation of a starch-based based hydrogel nanocomposite prepared from starch and polyvinyl alcohol blend as polymeric matrix and fumarate-alumoxane (Fum-A) and maleic anhydride (MA) as cross-linking agents, for its use in NH_4^+ removal from aqueous solutions.

The adsorption efficiency of zeolite towards ammonium removal was studied by Yuanhao and Majid in 2015. They used batch adsorption experiments. The results showed that zeolite was effective in eliminating ammonia from aqueous solution. A low pH condition was suitable with the optimum pH found to be 6. High adsorbent dose generated a high removal rate and low adsorption capacity. Results of factorial design and response surface methodology proved that temperature was not a significant parameter. The adsorption kinetics followed the Pseudo-second order kinetic model ($R^2 = 0.998$). Equilibrium data were fitted well to Langmuir and Freundlich isotherm models.

2.12 DESORPTION

The evaluation of the reusability of an adsorbent is essential from a practical viewpoint. Once the saturation of an adsorbent takes place, suitable eluents are selected for the regeneration of the bed. After bed regeneration, the performance of the bed improves drastically. Desorption is the reverse process of adsorption, where the adsorbed substance is released from the surface. Desorption is used to regenerate the adsorbent after adsorption. After adsorption, the adsorbent is saturated with the adsorbate, and no further adsorption takes place. Replacement with fresh adsorbent is expensive, and hence, suitable solvents are selected that are used to take out the adsorbate from the surface of the adsorbent. Thus the adsorbent can be reused. The removal efficiency decreases with an increase in the adsorption-desorption

cycle. The critical aspect of the effective regeneration of an adsorbent is its return to the original state without changing its intended properties.

The regeneration of quarternized chitosan beads (QCB) loaded with both nitrate and phosphate ions was done with 0.025 M NaCl (Appunni and Meenakshi 2013). The optimum required contact time for complete desorption of nitrate and nitrate was found as 30 minutes, for this QCB was immersed in eluent at different time intervals of 5-30 minutes. 100 % of the actual adsorption capacity was obtained for adsorbent immersed for 30 minutes. The renewed adsorbents were used for adsorption studies. It was found a 99 % and 97.5 % of the actual adsorption efficiency for nitrate and phosphate were retained up to the 10th cycle.

The desorption studies on modified hydrated aluminium zeolite laded with ammonium and phosphate were performed by Diana *et al.*, 2015. The eluent solutions used were NaOH, NaHCO₃, Na₂CO₃, and mixtures of NaHCO₃/Na₂CO₃. The desorption efficiency of ammonium was obtained from 50 % to 92 % for the elution solutions used. The phosphate recovery was less varying from 20 to 79 %. One M NaOH was found as the better eluent than others.

Yian and Aiqin, 2009 checked the reusable ability of chitosan-g-poly (acrylic acid)/rectorite hydrogel composite used for the removal of ammonium ions. 0.1 mol/L sodium hydroxide solution was used successfully for complete desorption.

Mahatheva *et al.*, 2016 used iron-modified Dowex 21K XLT ion exchange resin for removing nitrate from water. The desorption of the adsorbent with 1 M KCl was done in three adsorption-desorption cycles. It

was observed a little reduction in adsorption capacity after each regeneration. No significant loss in the iron content of adsorbent occurred during recovery.

2.13 CHARACTERISATION OF ADSORBENTS

The study on exploring the potential use of amine cross-linked reed (ACR) for removing nitrate, phosphate, and Cr(VI) from aqueous solution in a fixed-bed column was conducted by Zhongfei et al., 2016. Results indicated that FTIR, Raman, and XPS of nitrate and phosphate laded ACR were quite different from those of Cr(VI) laden samples, which corresponded well to their adsorption properties. Results indicated that FTIR, Raman, and XPS of nitrate and phosphate laded ACR were quite different from those of Cr(VI) laden samples, which corresponded well to their adsorption properties.

Removal of nitrate by synthetic organosilica and organoclay was investigated by Moaaz *et al.* 2013. In this work, octadecyl trimethyl ammonium (ODTMA) chloride was used to prepare MCM-41 at room temperature. The cetyl trimethyl ammonium bromide was used to synthesize MCM-48 and layered organosilica material under hydrothermal conditions. The prepared organosilica materials, and the commercially available organoclay, Cloisite 10A, were characterized by powder X-ray diffraction (XRD) and tested with the occluded surfactant as sorbents for nitrate.

Deepak *et al.* 2015 investigated the phosphate removal on rice husk and fruit juice residue. The adsorption process was fitted with pseudo-first-order kinetics and Freundlich adsorption isotherm. The D-R isotherm showed the physical forces are dominating in the adsorption.

Thomas *et al.* 2008 experimented with wood particles activated with anionic polymer and iron salts for the remediation of phosphate from aqueous solutions. A decrease in the intensity of the phosphate with a reduction in particle size was observed in FTIR studies. A strong linear correlation between phosphorus and iron contents was found out.

Ammonium retention processes onto Cactus leave fibers using FTIR, EDX, and SEM analysis by Mohamed Ali *et al.* 2012. The results showed that ammonium retention onto these fibers occurred for a wide pH (6–10) and temperature ranges (20–60 °C), and the biosorption potential of Cactus leave fibers increased with temperature from 1.4 to 2.3 mg g⁻¹ for initial concentration of 50 mg/ L. The modeling studies showed that the pseudo-second-order model well described the ammonium biosorption, FTIR and EDX analysis before and after ammonium retention showed that the main mechanisms involved in the removal of ammonium were the ionic exchange by calcium ions as well as H⁺ and the complexation with carboxylic, alcoholic and phenolic groups. The surface of CLF determined by SEM revealed the presence of cracks and cavities, which may allow the intraparticle diffusion and the ion exchange processes.

Soleymanzadeha *et al.*, 2015 developed a nano biocomposites from sineguelas seed for cadmium removal. The synthesized material was characterized with different methods such as CHN elemental analysis, inductively coupled plasma/atomic emission spectroscopy (ICP–OES), Fourier transform-infrared spectroscopy (FT-IR), Brunauer–Emmett–Teller (BET), X-ray diffraction (XRD), transmission electron microscopy (TEM), energy dispersive X-ray (EDX) and the point of zero charge. It was observed a good dispersion of NZVI particles (10–70 nm) on the sineguelas waste.

2.14 ANALYTICAL METHOD

UV vis spectrophotometer was used for the analysis of nitrate nitrogen and ammonia nitrogen in the wastewater. UV vis spectrophotometer is an absorption spectrophotometer that works in the ultraviolet-visible spectral region. It measures the electronic transitions of atoms and molecules from the ground state to the excited state upon absorption of light in the UV-visible region. This electronic transition of atoms and molecules is a function of the composition of the sample solution. A blank is also used, which does not contain the sample. In wastewater analysis, an adequately diluted sample is taken for analysis. The working of the UV vis spectrophotometer is based on Beer-Lambert's law, which states that the absorbance is directly proportional to the concentration of absorbing species and the path length. In this device, absorbance is measured, which is related to the concentration of the substance under consideration. The measurement of UV absorption at 220 nm gives the determination of nitrates and organics if any. At 275 nm, the absorbance of dissolved organics takes place. So a second measurement is done at 275 nm to correct the nitrate value. The Nesslerization method is used in the determination of ammonia nitrogen at a wavelength of 430 nm (Yian *et al.*, 2009).

Ting wang *et al.*, 2014 synthesized iron nanoparticles by green tea and eucalyptus leaves extracts and conducted adsorption of nitrate in aqueous solution. They analyzed residual nitrate concentration in a UV vis spectrophotometer (722N) at 220 nm and corrected by subtracting a second absorbance at 275 nm.

The removal of nitrate using nano SiO₂-FeOOH-Fe-core-shell was carried out by Bekhradinassab *et al.*, 2014. The analysis of nitrate ions was

done using a UV vis spectrophotometer apparatus (HACH DR/5000) at a wavelength of 220 nm. They used 50 mL of distilled water acidified with 1 mL of 1 N HCl.

Appunni and Sankaran (2013) developed quarternary amine-modified chitosan beads for the removal of nitrate and phosphate anions. Ultraviolet Spectrophotometric Screening method was used for nitrate analysis in which the absorbance was measured at a wavelength of 220 nm, and phosphate was analyzed by Vanadomolybdophosphoric acid colorimetric method at a wavelength of 400 nm in a UV-Visible spectrophotometer (Spectroquant Pharo 300, Merck). The residual nitrate concentration after adsorption with the composite chitosan-melamine-glutaraldehyde was also done with UV vis spectrophotometry (Appunni and Sankaran 2014).

Cilai *et al.*, 2102 conducted a study on the effect of common ions on nitrate removal by zero-valent iron from an alkaline soil. Nitrate measurement was carried out by the ultraviolet spectrophotometric method at 220 nm and 275 nm using a UV1102 spectrophotometer.

Hualin *et al.*, 2013 analyzed the nitrate remaining in water after adsorption using the nanocomposite $\text{Fe}_3\text{O}_4/\text{ZrO}_2$ /chitosan using a UV vis spectrophotometer (WFZ UV-2000, Unico, USA).

UV-Apel P D spectrophotometer was used for the analysis of the concentration of ammonia in aqueous solution after adsorption by a starch-based hydrogel nanocomposite by Batool *et al.*, 2015.

The left out ammonium concentration in the supernatant solution after adsorption with zeolite synthesized from fly ash was analyzed spectrophotometrically by Nesslerization method (Mulan *et al.*, 2011)

Mohamed Bashir *et al.*, 2010 done the optimization of ammoniacal nitrogen removal from semi aerobic landfill leachate with ion exchange resin. The residual concentration of ammoniacal nitrogen was measured by the Nesslerisation method (Method: 8038) with a Hach's DR2010 spectrophotometer set at 425 nm.

2.15 CONTINUOUS REMOVAL IN PACKED BED ADSORPTION COLUMN

Adsorption is a transient process. The amount of material adsorbed within a bed depends both on position and time. The solution leaving the bed will have little or no solute remaining until the bulk of the bed becomes saturated. The breakpoint occurs when the concentration of the fluid leaving the bed spikes as unabsorbed solute begins to come out. Then it is conferred that the bed has become ineffective. Usually, a breakpoint composition is set as the maximum amount of solute that can be acceptably lost. In the column operation, the removal of pollutants is achieved continuously, and more control of the process is executed. The continuous adsorption column can be used for the treatment of both organic and inorganic pollutants. The removal of trace amounts of contaminants could be made through developing adsorption column in wastewater treatment systems. The data of continuous column studies can be used in the design of a packed bed column. Also, the prediction of breakthrough curves of fixed-bed columns in real water treatment processes can be made. The parameters affecting the breakthrough time and shape of the breakthrough curve are the initial concentration of the

feed solution, bed height, flow rate, and pH. Various studies have been conducted previously by conducting continuous experiments in a packed bed adsorption column for removal of nitrate in wastewater and analyzing the factors that influence the column operation. The accurate information obtained from the fixed bed column studies is guided to the ideal design of an adsorption system.

The influence of various parameters and breakthrough performance of the adsorption column were described by mathematical models of the column data. In modeling, first, the model parameters are estimated, and the experimental data are fitted to the various model equations. Thomas model, Yoon Nelson model, and Adam Bohart model are used commonly by multiple researchers to model the experimental column data. Adam Bohart, Thomas, Clark, and Yoon Nelson model was applied to fit the equilibrium column data of biosorption of phenol by immobilized activated sludge in a continuous packed bed column (Aksu and Gonen, 2004). Flow rate and initial phenol concentration were varied to the model column, and it was found that all models fitted to the column data. Thomas model is simple and reasonably accurate in predicting the performance of the column. Yoon Nelson model requires only fewer column data for prediction of breakthrough curves and is mostly applicable for single-component systems (Lim and Aris, 2014). Adam Bohart model is applicable only for the initial part of the breakthrough curve.

Asim *et al.*, 2013 investigated the removal characteristics of phosphate and nitrate by adsorption on boron waste (BW) and heat-treated boron waste (BW400) under batch equilibrium and column flow conditions. The effect of different flow rate (0.5 mL/min, 1 mL/min and 1.5 mL/min), various bed heights (6 cm, 9 cm and 12 cm) and effect of different of inlet concentration

(100 mg/L, 150 mg/L, 200 mg/L) were analyzed. Fixed-bed column studies were performed using a laboratory scale glass column with an internal diameter of 1 cm and a length of 12 cm. A stainless sieve was attached at the bottom of column with a layer of glass wool. The results of the column study showed that the adsorption capacity of both boron waste and treated boron waste was increased with increasing bed depth and initial influent concentration and decreased with increasing flow rate. The Breakthrough curves obtained from fixed-bed column tests showed that column with BW400 could be used for the uptake of phosphate and nitrate removal from aqueous solutions.

The simulation of a fixed bed adsorber packed with protonated cross-linked chitosan gel beads to remove nitrate from contaminated water was done by Jaffari *et al.*, 2004. It is observed that the trend of the breakthrough curve was not affected by sinusoidal variations of the superficial velocity, which confirms that the design can be carried out considering a conventional step injection. The packing length was more influential than the column diameter in the breakthrough curve analysis.

Auta and Hameed, 2014 conducted batch and fixed bed studies for the removal of methylene blue from aqueous solution using chitosan-clay composite. A comparison between modified ball clay (MBC) and chitosan composite (MB-CH) for removal of methylene blue has also been made. Adam Bohart model (A-B) and Yoon Nelson model were compared, and it was found that the experimental data fitted to the A-B model than Yoon Nelson model. The desorption efficiency of MB-CH was higher than MBC after five regeneration cycles.

Hekmatzadeh *et al.*, 2012 conducted studies on the modeling of nitrate removal by ion exchange resin IND NSSR in batch and fixed-bed experiments. Nitrate-rich groundwater and synthetic waters with varying initial nitrate concentrations were tested. The effect of the presence of sulfate and chloride are also studied. The resin bed height for all tests was set at 20.5 cm. The effect of flow rate varying from 0.69 to 2.11 L/h at a constant influent nitrate concentration of 120mg/L was studied. The influent nitrate concentration on the sorption performance of nitrate was examined at the values of 89.5 mg/L and 60.4 mg/L. It was found that the experimental breakthrough curves from column experiments were in good agreement with the model predictions ($R^2 > 0.96$). The prediction of column behavior can be made from the batch equilibrium data by using the mass action isotherm.

Lim and Aris (2014) modeled an adsorption column for removal of Cd(II) and Pb(II) ions in aqueous solution using dead calcareous ions as adsorbent. The study showed that when bed height was increased, the column exhaustion time also increased, causing an increase in the life span of the column. They applied the Thomas model, Yoon Nelson model, and Adam Bohart model to the experimental column data. The value of correlation coefficients indicated that Thomas model fitted better to Cd(II) column than to Pb(II) column. Yoon Nelson model was applicable for both the columns. Adam Bohart model assessed the saturation state of the column performance.

Zhongferi *et al.*, 2016 studied the use of amine cross-linked reed for removing nitrate, phosphate, and Cr (VI) from aqueous solutions in a fixed bed column. The effect of influent concentration (50 mg/L, 80 mg/L, and 120 mg/L) and flow rate (5 to 10 mL/min) was analyzed in a column of 20mm length, 12 mm diameter filled with 1.2 g adsorbent. It is found that the Thomas

model was suitable for the adsorption process. The value of Thomas model parameter k_{Th} was found to be decreased with influent concentration. This is attributed to the driving force for adsorption due to the difference in the concentration difference. The equilibrium adsorption capacities q_0 calculated from Thomas model were 107.3-122.3 mg/g for nitrate. The q_0 values for phosphate and chromium were 100.6-103.1 mg/g and 112.6-136.7 mg/g, respectively.

The applicability of the Thomas model for adsorption of Cr(VI) onto tea factory waste in a packed column was analyzed by Malkoc and Nuhoglu (2006). They observed close agreement between experimental data and the Thomas model. The fitting of the breakthrough curve was significant.

The use of activated carbon obtained from oil palm shells for phenol adsorption in a fixed bed column was done by Lua and Jia (2009). The column data was simulated by the linear driving force model based on the particle phase concentration difference (LDFQ). The model equation obtained was found to be in good agreement with the experimental column data.

The adsorptive removal of nickel (II) ions by crab shell in a packed column was investigated by Vijayaraghavan *et al.* (2004). The upflow mode was used in the column with an internal diameter of 2cm. The effect of bed height and flow rate on breakthrough curves was investigated. The Bed Depth Service Time Model (BDST) was used to describe the performance of the column.

Vinodhini and Nilanjana (2010) investigated the removal of Cr(VI) from tannery wastewater by neem sawdust in a fixed bed column. The effect of the parameters bed depth (5-15 cm) and flow rate (5-15 mL/min) were

studied. The neem sawdust dosage was increased from 10, 20, 30 mg for different bed heights 5,10, and 15 cm. The effect of co ions Na^+ , K^+ , Mg^{2+} , Ca^{2+} , SO_4^{2-} , PO_4^{3-} , NO_3^- and Cl^- was studied in the column. The percent removal of chromium obtained for bed heights 5 cm, 10 cm, and 15 cm were 67.81, 69.91, and 72.13, respectively. The percent removal of chromium for different flow rates 5, 10 and 15 mL/min for a bed height of 10 cm was 69.97, 65.46, and 62.9, respectively. It is found that the bed depth service model fits well with experimental data. The adsorption capacity estimated from the BDST model was 33010 mg/g.

2.16 SUMMARY

This chapter contains a detailed literature review on the sources of nitrogen contaminants (nitrate-nitrogen and ammonia nitrogen) in aqueous solution. The impacts of $\text{NO}_3\text{-N}$ and $\text{NH}_4^+\text{-N}$ on human being and all sorts of life has explained well. The advantages and disadvantages of different technologies for eliminating them are described. Benefits of adsorption, when compared to other water treatment methods, have been presented. The various adsorbents that are suitable for both nitrate nitrogen and ammonia nitrogen removal from aqueous solution, the mechanism of adsorption, kinetics, thermodynamics, and equilibrium models and desorption have been depicted. The advantages of the application of nano adsorbents in wastewater treatment and their characterization are presented in this section. The limitations of nanomaterials and the application of nanocomposite adsorbents have been highlighted.

A variety of research works involving the preparation of nano adsorbents and nanocomposites have been stated. A detailed literature review on the design, fabrication, and modeling of continuous fixed-bed adsorption columns for nitrate removal has been presented.

From the previous research works on both batch and continuous adsorption, we can summarize that adsorption using nanomaterials seen to be highly effective in the remediation of nitrate nitrogen and ammonia nitrogen from aqueous solution. To overcome the difficulty of separation of nanomaterials from the aqueous solution, they can be made composite with a suitable polymeric material, and they can be used effectively in a continuous fixed-bed column.



CHAPTER 3

MATERIALS AND METHODS

3.1 INTRODUCTION

In this chapter, the materials used for conducting adsorption tests for $\text{NO}_3\text{-N}$ and $\text{NH}_4^+\text{-N}$ removal for both batch and continuous experiments have been discussed. A detailed presentation of experimental procedures is included in this section. The experiments conducted for adsorption study is divided into three sections. In the first section, batch studies carried out for nitrate removal with iron loaded chitosan nutmeg shell powder (Fe-CH-NSP) and chitosan-bentonite nanocomposite films (CH-B-NCF) is discussed. The second part discusses the continuous experiments performed for $\text{NO}_3\text{-N}$ elimination in a fixed bed adsorption column and the mathematical modeling of the column. The third section focuses on batch adsorption of $\text{NH}_4^+\text{-N}$ with chitosan-bentonite nanocomposite film. The statistical validation of batch adsorption experiments of both $\text{NO}_3\text{-N}$ and $\text{NH}_4^+\text{-N}$ using nanocomposite films is done with response surface methodology.

3.2 PREPARATION OF NITRATE AND AMMONIUM STOCK SOLUTIONS.

Potassium nitrate (99.9%) for preparing nitrate stock solution was purchased from Sigma Aldrich. All the experiments are conducted on the basis of removal of nitrate as nitrogen. So the stock solution was prepared by dissolving 1.63g potassium nitrate in 1-liter ultrapure water to make 1000 mg/L $\text{NO}_3\text{-N}$ solution (Wen Song *et al.*, 2016). Ultrapure water was produced in situ using the Millipore Direct-Q3 UV system device. The required

concentration of nitrate solution was obtained by the serial dilution of the nitrate stock solution. Potassium nitrate was dried at 105⁰C for 24 hours before dissolution.

Ammonium chloride of 99.9 % purity was purchased from Sigma Aldrich. 1000 mg/L of NH₄⁺-N solution was prepared by adding 3.82 g ammonium chloride in 1-liter ultrapure water and stored. Ammonium chloride was also dried at 105⁰C for 1 h before dissolution to remove the moisture content. The working solutions for adsorption studies were obtained by diluting the stock solution. Both the stock solution were stored in stoppered glass jars.

3.3 PREPARATION OF ADSORBENTS

In this section preparation of the adsorbents has been discussed.

3.3.1 Preparation of Fe-loaded Chitosan Nutmeg Shell Powder

In the last few decades, researchers have been more attracted towards the synthesis of nanoparticles through environmentally benign routes. In the present work, nutmeg shell powder supported with chitosan is used as the biomaterial. The Fe-loaded chitosan nutmeg shell powder is synthesized based on the following procedure. The raw nutmeg shell coat was separated from its fruit and was water washed to remove the dirt. The shell is dried by keeping in an oven at 80⁰C for 4 h. After that, the shell is powdered and is sieved. The fraction of particles between 75 μm and 90 μm were selected. The particles were washed with hot distilled water and were dried at 70⁰C. Ten gram of prepared nutmeg shell powder was added to 100 mL of 1% acetic acid, and the solution is kept for mixing for 1 h in a magnetic stirrer at room temperature. At the same time, 1 g of powdered chitosan with a degree of deacetylation is dispersed in 100 mL 1 % acetic acid and kept in magnetic stirrer for 1 hour.

Both solutions were mixed and stirred for two hours using a magnetic stirrer to layout the biomaterial. Then add a 20 mL mixture of $\text{FeCl}_2 \cdot 4\text{H}_2\text{O}$ and $\text{FeCl}_3 \cdot 6\text{H}_2\text{O}$ to the above solution and is ultrasonically mixed for 30 minutes. 100 mL of 1 molar NaOH solution with temperature 50°C was added slowly and stirred for 30 minutes. The mixture is filtered using $0.2\ \mu\text{m}$ cellulose nitrate membrane filter paper in a vacuum filtration unit and kept for drying for 12 hour. After drying, the powder is washed by distilled water to neutral pH before use. Then dried at $70\text{-}80^\circ\text{C}$ for eight hours in a hot air oven (Zihong *et al.*, 2012; Arshadi *et al.*, 2015). The prepared adsorbents are stored in sealed plastic containers at room temperature. Fig 3.1 shows nutmeg and nutmeg shell, and Fig 3.2 depicts synthesized Fe-loaded chitosan nutmeg shell powder.



Fig 3.1 Nutmeg and nutmeg shell



Fig. 3.2. Synthesized Fe-loaded chitosan nutmeg shell powder

3.3.2 Preparation of Chitosan-Bentonite Nanocomposite Films

The chemicals bentonite nanoclay, chitosan with a deacetylation degree of 85.0%, and acetic acid were purchased from Sigma Aldrich and used without further purification. 100 mL of 1% acetic acid was taken in a beaker. Two grams of chitosan was added to it. A clear solution was obtained after magnetically stirring the solution for 10 hr. Further 0.5 g of bentonite was added into it and stirred for eight hour at 500 rpm. After that, the suspension was sonicated for 6 h. Half of the consequential solution was transferred into a glass petri dish. The film was then dried at 80°C for a period of 6 h. It was then unwrapped from the glass plate and was washed to remove any excess acetic acid. Then it was again dried for 2 h and cut into small pieces. A hand-held digital micrometer was used to measure the film thickness and found as 0.2 mm. These films are stored in sealed plastic containers to perform adsorption experiments. The synthesized nanocomposite films are shown in Fig 3.3. Fig. 3.4 shows the various stages of synthesis of nanocomposite films.



Fig. 3.3 Synthesized chitosan-bentonite nanocomposite films

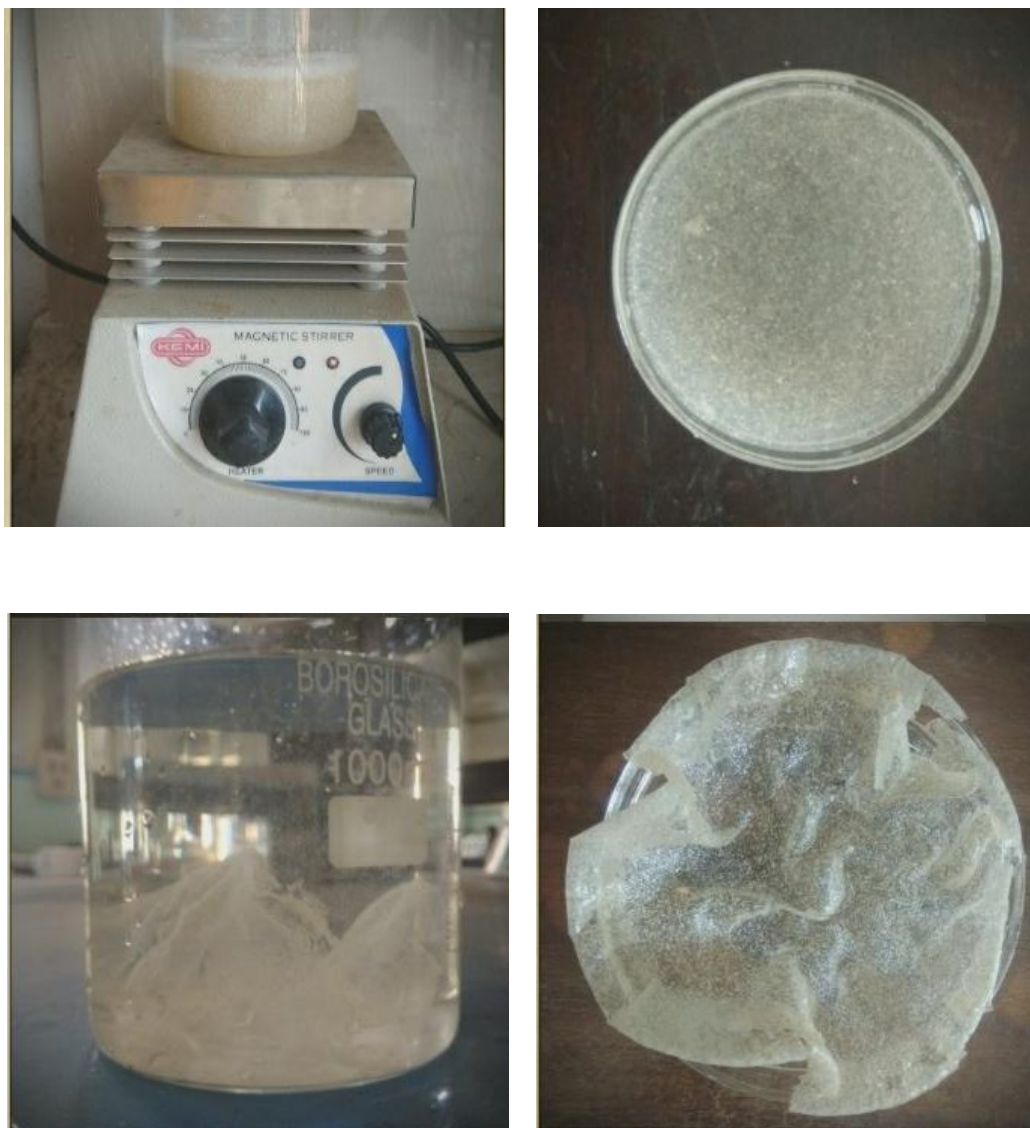


Fig. 3.4 Synthesis of chitosan bentonite nanocomposite films in the lab

3.4 ANALYTICAL METHOD FOR NITRATE NITROGEN AND AMMONIA NITROGEN DETERMINATION

The analysis of nitrate solution was achieved by the ultraviolet spectrophotometric screening method. The UV vis spectrophotometer (Hitachi U-2900) set at $\lambda_{\max}=220$ nm, and $\lambda_{\max}=270$ nm was used for nitrate determination (Cilai *et al.*, 2012; Yanhui *et al.*, 2011). The second measurement at $\lambda_{\max}=270$ is used to correct the nitrate value from the dissolved organic matter absorbed at 220 nm. One mL of 1N hydrochloric acid is added before analysis. The acidification helps to prevent interference from hydroxide or carbonate ions (Ying *et al.*, 2007). The spectrophotometer was first calibrated using nitrate solutions of different concentrations (Standard Methods for the Examination of Water and Wastewater, 1985). The calibration curve is given in Annexure I.

The residual concentration of ammoniacal nitrogen was determined by Nessler's reagent colorimetric method using UV vis spectrophotometer (Hitachi U-2900) set at $\lambda_{\max}=430$ nm (Yian *et al.*, 2009). Fifty mL of ammonium chloride solution of various concentrations was mixed with one mL of potassium tartrate. Then the solution is filtered. After that, add one mL Nessler's reagent. The solution was put for analysis after five minutes until the color change from yellow to brown. A blank solution without the ammonium chloride solution was taken in the cuvette. Both the sample and blank solutions were used in the UV vis spectrophotometer, and the standard calibration curve was obtained. This calibration curve was used to measure the concentration of the ammonium solution (Annexure I). Fig. 3.4 shows the sample of ammonium solution after adding Nessler's reagent.

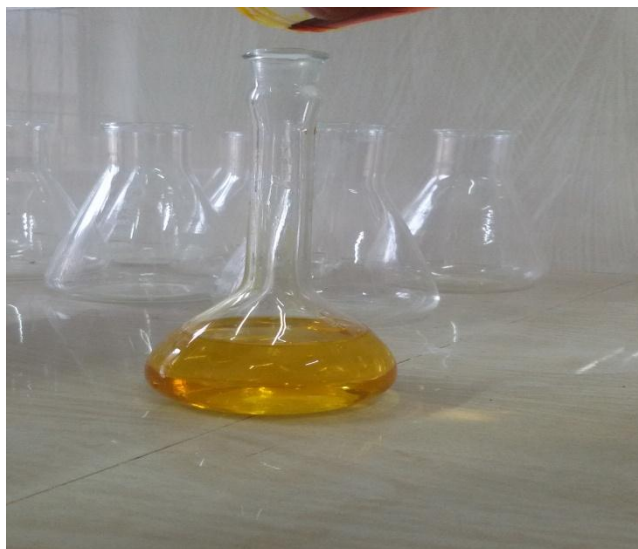


Fig. 3.5 Ammonium solution with Nessler's reagent for analyzing in UV vis spectrophotometer

3.5 CHARACTERIZATION OF THE ADSORBENTS

The surface morphology of Fe-CH-NSP and nanocomposite films was determined using a scanning electron microscope (JEOL-JSM-6390). The elemental composition of nanocomposite films before and after ammonia nitrogen adsorption was estimated using energy-dispersive X-ray spectroscopy (EDX). The crystal structure and basal spacing of iron loaded chitosan-nutmeg shell powder and nanocomposite films were obtained from the X-ray diffraction pattern (Standard X-ray Diffraction Powder Patterns, 1981). Bruker AXS X-ray powder diffractometer (Cu K α radiation) was used to find the crystal structure and basal spacing of nanomaterials in the present work. The thermogravimetric analyzer (TGA) was used to determine the thermal stability of nanocomposite films. STA 6000 Perkin Elmer TGA-DTA system was used for the thermal analysis in the present study. The inert atmosphere was created with nitrogen gas. Nitrogen gas with a flow rate of 50 mL/min results in a non-oxidative degradation.

Fourier transform infrared spectroscopy was used to analyze the functional group present in nutmeg shell powder, activated nutmeg shell powder, and nitrate loaded Fe-CH-NSP. Fourier transform infrared spectra of chitosan-bentonite nanocomposite films before and after ammonia adsorption have been carried out. Perkin Elmer FTIR spectrophotometer with 20 scans and resolution four was used for analyzing the functional groups in the adsorbents. The average particle size of nanocomposite films was calculated using Debye-Scherrer's formula (Annexure-II), which is given by equation 3.1.

$$D = \frac{K\lambda}{\beta \cos \theta} \quad (3.1)$$

where, D = mean diameter of nanoparticles

β = Full width at half maximum value of XRD diffraction lines in radians

λ = the wavelength of X-ray radiation source

θ = angle of incidence

K = the Scherrer constant with value from 0.9 to 1.

The thickness of chitosan-bentonite nanocomposite film was measured using a hand held digital micrometer.

3.6 BATCH ADSORPTION EXPERIMENTS

Adsorption experiments were carried out in a temperature-controlled incubated shaker (ROTEK Incubated shaker). A known volume of adsorbate solution was contacted with a definite amount of adsorbents to conduct batch adsorption experiments. Solution after adsorption was filtered to remove the adsorbent loaded with adsorbate and analyzed for residual concentration of adsorbate. Experiments were designed by Box-Behnken design under the

response surface methodology of Minitab. According to the design of experiments of RSM, batch experiments were conducted for both nitrate nitrogen and ammonia nitrogen removal. The efficiency of nitrate nitrogen and ammonia nitrogen adsorption capacity was determined using the following equations.

$$E(\%) = \frac{(C_0 - C_t)}{C_0} \times 100 \quad (3.2)$$

$$q(\text{mg/g}) = \frac{(C_0 - C_t)}{C_0} V/m \quad (3.3)$$

where C_0 is the concentration of nitrate or ammonium in the solution before adsorption in mg/L and C_t is the concentration of nitrate or ammonium in the solution after adsorption in mg/L and m is the mass of adsorbent in grams, and V is the volume of solution taken for adsorption in liters.

3.6.1 Batch Experiments for Nitrate Removal using Fe-CH-NSP and CH-B-NCF

Adsorption experiments were conducted by diluting the stock solution of nitrate using deionized HPLC grade water. Constant volume of nitrate solution was taken in stoppered flasks for the batch tests. After adding a definite amount of adsorbent, the bottles were shaken in an incubated shaker at 30⁰C. The supernatant solution after removing adsorbents was analyzed to calculate the adsorption efficiency. The Fe-CH-NSP was separated by vacuum filtration in a vacuum filtration unit. Whatman 0.2 μm cellulose nitrate membrane filter paper was used for vacuum filtration. The nitrate solution after adsorption with chitosan bentonite nanocomposite films was filtered with Whatman 0.45 mm

filter paper. One mL HCl solution was added to the solution after filtration and fed to UV vis spectrophotometer for analysis.

3.6.2 Effect of Various Parameters on Adsorption of Nitrate Nitrogen by Fe-CH-NSP and Chitosan-Bentonite Nanocomposite Films

The iron-loaded chitosan nutmeg shell powder and nanocomposite films synthesized in the laboratory were used for the removal of nitrate from synthetically prepared wastewater. First, the effect of pH on nitrate removal with Fe-CH-NSP was studied by keeping the initial concentration at 50 ppm and adsorbent concentration as 0.05 g/ 100 mL of adsorbate solution. pH was varied from 2 to 12, and the bottles were shaken in a temperature-controlled incubated shaker set at 120 rpm and 30°C for 90 minutes. The pH was adjusted by adding 0.1N HCl or 0.1 N NaOH. The solutions after adsorption were vacuum filtered and analyzed. The effect of temperature on adsorption was studied, keeping pH as 8.0 and time as 90 minutes. The initial concentration and adsorbent dosage were 50 mg/L and 0.05 g/ 50 mL, respectively, and the temperature of adsorption was varied from 30°C to 70°C. After adsorption experiments, the solution with Fe-CH-NSP was vacuum filtered and kept for analysis. The effect of pH on nitrate removal by chitosan bentonite nanocomposite films was conducted by contacting 50 mg/L solution with 0.1g of the adsorbent. The volume of the solution taken was 100 mL. The solution was shaken for one hour at an agitation speed of 120 rpm. The pH was varied from 2-12. The temperature influence of nanocomposite films on nitrate adsorption was studied by changing the temperature from 30°C to 70°C in a 100 mL nitrate solution of concentration 70 mg/L. The amount of adsorbent added was 0.1g. The solution with CH-B-NCF was filtered using Whatman 0.45 mm filter paper. The consequential filtrate solution was

analyzed using a UV vis spectrophotometer. After conducting batch experiments, the efficiency and adsorption capacity were evaluated.

3.6.3 Equilibrium Studies for Nitrate Removal Using Fe-CH-NSP and Chitosan-Bentonite Nanocomposite Films

The equilibrium studies on nitrate uptake with chitosan bentonite nanocomposite films were carried out by varying the initial concentration from 20 mg/L to 100 mg/L. 0.1 g adsorbent was added to a 100 mL nitrate solution. Then the flasks were shaken in a temperature-controlled incubated shaker at 120 rpm and 30°C until equilibrium concentration between the adsorbent and adsorbate was attained. The filtered solution after adsorption was analyzed for residual nitrate concentration. Initial concentrations varying from 20 ppm to 120 ppm of 100 mL nitrate solution was taken for the equilibrium study with Fe-CH-NSP. 0.1 g of Fe-CH-NSP was added, and the experiments were done at temperature, 30°C. The isotherm model represents an equilibrium between adsorbate and adsorbent. Four equilibrium models were analyzed in the present study. Langmuir, Freundlich, Tempkin, and Dubinin-Radushkevich models were applied to equilibrium data to represent the equilibrium between nitrate in the adsorbent and adsorbate. Langmuir model represents monolayer adsorption. In the Langmuir model, adsorbent has a finite number of identical sites, low coverage and identical heats of adsorption due to homogeneous sites (Xing Xu *et al.*, 2013 *b*). Adsorbed molecules are not interactive according to Langmuir model. In the Freundlich model, adsorption takes place in homogeneous sites of the adsorbent. Nitrate is adsorbed in a heterogeneous surface of the adsorbent by the Freundlich model. The Tempkin isotherm model was used to evaluate the adsorption potential of the adsorbent. According to Tempkin isotherm, a linear decrease of adsorption energy takes

place as the degree of achievement of the sorption centers of an adsorbent is increased (Hameed and Daud, 2008). The D-R isotherm is used to measure the apparent energy of adsorption. The Langmuir model, Freundlich, Tempkin and D-R isotherm equations are given by the following equations.

$$q_e = \frac{q_m K_L C_e}{1 + K_L C_e} \quad (3.4)$$

$$\frac{C_e}{q_e} = \frac{1}{K_L q_m} + \frac{C_e}{q_m} \quad (3.5)$$

$$q_e = K_f C_e^{\frac{1}{n}} \quad (3.6)$$

$$\ln q_e = \ln K_f + \frac{1}{n} \ln C_e \quad (3.7)$$

$$q_e = B \ln A + B \ln C_e \quad (3.8)$$

$$\ln q_e = \ln q_s - K_{ad} D^2 \quad (3.9)$$

Equation (3.4) represents the Langmuir model, and equation (3.5) represents the linearized form of Langmuir equation. Equation (3.6) represents the Freundlich model, and (3.7) represents the linearized form of Freundlich equation. The equation (3.8) and equations (3.9) represent Tempkin and D-R isotherm models, respectively. C_e represents the equilibrium concentration of the solution in mg/L, q_e is the adsorption capacity in mg/g at equilibrium, q_m is related to the maximum adsorption capacity (mg/g), and K_L is the Langmuir adsorption constant and is related to the energy of adsorption. q_m and K_L is calculated from the slope and intercept of the plot between C_e vs. C_e/q_e . The values K_f and n are derived from the intercept and slope of the graph between $\ln C_e$ and $\ln q_e$. K_f is the Freundlich constant, which represents adsorption capacity ($\text{mg/g}(\text{L}/\text{mg})^n$), and the constant n represents adsorption intensity

(Hernandez-Apaolaza, L. and F. Guerrero, 2008). 'A' is Tempkin isotherm equilibrium binding constant (L/g), and B is constant related to the heat of sorption in kJ/mol. The Tempkin isotherm constant b_T is calculated as,

$$b_T = \frac{RT}{B} \quad (3.10)$$

Where R is the universal gas constant and T is the temperature. In equation 3.9, q_s , K_{ad} , and D are theoretical isotherm saturation capacity (mg/g), Dubinin-Radushkevich isotherm constant related to mean sorption energy (mol^2/kJ^2), and Polanyi potential respectively. The mean free energy, E for removing a molecule from its sorption site to infinity is related to K_{ad} as

$$E = \frac{1}{\sqrt{-2K_{ad}}} \quad (3.11)$$

The value of $E > 8$ kJ/ mole point to chemical sorption and less than 8 kJ/ mol designate physisorption.

3.6.4. Kinetic Studies for Nitrate Removal Using Fe-CH-NSP and Chitosan-Bentonite Nanocomposite Films

The kinetic studies were conducted by shaking 100 mL of 70 ppm solution containing 0.1 g adsorbent. The time was varied between 20 minutes to 120 minutes. The temperature was kept at 30°C, and the agitation speed was 120 rpm. For kinetic studies using Fe-CH-NSP, 100 ppm nitrate solution at pH 8.0 was agitated for time intervals 30 to 180 minutes at 30 °C and 120 rpm. 0.1 g adsorbent was added to 100 mL of adsorbate solution and mixed thoroughly. After shaking, the solutions were filtered and analyzed in a UV vis spectrophotometer. The kinetic data were fitted to Lagergren's pseudo-first-order, pseudo-second-order, second-order, intraparticle diffusion model and Dunwald-Wagner diffusion model to test the kinetics of adsorption of nitrate on the surface of both adsorbents

Lagergren equation is given by equation (3.12), pseudo-second-order equation is represented by equation (3.13), the second-order equation is given in equation (3.14), intraparticle diffusion equation is given in (3.15) and Dunwald-Wagner diffusion model equation is represented in equation (3.16).

$$\ln\{(q_e - q_t)\} = \ln q_e - k_1 t$$

(3.12)

$$\frac{t}{q_t} = \frac{1}{k_2 q_e^2} + \frac{t}{q_e} \quad (3.13)$$

$$\frac{1}{q_e - q_t} = \frac{1}{q_e} + K_2 t \quad (3.14)$$

$$q_t = k_d t^{0.5} \quad (3.15)$$

$$\log\left(1 - \left(\frac{q_t}{q_e}\right)^2\right) = -\frac{k_{DW}}{2.303} \times t \quad (3.16)$$

k_1 is the Lagergren pseudo first order constant (min^{-1}), k_2 is the pseudo second order rate constant for adsorption ($\text{g mg}^{-1} \text{min}^{-1}$), K_2 is the second order rate constant ($\text{g mg}^{-1} \text{min}^{-1}$), k_d ($\text{mg g}^{-1} \text{min}^{-1/2}$) is the rate constant for intraparticle diffusion and k_{DW} is the Dunwald-Wagner rate constant. q_e is the amount of anion adsorbed at equilibrium and q_t is the amount of anion adsorbed at time t in mg/g .

3.6.5 Thermodynamic Studies For Nitrate Removal Using Fe-CH-NSP and Chitosan-Bentonite Nanocomposite Films

The thermodynamic investigation for nitrate uptake with Fe-CH-NSP was achieved by conducting batch adsorption experiments at different temperatures ranging from 30 to 70 degree celsius. The initial solution concentration was 50 mg/L . The adsorbent dosage was 0.05g /50 mL. pH was maintained at 8.0, and

shaking speed was 120 rpm. The final concentration was measured after 90 minutes using UV vis spectrophotometer at 220 nm. The time of shaking, initial concentration, pH, and adsorbent dosage was 60 minutes, 70 ppm, 4, and 0.1g/100mL, respectively, for adsorption with chitosan-bentonite nanocomposite films. The thermodynamic constants such as Gibbs free energy, the thermodynamic equilibrium constant, entropy change, and enthalpy change was determined.

The thermodynamic equilibrium constant is determined using the equation given below (Mehmet Ugurlu and M Hamdi Karaoglu, 2011).

$$K_d = \frac{C_0 - C_t}{C_t} \left(\frac{V}{m} \right) \quad (3.17)$$

$(C_0 - C_t)$ is the concentration of nitrate in the adsorbent and C_t is the concentration in the solution in mg/L. Thermodynamic parameters of adsorption like Gibbs free energy change (ΔG) kJ/mol, enthalpy change (ΔH) kJ/mol and entropy change (ΔS) kJ/mol K are determined using equations (3.18), (3.19) and (3.20) respectively.

$$\Delta G = -RT \ln K_d \quad (3.18)$$

$$\Delta G = \Delta H - T\Delta S \quad (3.19)$$

$$\ln K_d = \frac{\Delta S}{R} - \frac{\Delta H}{RT} \quad (3.20)$$

R is the universal gas constant in J/mol K, and T is the absolute temperature in K.

3.6.6 Response Surface Methodology for Nitrate Nitrogen Removal Using Nanocomposite Films

The design of experiments using Minitab was used to develop the model equation and optimization of nitrate removal using chitosan-bentonite

nanocomposite films. Conventional methods of changing one parameter and keeping the other influencing parameters constant and performing the adsorption experiments are time-consuming. When more than one variable influences a process, the correct approach is to use a factorial method. Response surface methodology consists of a group of empirical techniques devised to generate the relationship between a group of controlled experimental parameters and measured responses. The advantage of RSM is that it is cost-effective, smooth working, and accurate for the optimization of the output response. Surface plots or contour plots are used to represent the response graphically. The Box-Behnken method demands minimum experimental runs and is used for the optimization of three or higher number of variables affecting the process (Batool *et al.*, 2015). The design of experiments was carried out first using initial concentration, pH, time, and temperature. Then the experiments were conducted. Efficiency was found out and analyzed using RSM.

The response surface is given by $Y = (X_1, X_2, X_3 \dots X_K)$, if all the variables are assumed to be measurable. Y is the efficiency of nitrate removal by adsorption which is called response variable and X_i is called variables of action called factors. The second-order model is assumed in RSM. The mathematical model equation of the second order was developed using response surface methodology, and an optimal set of parameters that maximize the efficiency was found out. The mathematical model equation representing Box- Behnken design is given by equation 3.21

$$Y = \beta_0 + \beta_1 X_1 + \beta_2 X_2 + \beta_3 X_3 + \beta_4 X_4 + \beta_{11} X_1^2 + \beta_{22} X_2^2 + \beta_{33} X_3^2 + \beta_{44} X_4^2 + \beta_{12} X_1 X_2 + \beta_{13} X_1 X_3 + \beta_{14} X_1 X_4 + \beta_{23} X_2 X_3 + \beta_{24} X_2 X_4 + \beta_{34} X_3 X_4 \quad (3.21)$$

The four factors in the present study were designated as initial concentration (X_1), pH (X_2), time (X_3) and temperature (X_4). They were prescribed in three levels coded as +1 for high, 0 for intermediate and -1 for low value. β_0 is a constant, $\beta_{12}, \beta_{13}, \beta_{14}, \beta_{23}, \beta_{24}, \beta_{34}$ are called interaction coefficients, $\beta_{11}, \beta_{22}, \beta_{33}, \beta_{44}$ are quadratic coefficients, $\beta_1, \beta_2, \beta_3$ and β_4 are regression coefficients for linear effects and Y is the response variable under study. Linear regression coefficient (R^2) between experimental and predicted value of Y was determined to find the quality of fit of model. Response optimizer of RSM gave the optimum conditions of operating parameters for maximum removal.

The Box-Behnken method under the response surface methodology of Minitab was used for the optimization of nitrate removal using chitosan-bentonite nanoclay adsorbent. All the experiments were conducted at 30°C temperature and 120 rpm shaking speed according to the design of experiments provided by Box Behnken design. A total of 27 experimental runs were conducted batchwise at pH 4.0. pH was adjusted by 0.1 N NaOH and 0.1 N HCl. After 27 sets of batch experiments, the response surface was analyzed. Response optimizer gave the optimum values of initial concentration, temperature, pH, and time for maximum removal. Surface plots showing the combined effect of variables were plotted.

3.6.7 Desorption Studies of Nitrate Nitrogen with CH-B-NCF

The desorption study is essential to get information regarding the reusability of the adsorbent. In the present study, first adsorption experiments were conducted at 120 rpm and 30°C. For the first cycle of adsorption-desorption experiments, 0.1 g of nanocomposite films were added to 100 mL of 60 ppm nitrate solution. The pH of the nitrate stock solution was maintained at 4.0 by adding 0.1N HCl. The solution was shaken for 60 minutes in a

temperature-controlled incubated shaker, and after adsorption, the residual solution was filtered and analyzed using a UV vis spectrophotometer. After adsorption, the nanocomposite films were washed with HPLC grade water to remove the residual nitrate ions. The adsorbent films were then dried in an oven. The dried adsorbents were then added to the stripping solution. The regenerating solution used was 100 mL of 1 M NaCl at pH 4.0. Then the bottle was placed in an incubated shaker and agitated for 60 minutes at room temperature. Then the solution was filtered and analyzed for nitrate in the UV vis spectrophotometer. Percentage desorption was determined. The same procedure was repeated. Five cycles of adsorption-desorption experiments were conducted, and the time of reuse was analyzed for chitosan-bentonite nanocomposite films.

3.6.8 Adsorption Using Nanocomposite Films for Ammonia Nitrogen

The adsorption efficiency of chitosan bentonite nanocomposite films towards ammonia nitrogen is investigated by performing batch adsorption experiments. To find the effect of pH on adsorption efficiency, 50 mL of solution was agitated with 0.1 g of adsorbent. The concentration of the solution was 50 mg/L. The solution was taken out after one hour and tested for residual ammonia nitrogen concentration. The pH was adjusted with 0.1 M HCl or 0.1 M NaOH. The effect of temperature on adsorption was studied, keeping pH 6.0 and time as 90 minutes. The initial concentration and adsorbent dosage were 50 mg/L and 0.1 g/50 mL, respectively, and the temperature of adsorption was varied from 30°C to 70°C.

For isotherm studies, 50 mL of ammonium solution having different initial concentration was agitated with 0.1 g of chitosan- bentonite nanocomposite films. The initial concentration was varied from 10 mg/L to 50

mg/L. The time and speed of agitation were 100 minutes and 120 rpm, respectively. The isotherm data obtained were analyzed with Langmuir and Freundlich isotherm models. The kinetic studies of adsorption were performed on a series of solutions with an initial concentration of 28 mg/L and pH six at different time intervals (20, 40, 60, 80, 100, 120, and 140 minutes) until equilibrium was reached. The amount of adsorbent used was 0.1 g/ 50mL. The temperature and agitation speed were maintained at 30⁰C and 120 rpm. After shaking, the solutions were analyzed in the UV vis spectrophotometer at 430 nm. The kinetic data were fitted to Lagergren's pseudo-first-order, pseudo-second-order, second-order, intraparticle diffusion model, and Dungwald-Wagner film diffusion model to test the kinetics of adsorption of ammonium on the surface of chitosan-bentonite nanocomposite films (Zhu *et al.*, 2011). Thermodynamic parameters ΔG , ΔH , and ΔS , were evaluated from the data obtained from the study on the effect of temperature.

In the present work, 0.5 M NaOH solution has been used for desorption experiments. 50 mL of 0.5 M NaOH solution was mixed with 2 g of chitosan-bentonite nanocomposite films laden with ammonium ions. The mixture was stirred for 30 minutes at an agitation speed of 120 rpm at room temperature. The adsorbent residue after shaking was then separated from the solution using Whatman 0.45 mm filter paper. It was then washed with 50 mL of distilled water for 10 minutes. The nanocomposite films obtained after washing was dried at 100⁰C for 3 hrs. The study on pH effect varying from 2-10 and effect of temperature study (30⁰C to 70⁰C) were repeated with the regenerated adsorbents.

3.6.9 Design of Experiments for Ammonia Nitrogen Adsorption Using Chitosan-Bentonite Nanocomposite Films

Adsorption experiments were performed according to the design of experiments given by Box-Behnken design under the response surface methodology of Minitab 18. Optimization of operating parameters for ammonia nitrogen removal was carried out using RSM. Response surface methodology was also used to study the interaction between variables and ANOVA (Analysis of variance). RSM gave 27 sets of experimental combinations. The parameters for the batch study were initial concentration, temperature, time, and pH. All the batch tests were conducted at 303 K and 120 rpm shaking speed. The pH was adjusted using 0.1N HCl and 0.1N NaOH. After adsorption, filtration was carried out using Whatman 0.45 mm filter paper. After filtration, the concentration of the solution was determined using a previously calibrated UV vis spectrophotometer at 430nm.

3.7 REMOVAL OF NITRATE NITROGEN IN CONTINUOUS FIXED BED ADSORPTION COLUMN USING CHITOSAN-BENTONITE NANOCOMPOSITE FILM AS ADSORBENT

Continuous removal of nitrate-nitrogen from aqueous solution was accomplished using a fixed bed adsorption column. A schematic diagram showing the principle of working of the packed bed adsorption column is shown in Fig. 3.6.

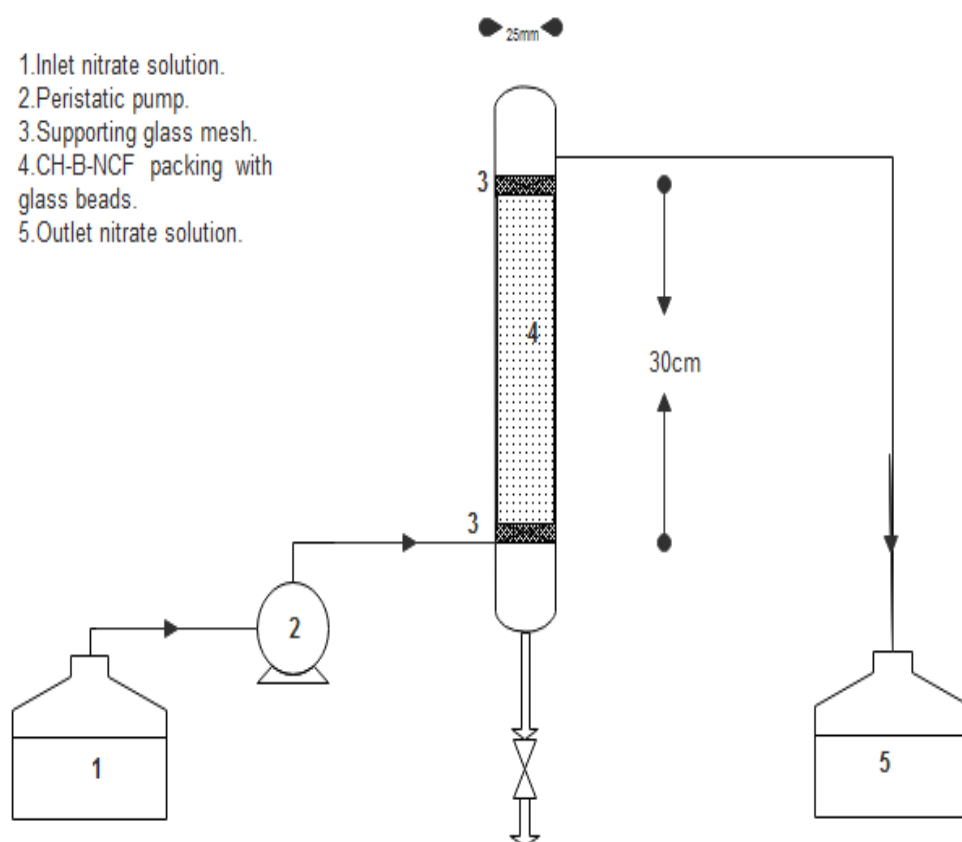


Fig. 3.6. Schematic of the experimental packed bed column with proper dimensions

Fixed bed column studies were conducted using a perspex glass column of 30 mm outer diameter, 25 mm inner width and 300 mm height (Lim and Aris, 2014). The schematic diagram of the nitrate adsorption column is shown in Fig 3.6. The column was packed with the required amount of adsorbent uniformly mixed with glass beads. The introduction of glass beads helps to retard the fluidization and bypass flow of the bed. Two supporting layers of pre-equilibrated glass mesh were provided at the bottom and top of the column to prevent the loss of adsorbent during the filtration process. Five liters of nitrate solution was stored in a glass vessel. A silicon tube of 2 cm diameter and 2 mm

thickness was used to connect the glass vessel containing the stock solution, peristaltic pump, and the glass column. The trapped air in the bed was removed by wetting the column with deionized water. The column was charged with a nitrate solution of 70 mg/L initial concentration in the upflow mode. The influent flow rate of 6mL/min, 10 mL/min, and 15 mL/min are achieved with the help of a peristaltic pump. The calibration details of the peristaltic pump are given in (Annexure-III). The treated nitrate solution was collected at various time intervals until the bed got saturated. The nitrate solution after adsorption was filtered using Whatman 0.45 mm filter paper and analyzed for residual nitrate concentration. Fig. 3.7 is the experimental set up for a fixed-bed column for nitrate removal. The effect of bed height and flow rate were studied for continuous experiments. All the tests were performed at room temperature. The adsorbent dosage for the study was 30% of the bed height. The pH of the nitrate solution was kept at 4 using 0.1 N HCl. The analysis of the breakthrough curve and the mathematical determination of column parameters are done. The mathematical modeling of the continuous adsorption system is also performed.



Fig. 3.7 Nitrate fixed bed column using CH-B-NCF

The column performance is evaluated by evaluating C_f/C_0 , where C_f is the effluent concentration, and C_0 is the influent concentration in mg/L, respectively. The nitrate adsorption breakthrough profiles were obtained from C_f/C_0 against time plots. Adsorbed anion concentration was also plotted against time to analyze the amount of nitrate adsorbed in each set of experiments. The adsorbed anion concentration in the bed is obtained using Eqn 3.22

$$C_{ad} = C_0 - C_f \quad (3.22)$$

The treated volume of nitrate solution collected at any time is given by equation 3.23

$$V_{eff} \text{ (mL)} = Q t_{total} \quad (3.23)$$

Q represents the volumetric influent flow rate in mL/min and t_{total} is the total flow time in minutes. The total adsorbed nitrate ion q_{total} (mg) is obtained by finding the area under the plot from the integral of adsorbed concentration C_{ad} versus time. The total adsorbed nitrate is given by equation 3.24 (Auta and Hameed 2014).

$$q_{total} = \frac{QA}{1000} = \frac{Q}{1000} \int_{t=0}^{t=t_{total}} C_{ad} dt \quad (3.24)$$

The total amount of nitrate ions delivered to the column m_{total} in mg is obtained from equation (3.25).

$$m_{total} = \frac{C_0 Q t_{total}}{1000} \quad (3.25)$$

Total removal percentage of $\text{NO}_3\text{-N}$ is the ratio of total adsorbed ion in the column to the total ion delivered to the column. Percentage total removal of nitrate ions is given by equation (3.26).

$$\% \text{ removal} = \frac{q_{total}}{m_{total}} \times 100 \quad (3.26)$$

The equilibrium nitrate uptake q_{eq} also known as the column maximum adsorption capacity, which is obtained by dividing the total anion adsorbed with mass of adsorbent (X) in the column. Equation 3.27 gives column maximum adsorption capacity

$$q_{eq} = \frac{q_{total}}{X} \quad (3.27)$$

At equilibrium, the unadsorbed nitrate ion concentration is given by equation 3.28

$$C_{eq} = \frac{m_{total} - q_{total}}{V_{eff}} \times 1000 \quad (3.28)$$

Three well-known models, Thomas model, Yoon Nelson model, and Adam Bohart model, were used in the present study for mathematical modeling. The various models applied to the column data is described below.

3.7.1 Thomas Model

The Thomas model is widely used for the design of the adsorption column and was developed in 1948. The model is often used to explain the breakthrough of the packed bed column and the parameters affecting the column. The underlying assumptions of Thomas or reaction model are: (i) negligible axial and radial dispersion in the fixed bed column; (ii) the adsorption is described by a pseudo-second-order reaction rate principle which reduces to Langmuir isotherm at equilibrium; (iii) constant column void fraction; (iv) consistent physical properties of the adsorbent solid-phase and the fluid phase; (v) isothermal and isobaric process conditions; (vi) the intraparticle diffusion and external resistance during the mass transfer processes are considered to be negligible (Jaafari *et al.*, 2004). The linearized

form of the Thomas model is given in equation 3.29. Parameters of the Thomas model were determined, and breakthrough curves were predicted

$$\ln\left(\frac{C_0}{C_f} - 1\right) = \frac{k_{Th}q_0m}{Q} - k_{Th}C_0t \quad (3.29)$$

where, k_{Th} (mL/min.mg) is the Thomas kinetic constant; q_0 (mg/g) is the maximum solid-phase concentration; C_0 (mg/L) is the influent nitrate concentration; C_f (mg/L) is the effluent concentration at time t ; m (g) the mass of adsorbent and Q is the volumetric influent flow rate. A linear plot of $\ln[(C_0/C_f) - 1]$ against time, t was employed to determine the values of q_0 and k_{Th} from the intercept and slope of the plot. The experimental column data has been compared with the data predicted by the Thomas model, and thus the model is validated.

3.7.2 Yoon Nelson model

Yoon and Nelson developed a model based on the assumption that the rate of decrease in the probability of adsorption of adsorbate molecules is proportional to the probability of the adsorbate adsorption and the adsorbate breakthrough on the adsorbent (Lim and Aris, 2014). The Yoon– Nelson model is a linearized model for a single component system and involves fewer column parameters. It gives time for 50% adsorbate breakthrough. The mathematical representation of the Yoon Nelson model is described in equation (3.30).

$$\ln \frac{C_f}{C_0 - C_f} = k_{YN}t - \tau k_{YN} \quad (3.30)$$

k_{YN} is the Yoon Nelson rate constant (minute⁻¹) and τ is time required for 50 % nitrate anion breakthrough in minutes. No other physical data is required in Yoon Nelson model and hence it is a straightforward model. A plot

of $\ln \frac{C_f}{C_0 - C_f}$ versus time will give the parameters of Yoon Nelson model. The fit of experimental data was checked using the model.

3.7.3 Adam Bohart model

Adam–Bohart model is used for the narration of the first part of the breakthrough curve, up to 10-50%. This model establishes the fundamental equations describing the relationship between C_t/C_0 and t in a fixed bed adsorption system (Lim and Aris, 2014). Adam Bohart model is based on the theory of surface reaction. The surface reaction theory assumes that equilibrium is not immediate; therefore, the rate of the adsorption is proportional to the adsorption capacity, which remains on the adsorbent. This approach focused on the estimation of characteristic parameters such as maximum adsorption capacity (N_0) and A-B kinetic constant (k_{AB}) using a quasi chemical kinetic rate expression. The Adam Bohart model expression is given in equation (3.31).

$$\ln \frac{C_f}{C_0} = k_{AB} C_0 t - \frac{k_{AB} N_0 Z}{U_0} \quad (3.31)$$

k_{AB} is the Adam Bohart kinetic constant (L/mg min). N_0 represents the saturation concentration (mg/L) and Z is the bed depth (cm). U_0 is the linear velocity (cm/min) and it was calculated from the volumetric flow rate and cross section area of the bed. A plot of $\ln \frac{C_f}{C_0}$ was made with time to get k_{AB} and N_0 . The column data was compared with the data predicted by the model and the linear regression coefficient between experimental data and predicted data was determined (Wan *et al.*, 2012)

3.8 SUMMARY OF THE CHAPTER

This chapter includes a detailed study on the various materials and methods used in the removal of nitrate-nitrogen with two composites, namely iron loaded chitosan nutmeg shell powder (Fe-CH-NSP) and chitosan-bentonite nanocomposite films. The materials and methods required for ammonia nitrogen adsorption with chitosan-bentonite nanocomposite films from aqueous solutions were also explained in this chapter. The synthesis and characterization of the nanomaterials are being discussed. The performance of chitosan bentonite nanoclay films for nitrate elimination in a fixed bed adsorption column has also been described. Modeling of the column using the Thomas model, Yoon Nelson model, and Adam Bohart model and their equations have been depicted in this chapter.

.....❁.....

CHAPTER 4

RESULTS AND DISCUSSION

4.1 INTRODUCTION

The risk produced by nitrogen contamination should be remediated to protect our ecosystem. Adsorption is an effective method for the wastewater discharges carrying nitrate nitrogen ($\text{NO}_3\text{-N}$) and ammonia nitrogen ($\text{NH}_4^+\text{-N}$). In the current study, two new kinds of adsorbents were synthesized, namely Fe-loaded chitosan nutmeg shell powder (Fe-CH-NSP) and chitosan bentonitenanocomposite films (CH-B-NCF). The adsorption of $\text{NO}_3\text{-N}$ with these adsorbents has been investigated. The removal of ammonia nitrogen with nanocomposite films has also been studied. The method of synthesis of the adsorbents and adsorption process has been explained in chapter 3 (Section 3.3). The characterization of synthesized adsorbents with SEM-EDAX, TEM, FTIR, TGA, and XRD have also been described in this chapter. Statistical validation by RSM has been carried out for adsorptive removal of both $\text{NO}_3\text{-N}$ and $\text{NH}_4^+\text{-N}$ with chitosan-bentonitenanocomposite films. The continuous adsorption study for nitrate-nitrogen has been carried out. The chitosan bentonitenanocomposite films were selected for the fixed bed column studies due to the following reasons: (1) Harsh chemicals are not used for the preparation of the nanocomposite films. (2) The effortless separation of nanocomposite films and uncomplicated column operation. The mathematical modelling of the fixed bed nitrate column is also included in this chapter.

4.2 BATCH ADSORPTION STUDY FOR NITRATE NITROGEN REMOVAL USING Fe-CH-NSP

Nutmeg shell powder and chitosan in a ratio of 10:1 were used as a source of biomaterial for the development of composite bio sorbent. The Fe-loaded nutmeg shell powder with chitosan as a bridging reagent was used in batch adsorption of nitrate-nitrogen from aqueous solution. The activation by iron nano particles increased the number of available binding sites (Francesca Pagnanelli, *et al.*, 2010)

4.2.1 Effect of pH and Temperature on Nitrate Removal by Fe-CH-NSP

The batch experiments to find the effect of pH and temperature on adsorption efficiency was conducted at room temperature and 120 rpm speed. Fig. 4.1 shows the effect of pH and temperature on percent removal of nitrate-nitrogen onto Fe-CH-NSP. The effect of pH study shows that acidic medium is favourable for adsorption. The percent removal of NO₃-N obtained for pH of 2, 4, 6, 8, 10 and 12 are 60, 62, 78, 80, 42, and 30 % respectively. A higher replacement of nitrate-nitrogen was seen in the pH range of 6 to 8. Maximum removal was (80%) was obtained at pH 8. It is observed that adsorption of nitrate decreased after pH 8. The formation of iron based oxides on the surface of Fe- loaded chitosan nutmeg shell powder might be takes place at pH 8, and after that the surface doesn't provide any electrostatic attraction to the nitrate anions (Ahmed *et al.*, 2016). The acidic or alkaline nature of the solution affects the degree of speciation of nitrate ions. The -COOH, -COO, -OH and Fe³⁺ groups in the composite are playing a vital role in the adsorption process. The easy protonation of the functional groups at acidic pH causes an increase in adsorptive capacity. At extreme acidic conditions the protonation of nitrate ions and the solution enriched with H⁺ ions causes a slight decrease in the

adsorption of nitrate anions. As pH increases, the electrostatic interaction between anions and adsorbent increases and adsorption capacity is increased. At high alkaline conditions, a stronger contest is there between the OH⁻ ions and NO₃⁻ ions to the adsorbent active sites. Hence poor adsorption is observed at pH 10 and pH 12. According to Pearson's principle of hard and soft acids and bases (HSAB) nitrate anions are categorized as hard acids. Also, the Fe³⁺ incorporated chitosan acts as a hard base. So a hard acid- base contact exists amid them (Pahlavanzadeh, *et al.*, 2012).

The analysis of the effect of temperature on the percentage of nitrate-nitrogen uptake shows that the NO₃-N uptake efficiency increased from 20°C to 30°C and reached a maximum and then slows down when the temperature was raised from 30°C to 70°C. The adsorption of NO₃-N onto Fe-CH-NSP at different temperatures 30°C-70°C showed a reduction in adsorption with the raise in temperature. The percent removal of NO₃-N obtained for temperatures 20, 30, 40, 50, 60, and 70°C were 87.6, 88.04, 86.96, 85.71, 84.18, and 81.2 % respectively for an initial nitrate concentration of 50 mg/L. Favourable adsorption could be seen in a range of 30°C-60°C. Maximum removal was found at 30°C. All other experiments were performed at this temperature. At higher temperatures, desorption of adsorbed nitrate ions may lead to a decreased adsorption capacity (Manalet *et al.*, 2008).

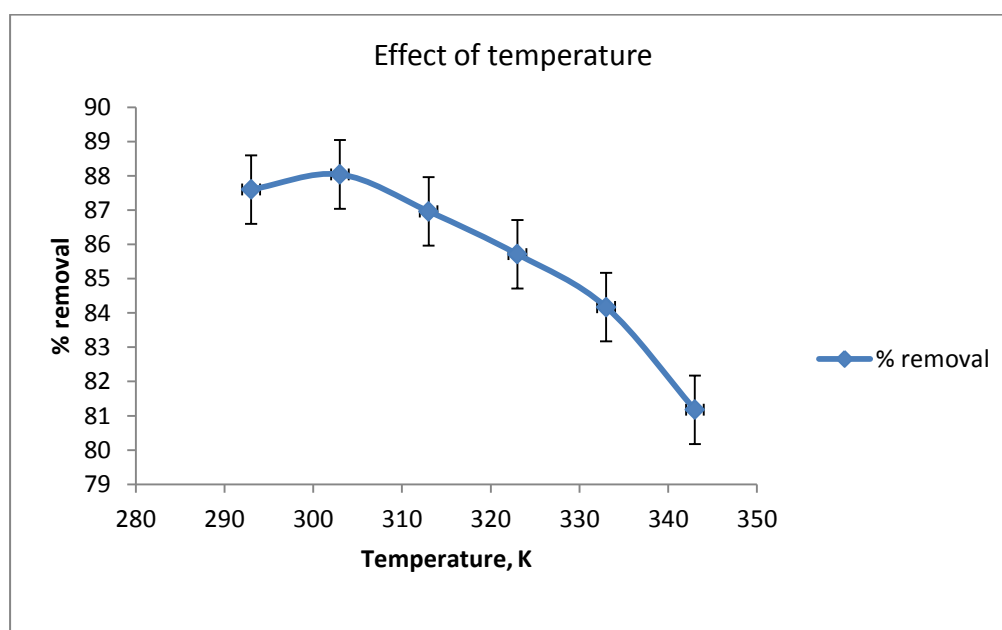
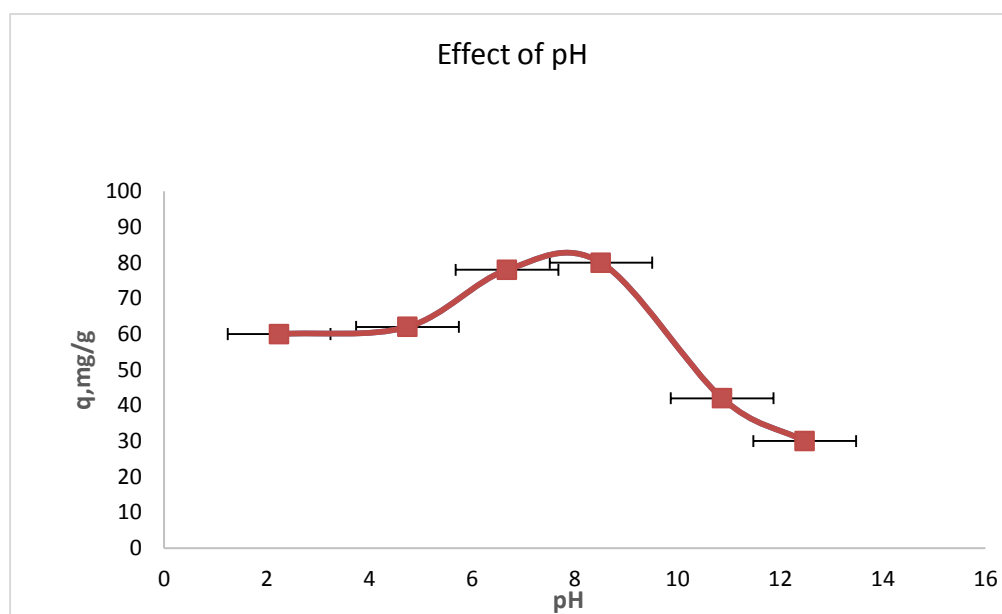


Fig 4.1 Effect of pH and temperature on adsorption efficiency removal of $\text{NO}_3\text{-N}$ onto Fe-CH-NSP.

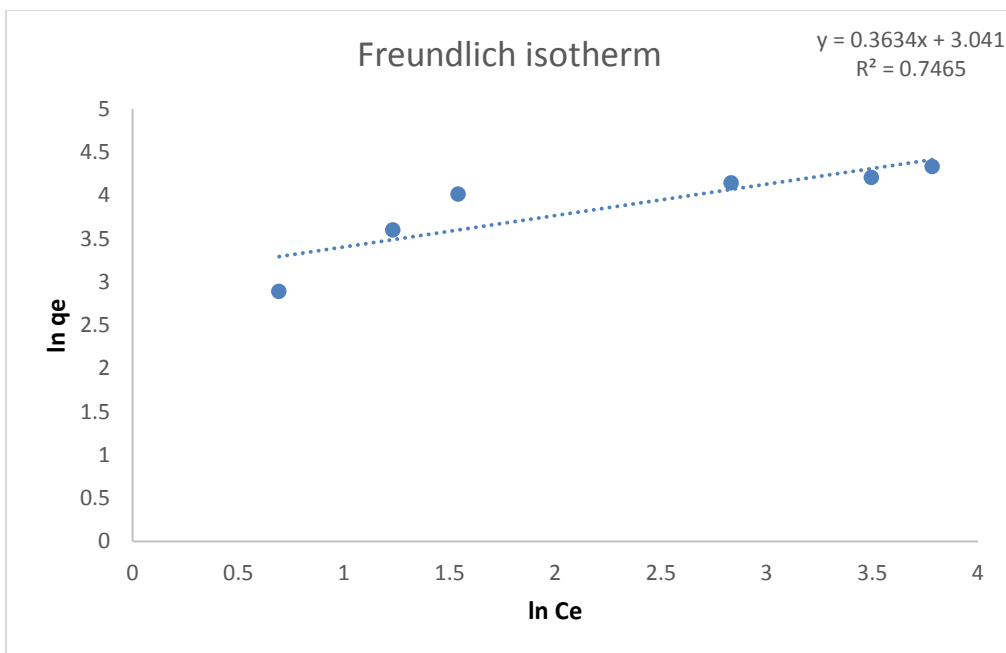
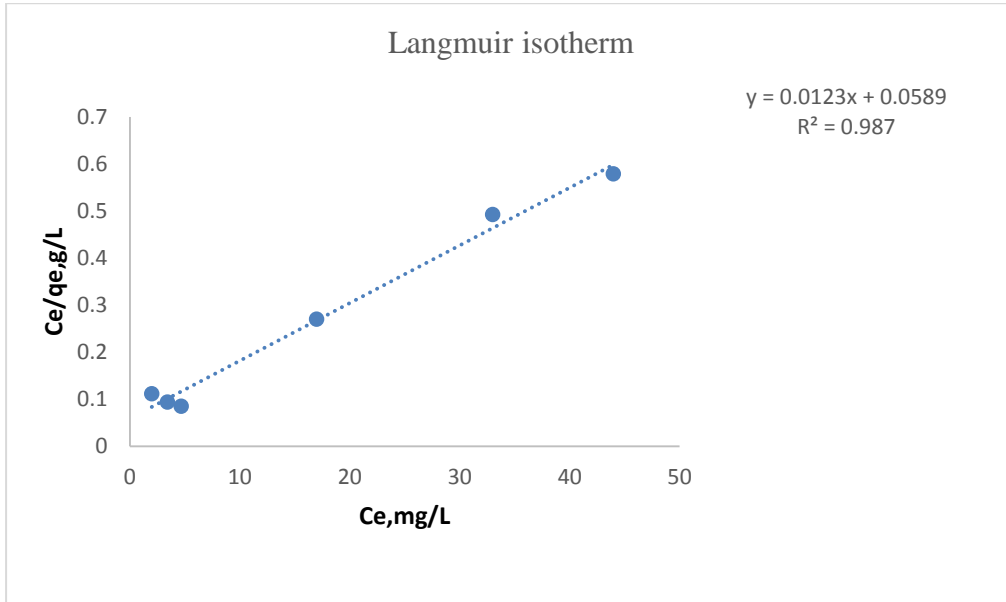
4.2.2 Adsorption Isotherms of Nitrate Nitrogen Removal onto Fe-CH-NSP

Four adsorption isotherms, Langmuir, Freundlich, Tempkin, and Dubinin-Radushkevich (D-R) isotherms were analyzed for the removal of $\text{NO}_3\text{-N}$ with Fe-CH-NSP. The isotherm plots are shown in Fig 4.2. The parameters of equilibrium isotherm have been summarized in Table 4.1. Langmuir, Freundlich, Tempkin, and D-R isotherm plots had R^2 values of 0.99, 0.75, 0.86, and 0.98, respectively. The regression coefficients of four models were in the order of Langmuir>D-R>Tempkin>Freundlich. The equilibrium data fitted more to the Langmuir isotherm model. The maximum adsorption capacity q_m calculated from the Langmuir Isotherm model was 83.33 mg/g. R_L is a dimensionless separation factor calculated from the Langmuir isotherm model. For positive adsorption, the value of the separation factor should lie between zero and one. The case of $R_L=0$, occurs if k is very large, which means that adsorption is too strong. That is why $R_L=0$ is named irreversible. The condition of $R_L = 1$ can occur only if $k=0$. This means that the adsorption isotherm is a straight line. So this is linear adsorption. For unfavorable adsorption the value of R_L is greater than 1. In the current study values of R_L obtained for concentrations 20, 40, 60, 80 100 and 120ppm was 0.242, 0.121, 0.081, 0.0604, 0.048, and 0.040 respectively. Here the values of R_L at all concentrations are less than one, which shows that adsorption is favorable. The inverse relationship between R_L and initial concentration indicates that favorable removal could be observed at higher initial concentrations. The Freundlich constants K_f and $\frac{1}{n}$ have been calculated and obtained as 20.9 and 0.363, respectively. The value of $\frac{1}{n} < 1$ indicates the favorable nature of adsorption, and the value of $\frac{1}{n}$ more close to zero shows that the surface is more heterogeneous (Qili *et al.*, 2015).

The D-R isotherm assumed that the characteristics of the sorption curves are related to the porosity of the adsorbent (Foo and Hameed 2010). The high regression coefficient of Dubinin-Radushkevich isotherm ($R^2=0.98$) substantiates the porous nature of the prepared Fe-CH-NSP particles. The theoretical saturation capacity q_s and Dubinin-Radushkevich isotherm constant K_{ad} were obtained as $q_s = 69.55$ mg/g, and $K_{ad}=1.0 \times 10^{-6}$, respectively. The value of q_s obtained from D-R isotherm is almost equivalent to the maximum adsorption capacity calculated from Langmuir isotherm, $q_e=83.33$ mg/g. The energy required by a molecule to move from its site to infinity is called the mean free energy, E (Sudipta *et al.*, 2009). The value of E computed using D-R isotherm was obtained as $E=0.707$ kJ/mol. The value of Tempkin isotherm equilibrium binding constant (A) was obtained as $A=3.0312$ L/g. The constant related to the heat of sorption is obtained as $B=15.61$ kJ/mol. The constant related to heat of sorption $B < 25$ J/mol indicates physisorption. The relatively high value of value B indicates that both physisorption and ion exchange play a major role in the adsorption. The Tempkin isotherm constant is obtained as $b_T=161.38$ (Deepak *et al.*, 2017).

Table 4.1 Equilibrium parameters for adsorption of $\text{NO}_3\text{-N}$ on Fe-CH-NSP.

Langmuir			Freundlich			Tempkin			Dubinin-Radushkevich		
$q_{m,}$ (mg/g)	K_L (L/mg)	R^2	K_f (mg/g)(L/mg) ⁿ	n	R^2	A (L/g)	B (J/mol)	R^2	q_s (mg/g)	K_{ad}	R^2
83.33	0.2069	0.98	20.93	2.75	0.75	3.0312	15.61	0.86	69.546	1.00E-06	0.978



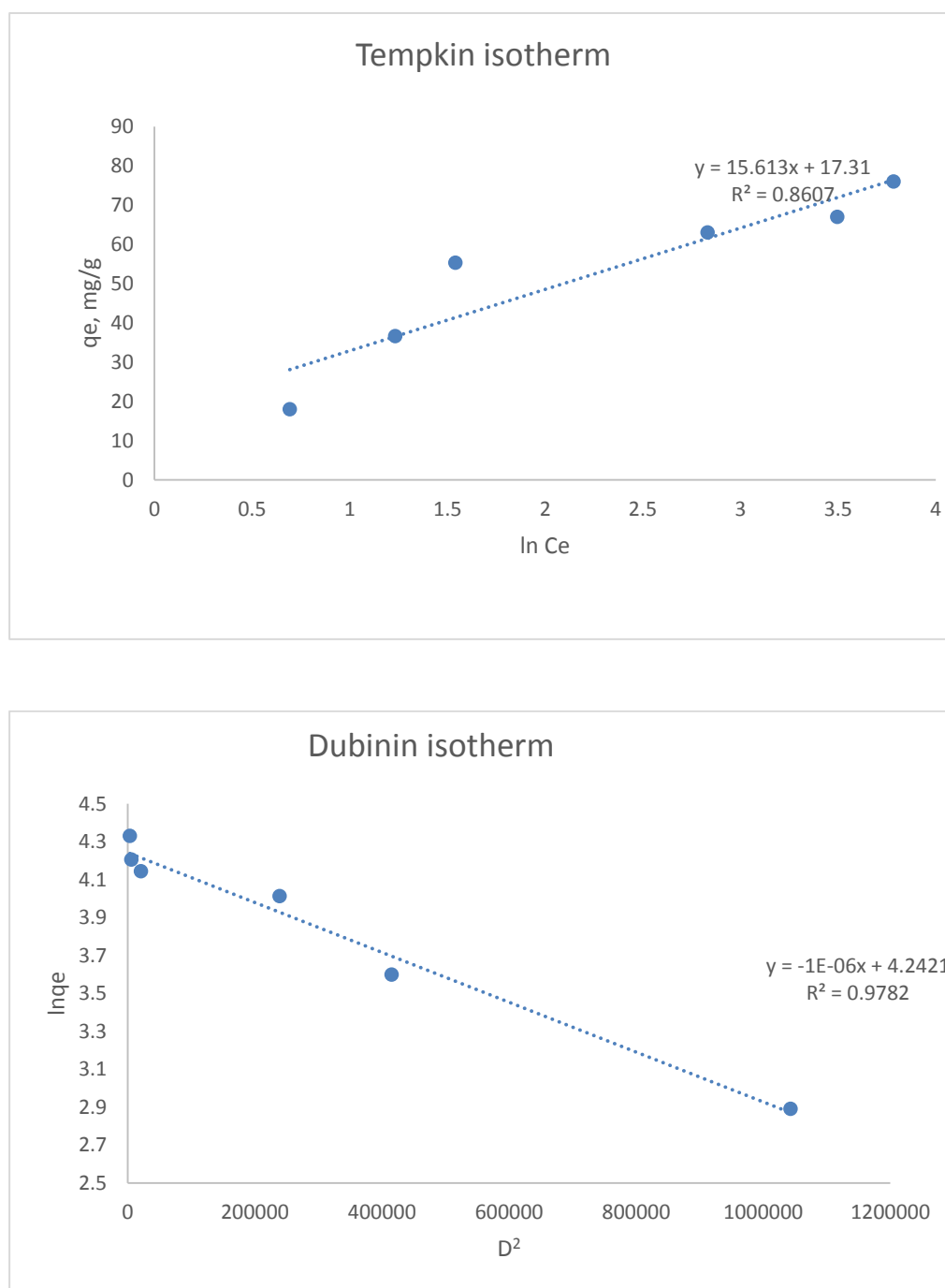


Fig 4.2 Langmuir, Freundlich, Tempkin and Dubinin-Radushkevich isotherm of $\text{NO}_3\text{-N}$ adsorption using Fe-CH-NSP.

The plot of comparison of four isotherm equilibrium q_e with experimental data is shown in Fig 4.3. The sorption competence of various adsorbents for removal of nitrate-nitrogen were 13.06 mg/g for iron nanoparticles synthesized by green tea leaves (Ting *et al.*, 2014), 27.55 mg/g for activated carbon prepared from sugar beet bagasse (Hakan and Gul, 2010), 52.8 mg/g for wheat straw resin (Xing *et al.*, 2010), 32.8 mg/g for pine sawdust (Anni *et al.*, 2014), 102.04 mg/g for magnetic amine cross-linked corn stalk (Wen *et al.*, 2016), and 26.13 mg/g for olive stone (Imen *et al.*, 2015). The maximum adsorption capacity of modified NSP, which is a local resource, is 83.33 mg/g which is higher or comparable with the results reported by others.

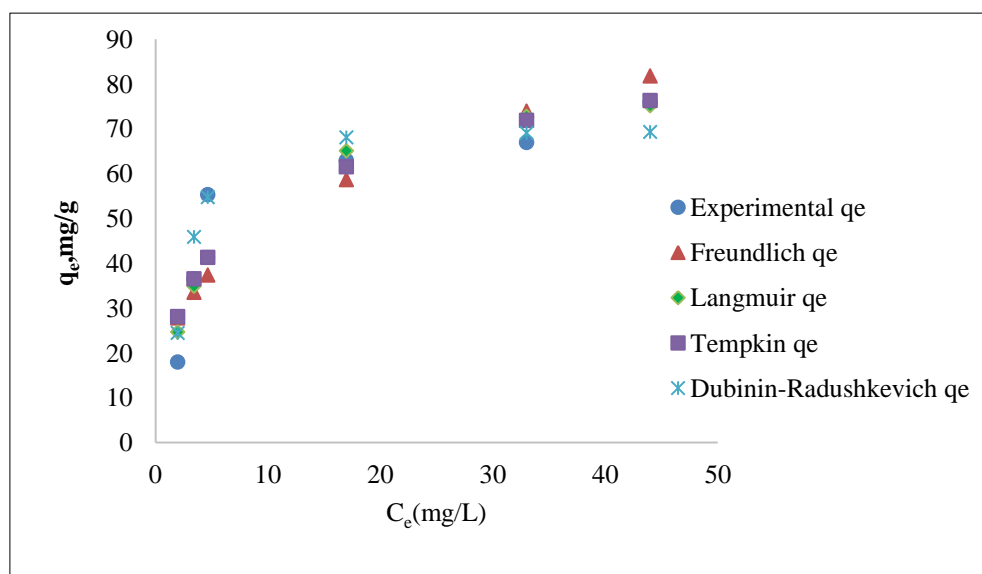
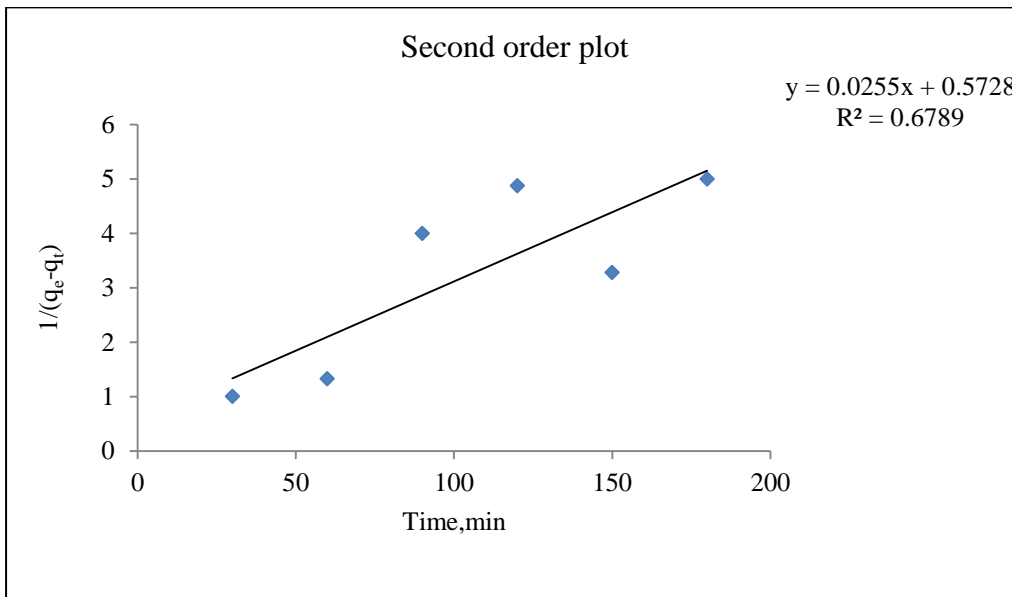
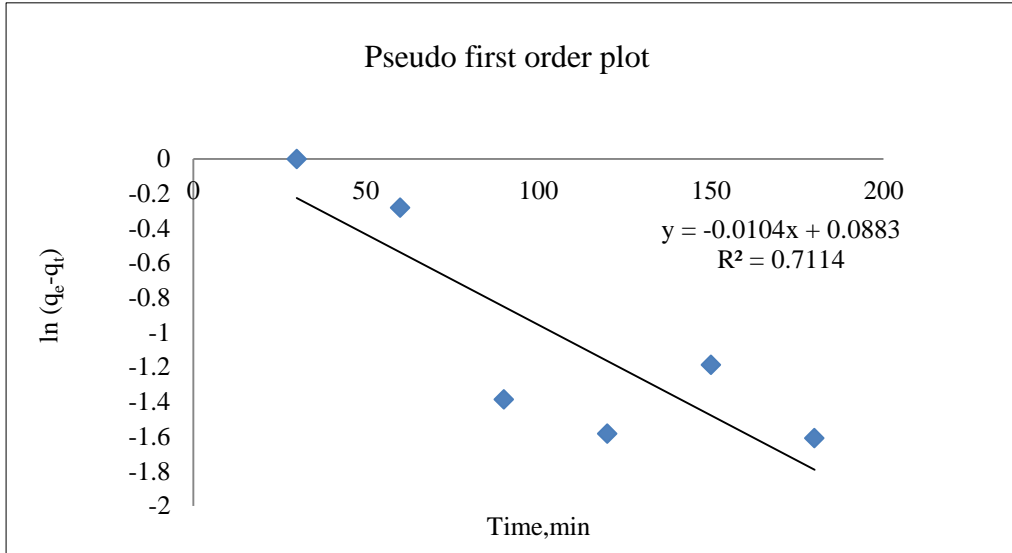


Fig 4.3 Equilibrium isotherms for $\text{NO}_3\text{-N}$ removal from aqueous solution onto Fe-CH-NSP.

4.2.3 Kinetics of Adsorption of NO₃-N onto Fe-CH-NSP.

Kinetic studies were conducted to investigate the velocity of adsorption, the controlling mechanism of adsorption, rate-limiting step, and parameters governing the sorption. The adsorption experiments were done at different time intervals and the residual nitrate concentration was measured in the UV-vis spectrophotometer. The difference in solute concentration between adsorbent and adsorbate causes significant removal within 60 minutes. The equilibrium was reached in 90 minutes (94.7%). The aggregation of nitrate anions and the unavailability of adsorption sites on Fe-CH-NSP results in a plateau after 90 minutes (Sachinet *al.*, 2011). Three kinetic reaction models, namely, the pseudo first order, pseudo second order, and the second order model were analyzed. The kinetic plots have shown in Fig 4.4. Two kinetic diffusion models, Morris–Weber intraparticle diffusion model and Dunwald-Wagner film diffusion model, were also analyzed in the present study. The kinetic constants and correlation coefficients for the three kinetic reaction models have presented in Table 4.2. The linear correlation coefficient for the pseudo-first-order ($R^2=0.71$) and second-order model ($R^2=0.68$) were lower compared to the pseudo-second-order model ($R^2=0.99$). The results point to that, data fits more to pseudo-second-order kinetics. The second order model was poorly fitting to the data. The pseudo first order model showed a little fit, which may be due to the reduction kinetics of nano zero valent iron. The calculated q_e value using pseudo second order kinetics is 50 mg/g, while the experimental q_e value was 47.5 mg/g. It was almost comparable to the q_e value of pseudo-second-order kinetics, which proves that the adsorption of NO₃-N using Fe loaded chitosan nutmeg shell powder is pseudo second order. The results suggested that nitrate removal by Fe loaded chitosan nutmeg shell powder is due to both adsorption and reduction but is dominated by adsorption kinetics (Ting *et al.*, 2014). The pseudo-second-order rate constant was obtained as 0.0006 g mg⁻¹ min⁻¹.



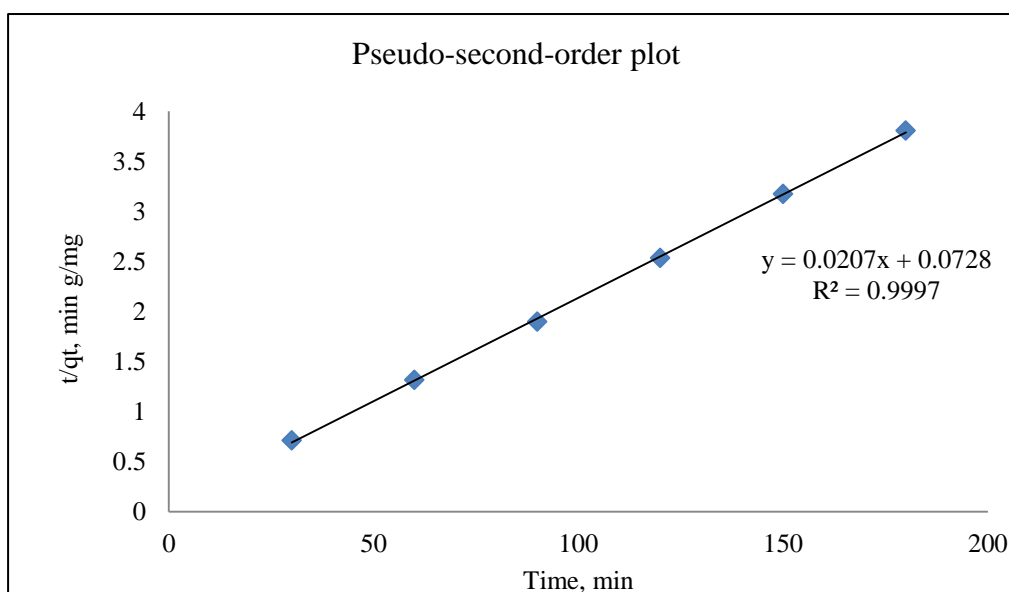


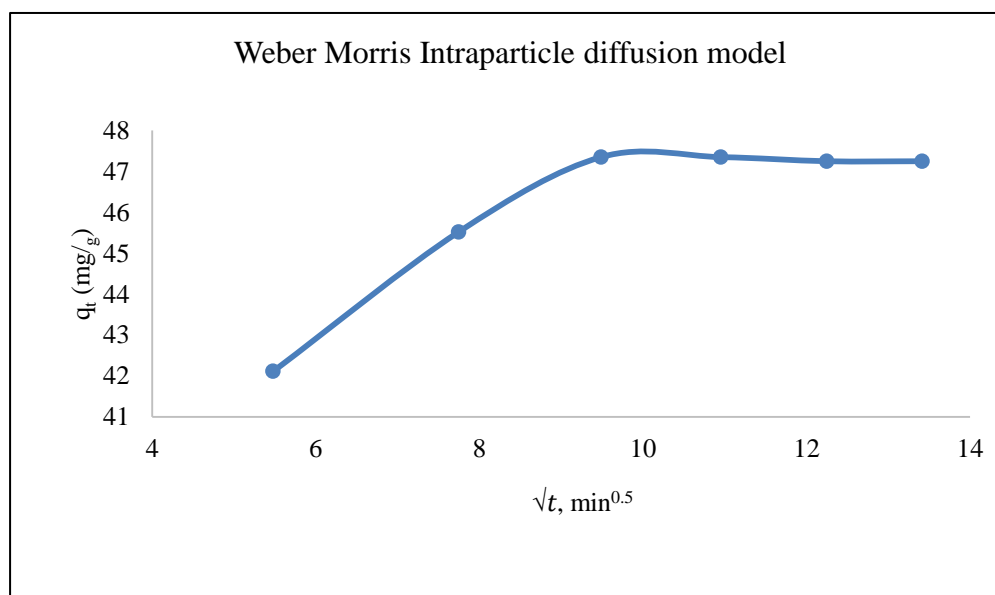
Fig 4.4 Kinetics of adsorption of nitrate nitrogen onto Fe-CH-NSP-pseudo first order, second order, and pseudo second order models.

Table 4.2 The kinetic constants and correlation coefficients for adsorption of $\text{NO}_3\text{-N}$ onto Fe-CH-NSP.

Experimental	Pseudo first order			Second order			Pseudo second order		
q_{exp} , mg/g	q_{eq} , mg/g	R^2	k_1 , min^{-1}	q_{eq} , mg/g	R^2	K_2 , $\text{g}\cdot\text{mg}^{-1}\cdot\text{min}^{-1}$	q_{eq} , mg/g	R^2	k_2 , $\text{g}\cdot\text{mg}^{-1}\cdot\text{min}^{-1}$
47.5	1.1	0.71	0.01	17.48	0.67	0.025	50	0.99	0.0006

Figure 4.5 represents Weber-Morris intraparticle diffusion plot and Dunwald-Wagner liquid film, diffusion model. In the present study, the intraparticle rate constant k_d is $0.609 \text{ mm}^2/\text{min}$ and intercept, C is 40.1,

respectively ($R^2=0.732$). The relatively big value of C indicates a more significant boundary layer effect (Alagumuthu. and Rajan 2010). In the Weber-Morris intraparticle diffusion plot the initial curve represents the boundary layer effect, and the straight line represents intra-particle-diffusion. Since the plot is not passing through the origin, the intraparticle diffusion is not the sole rate-limiting step. It indicates the possibility of both particle and pore diffusion in the adsorption process. The Dunwald-Wagner liquid film diffusion model is based on Fick's second law for diffusion into or out of a sphere Dunwald-Wagner rate constant is $k_{DW}=0.099 \text{ min}^{-1}$ ($R^2=0.71$). The diffusion coefficient in the biosorbent phase was calculated and obtained as $D_{DW}=1.31 \times 10^{-5} \text{ mm}^2 \text{ min}^{-1}$. The intraparticle diffusion and film diffusion constants and correlation coefficients for adsorption of $\text{NO}_3\text{-N}$ onto Fe-CH-NSP is given in Table 4.3.



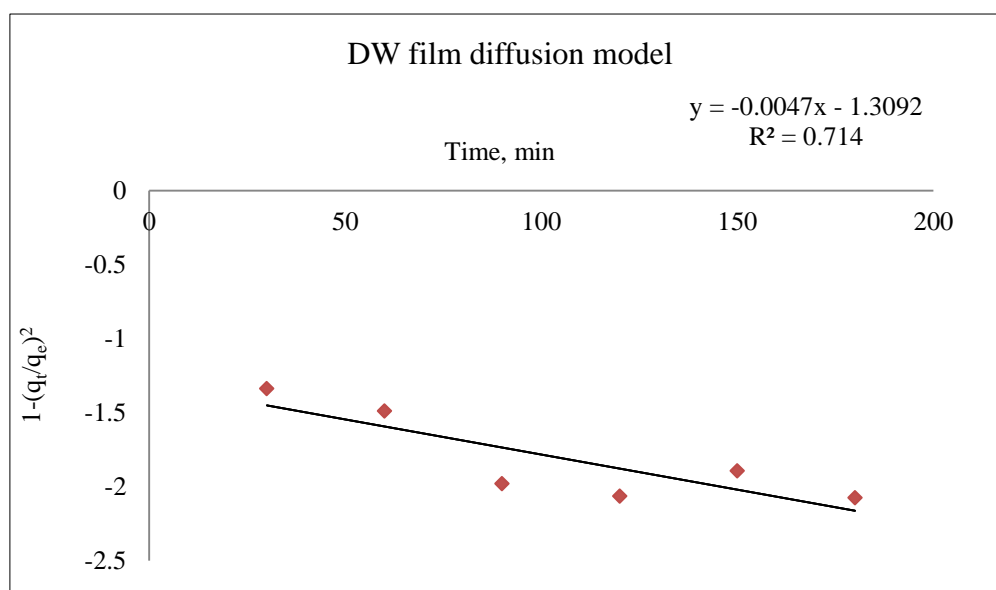


Fig 4.5 Kinetics of adsorption diffusion model of $\text{NO}_3\text{-N}$ onto Fe-CH-NSP, Weber-Morris intraparticle diffusion model and Dunwald-Wagner film diffusion model.

Table 4.3 The intraparticle diffusion and film diffusion constants and correlation coefficients for adsorption of $\text{NO}_3\text{-N}$ onto Fe-CH-NSP.

Intra-particle diffusion			Film diffusion		
$k_d, \text{mg/g min}^{-1/2}$	C, constant	R^2	$k_{DW} \text{min}^{-1}$	$D_{DW} \text{mm}^2/\text{min}$	R^2
0.61	40.1	0.73	0.009	1.3×10^{-5}	0.71

4.2.4 Effect of Temperature on Adsorption of Nitrate Nitrogen Using Fe-CH-NSP

The thermodynamic parameters were evaluated by conducting the adsorption of nitrate-nitrogen onto Fe-CH-NSP at varying temperatures. A decrease in adsorption efficiency was observed with an increase in temperature. The q_e values obtained for temperatures 30, 40, 50, 60 and 70⁰C were 44.02, 43.48, 42.86, 42.09, and 40.59 mg/g respectively for $C_0=50 \text{ mg/L}$.

Noticeable decrease in adsorption capacity was found at a temperature higher than 60°C. The weakening of the ion exchange mechanism and electrostatic interaction at higher temperatures makes the adsorption process exothermic. The ΔH and ΔS values of the process determined graphically and are shown in Fig4.6.

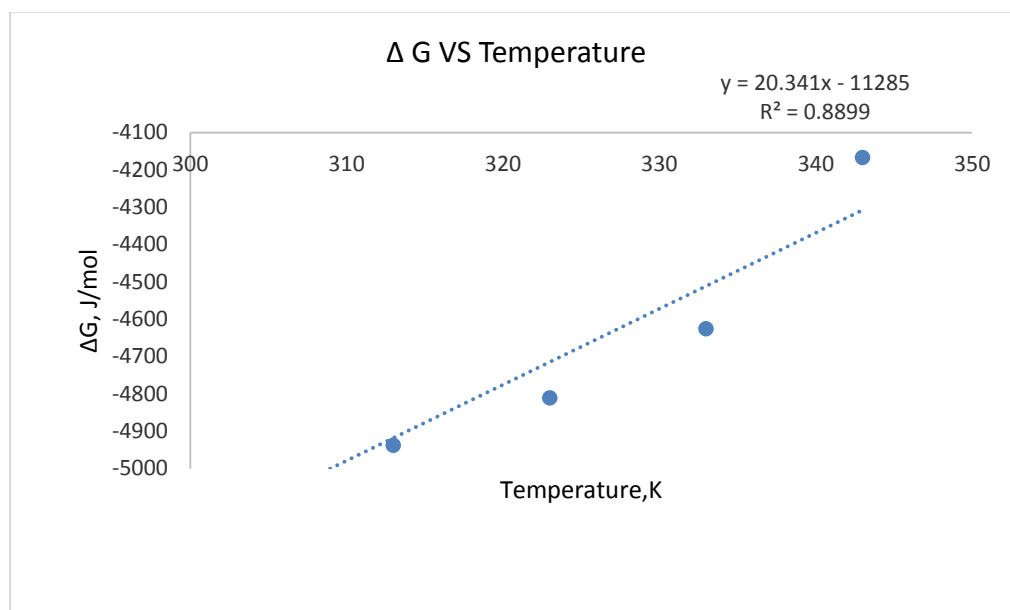


Fig 4.6 Thermodynamic plot for the adsorption of $\text{NO}_3\text{-N}$ onto Fe-CH-NSP.

The change of thermodynamic parameters with temperatures is summarized in Table 4.4. The negative values of Gibb's energy specify that the process is spontaneous and feasible (Ramalingam *et al.*, 2015). The change in enthalpy is found to be -11.285 kJ/mol, which establishes the exothermic nature of the process. The value of ΔS is 0.0203 J/K, which is closer to one indicates a gradual increase in randomness and impulsiveness throughout the adsorption process (Ranjan K R *et al.*, 2015).

Table 4.4 Thermodynamic parameters of adsorption of NO₃-N onto Fe-CH-NSP.

Temperature (⁰ K)	q _e (mg/g)	ΔG (kJ/mol)	ΔH, (kJ/mol)	ΔS (J/K)
303	44.02	-5.02	-11.285	0.0203
313	43.48	-4.93		
323	42.85	-4.81		
333	42.08	-4.62		
343	40.58	-4.16		

4.2.5 Characterisation of Fe-CH-NSP

Morphological characterisation of Fe-CH-NSP was performed using scanning electron microscopy and transmission electron microscopy. FTIR and XRD was used to analyze the functional groups and crystal structure of Fe-CH-NSP.

4.2.6 Morphological Behavior by SEM and TEM Analysis

The surface topography and morphological uniqueness of the adsorbents are obtained by scanning electron microscopy. The surface morphology of Fe-CH-NSP before and after adsorption is shown in figure Fig 4.7 and Fig 4.8, respectively. The abundant porous and irregular structure of the Fe loaded nutmeg shell powder could enable the easy access of nitrate anions into it. From the microphotograph, it is evident that the nanomagnetic particles are dispersed well in the chitosan-nutmeg shell matrix. The heterogeneous surface also depicts the presence of different constituents in the composite. The Fe loaded nutmeg shell powder has very small cavities with excellent size distribution. It is due to the cross-linking of iron nanoparticles in the suspension of biopolymers in an aqueous solution (Ramalingamet *al.*,

2015). The nitrate adsorption onto Fe-CH-NSP, leads to the reduced porosity and coarse surface of the adsorbent and it is an evidence for the fact that nitrate ions occupied the adsorption sites. The clustered or aggregated structure of adsorbent after adsorption explains the filling of reactive sites.

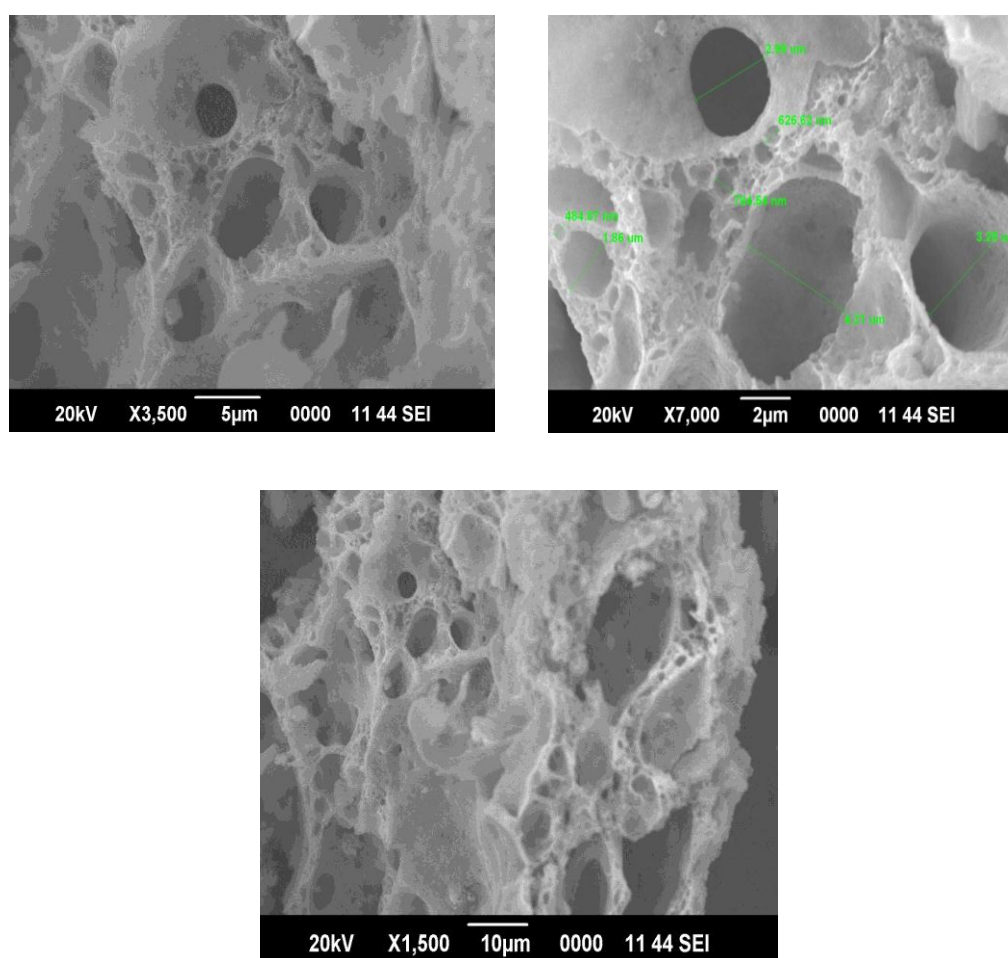


Fig 4.7 SEM images of Fe-CH-NSP at different magnifications before nitrate adsorption.

Fig 4.9 shows the TEM image of the Fe-CH-NSP particles. TEM results showed the development of polydispersed nanoparticles of size ranging from 20 to 200 nm (Machado *et al.*, 2013). TEM analysis on nanoscale shows information on the size and morphology of activated nutmeg shell powder. Lower magnification images are obtained, typically capturing between 100 particles per image. The TEM gives direct imaging of the atomic structure, while HRTEM is a specialized mode of TEM. HRTEM make use of both transmitted and scattered beams to generate an interference image.

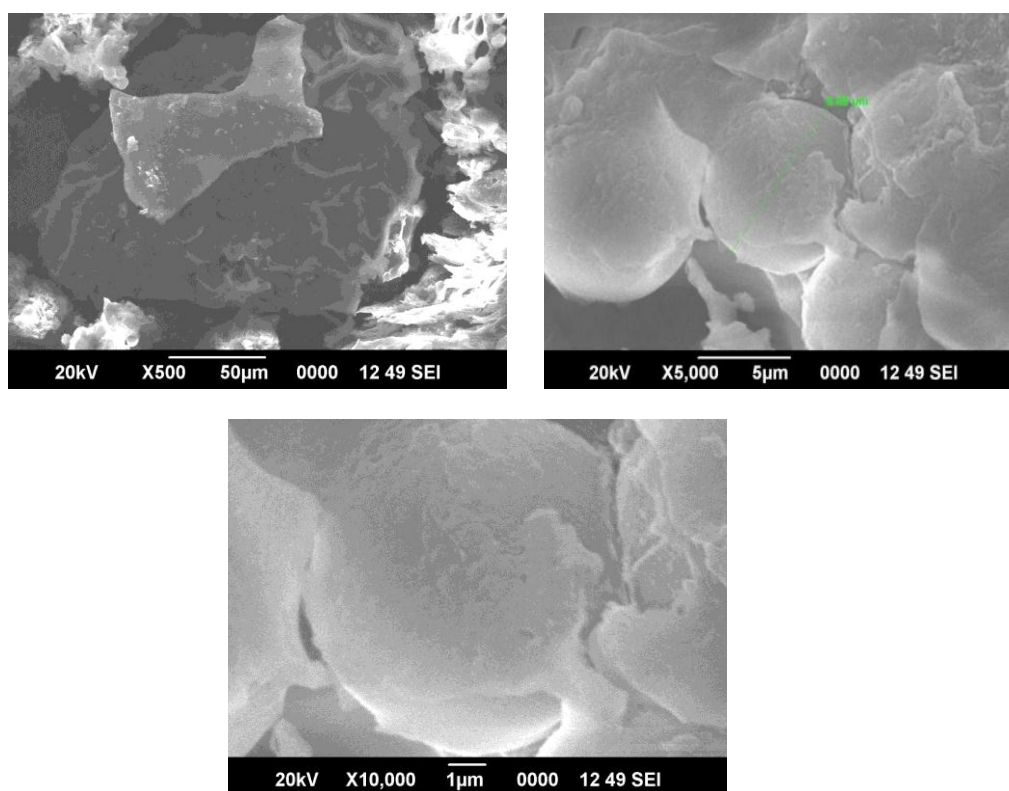


Fig 4.8 SEM images of Fe-CH-NSP after nitrate adsorption.

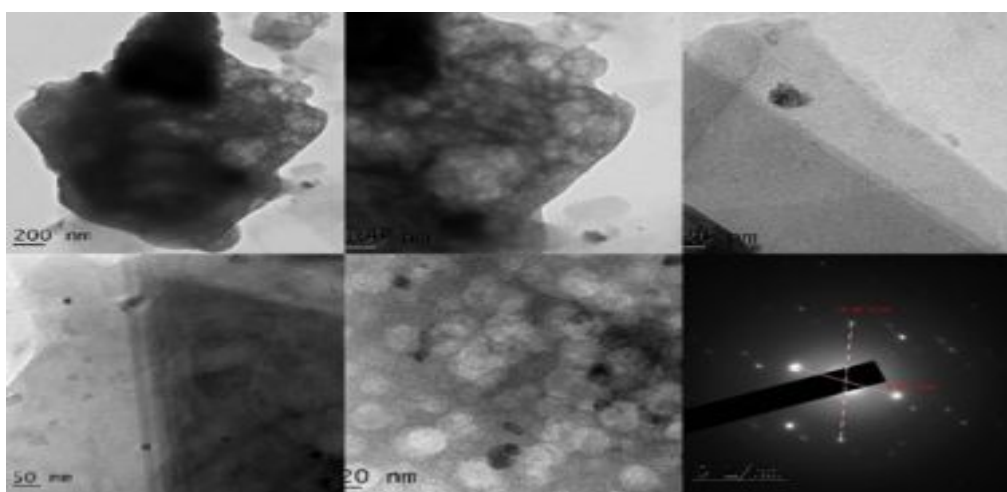


Fig 4.9 TEM image of Fe-CH-Nutmeg shell powder.

4.2.7 FT-IR Analysis of Nitrate Nitrogen Removal by Fe-CH-NSP

FT-IR analysis was carried out to recognize the contact among biomolecules of nutmeg shell powder, chitosan and metal ions, accountable for the formation of iron nanoparticles. Fig 4.10 shows the spectral analysis of the raw nutmeg shell powder. The band at 3298 cm^{-1} seen in NSP is credited to O-H stretching of phenolic compounds (Gonzalo *et al.*, 2009). The peak at 2937 cm^{-1} indicates the presence of $-\text{CH}_2$ stretching of aliphatic compound. The presence of stretching vibration of carboxylate functional groups are shown by the peaks at about 1632 cm^{-1} and 1514 cm^{-1} . The peaks at 1032 cm^{-1} and 1151 cm^{-1} represent the C-OH stretching vibration (Zihong *et al.*, 2012). Fig 4.11 depicts the Fe loaded chitosan nutmeg shell powder. The peak at 3298 cm^{-1} disappears in activated NSP. The new peak appeared at 3738 cm^{-1} is attributed to the amide - NH stretch which clearly shows the binding of chitosan to the composite. The new bands at 653 cm^{-1} , 538 cm^{-1} , 457 cm^{-1} , 480 cm^{-1} seen in the activated NSP demonstrate the presence of Fe-O bonds confirming the formation of iron nanoparticles (Arshadi *et al.*, 2015). Fig 4.12 depicts the Fe loaded chitosan nutmeg shell powder after nitrate adsorption.

It is observed that considerable change in the frequency of adsorbent after adsorption is mainly in the series of 1000cm^{-1} and 1600cm^{-1} , where C=O, C-O, C-N are present. All these functional groups are contributing to adsorption process through electrostatic attraction and ion exchange. The disappearance of various bands after equilibration with nitrate solution including the band at 653 cm^{-1} clearly postulates the interaction of $\text{NO}_3\text{-N}$. The peaks at 1369 cm^{-1} , 1338 cm^{-1} , and 1306 cm^{-1} attributed to O-H bending vibration get shifted to 1375 cm^{-1} after adsorption. This band at 1375 cm^{-1} visible in the FTIR spectra of adsorbent after adsorption is due to residual nitrates. The appearance of new peaks after nitrate adsorption might be due to the inner sphere surface complexation between Fe-O-N and functional groups. The characteristic bands representing both chitosan and nutmeg shell are present in the composite. All these observations pinpoint to the strong interaction between functional groups and adsorbate.

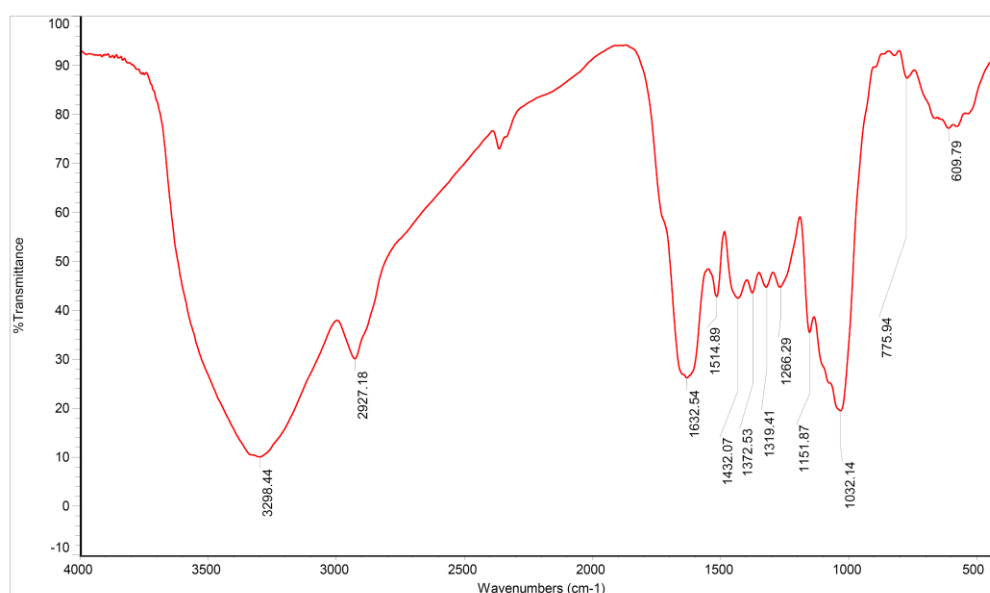


Fig 4.10 FTIR of raw nutmeg shell powder.

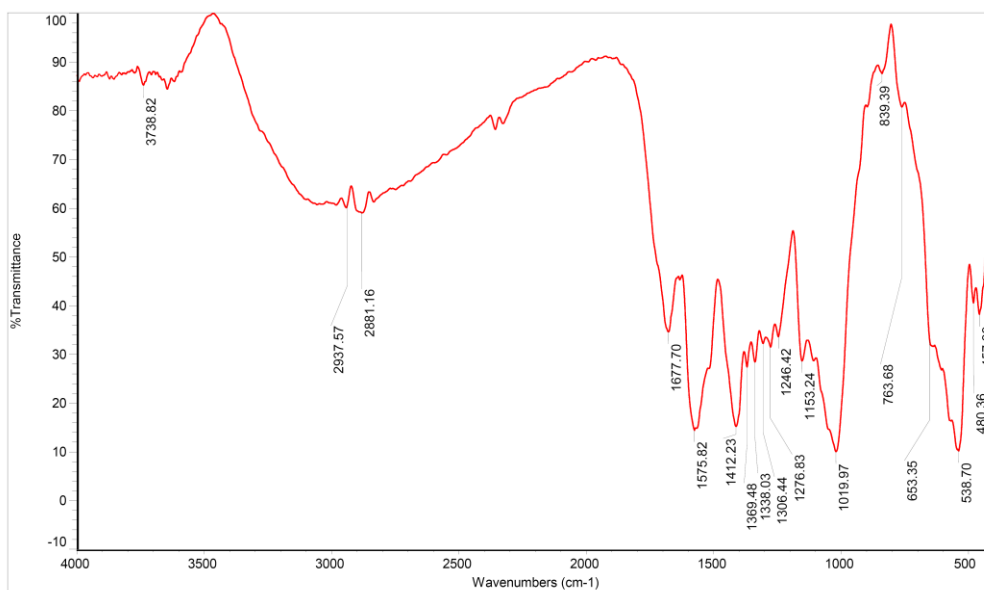


Fig 4.11 FTIR of Fe-loaded chitosan nutmeg shell powder.

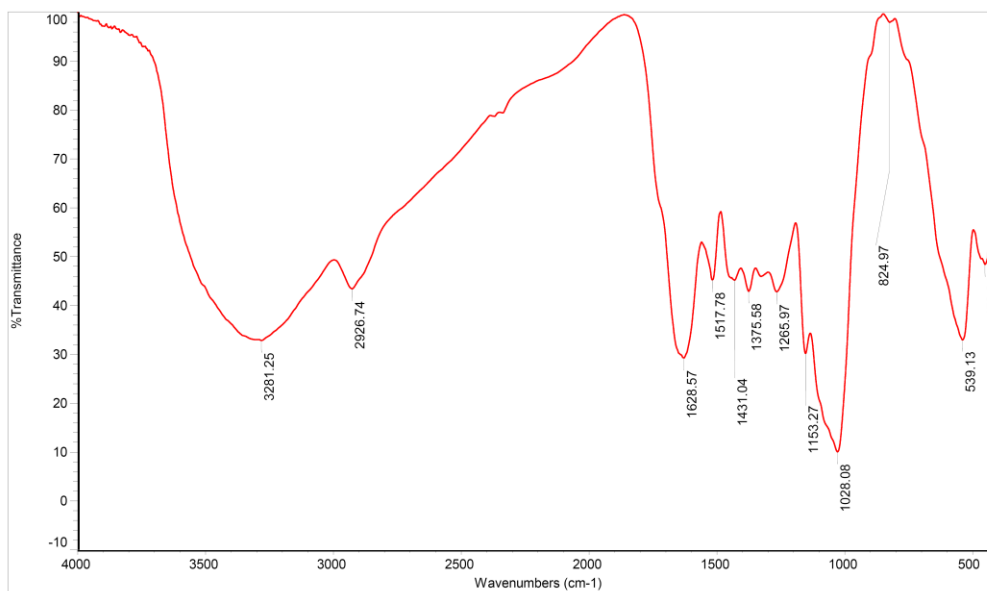


Fig. 4.12 FTIR of Fe-CH-NSP after nitrate adsorption.

4.2.8 X-ray Diffraction Pattern of Fe-CH-NSP.

The interference effect and the diffraction pattern produced by the scattering of X-rays on atoms of a crystal indicate the characteristics of the substance. The scanning of the material was done at 2θ value ranging from 3° to 80° at a wavelength of 1.5406 \AA in a X-ray diffractometer. The X-ray diffraction pattern of iron nanoparticles loaded nutmeg shell powder is shown in Fig. 4.13. X-ray diffraction pattern of Fe-CH-NSP showed the presence of iron oxides and Fe(0). The characteristic peaks in the XRD spectrum of the composite are due to their regular layered structure. The peaks indicated the d-spacing in the formation of composite. The peaks in the XRD curve were compared with that of standard data and are similar. XRD patterns of iron nanoparticles match with those presented in previous works (Arshadi, *et al.*, 2015). The peaks at 2θ of 36° , 38° point to the existence of magnetite or maghemite while the peak at 48.9° and 53.8° is of Fe (0). The Fe-O provides a conductive environment in solution. XRD pattern of magnetized biosorbent after contacting with the nitrate solution is shown in Fig 4.14. The interaction between the adsorbent and adsorbate could be seen in the XRD image. The XRD results thus not only confirmed successful alteration of the NSP with Fe ions and chitosan but also the interaction with the atoms in the adsorption process.

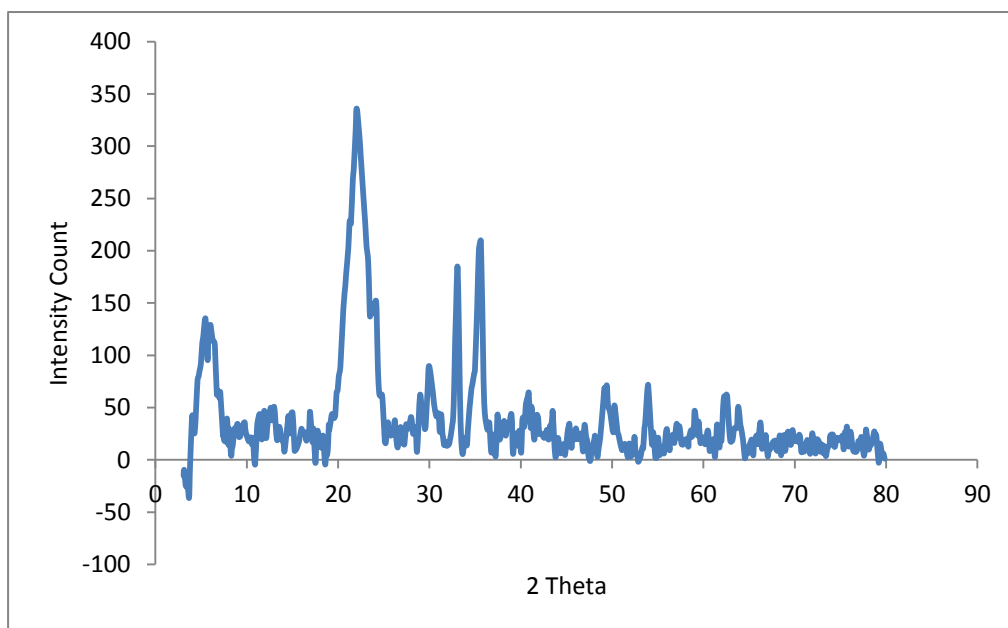


Fig4.13 XRD spectra of Fe-CH-NSP.

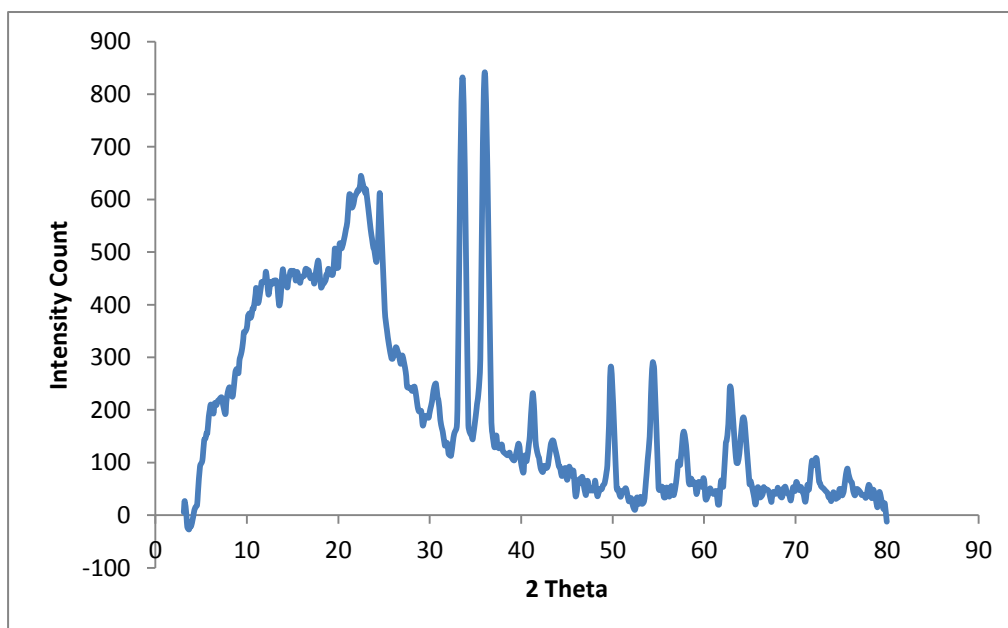


Fig 4.14XRD spectra of Fe-CH-NSP after adsorption of $\text{NO}_3\text{-N}$.

4.3 BATCH ADSORPTION OF NITRATE NITRATEGON BY CHITOSAN-BENTONITE NANO COMPOSITE FILMS.

The present section discusses the effectiveness of synthesized chitosan bentonite nano clay films (CH-B-NCF) for nitrate uptake through the batch adsorption process. The films used in all the experiments have a thickness of 0.2 mm and a diameter of 6.5 mm. The methods of preparation of nitrate solution, nitrate analysis, and synthesis of nanocomposite film have been described in chapter 3. This study had the following objectives in mind: (i) investigation of the influence of pH on nitrate adsorption; (ii) study of equilibrium adsorption isotherms, kinetics of adsorption, and thermodynamics of nitrate sorption on nanocomposite films; (iii) study of the combined effect of variables using response surface methodology and determination of optimum conditions for NO₃-N removal using the response optimizer of Box-Behnken design and (iv) regeneration of the nanocomposite films by batch-wise desorption studies with 1 M NaCl.

4.3.1 Effect of pH on Nitrate Nitration Uptake by Chitosan Bentonite Films.

The surface charge and functional group dissociation of active sites of the adsorbent are influenced by the pH of the working adsorption solution. The consequence of pH variation on adsorption efficiency of nitrate between pH 2 to 12 is shown in Fig. 4.15. It was observed that maximum removal of nitrate occurs at a pH of 4. The adsorption capacity at pH 4 was 46 mg/g. The nitrate percentage removal at pH 2.0 was 72 %, and as pH increased, the adsorption efficiency also increased up to pH 4.0 (92%). At acidic pH, the surface of the adsorbent gets protonated, and the functional groups which contribute to electrostatic attraction become positively charged. It is reported in the literature that at pH below 5, almost 90 % of the total amine groups in

the chitosan become protonated and at neutral pH, the protonation efficiency is decreased to 50% (Sudipta *et al.*, 2009). The hydroxyl, amino, carboxylic, and carbonyl group present in the nanocomposite films are positively charged at low pH and negatively charged at higher pH. So, high adsorption capacity at low pH is mainly due to the strong electrostatic interaction between the positively charged sites of nanocomposite films and the negatively charged nitrates. The higher adsorption of nanocomposite films also postulates that the cross-linking treatment of the chitosan with bentonitenanoclay reinforced its chemical stability at acidic pH. At pH 2, there was some restriction in the free movement of nitrate ions toward the adsorption sites due to more H⁺ ions in the solution, which slightly decreases the adsorption efficiency. Also, there will be a competition of Cl⁻ ions with nitrate anions. The sharp decrease in percentage nitrate removal (30%) occurred when pH reached 12.0. It is ascribed to the increase in diffusion resistance due to the contest between hydroxide and nitrate ions for adsorption sites. At high alkalinity, the adsorption efficiency decreased significantly due to the electrostatic repulsion among deprotonated amine groups and negatively charged nitrate ions (Appunni and Meenakshi., 2013).

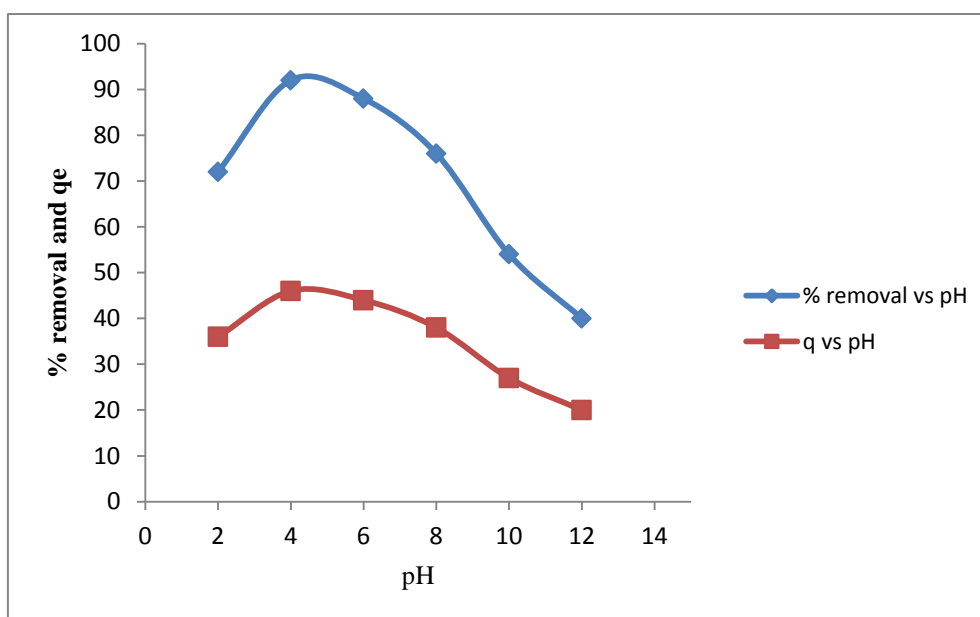


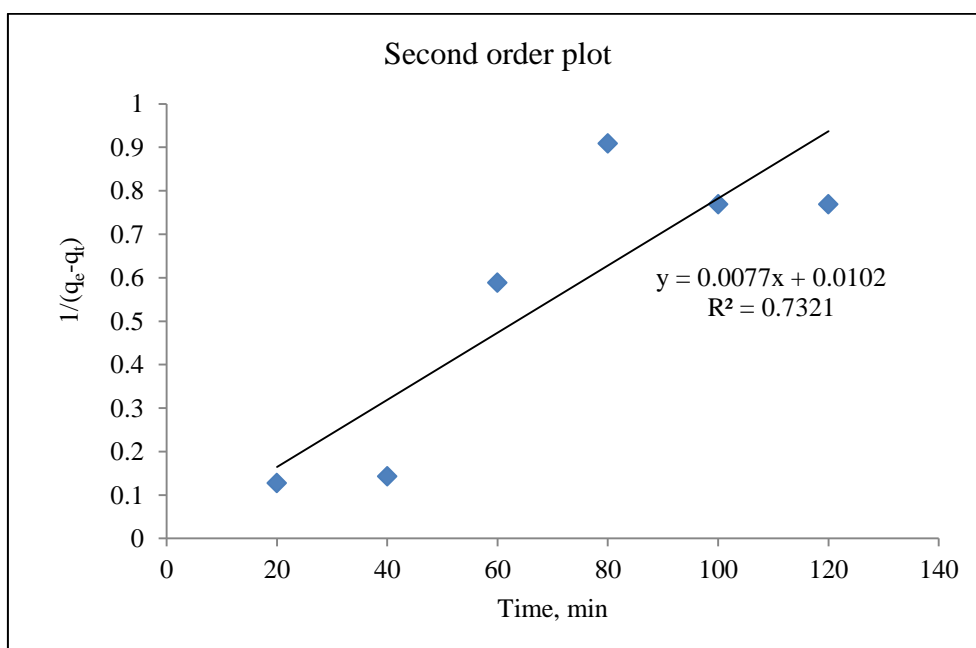
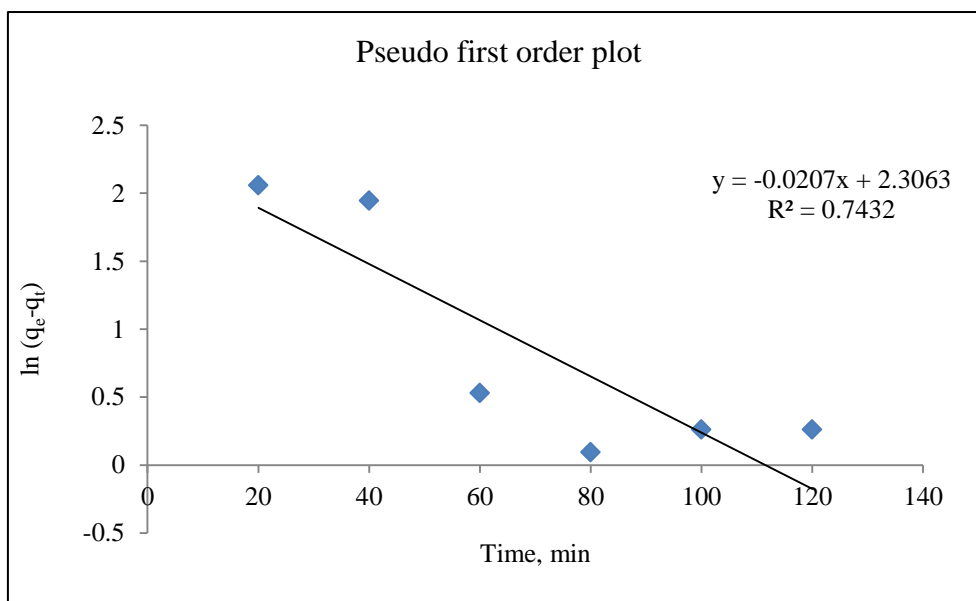
Fig 4.15 Influence of pH on nitrate adsorption (initial nitrate concentration 50 mg nitrate/L and nanocomposite film dose 0.1 g/100 mL).

4.3.2 Adsorption Kinetics

The controlling mechanism and rate-limiting step of an adsorption process are obtained from the kinetic analysis. The adsorption kinetic data were analyzed using pseudo-first-order, second-order, and pseudo-second-order kinetic models, which are shown in Fig 4.16. The kinetic data were obtained by conducting the adsorption experiments at different time intervals and measuring the final concentration (Annexure-IV). Two adsorption kinetic diffusion models- intraparticle diffusion model, and Dunwald Wagner film diffusion model are also studied and are shown in Fig 4.17. The kinetic parameters and correlation coefficients of three kinetic models have tabulated in Table. 4.5. The R^2 values of pseudo-second-order, pseudo-first order and the second-order were obtained as $R^2=0.99$, $R^2=0.74$, and $R^2=0.73$, respectively. This shows that the reaction follows pseudo-second-order. The

experimental q_e value was 64.3 mg/g, and q_e calculated using pseudo-second-order kinetics was 71.42 mg/g. The pseudo-first-order model showed a little fit with $R^2=0.74$ while second order showed poor fit. In literature, it is reported that the kinetics of most of the adsorption process with modified chitosan and clay composites are following the pseudo-second model (Moazz *et al.*, 2013; Appunni and Meenakshi, 2014). In the pseudo-second-order kinetic model, the rate-controlling step involved is the chemical sorption involving valence forces through the sharing or exchange of electrons between sorbent and sorbate (Mohammadali *et al.*, 2010). The pseudo-second-order rate constant was obtained as $0.00426 \text{ g mg}^{-1} \text{ min}^{-1}$.

Weber-Morris intraparticle diffusion and Dunwald-Wagner liquid film diffusion plots are presented in Fig 4.17. In the present study, the intraparticle rate constant is $2.35 \text{ mg/g/min}^{1/2}$, and the slope is 41.4, respectively ($R^2=0.8$). The value of the slope C gives an idea about the boundary layer thickness (Siva *et al.*, 2012). The relatively high value of C indicates a more significant boundary layer effect. In the Weber-Morris intraparticle diffusion plot, the initial curve represents the boundary layer effect, and the straight line represents intra-particle-diffusion. The multilinearity in the plot shows that the intraparticle diffusion is not the sole rate-limiting step. There is a possibility of both particle and pore diffusion in the adsorption process. Dunwald-Wagner rate constant obtained is $k_{DW}=0.05 \text{ min}^{-1}$ with $R^2=0.75$. Table 4.6 contains the intraparticle diffusion and film diffusion constants and correlation coefficients for adsorption of $\text{NO}_3\text{-N}$ onto CH-B-NCF.



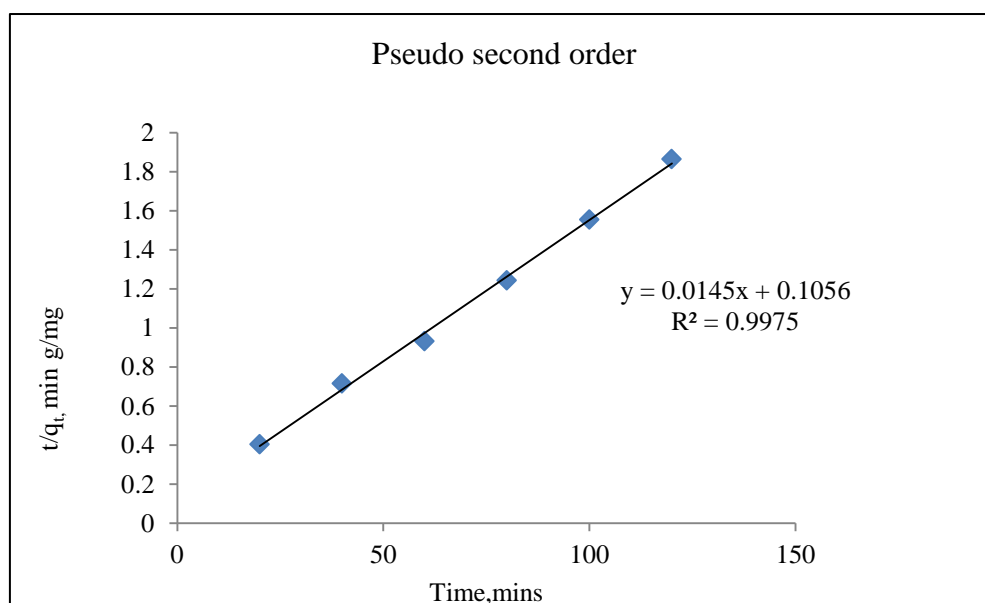


Fig 4.16 Kinetics of adsorption of nitrate nitrogen onto CH-B-NCF, pseudo first order, second order, and pseudo second order models.

Table 4.5 The kinetic constants and correlation coefficients for adsorption of nitrate on to chitosan bentonitenanocomposite films.

Experimental	Pseudo first order			Second order			Pseudo second order		
	q _{ecal} , mg/g	R ²	k ₁ min ⁻¹	q _{ecal} , mg/g	R ²	K ₂ , g.mg ⁻¹ min ⁻¹	q _{ecal} , mg/g	R ²	k ₂ , g.mg ⁻¹ min ⁻¹
64.3	10.03	0.74	0.002	100	0.73	0.007	71.42	0.99	0.004

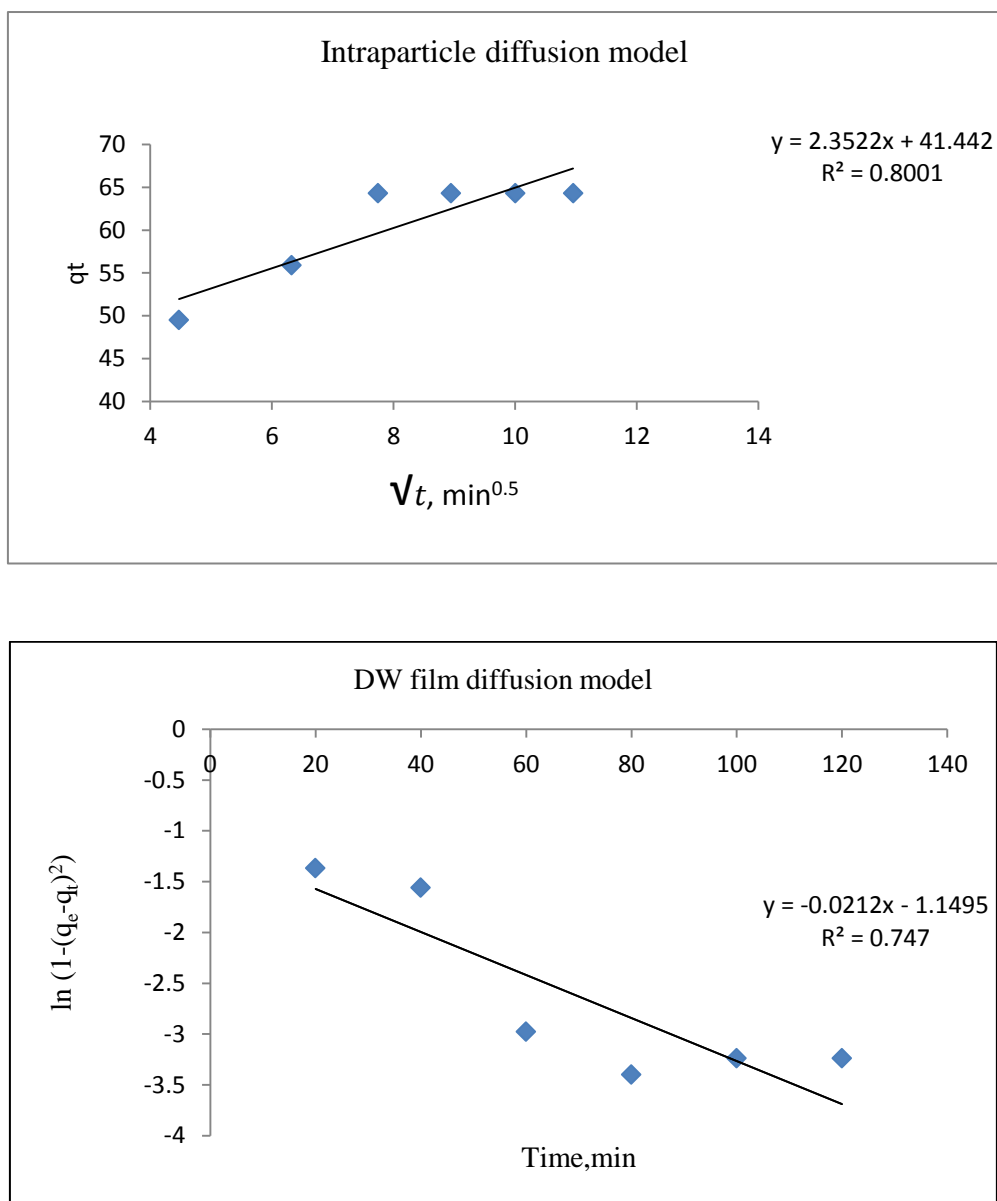


Fig 4.17 Kinetics of adsorption diffusion model of nitrate nitrogen onto chitosan bentonite nanocomposite films, Weber-Morris intraparticle diffusion model and Dunwald-Wagner film diffusion model.

Table 4.6 The intraparticle diffusion and film diffusion constants and correlation coefficients for adsorption of NO₃-N onto CH-B-NCF.

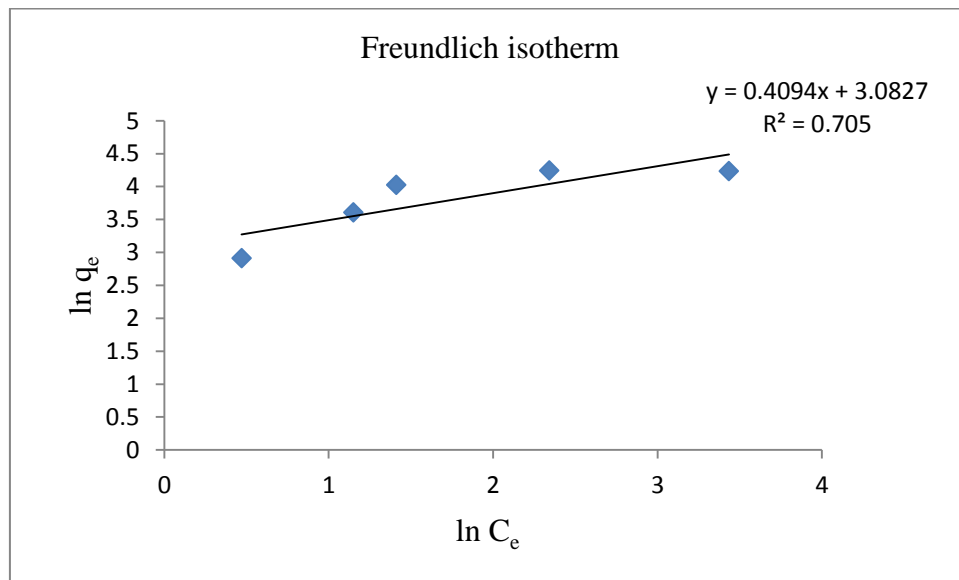
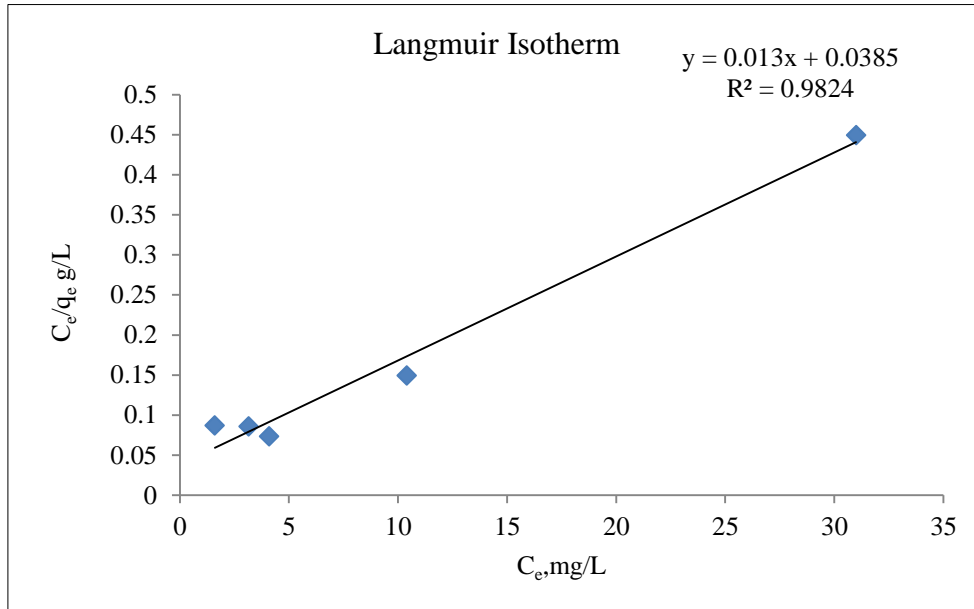
Intraparticle diffusion			Film diffusion	
k_d , mg/g min ^{-1/2}	C, intraparticle constant	R ²	k_{DW} min ⁻¹	R ²
2.35	41.44	0.8	0.05	0.75

4.3.3 Adsorption Isotherm

The experimental data of equilibrium studies of adsorption of nitrate-nitrogen onto CH-B-NCF were treated with four well-known isotherms—Langmuir, Freundlich, Tempkin, and Dubinin-Radushkevich models. Previous studies have generally used these adsorption isotherm models to explain nitrate adsorption (Appunni and Meenakshi, 2013). The four isotherm plots are shown in Fig 4.18. The Langmuir and Dubinin-Radushkevich models show the squared correlation coefficient as $R^2=0.98$ and $R^2=0.96$ respectively. The R^2 values of Freundlich and Tempkin are 0.75 and 0.86, respectively. The results proved that the equilibrium data were fitted best to Langmuir and Dubinin-Radushkevich models. The fit to Langmuir model describes the formation of a monolayer nitrate ion region on the outer surface of nanocomposite films. The equilibrium distribution of nitrate ions between nanocomposite films and the aqueous solution takes place during adsorption. The Dubinin-Radushkevich model is used for the estimation of apparent free energy and characteristics of the porosity of the adsorbent. The isotherm parameters are summarized in Table 4.7. The maximum monolayer adsorption capacity q_m calculated from the Langmuir model was 76.92 mg/g. The nitrate adsorption capacities of the chitosan derivative adsorbents are tabulated in Table 4.8. The findings showed that the adsorption capacity of the prepared nanocomposite film was higher or comparable with the other adsorbents. The main novelty is that no toxic or intensive chemicals were used in the cross-

linking of chitosan with bento nitenanocaly. Only acetic acid was used for the preparation process. The higher adsorption of nitrate ions also shows that the nanocomposite films have a more specific surface area, pore-volume, and average pore width.

The essential characteristics and favourability of the Langmuir isotherm model are expressed in terms of a dimensionless constant R_L (Rangabhashiyam *et al.*, 2014). It is commonly known as the separation factor. Value of $R_L < 1$ indicates that adsorption is favorable, and $R_L > 1$ indicates unfavorable adsorption. In the present work, values of R_L were in the range of 0.13 to 0.02 for concentrations ranging from 20 ppm to 100 ppm. The inverse relationship between R_L and initial concentration indicates that favorable removal can be achieved at higher initial concentrations. Freundlich constants K_f and $1/n$ have been found as 21.8 and 0.4 ($R^2=0.71$), respectively. Since $n > 1$, it is a favourable adsorption. The D-R isotherm constants are obtained as $q_s=68.64$ mg/g, and $K_{ad}=9.00E-07$ ($R^2=0.96$). The theoretical saturation capacity q_s calculated by D-R isotherm is almost comparable with the maximum adsorption capacity calculated from Langmuir isotherm $q_m=76.92$ mg/g. The mean free energy computed was $E=0.75$ kJ/mol, the energy demand by a molecule to move from its site to infinity (Qili Hu *et al.*, 2015). $E < 25$ kJ/mol indicates physisorption. The Tempkin constants were obtained as $A=3.26$ mg/L, $B=16.97$ J/mol, and $b_T=148.44$. The constant associated to the heat of sorption is $B < 25$ J/mol indicates physisorption. The equilibrium adsorption capacity calculated using the four isotherms ($q_{e, cal}$) of NO_3-N onto nanocomposite films was plotted as a function of equilibrium concentration, C_e . Fig 4.19 shows the fitting curve between four isotherms. From the R^2 values, the best aptness order was Langmuir>D-R>Tempkin>Freundlich. Figure 4.19 shows the a plot between experimental and theoretical q_e values and equilibrium concentration C_e .



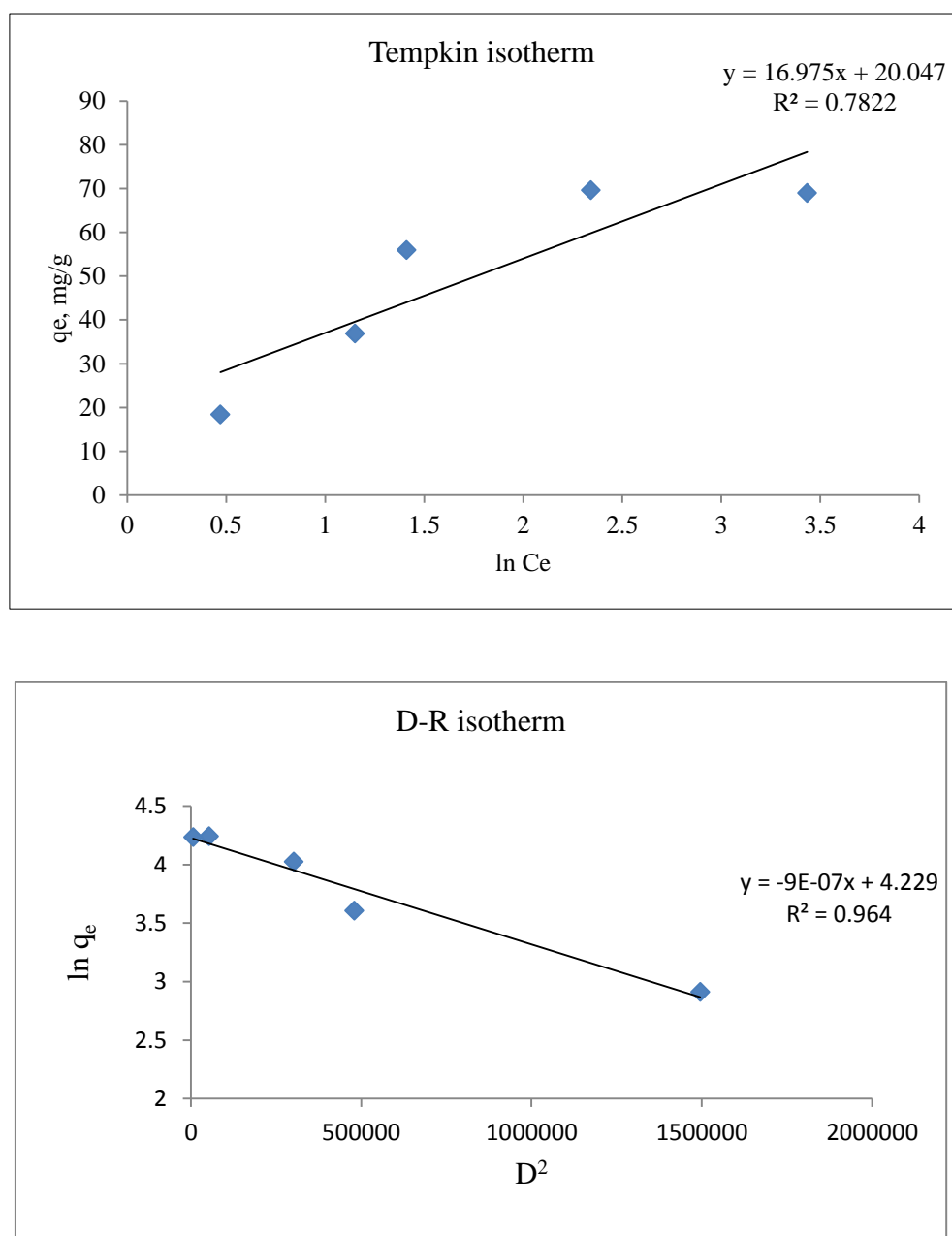


Fig 4.18 Langmuir, Freundlich, Tempkin and Dubinin-Radushkevich isotherm of $\text{NO}_3\text{-N}$ adsorption using CH-B-NCF.

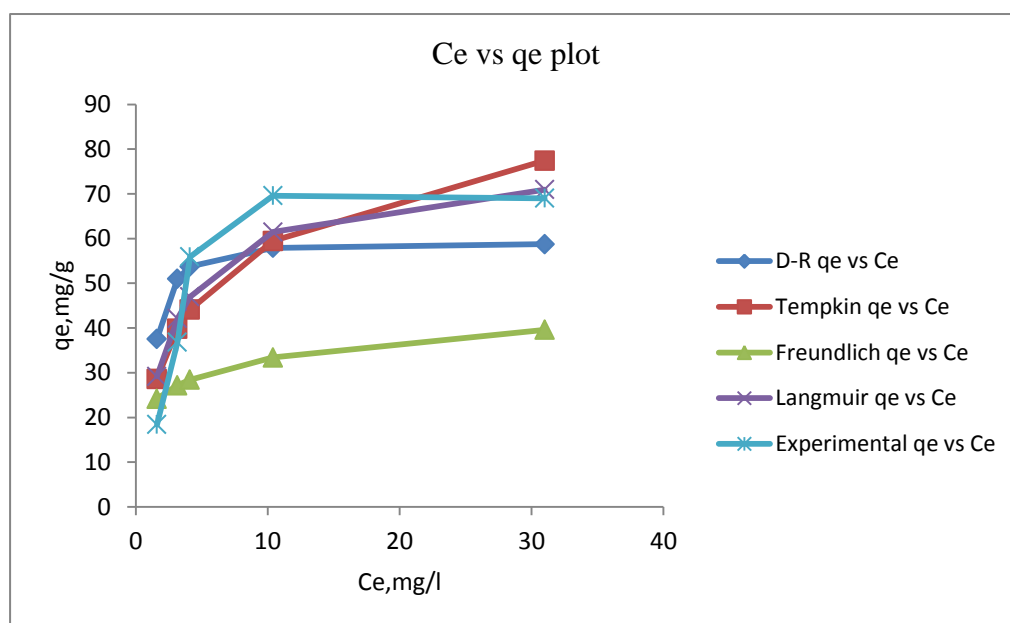


Fig 4.19 Equilibrium isotherms for NO₃-N removal from aqueous solution onto CH-B-NCF.

Table 4.7. Equilibrium parameters for adsorption of NO₃-N on to chitosan bentonitenanocomposite films

Langmuir			Freundlich			Tempkin			Dubinin-Radushkevich		
q _m , (mg/g)	K _L (L/mg)	R ²	K _f , (mg/g)(L/mg) ⁿ	n	R ²	A (L/g)	B (J/mol)	R ²	q _s (mg/g)	K _{ad}	R ²
76.92	0.34	0.98	21.8	2.4	0.71	3.26	16.97	0.78	68.64	9.00E-07	0.96

Table 4.8. The nitrate adsorption capacities of the chitosan derivative adsorbents

Adsorbent	Adsorption capacity (mg/g)	Reference
Cross-linked chitosan treated with GTAC	67.5	Appunni and Meenakshi.,2013
Chitosan-bentonite nanocomposite films	76.9	Present study
Chitosan beads cross-linked with epichlorohydrin	103.1	Chatterjee <i>et al.</i> , 2009
Chitosan beads conditioned with sodium bisulphat	93.6	Chatterjee <i>et al.</i> , 2009
Chitosan beads cross-linked with epichlorohydrin and conditioned with sodium bisulphate	104.1	Chatterjee <i>et al.</i> , 2009
Chitosan beads non cross-linked	90.7	Chatterjee <i>et al.</i> , 2009
Chitosan hydrogel beads	92.1	Chatterjee <i>et al.</i> , 2009
Chitosan coated zeolite (protonated with H ₂ SO ₄) in cold regions	0.6 meq/g	Arora <i>et al.</i> , 2010
Chitosan coated zeolite (protonated with HCl) in cold regions	0.74 meq/g	Arora <i>et al.</i> , 2010

4.3.4 Thermodynamics of Nitrate Nitrate Adsorption

Temperature is a highly noteworthy parameter in the adsorption process. A series of batch experiments at 30, 40, 50, 60, and 70⁰C were performed to study the influence of temperature rise on the adsorption capacity of chitosan bentonite nanocomposite films on nitrate-nitrogen (Annexure-IV). The experimental results revealed that low temperatures benefit the adsorption of nitrate onto nanocomposite films. The q_m values obtained for temperatures 30, 40, 50, 60 and 70 ⁰C were 64.3 mg/g, 65.4 mg/g, 57.2 mg/g, 50.4 mg/g and 45.6 mg/g respectively for an initial

concentration of 70 mg/L. The results suggest that the adsorption capacity is affected by temperature. Fig. 4.20 shows the free energy change of adsorption of nitrate ions using chitosan bentonite nanocomposite films with temperature. A slight increase in adsorption capacity at 40 °C may be due to the enhancement of retarding forces acting on the adsorbent surface. The values of thermodynamic parameters have gathered in Table 4.9. The negative values of ΔG indicate that the adsorption process is favorable, and this also indicates that the process is spontaneous. The increase in the values of the magnitude of Gibbs free energy change with temperature shows that there is an increase in the spontaneity of the adsorption process with temperature. The positive value of ΔS also postulate it. The negative value of ΔH shows that the adsorption is exothermic. The positive value of ΔS indicates the increase in randomness at the solid-solution interface during the binding of nitrate into the active site of the chitosan bentonite nanocomposite films.

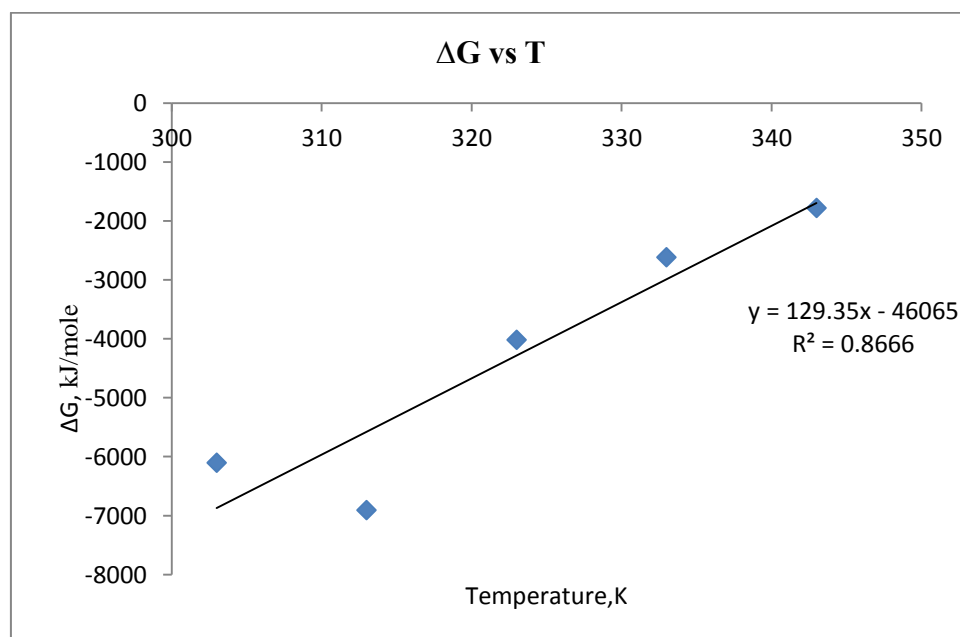


Fig. 4.20. Free energy change of adsorption of nitrate ions using chitosan bentonite nanoclay adsorbent versus temperature

Table 4.9. Thermodynamic parameters of adsorption of nitrate onto nanocomposite film

Temperature, K	K_d	ΔG , kJ/mole	ΔH , kJ/mole	ΔS , kJ/K
303	11.28	-6.10	-46.07	0.129
313	14.22	-6.91		
323	4.47	-4.02		
333	2.57	-2.6148		
343	1.87	-1.78		

4.3.5 Desorption Studies of Nitrate Nitrogen

The regeneration and reuse of costly adsorbents are necessary for the economical operation of an adsorption process in wastewater treatment systems. The multiple uses of adsorbents can be achieved by eliminating the adsorbate with suitable eluents. In the present work 1 M NaCl solution has been used for desorption experiments. Regeneration of nanocomposite films adsorbed with nitrate was done in batch experiments. The desorption study of nanocomposite adsorbents was conducted using a 1 M sodium chloride solution. The initial concentration of nitrate taken was 60 ppm (Annexure-IV). Adsorption experiments were done with an adsorbent dosage of 0.1 g/100 mL. The time of shaking was 60 minutes. The saturated films were shaken in a shaker with an eluent solution. After the first cycle, adsorption efficiency was 93.16 %. After adsorption, desorption was conducted using a 100 mL NaCl solution, and the percentage desorption after the first adsorption-desorption cycle was 96.36 %. In the second cycle, the adsorption efficiency was decreased to 85.83%, and desorption efficiency was 81.25%. Adsorption efficiency was decreased to 78.12%, followed by a desorption efficiency of

75.0% in the third cycle. After the fourth cycle, the adsorption and desorption efficiencies were 74.4% and 69%, respectively. The fifth cycle gave an adsorption efficiency of 73.3% and a desorption efficiency of 66.7%. The decrease in concentration gradient in consecutive periods causes a fall in adsorption efficiency. The virgin adsorbent used in the first cycle results in highest nitrate uptake. The desorption of chemically bonded nitrate is due to the formation of soluble sodium nitrate. The desorption efficiency decreases in the successive cycles should be due to a reduction in the activity of adsorbent. This study shows that chitosan-bentonite nanocomposite films can be reused in wastewater treatment plants using sodium chloride as eluent. The relation between the regeneration cycle and adsorption-desorption efficiency is shown in Fig. 4.21.

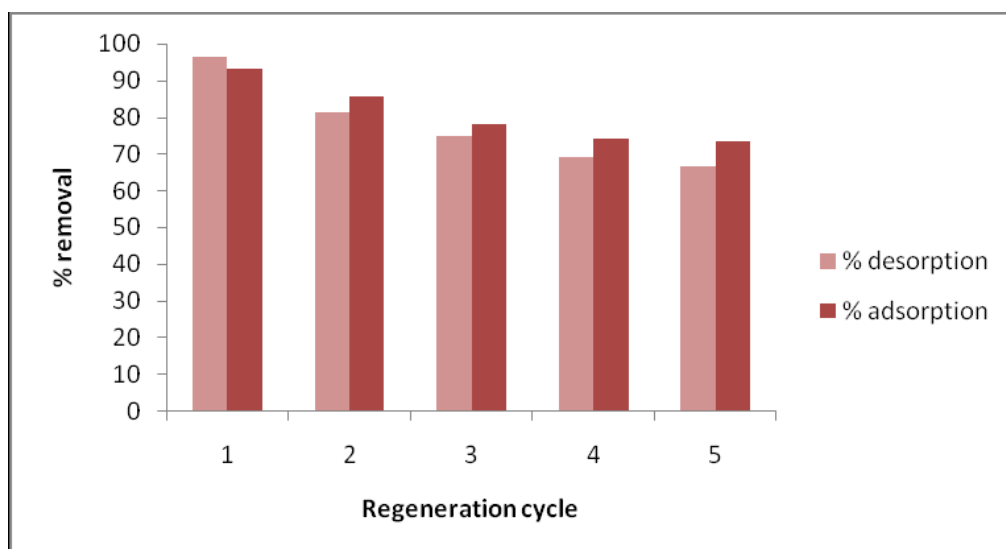


Fig. 4.21 :Desorption of nanocomposite films loaded with nitrate by 1 M NaCl

4.3.6 Response Surface Methodology for Analysis of Nitrate Removal Using Chitosan-Bentonite Nanocomposite Films

The optimum conditions for adsorption of nitrate-nitrogen by nanocomposite films were determined by Box Behnken design under response surface methodology. Optimization studies were conducted with 0.1 g of adsorbent in a 100 mL solution. The speed of shaking was 120 rpm. The four parameters for study in uncoded units were pH, temperature, initial nitrate concentration, and time of adsorption. The range of variables chosen for the experimental design of the adsorption process is shown in Table 4.10.

Table 4.10 Coded levels of independent variables in Box-Behnken design for NO₃-N using nanocomposite films

Variables	Actually coded levels	
	Low (-1)	High (-1)
pH	2	12
Temperature	30	70
Initial Concentration	20	100
Time of Contact	20	120

The design of experiments gave 27 different combinations of the parameters as shown in Table 4.11.

Table 4.11. Design of experiments for nitrate removal using chitosan bentonite nanocomposite films

Sl. no.	pH	Temperature, °C	Initial concentration, mg/L	Time, minutes	Final Concentration, ppm	$q = (C_0 - C_t)/m$, mg/g	$E\% = \frac{(C_0 - C_t) \times 100}{C_0}$	P %
1	7	50	60	70	9	51	85	81.43
2	7	50	100	20	18	82	82	86.93
3	2	30	60	70	10.2	49.8	83	84.76
4	12	30	60	70	9.6	50.4	81	85.26
5	7	30	20	70	4	16	80	77.01
6	2	70	60	70	14.4	45.6	76	78.6
7	7	50	20	120	5.2	14.8	74	75.93
8	12	70	60	70	15.6	44.4	74	77.1
9	7	70	60	20	16.8	43.2	72	75.35
10	2	50	20	70	5.2	14.8	74	73.68
11	2	50	100	70	11	89	89	89.68
12	7	70	60	120	12	48	80	80.35
13	7	50	60	70	11.4	48.6	81	81.43
14	7	50	20	20	5.8	14.2	71	70.93
15	12	50	100	70	12	88	85	89.18
16	7	70	100	70	14	86	86	85.85
17	7	30	60	20	10.2	49.8	83	82.51
18	7	70	20	70	6	14	70	69.85
19	7	50	60	70	10.8	49.2	82	81.43
20	2	50	60	20	15	45	75	76.18
21	7	30	60	120	9	51	85	87.51
22	7	30	100	70	8	92	92	93.01
23	2	50	60	120	7.2	52.8	88	87.18
24	12	50	60	120	11.4	48.6	80	80.68
25	12	50	60	20	10.8	49.2	79	81.68
26	7	50	100	120	8	92	92	91.93
27	12	50	20	70	5.2	14.8	72	73.18

The analysis was done in coded units. The model equation in uncoded units is obtained from RSM and is given by equation 4.1.

$$\begin{aligned} \% \text{ removal} = & 0.676 + 0.0104 \text{ pH} - .00144 \text{ Temp} + 0.0016 \text{ Initial conc} + 0.00134 \text{ time} \\ & - 0.00005 \text{pH} * \text{Temp} - 0.00012 \text{ pH} * \text{Time} \end{aligned} \quad (4.1)$$

The percentage of nitrate removal obtained experimentally, and that predicted by the model do not show much deviation with the $R^2=0.89$ (Fig. 4.22). This showed that the model fitted well with the experimental data.

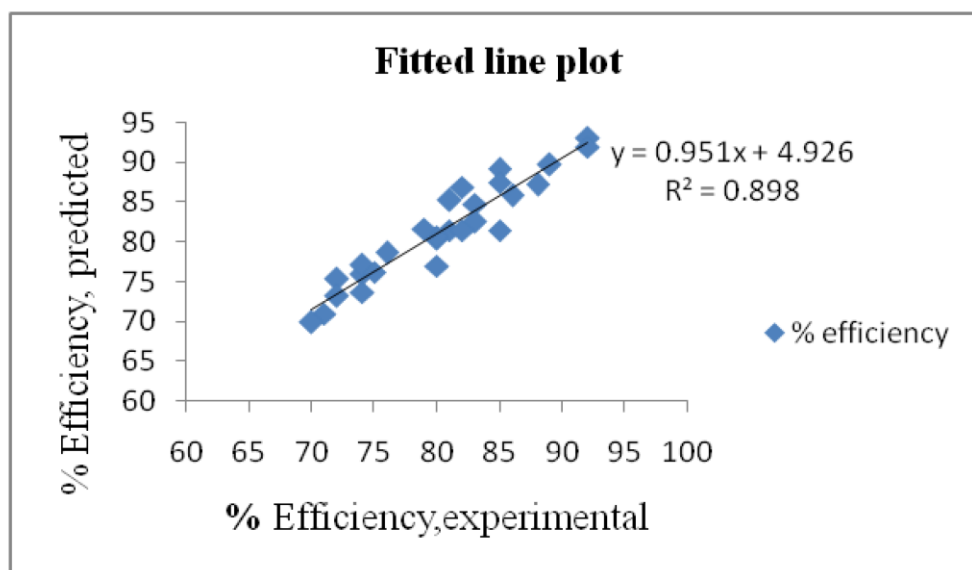


Fig. 4.22 Experimental versus predicted efficiency for adsorption of nitrate onto nanocomposite films

The response optimizer gave the optimum values of the parameters affecting the removal efficiency of nitrate nitrogen. Optimum conditions were obtained by taking top points of response surface plots (Peijinget *al.*, 2018; Miao *al.*, 2010). From the optimization plot of Minitab 19, 88.43 % removal of

nitrate was obtained at 100 mg/L initial nitrate concentration with 0.1 g/ 100 mL of nanocomposite film added to the solution. The time of shaking was 120 minutes at pH 2.0. When the experiment has been conducted batch-wise under these conditions, 85 % nitrate removal was observed. Thus the model was theoretically validated. The optimizer plot for adsorption of nitrate onto nanocomposite films is shown in Fig. 4.23.

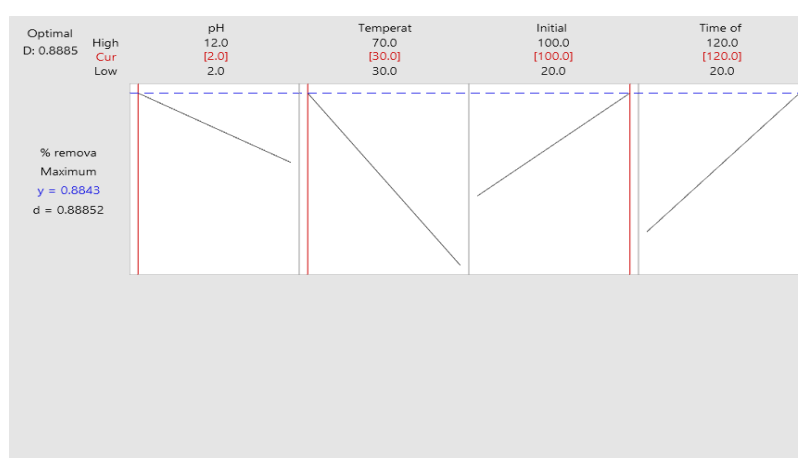


Fig. 4.23 Optimizer plot of for adsorption of nitrate onto nanocomposite films

4.3.7 Combined Effect of Variables on Nitrate Nitrogen Removal

The combined effect of pH, temperature, initial concentration, and time was analyzed using Minitab 19. The adsorption experiments were conducted with 1 g/L adsorbent dosage and 120 rpm shaking speed. The removal of nitrate first increased with time, and finally, an equilibrium was achieved. With an increase in the initial concentration, the driving force for adsorption was increased. So initially, the removal was increased. The number of active sites is constant, with an increase in initial concentration. The accumulation of nitrate near the CH-B-NCF results in a decrease in the percentage removal. Finally, equilibrium was attained between the adsorbent and adsorbate. Surface plots for the combined effect of pH, temperature, initial concentration, and time are shown in Fig. 4.24.

The combined effect of pH and temperature was mostly influencing the nitrate uptake. From the model equation, it can be seen that the combined effect of pH and time has also affected the nitrate percentage removal. The nitrate removal efficiency was less significant by the combined effect of initial concentration and time.

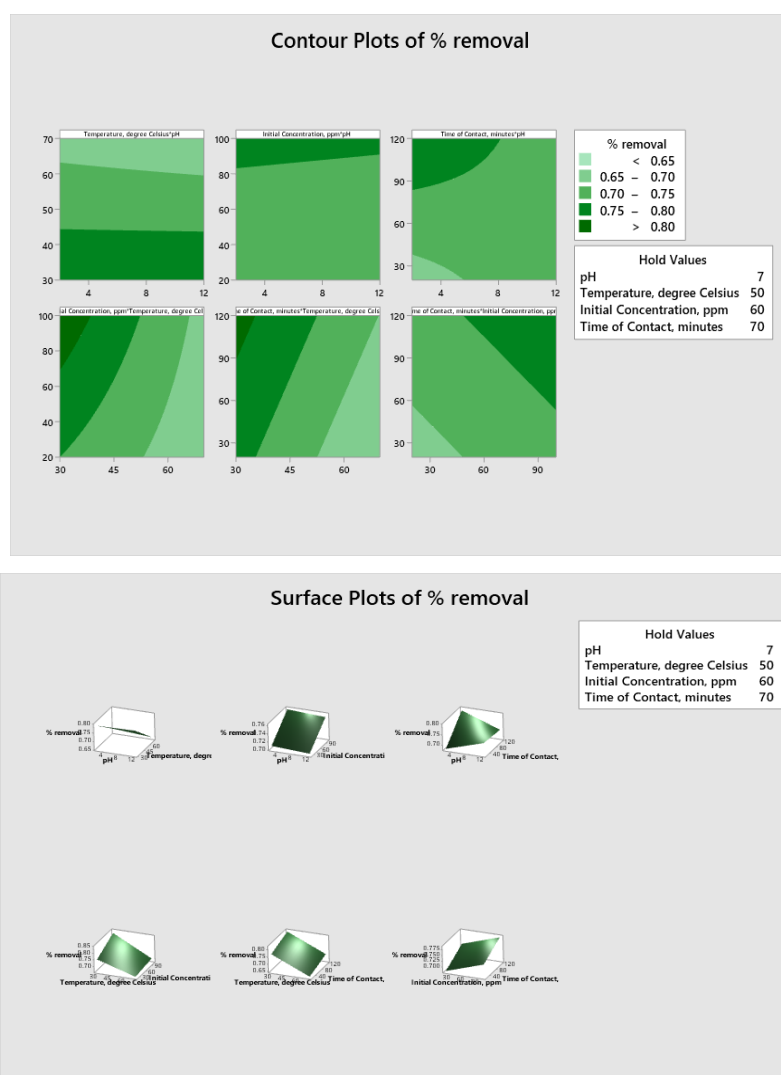


Fig 4.24 Contour and surface plots for combined effect of variables for nitrate removal by nanocomposite films

4.3.8 Characterisation of Chitosan Bentonite Nanocomposite Films

The surface physical morphology of the chitosan bentonite nanocomposite films was done with scanning electron microscopy. The basal spacing of nanocomposites was determined using X-ray diffraction. The thermal stability of the CH-B-NCF was analyzed in a thermogravimetric analyzer.

4.3.9 Surface Morphology Analysis by Scanning Electron Microscopy

The surface morphology of nanocomposite films was analyzed by scanning electron microscopy. Fig 4.25 shows the SEM image of prepared chitosan bentonite nanocomposite films. The richly porous structure of the films could enable the easy access of adsorbates into them. The bulk like agglomerates seen in the morphograph shows that nanoclay was well embedded in the chitosan matrix. (Qili *et al.*, 2015; Majid *et al.*, 2014).

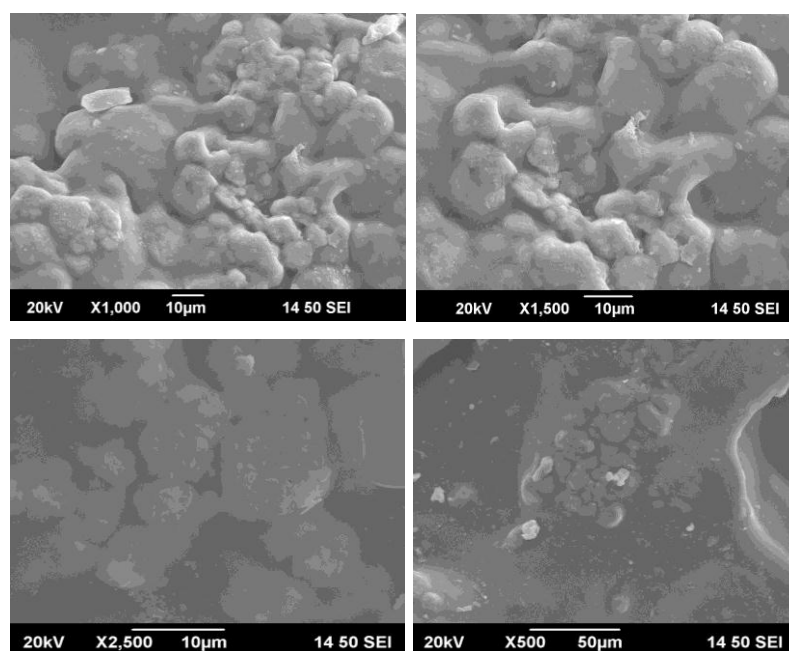


Fig 4.25 SEM of chitosan-bentonite nanocomposite films at different magnifications

The heterogeneous surface seen in the SEM image indicated the scattering of nanoclay in the chitosan surface. The uneven surface of the film suggests the immense opportunity of uptake of nitrate and ammonium ion by the adsorbent.

4.3.10 .X-ray Diffraction

The X Ray Diffraction is a fast resolution method used primarily to identify the crystal phase of a crystalline material. The XRD also can provide information about the morphology. The material to be analyzed is finely ground, homogenized and the average composition of its volume is determined. X-ray diffraction gives information of the variation of structure of chitosan after blending with nanoclay. Fig. 4.26 shows XRD of chitosan bentonite nanoclay films. The standard data of chitosan patterns exhibited the characteristic peaks centered at 10 and 20 degrees in 2θ . The main characteristic of basal spacing of bentonitenanoclay is at $2\theta = 5.778$ which could be seen in the XRD of the composite structure (Miltiadis *et al.*, 2013). The nanocomposite synthesized from two raw components indicating that nanocomposite molecules partially intercalate into the interlayer spaces. Fig 4.27 depicts X Ray Diffraction pattern of nanocomposite films after nitrate adsorption. The considerable change in crystalline peak to amorphous nature indicates the adsorption of nitrate anions. The change in the intercalary spacing is also seen in XRD spectra. The disappearance of peaks shows indistinct intercalation or incomplete exfoliation on the structure of CH-B-NCF. The characteristic peaks and the d spacing of nanocomposite are shown in Table 4.12. Using Deybe-Scherrer formula the average particle crystallite size of nanoclay composite film was determined as 9.86 nm.

Table 4.12 The characteristic peaks and intergallery spacing of chitosan bentonite nanocomposite film.

Chitosan Bentonitenanocomposite films				
Peak position $2\theta^\circ$	d spacing, \AA°	FWHM $^\circ$	D_p (nm)	D_p Average (nm)
5.365	16.46	1.315	6.05	9.86
19.438	4.56	0.686	11.65	
61.438	1.51	0.784	11.79	

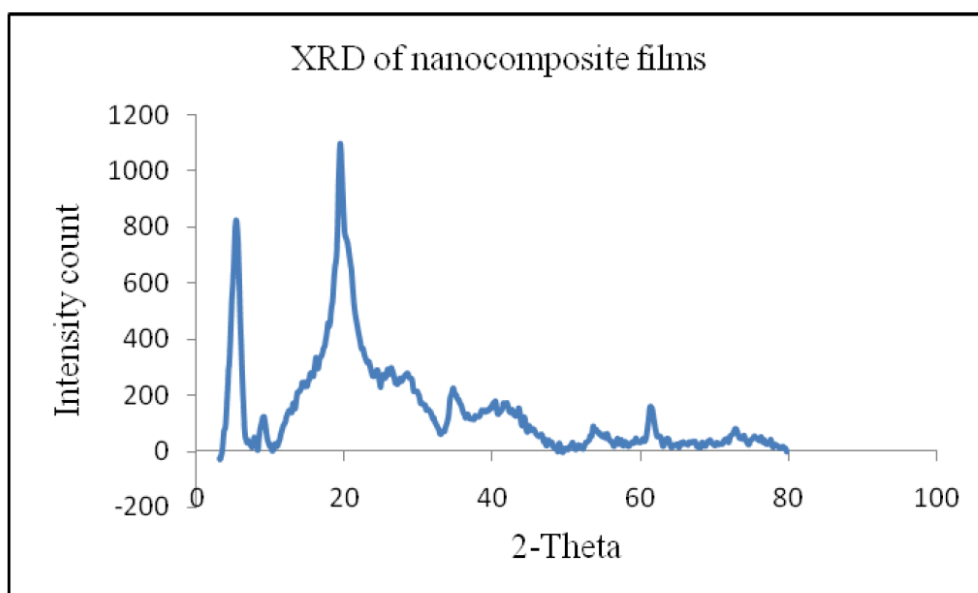


Fig. 4.26. XRD of chitosan bentonite nanoclay film

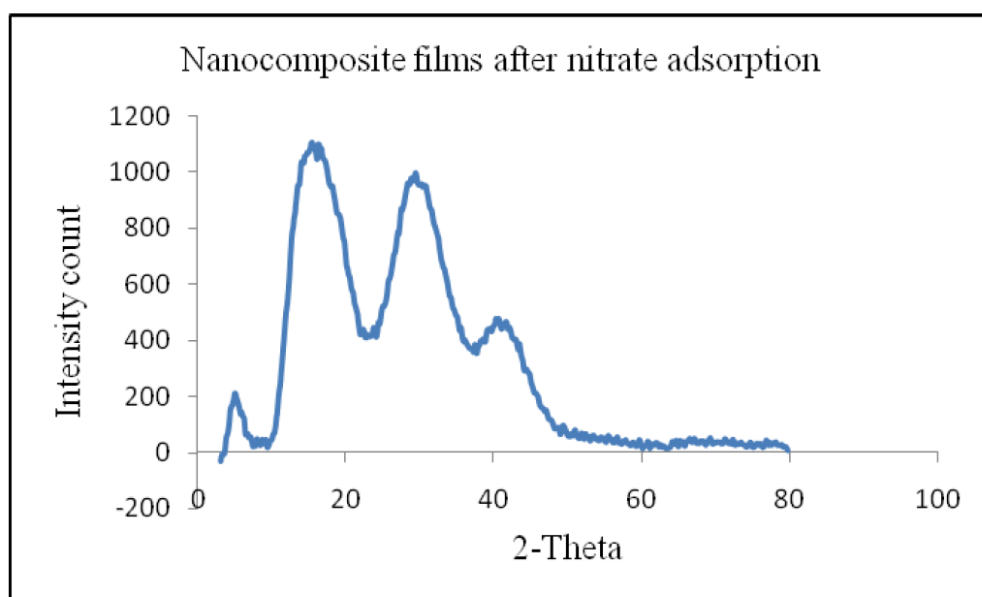


Fig. 4.27. XRD of chitosan bentonite nanoclay film after nitrate adsorption

4.3.11 Thermogravimetric Analysis

Thermally stable porous materials are most suitable as adsorbents in adsorption process. The thermal stability of the nanofilm was analyzed by heating the film from 30°C to 800°C at the rate of 10°C per minute. Nitrogen was the carrier gas with a flow rate of 50 mL/min. The use of nitrogen gas results in a non-oxidative degradation. The weight loss was noted. The initial weight loss was very small. The primary degradation happened between the temperature ranges 30-250 °C. The initial weight loss is due to the loss of adsorbed or bound moisture. This results in a 14 % weight loss. After 270°C the second stage of degradation starts and the weight loss was rapid. There was 44.26 % weight loss arising in the second stage and it was continued up to 530 °C. The quick weight loss is owing to the degradation of inorganics and deacetylation of chitosan bentonite nanofilms. Carbon monoxide (CO), CO₂ (Carbon dioxide), and water (H₂O) are the consequential products of

deterioration of inorganics in the nanofilm (De Silva *et al.*, 2013). On completion of 800°C only 7.5% of the material was remaining. So enhancement of thermal stability of chitosan by the addition of bentonitenanoclay occurs due to the formation of char as barrier which reduces the loss of volatile matter from the film. The weight loss with change in temperature for chitosan bentonitenanocomposite films is shown in Fig. 4.28. From the figure it is clear that the thermogram of chitosan-bentonite composite shows multistep degradation. The cross linking with bentonitenanoclay caused a significant delay in the degradation and increased the thermal stability of chitosan.

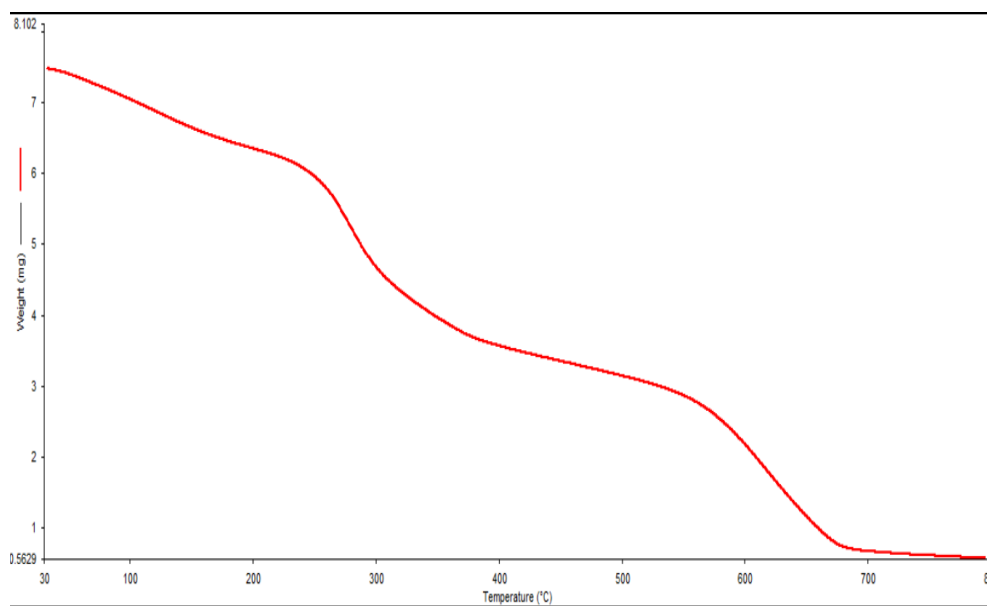


Fig. 4.28. TGA of chitosan bentonitenanocomposite films

4.4 CONTINUOUS REMOVAL OF NITRATE NITROGEN IN PACKED COLUMN USING NANOCOMPOSITE FILMS

The application of an adsorption system in practice is commonly carried out in the fixed bed mode. The column operation provides more proficient utilization of the adsorbent's capacity compared to the batch process. The data obtained from the column adsorption experiment were applied into mathematical theories to get information on the influencing parameters. In the present study, chitosan-bentonite nanocomposite films with glass beads are packed in the column, and nitrate solution of initial concentration 70 mg/L is passed through it. The change in effluent concentration with specific time intervals is noted. The performance of the continuous packed bed adsorption column was studied by plotting the breakthrough curves. The plot of the ratio of outlet nitrate concentration to the inlet nitrate concentration (C_t/C_0) against time gives breakthrough curve (Hekmatzadeh *et al.*, 2012). The column was operated at different bed height and flow rate of nitrate solution. The effect of change in parameters on the breakthrough performance of the column is given in Annexure-IV. The amount of adsorbent taken was 30% of bed height.

4.4.1 Effect of Bed Height on Breakthrough Curves

The experiments on three different bed heights were conducted to evaluate the effect of bed height for continuous removal of nitrate in the packed bed adsorption column. The bed heights applied were 10 cm, 15 cm, and 20 cm to determine the breakthrough of the nitrate solution. The flow rate of 70 ppm nitrate solution was maintained at 6 mL/min, and the pH of the stock solution was 4.0. When bed height changes, consequently, there will be a change in the nanocomposite adsorbent weight in the column. The mass of films was 3 mg, 4.5 mg, and 6 mg for bed heights 10 cm, 15 cm, and 20 cm, respectively. Fig 4.29 represents the breakthrough curves at bed heights of 10, 15 and 20 cm. The plot clearly shows that the amount of nitrate adsorbed

increased with an increase in bed height. The slightly different shape and gradient of the breakthrough curve could be seen with the variation of bed height. The lower bed depth of 10 cm gets saturated more than the higher bed depth of 15 cm and 20 cm. More volume of effluent can be treated when we increase the bed height. As the bed height of the column was increased, the breakthrough curve shifted from left to right. The breakthrough occurred slowly for the 20 cm bed than for 10 and 15 cm beds. At lower bed height, axial dispersion predominates, and consequently, the nitrate ions do not get enough time for diffusion onto the surface of the adsorbent (Xu Xing *et al.*, 2011). Also, the adsorption capacity was found to increase with bed depth. The increase in nitrate uptake capacities with higher bed height in the column is due to the increase in specific surface area of the adsorbent. So more nitrate ions can be fixed on the active sites of the nanocomposite film. The exhaustion time of adsorbent was increased for higher depths (Vinodini V and Nilanjana Das, 2014). The longer bed of 20 cm gave a delayed exhaustion time of 40 hrs. The delayed exhaustion time shows that the bed is able to operate for a longer period without changing the nanocomposite packing. The higher nitrate sorption capacity at higher bed depth can also be attributed to the sufficient residence time of the anion in the adsorption column (Auta and Hameed, 2014). This provides ample time for diffusion or interaction of the nitrate molecules with nanocomposite films. The total removal percentage of nitrate column was seen to increase with bed height. For bed heights, 10, 15, and 20 cm, total removal of nitrate was 51.92, 53.66, and 55.64, respectively. The unadsorbed nitrate ion is denoted as C_{eq} in mg/L. In the present study, it is seen that as the bed height increased from 10 cm to 20 cm, the unadsorbed nitrate from the column decreases from 33.06 mg/L to 31.05 mg/L. So the results inferred that length of the bed height significantly influenced both column breakthrough time and the nanofilm bed performance. The plot of the amount of nitrate adsorbed versus time has shown in Fig. 4.30.

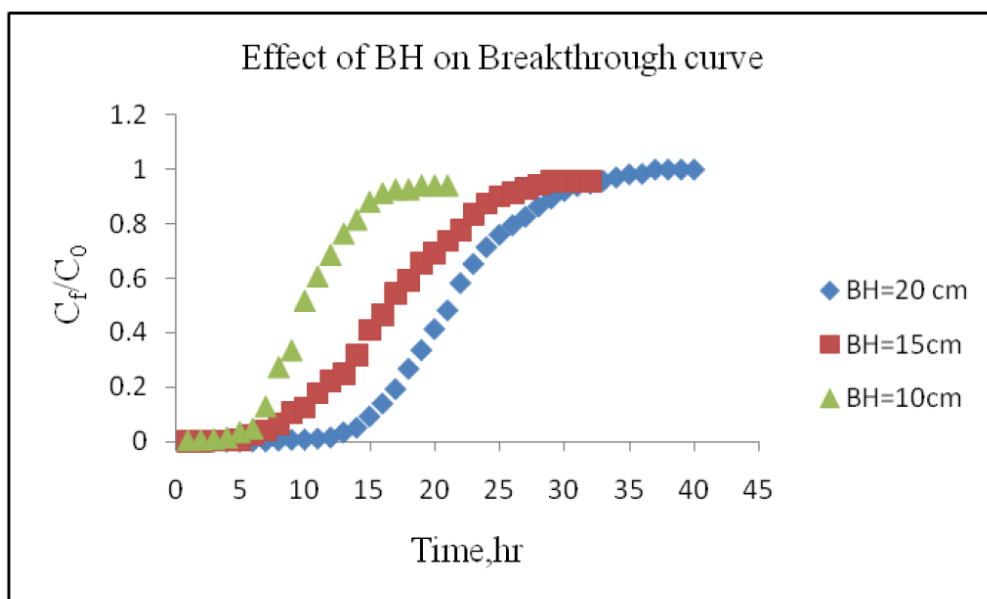


Fig. 4.29 Effect of bed height on breakthrough curves

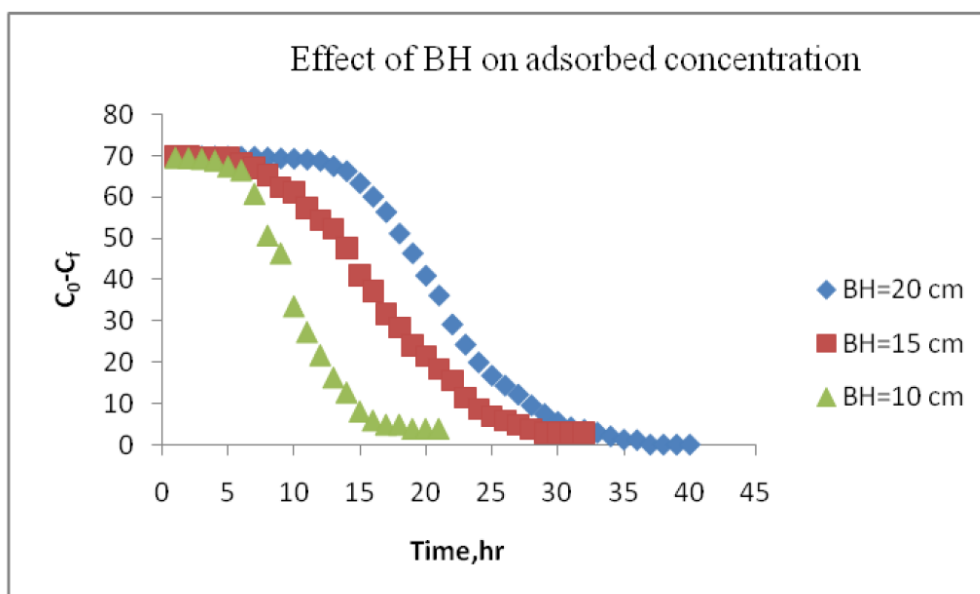


Fig. 4.30 Effect of bed height on adsorbed concentration in continuous packed bed nitrate column

4.4.2 Effect of Flow Rate on the Performance of Packed Column

Flow rate is one of the critical parameters in evaluating the adsorption performance of sorbent in continuous column studies. Three different influent flow rates of 6, 10, and 15 mL/min were used to study the effect of flow rate on the adsorption capacity of the bed on nitrate-nitrogen removal. The bed height, pH, and initial concentration were kept at 15 cm, 4.0, and 70 ppm, respectively. The saturation of the bed occurred quicker, with an increase in flow rate. Fig 4.31 shows the breakthrough curve for various flow rates of nitrate solution. There was a shift in the breakthrough curve from right to left with an increase in the flow rate of the nitrate solution. This is due to the fact that with the increase in flow rate, the residence time of the nitrate ions decreases, and there is no sufficient time for diffusion into the active sites of the chitosan-bentonitenanocomposite. The nitrate ions get adequate time for diffusion at a lower flow rate. The anion solution leaves the column quickly at a higher flow rate, so enough time is not there to reach the equilibrium (Hekmatzadeh, *et al.*, 2012). As a result, the percentage removal of nitrate decreased, and an increase in breakthrough was observed with the increase in the flow rate of influent nitrate solution.

The total removal percentage of nitrate ion for the flow rate of 6 mL/min, 10 mL/min, and 15 mL/min were obtained as 53.68, 51.65, and 51.58%, respectively. A drastic increase in the breakthrough was seen in the first part of the column operation at a higher flow rate of 15 mL/min. The contact period between the nitrate solution and the adsorbent bed was short at a flow rate of 15 mL/min. Therefore the adsorption was not complete and resulted in a steep breakthrough in the initial part of the column operation. The total amount of nitrate ions delivered to the column and the total anion adsorbed by the column is increased with the increased flow rate (Lim and Aris, 2014). The intense competition for the limited active sites of the nanocomposite films by the numerous nitrate molecules present in the higher flow of solution caused a decrease in sorption capacity at 15 mL/min (Autaand

Hameed, 2014). It is inferred that higher bed height and low flow rates are recommended for the best performance of the fixed bed column. Fig 4.32 gives the plot of effect of adsorbed nitrate concentration on breakthrough curve.

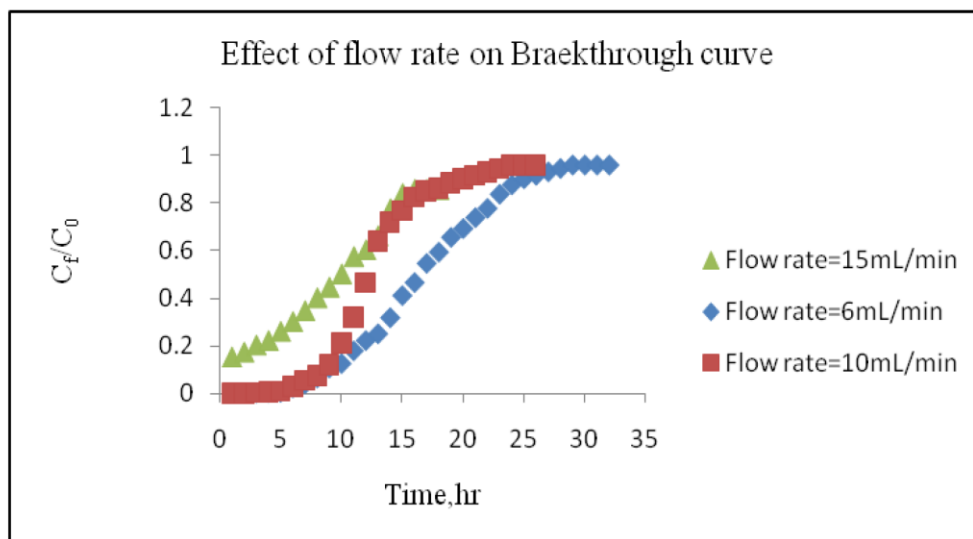


Fig. 4.31. Effect of flow rate on breakthrough curves

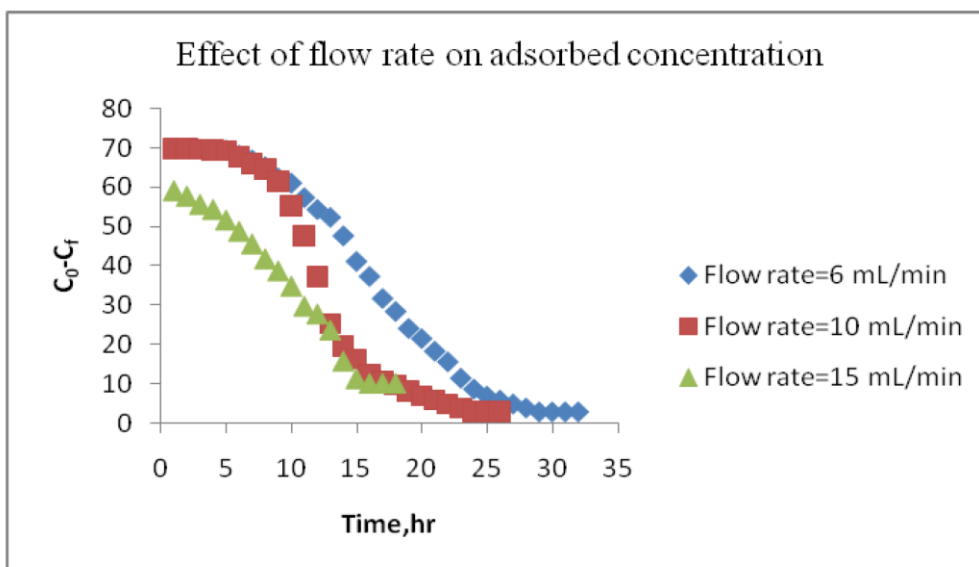


Fig. 4.32 Effect of flow rate on adsorbed concentration

From the continuous study of nitrate removal in the fixed bed adsorption column with chitosan-bentonite clay nanocomposite films, it is found that that lower flow rate and large bed depth is favourable for treating higher volume of the aqueous solution. Slower breakthrough and longer residence time of nitrate ions in the bed could be achieved at lower infiltration velocity and higher bed height. Mathematical description of column parameters for various experimental conditions are shown in Table 4.13. Q represents the volumetric influent flow rate and t_{total} is the total flow time in minutes. V_{eff} is the treated volume of nitrate solution in mL. The total adsorbed nitrate ion is represented by q_{total} while m_{total} is the total amount of nitrate ion delivered to the column.

Table 4.13 Mathematical description of fixed bed nitrate column parameters ($C_0=70$ mg/L)

Sl No	Q , mL/min	Bed Height, cm	Mass of adsorbent, g	t_{total} , minute	V_{eff} , mL	A_s , Area	q_{total} , mg	m , mg _{total}	% Total removal	q_{eq} , mg/g	C_{eq} , mg/L
1	6	10	3	1260	7560	45776	274.656	529.2	51.9	91.55	33.66
2	6	15	4.5	1920	11520	72153	432.918	806.4	53.66	96.20	32.42
3	6	20	6	2400	14400	93480	560.88	1008	55.64	93.48	31.05
4	6	15	4.5	1920	11520	72153	432.918	806.4	53.68	96.20	32.42
5	10	15	4.5	1560	15600	56409	564.09	1092	51.65	125.35	33.84
6	15	15	4.5	1080	16200	38995	584.925	1134	51.58	129.98	33.89

4.5 MODELING OF PACKED BED ADSORPTION COLUMN.

4.5.1 Thomas Model

The column data for different bed heights and flow rate were fitted to the linearized form of Thomas model. The model parameters k_{Th} (mL/min mg) and maximum solid phase concentration q_0 (mg/g) were determined from the experimental data by plotting $\ln \frac{C_0}{C_f} - 1$ versus time. Plots for determining k_{Th} and q_0 for varying bed height and flow rate is shown in Fig. 4.33 and Fig 4.34 respectively. The excellent fit of Thomas model shows that the external and internal diffusions were not the limiting steps. Similar trends have been reported elsewhere for nitrate adsorption onto amine cross linked reed (Zhongfei *et al.*, 2016).

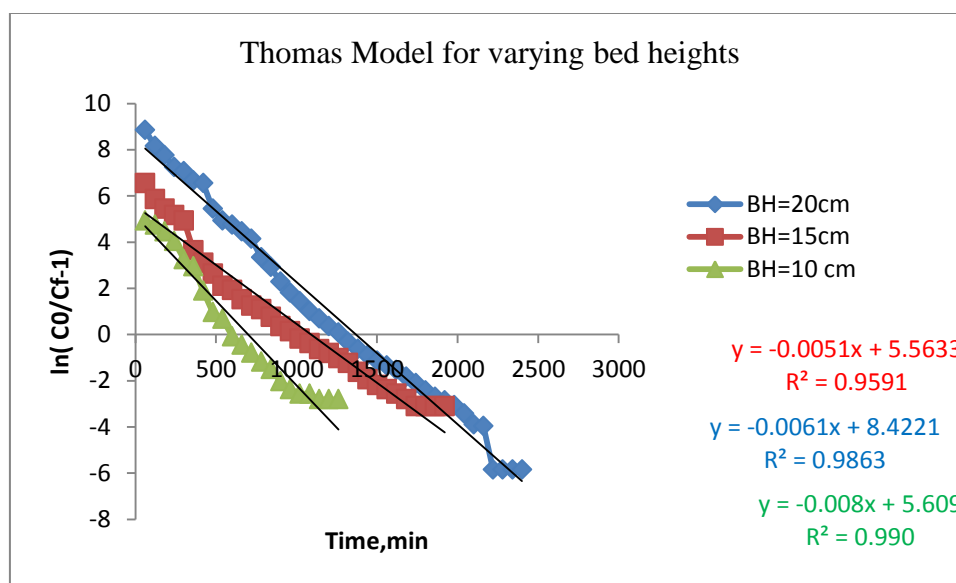


Fig. 4.33. Plot for determining Thomas kinetic coefficient k_{Th} (mL/min mg) and maximum solid phase concentration q_0 (mg/g) for varying bed height

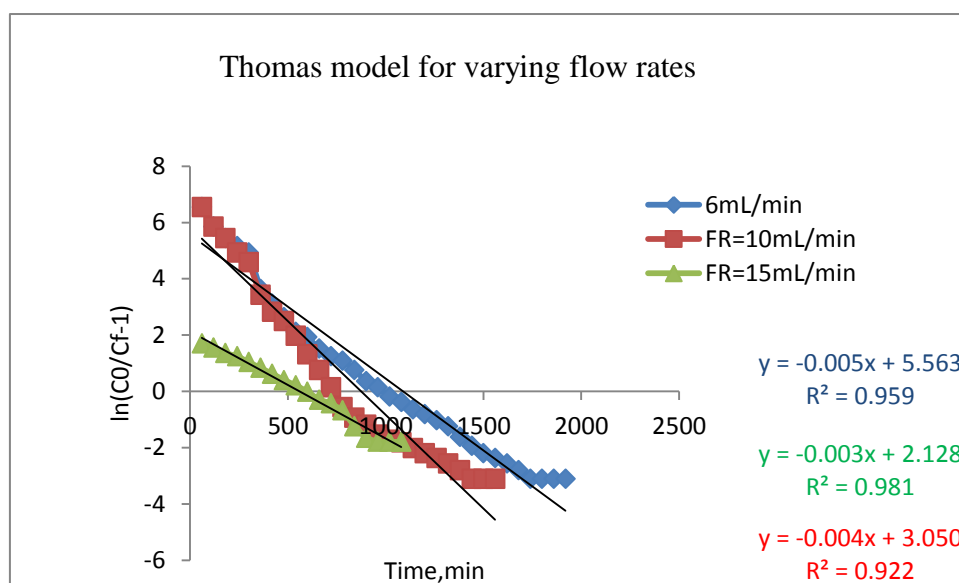


Fig. 4.34 Plot for determining Thomas kinetic coefficient k_{Th} (mL/min mg) and maximum solid phase concentration q_0 (mg/g) for varying flow rate

Breakthrough curves predicted by Thomas model were compared with the experimental breakthrough curves. Fig 4.35 shows the comparison of experimental and theoretical breakthrough curves predicted by Thomas model for varying bed height. The smooth curve represents the prediction by Thomas model. The experimental and theoretical breakthrough curves predicted by Thomas model were superimposed, which indicates that there is a fit between experimental and predicted values of C_f/C_0 . Fig. 4.36 shows the comparison between experimental breakthrough curves and that predicted by Thomas model for varying flow rate.

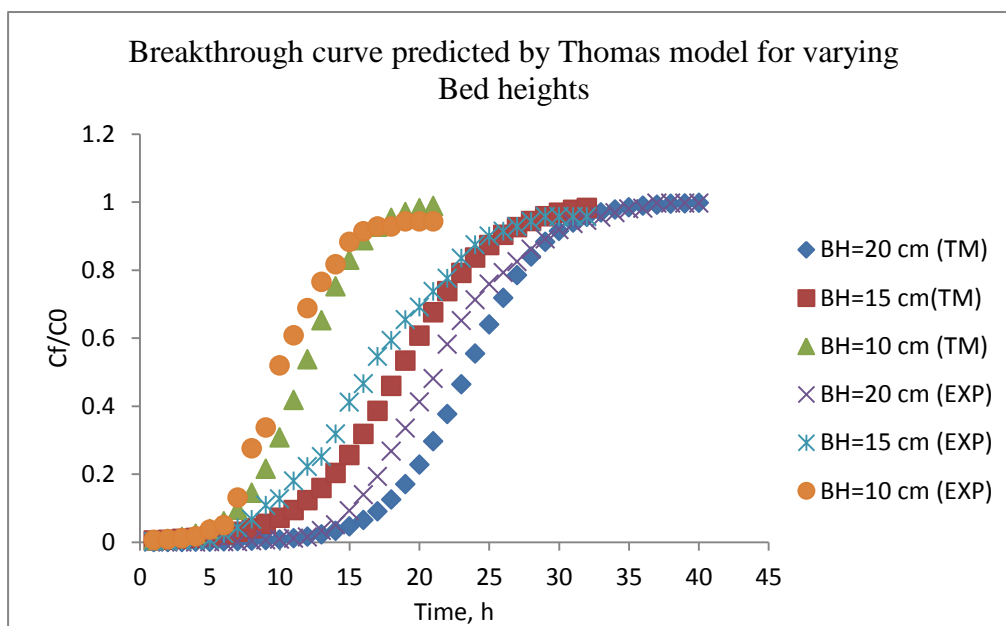


Fig. 4.35 Comparison of experimental and theoretical breakthrough curves predicted by Thomas model for varying bed height

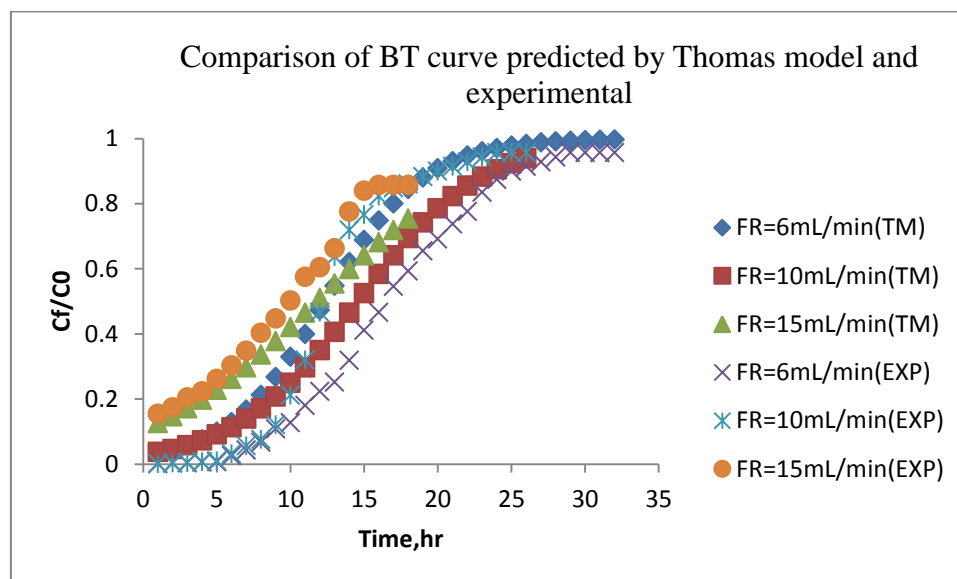


Fig. 4.36 Comparison of experimental and theoretical breakthrough curves predicted by Thomas model for varying flow rate

Thomas model is commonly used for the prediction of breakthrough analysis. The simplicity and accuracy of Thomas Model make it to suitable for the description of the breakthrough performance of the fixed bed adsorption column. The correlation coefficients in the determination of coefficients of the Thomas model for varying bed heights of 10 cm, 15 cm, and 20 cm were $R^2=0.99$, $R^2=0.97$ and $R^2=0.94$. The value of k_{Th} was decreased (0.11 to 0.057) with bed heights increasing from 10 cm to 20 cm. It was attributed to the increased surface area of the nanocomposite films (Lim and Aris, 2014). Therefore higher bed heights would increase the adsorption of nitrate anions. It was found that q_0 first increased and then decreased. The same results were also obtained for experimental data. The higher regression coefficients for varying bed depths showed that the parameters of the Thomas model were determined without much error. The value of Thomas kinetic coefficient for influent nitrate velocity of 6 mL/min, 10 mL/min, and 15 mL/min were calculated and obtained as 0.071, 0.086, and 0.128 mL/min mg. The increase in k_{Th} with flow rate shows that the low flow rate is favorable for better adsorption. The parameters predicted by Thomas model for different experimental conditions in nitrate fixed bed adsorption column is shown in Table 4.14.

Table 4.14 The Thomas model parameters at different flow rates and bed heights (initial concentration = 70 mg NO₃-N/L)

Model	Parameter	Q= 6 mL/min	Q=10 mL/min	Q=15 mL/min	BH=10 cm	BH=15 cm	BH=20 cm
Thomas model	k_{Th} , mL/min	0.071	0.086	0.128	0.114	0.071	0.057
	mg						
	q_0 (mg/g)	114.29	165.28	146.09	98.16	115	97.93
	R^2	0.97	0.96	0.98	0.99	0.97	0.94

4.5.2 Yoon Nelson Model

The Yoon-Nelson model is applied in the continuous adsorption study of nitrate ions onto nanocomposite films. The requirement of fewer column data makes Yoon Nelson model a simple theoretical model. This model is suitable for single-component systems (K. Garg and K. Kadirvelu, 2013). The Yoon Nelson rate constant (k_{YN}) and time for 50% of adsorbate breakthrough (τ) were obtained from the linearized Yoon-Nelson equation. In the present work, the fit of experimental data was checked for the packed bed nitrate adsorption column. k_{YN} and τ are determined graphically by plotting $\ln(C_f/(C_0 - C_f))$ versus time. The plot for determining the Yoon Nelson coefficient for varying bed height and varying flow rates is depicted in Fig. 4.37 and Fig 4.38 respectively.

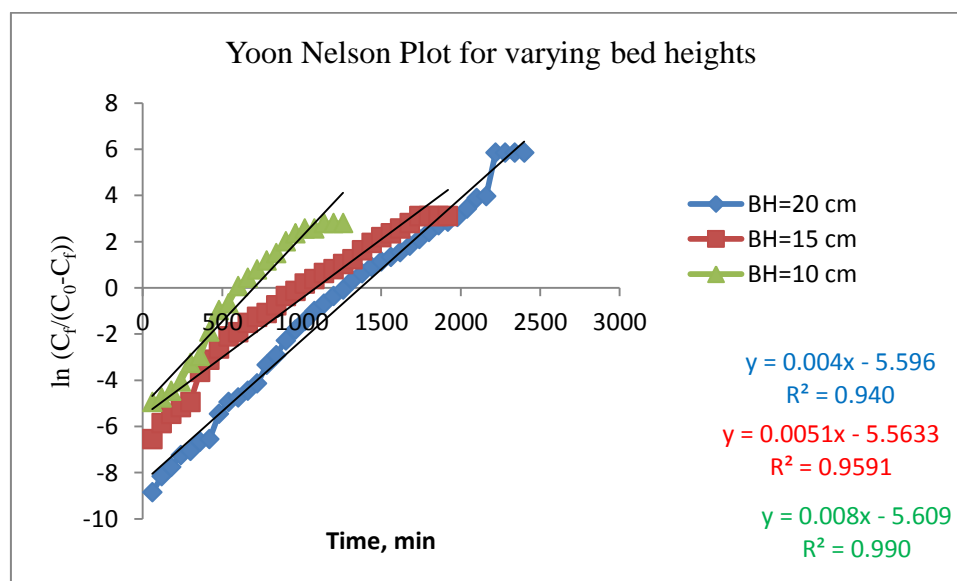


Fig. 4.37 Yoon Nelson parameters determination for varying bed height

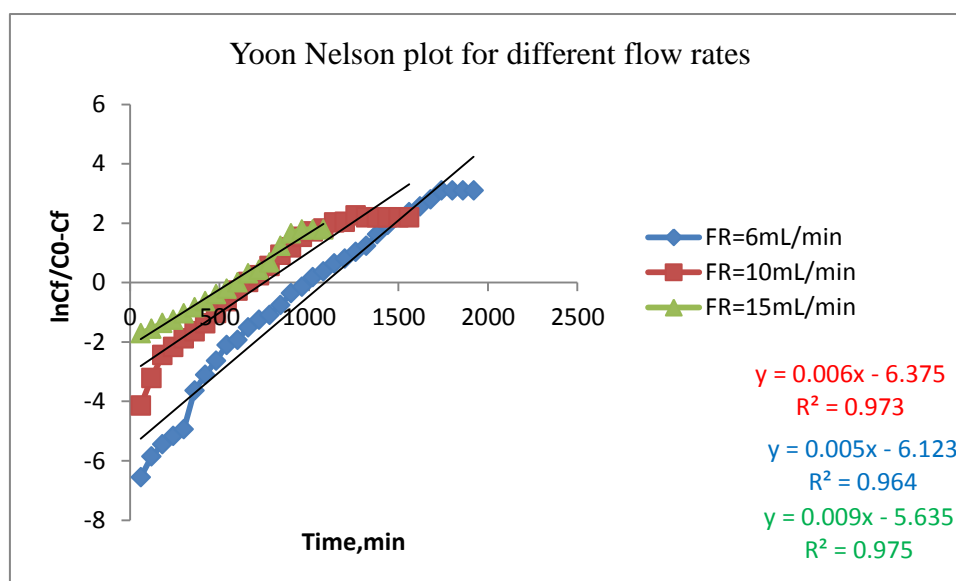


Fig. 4.38 Determination of coefficients in the Yoon Nelson model for varying flow rate

The time for 50% breakthrough predicted by Yoon Nelson model for different bed heights 10 cm, 15 cm, and 20 cm was obtained as 11.7 h, 20.5 h, and 23.3 h, respectively. The correlation coefficients for determining the parameters of Yoon Nelson model for varying bed heights lie between 0.94-0.99 which shows that this model is to some extent ahead of the experimental data. For 20 cm bed depth, the 50% breakthrough time was very close to experimental results. This confirms that longer beds are preferable for better performance. The time for 50% breakthrough predicted by Yoon Nelson model for various flow rates 6 mL/min, 10 mL/min, and 15 mL/min were 20.4 h, 17.7 h, and 10.4 h respectively. The results showed that the time required for a 50% breakthrough, ' τ ' decreased with an increase in flow rate. A similar observation was made during the sorption of nitrate with Purolite A520E resin in a fixed bed column (Nur T *et al.*, 2014). Also, to note was the correlation coefficient for determining the parameters of the Yoon Nelson model for different flow rates lie between 0.96-0.97. This study proved that the Yoon

Nelson model is an excellent method for determining the 50% breakthrough time for the nitrate column for varying flow rates. The parameters of the Yoon Nelson model for changing bed height and flow rate are shown in Table 4.15. Breakthrough curves predicted by Yoon Nelson model were analyzed graphically for change in bed height and flow rate. Fig. 4.39 and Fig 4.40 show the comparison of breakthrough curves predicted by Yoon Nelson model for varying bed height and flow rate respectively.

Table 4.15. The Yoon Nelson model parameters at different flow rates and bed heights (initial concentration = 70 mg N/L)

Model	Parameter	Q= 6 mL/min	Q=10 mL/min	Q=15 mL/min	BH=10 cm	BH=15 cm	BH=20 cm
Yoon Nelson model	k_{YN} , minute ⁻¹	0.005	0.006	0.009	0.008	0.005	0.004
	τ , hrs	20.4	17.7	10.4	11.7	20.5	23.3
	R ²	0.96	0.97	0.97	0.99	0.97	0.94

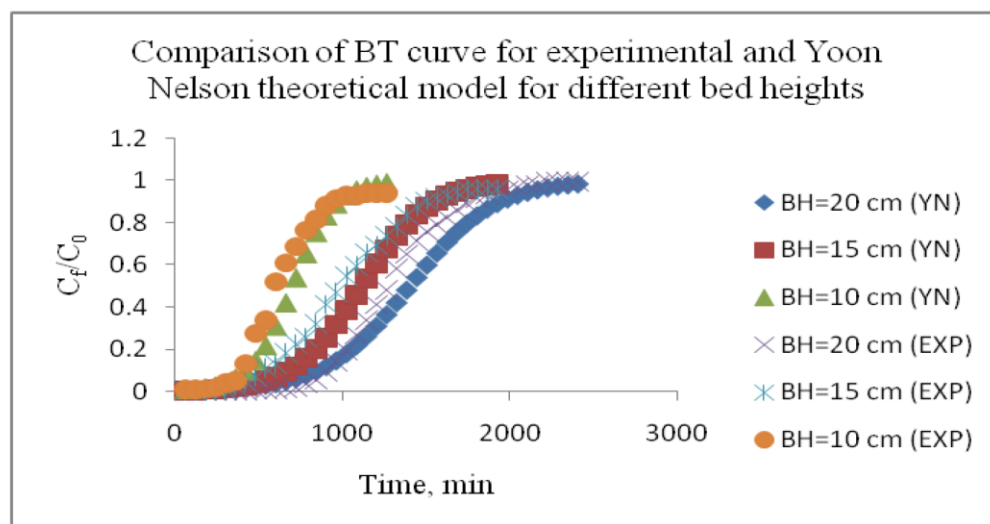


Fig. 4.39 Comparison of experimental and theoretical breakthrough curves by Yoon Nelson model for varying bed height

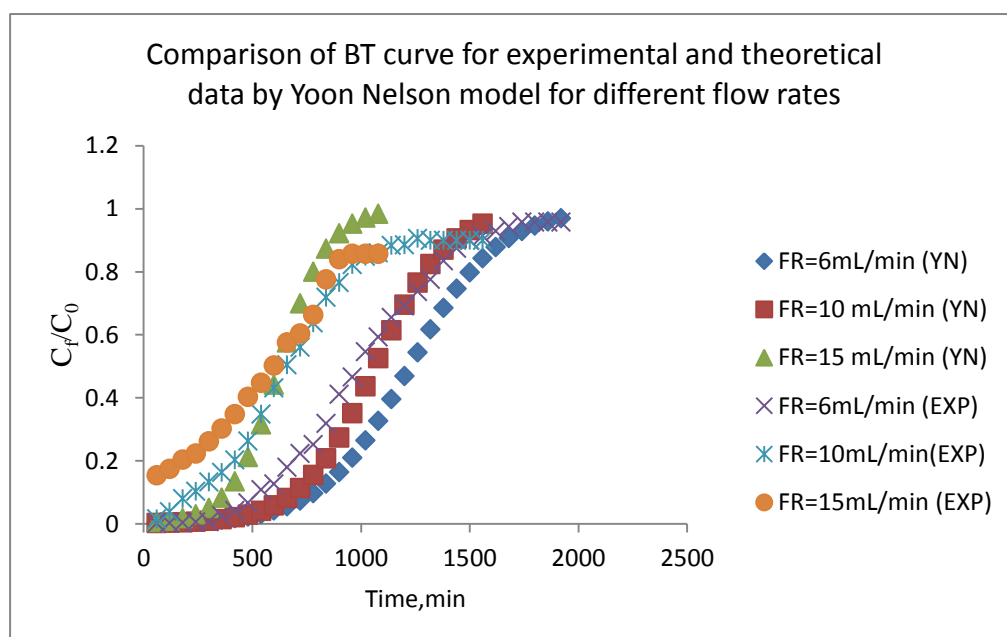


Fig. 4.40 Comparison of experimental and theoretical breakthrough curves by Yoon Nelson model for different flow rates

4.5.3 Adam Bohart Model

The Adam Bohart model is usually selected for interpretation of the breakthrough time in the initial state of adsorption operation. In the current work on adsorption of nitrate on chitosan-bentonitenanocomposite film in a packed adsorption column, Adam Bohart kinetic constant k_{AB} and saturation concentration N_0 were determined. The Adam Bohart parameters have been obtained from the plot of $\ln(C_t/C_0)$ vs. time. Fig 4.41 and Fig 4.42 depicts the plot for the determination of Adam Bohart model parameters for different bed heights and flow rates.

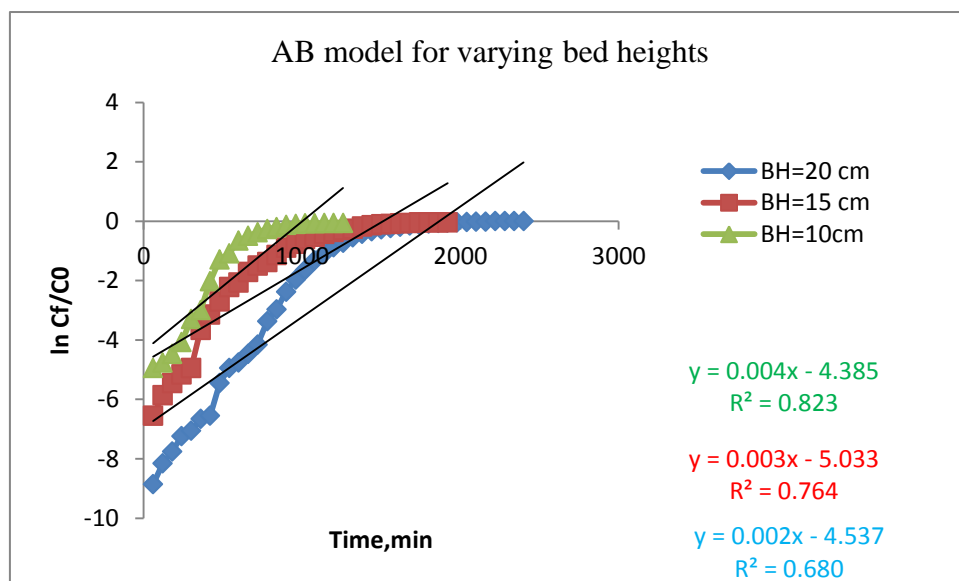


Fig. 4.41 Determination of Adam Bohart model parameters for bed height = 10 cm, 15 cm and 20 cm

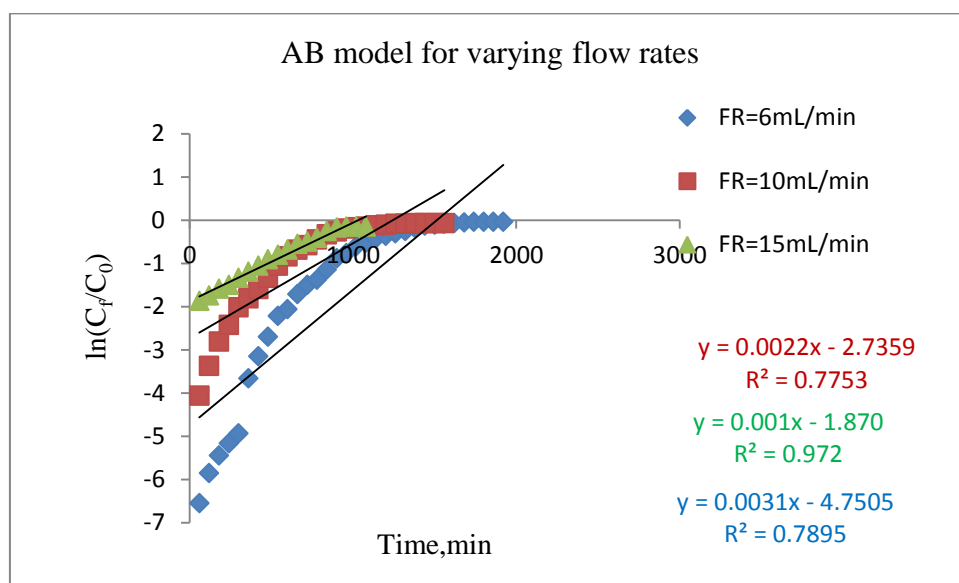


Fig. 4.42 Determination of Adam Bohart model parameters for different flow rate

Table 4.16 gives the computed Adam-Bohart model parameters at different flow rates and bed heights for initial nitrate concentration of 70 mg/L. The A-B constant, k_{AB} values for different bed heights 10 cm, 15 cm, and 20 cm was computed as 5.71, 4.28, and 2.85 respectively. An increase in the model's saturation concentration N_0 was also observed with an increase in bed height. The linear regression coefficient was in the range 0.68-0.82 for all the three-bed heights. When the flow rate was increased, the values of N_0 is increased. As the flow rate increases, the volume of nitrate solution that entered the column was higher and caused the earlier saturation of the nanocomposite film packing. This shows that the physical mass transfer of the packed bed is contributing to adsorption kinetics (Xing *et al.*, 2013). The linear regression coefficient for determining Adam Bohart parameters for the three flow rates lie between 0.76-0.93.

Table 4.16. The Adam-Bohart model parameters at different flow rates and bed heights (initial concentration = 70 mg N/L)

Model	Parameter	Q= 6 mL/min	Q=10 mL/min	Q=15 mL/min	BH=10 cm	BH=15 cm	BH=20 cm
Adam Bohart Model	k_{AB} , L/mg.min (10^{-5})	4.28	5.71	5.71	5.71	4.28	2.85
	U_0 , cm/min	1.22	2.04	3.57	1.22	1.22	1.22
	N_0 , mg/L(10^3)	9.6	12.6	15.4	9.4	9.6	9.71
	R^2	0.76	0.84	0.93	0.82	0.76	0.68

The breakthrough curves predicted by the A-B model and experimental values were plotted and compared. From the plot of breakthrough curves for the three-bed heights (Fig. 4.43), it can be observed that the curves were overlapping in the initial part of the column operation, but showed considerable change at the right end. The comparison between experimental and theoretical breakthrough curves for three different flow rates by Adam Bohart model is shown in Fig. 4.44. With an increase in the flow rate, bed saturation occurred faster. This is because more adsorbate enters the active site of the adsorbent when the flow rate is increased.

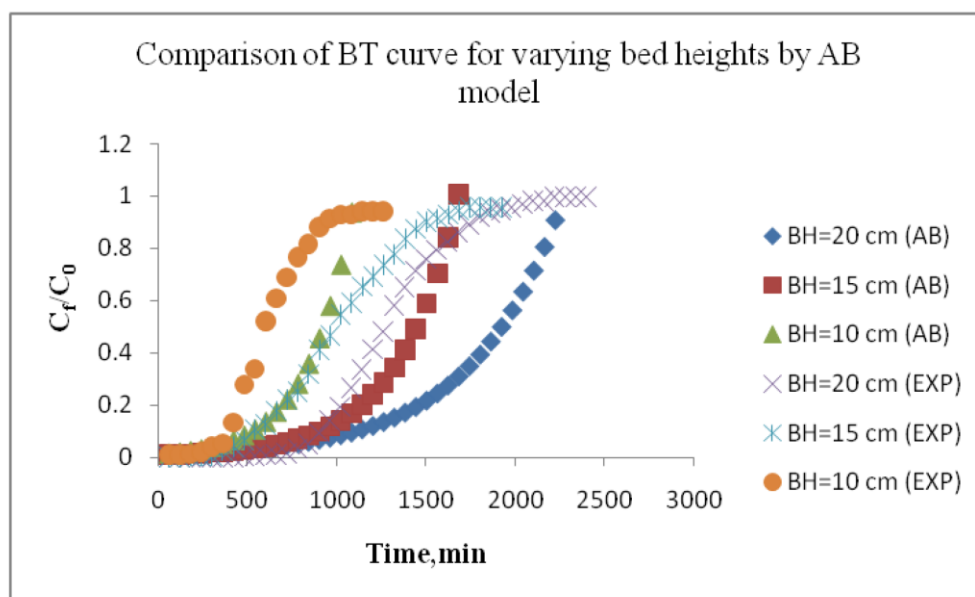


Fig. 4.43 Breakthrough curves by Adam Bohart Model and experimental for bed height=10 cm, 15 cm and 20 cm

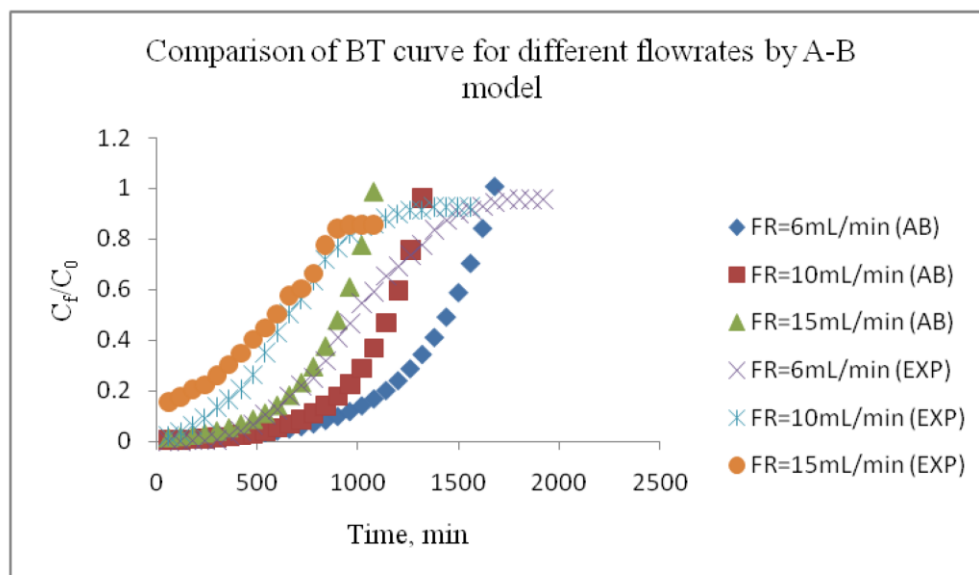


Fig. 4.44 Breakthrough curves by Adam Bohart Model and experimental for varying flow rate $Q=6\text{mL}/\text{min}$, $10\text{mL}/\text{min}$ and $15\text{mL}/\text{min}$.

4.5.4 Comparison of Thomas model, Yoon Nelson model and Adam Bohart model

The correlation between experimental and theoretical data of column operation was compared with three models. Correlation coefficients for three-bed heights 10 cm, 15 cm, and 20 cm at a flow rate of 6 mL/min for Thomas and Yoon Nelson model is above 0.9. This shows that Thomas model and Yoon Nelson model were fitted to the experimental data well. The R^2 values for different flow rates also show a significant correlation with $R^2 > 0.9$. The exception indicates at an infiltration velocity of 10 mL/min. Adam Bohart correlation coefficients were low, and this model fitted only to the first part of the column operation for varying bed height and flow rate.

Comparison of $(C_f/C_0)_{\text{theoretical}}$ and $(C_f/C_0)_{\text{experimental}}$ data for varying bed height and flow rate by Thomas model is shown in Fig. 4.45 and Fig 4.46. The verification of $(C_f/C_0)_{\text{theoretical}}$ and $(C_f/C_0)_{\text{experimental}}$ by Yoon Nelson model for various bed height and flow rate is given in Fig. 4.47 and and Fig 4.48. The experimental and theoretical data validation by Adam Bohart model for different bed height and flow rate is given by Fig. 4.49. and Fig 4.50 respectively.

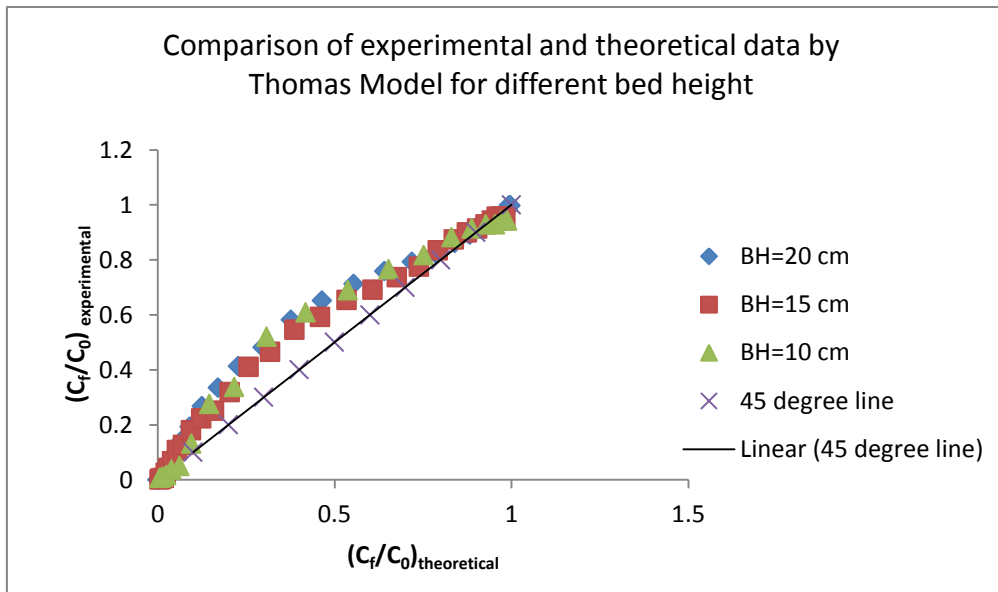


Fig. 4.45 Comparison of $(C_f/C_0)_{\text{experimental}}$ and $(C_f/C_0)_{\text{theoretical}}$ by Thomas model for varying bed height

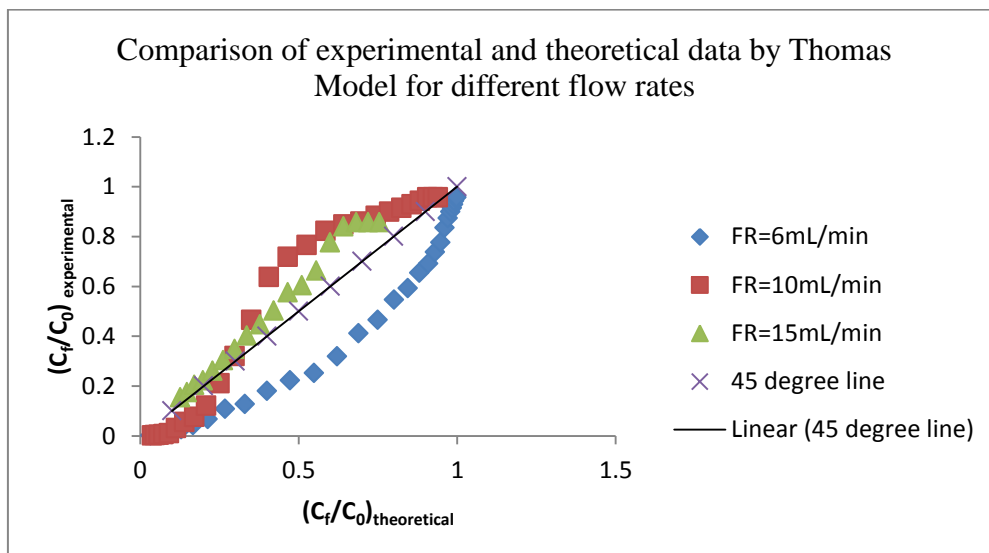


Fig. 4.46 Comparison of $(C_f/C_0)_{\text{experimental}}$ and $(C_f/C_0)_{\text{theoretical}}$ by Thomas model for varying flow rate

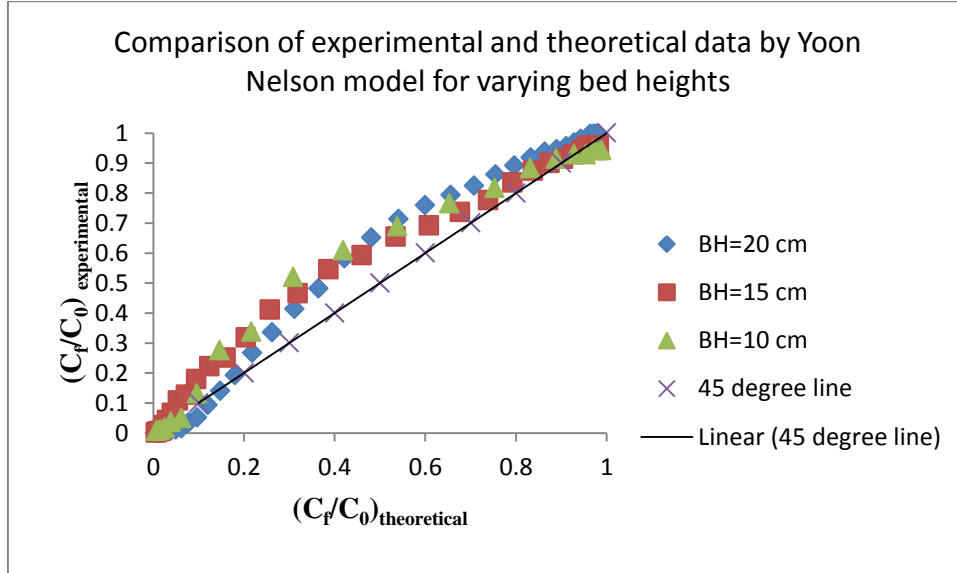


Fig. 4.47 Comparison of $(C_f/C_0)_{\text{experimental}}$ and $(C_f/C_0)_{\text{theoretical}}$ by Yoon Nelson model for varying bed height

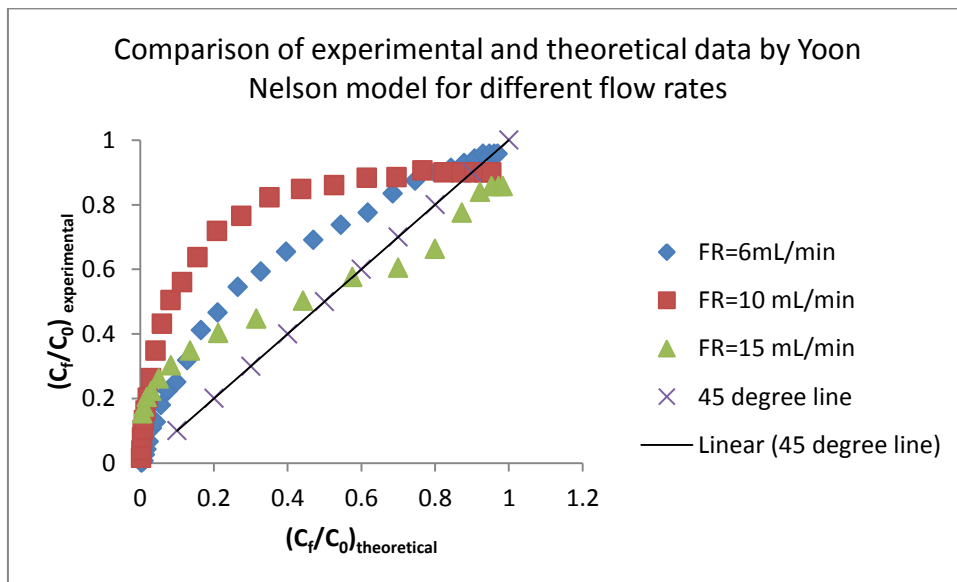


Fig. 4.48 Comparison of $(C_f/C_0)_{\text{experimental}}$ and $(C_f/C_0)_{\text{theoretical}}$ by Yoon Nelson model for varying flow rate

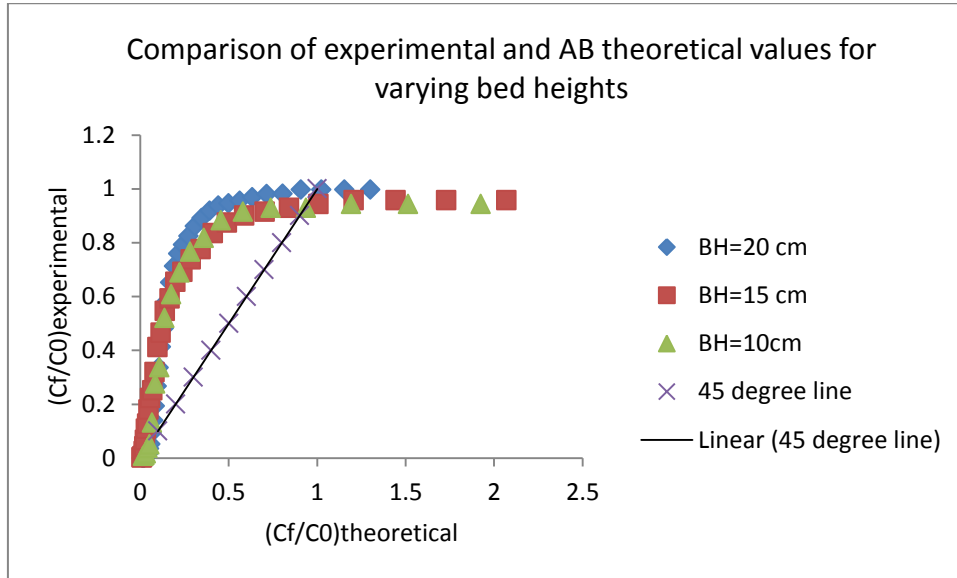


Fig. 4.49 Comparison of $(C_f/C_0)_{\text{experimental}}$ and $(C_f/C_0)_{\text{theoretical}}$ by Adam Bohart model for varying bed height

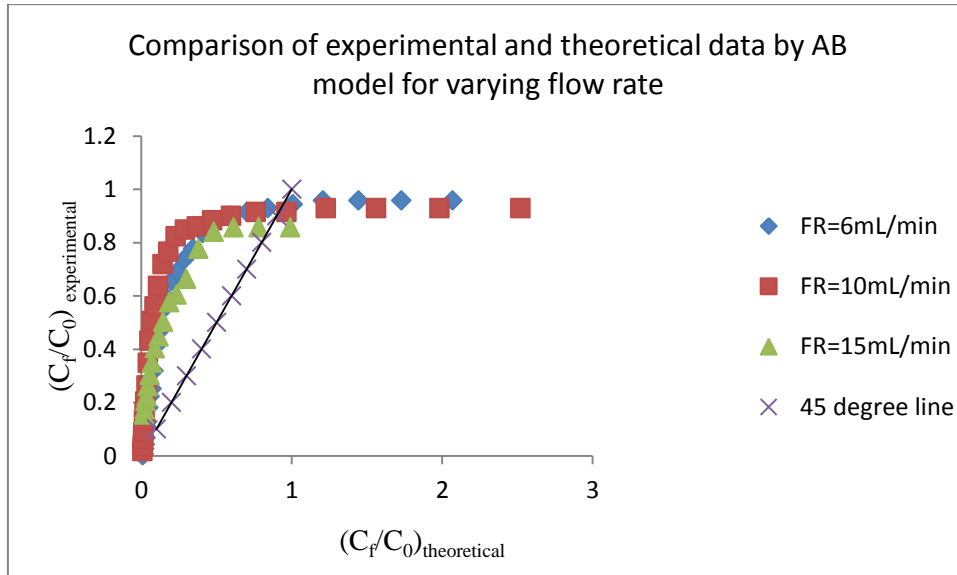


Fig. 4.50 Comparison of $(C_f/C_0)_{\text{experimental}}$ and $(C_f/C_0)_{\text{theoretical}}$ by Adam Bohart model for varying flow rate.

Correlation coefficients for experimental versus theoretical C_f/C_0 by Thomas model, Yoon Nelson model, and Adam Bohart model for different bed heights and flow rates are shown in Table 4.17 and Table 4.18 respectively. The calculated R^2 values for the experimental conditions $Q=6\text{ mL/min}$, $Z=15\text{ cm}$ in the varying bed heights, and varying flow rates shows close agreement ($R^2=0.91$ and 0.97 for Thomas model and $R^2=0.97$ and 0.94 for Yoon Nelson model). The lower R^2 value of Adam Bohart's model shows the poor fit of the model to the data. Considering the higher R^2 values and trend of the model parameters, it can be concluded that Thomas model and Yoon-Nelson model best described the continuous adsorption process.

Table 4.17 Correlation coefficients for Thomas model, Yoon Nelson model and Adam Bohart model for different bed heights

Q , mL/min	Z , cm	R^2 (Thomas model)	R^2 (Yoon Nelson model)	R^2 (Adam Bohart Model)
6	10	0.962	0.962	0.56
6	15	0.912	0.97	0.59
6	20	0.901	0.98	0.66

Table 4.18 Correlation coefficients for Thomas model, Yoon Nelson model and Adam Bohart model for different flow rates.

Q , mL/min	Z , cm	R^2 (Thomas model)	R^2 (Yoon Nelson model)	R^2 (Adam Bohart Model)
6	15	0.974	0.935	0.59
10	15	0.978	0.74	0.43
15	15	0.74	0.978	0.78

4.6. BATCH ADSORPTION STUDY OF AMMONIA-NITROGEN REMOVAL USING CHITOSAN-BENTONITE NANOCOMPOSITE FILMS.

The adsorption efficiency of ammonia nitrogen using chitosan-bentonite nanocomposite films synthesized in the laboratory was analyzed through batch adsorption experiments. Batch experiments were conducted with 0.1 g of the adsorbent for ammonium chloride samples of volume 50 mL kept in a temperature controlled incubated shaker at 120 rpm. The residual concentration of ammoniacal nitrogen was determined by Nessler's reagent colorimetric method using UV-VIS spectrophotometer set at $\lambda_{\max} = 430$ nm. The influence of pH on ammonia adsorption is discussed in this section. Kinetics of adsorption, equilibrium isotherm and thermodynamic studies using novel chitosan nanoclay composite for ammonia uptake were analyzed. The combined effect of variables was studied using response surface methodology and the optimum conditions were determined for ammonia nitrogen removal using the response optimizer of Box-Behnken design. The regeneration of nanocomposite films loaded with ammonium ions has been carried out with 0.5 mol/L NaOH solution as eluent. The effect of pH and effect of temperature study has been repeated with recycled nanocomposite films.

4.6.1 Effect of pH on Ammonia Nitrogen Removal by CH-B-NCF

To study the effect of pH on adsorption of ammonia nitrogen, 0.1 g of nanocomposite films was added in 50 ml of 50 mg/L NH_4^+ -N solution. Then the solution was shaken for 60 minutes in an incubated shaker at 303K. The pH was varied from 2 to 10. The effect of pH on % removal of ammonia nitrogen and adsorption capacity is shown in Fig. 4.51. As pH was increased, the efficiency of adsorption of NH_4^+ -N increased and maximum removal was

obtained at pH 6. A sudden decrease in the adsorption capacity was seen both at strongly acidic medium and at strongly alkaline range. NH_4^+ and $\text{NH}_3\cdot\text{H}_2\text{O}$ are the two forms of ammonia nitrogen in solution. NH_4^+ is the main form of existence in acidic or neutral conditions. In alkaline conditions, NH_4^+ changes into $\text{NH}_3\cdot\text{H}_2\text{O}$, which is not conducive to the adsorption of ammonia nitrogen and lowers the adsorption efficiency. Ammonia nitrogen is neutralized by hydroxyl ion and rendering it uncharged in alkaline medium. The solution enriched with H^+ in the acidic condition will also hinder the adsorption of ammoniacal nitrogen. The $-\text{COOH}$ and $-\text{COO}^-$ are the two vital functional groups responsible for adsorption. The ionization of the, $-\text{COOH}$ and $-\text{COO}^-$ takes place both at acidic and basic medium. Accordingly there will be decrease in the electrostatic attraction between nanocomposite films and ammonium ions. The pH value of the original working solution was 6.4. Therefore the pH of the working standard ammonia nitrogen is not adjusted in further experiments.

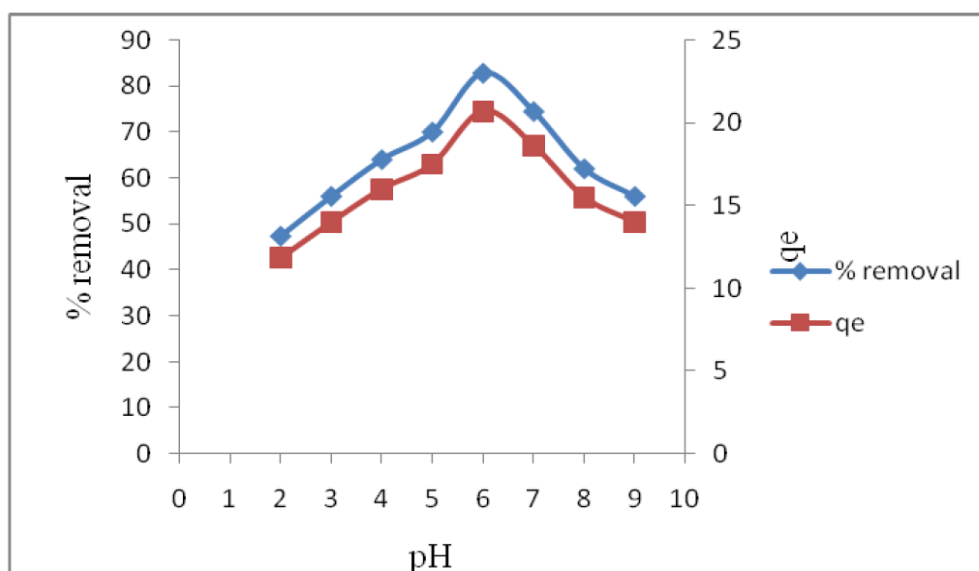


Fig. 4.51 Effect of pH on percentage removal and adsorption efficiency of ammonia nitrogen using CH-B-NCF

4.6.2. Adsorption Isotherms of Ammonia Nitrogen Uptake onto Chitosan Bentonite Nanocomposite Films.

The equilibrium studies were carried out by changing the initial concentration from 10 mg/L to 50 mg/L at room temperature. The adsorbent dosage was 0.1 g/ 50 m L. Shaking was performed at 120 rpm and 100 minutes. Langmuir and Freundlich adsorption isotherms were analyzed in the ammonia nitrogen removal with CH-B-NCF. The isotherm plots have shown in Fig.4.52. The estimated model parameters of equilibrium isotherm have been summarized in Table 4.19. Langmuir, Freundlich, isotherm plots had R^2 as 0.81, 0.93 respectively. It is evident that the Freundlich isotherm was suitable than Langmuir isotherm for fitting to experimental data. The Freundlich adsorption gives an approach to surface heterogeneity and an exponential distribution of active sites and their energies (Xinggong Wang *et al.*, 2014). The Freundlich constants K_f is related to adsorption capacity, and n is indicating the favourability of adsorption. Both K_f and $1/n$ have been calculated and obtained as 2.33 L/g and 0.77, respectively. The value of $1/n$ in the range of $0.1 < 1/n < 1$ indicates the adsorption of $\text{NH}_4^+\text{-N}$ is favorable. The maximum adsorption capacity q_m calculated from the Langmuir Isotherm model was 37.01 mg/g. The value of Langmuir constant obtained was $K_L = 0.06$ L/mg. The value of R_L , which is an authoritative feature of the Langmuir isotherm model, should lie in the range $0 < R_L < 1$ for favorable adsorption. Here the values of R_L at all concentrations are less than one, which shows that adsorption is favorable. It was found that the R_L values were decreasing with increasing initial concentration. The results showed that more ammonia nitrogen molecules are penetrating the composite by diffusion in the initial stage of adsorption. The adsorption sites like $-\text{COO}-$, $-\text{OH}$ are getting saturated by electrostatic attraction. The adsorption capacities of different adsorbents for removal of ammonia nitrogen has given in Table 4.20. In this study, the value of q_m is 37.01 mg/g, which is higher than the results made by the above scientists for the removal of ammonia nitrogen.

Table 4.19 Equilibrium parameters for adsorption of NH_4^+ -N on to chitosan bentonitenanocomposite films

Langmuir Isotherm			Freundlich Isotherm		
q_m , mg/g	b, L/mg	R^2	K_f , mg/g(mg/L) ⁿ	n	R^2
37.01	0.06	0.81	2.33	1.28	0.93

Table 4.20 Ammonia nitrogen adsorption capacities of various adsorbents

Adsorbent	Adsorption Capacity (mg/g)	Reference
Zeolite synthesized from fly ash	24.3	Mulan et al., 2011
Chitosan polyacrylic acid composite	21.1	Yian et al., 2009
Starch based hydrogel nanocomposite	19.0	Batool et al., 2015
Chitosan bentonite nanocomposite films	37.0	Present study

Fig 4.53 shows the equilibrium data of ammonia nitrogen removal from aqueous solution fitted to Langmuir and Freundlich isotherms. A slight variation is seen at higher initial concentrations.

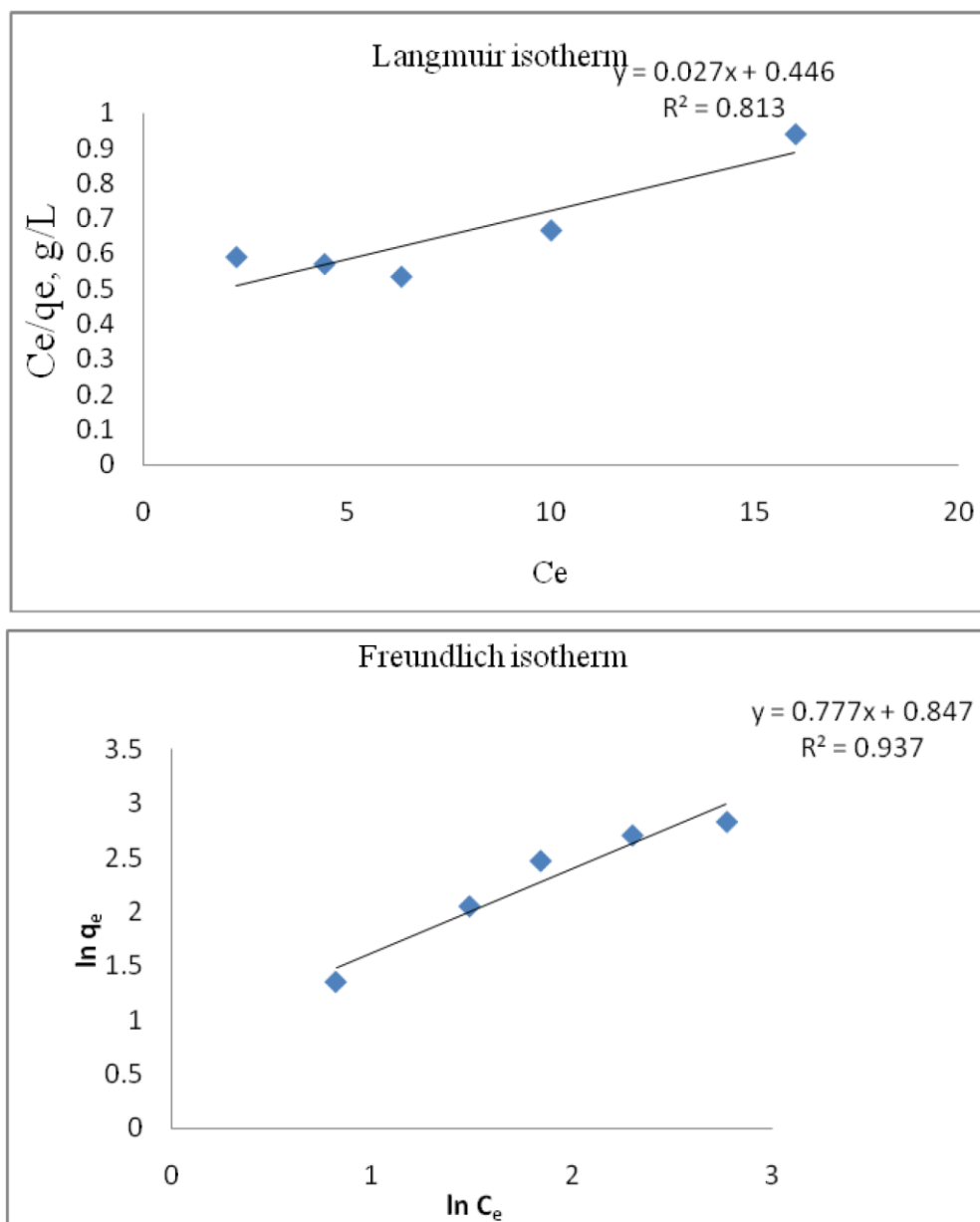


Fig 4.52 Langmuir and Freundlich isotherm plots for ammonia nitrogen adsorption onto CH-B-NCF.

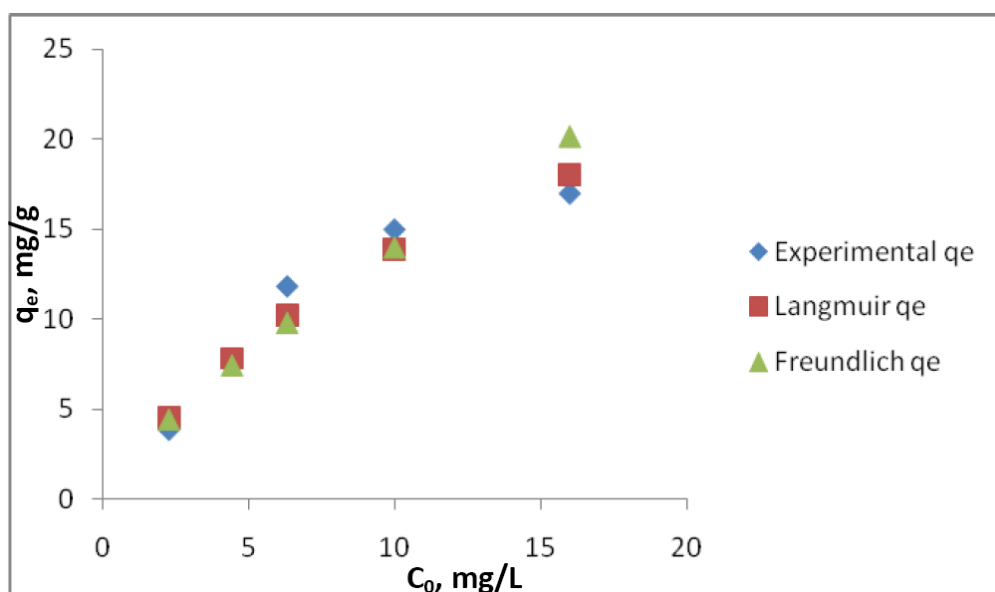
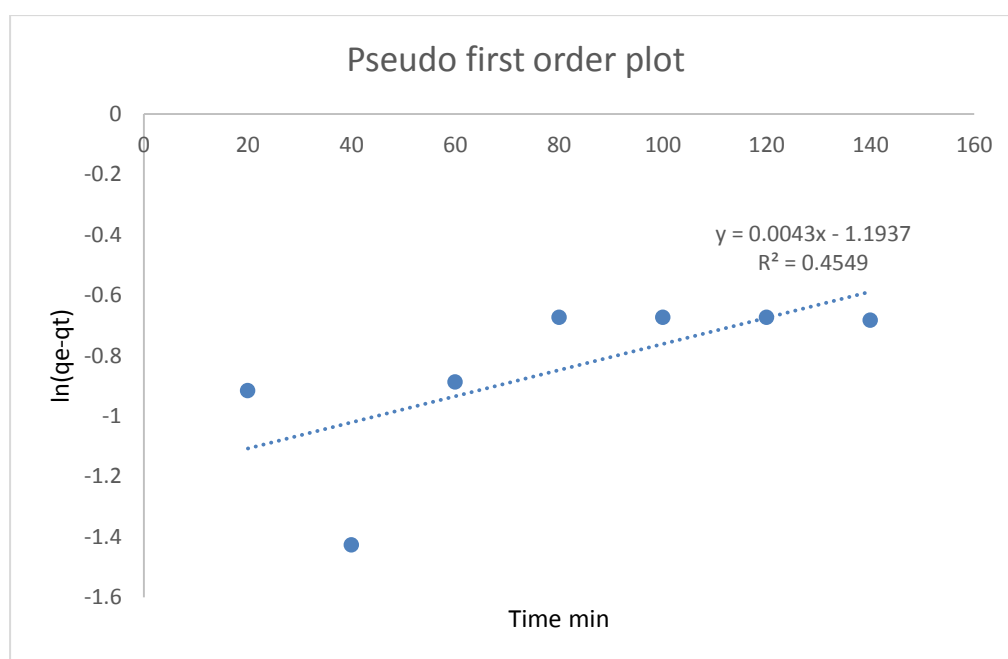


Fig 4.53 Equilibrium data of ammonia removal from aqueous solution fitted to Langmuir and Freundlich isotherms

4.6.3. Kinetics of Adsorption of Ammonia Nitrogen onto CH-B-NCF

Kinetic analysis is a prerequisite to find the frequency of adsorption and rate-limiting step that is involved in the design of adsorption on a large scale. In this study, the adsorption was rapid, and the removal efficiency was improved with the rise in adsorption process time and reached equilibrium in 60 minutes. The insignificant removal efficiency after one hour is attributed to the low solute concentration gradient and lack of adsorption sites. Here pseudo-first-order, second order, and pseudo-second-order kinetic models were used to analyze the data obtained. Fig 4.54 shows the kinetic plots of adsorption of ammonia nitrogen onto CH-B-NCF. The kinetic parameters and correlation coefficients of three kinetic models have tabulated in Table.4.20. The R^2 values of pseudo-second-order, pseudo-first-order, and the second-order were obtained as $R^2=0.99$, $R^2=0.45$, and $R^2=0.38$, respectively. This

shows that the reaction follows pseudo-second-order. The very small R^2 values indicates that pseudo-first-order and second-order models are poorly fitted to the adsorption of ammonium ions on the surface of nanocomposite films. The experimental q_e value was 11.4 mg/g, and q_e calculated using pseudo-second-order kinetics was 11.49 mg/g. The fitting of ammonium adsorption kinetic data to pseudo-second-order model was observed by other researchers can be seen in the literature (Aref *et al.*, 2014; Haiming *et al.*, 2010) The pseudo-second-order rate constant was obtained as $0.00426 \text{ g mg}^{-1} \text{ min}^{-1}$. The kinetic constants have been depicted in Table 4.21



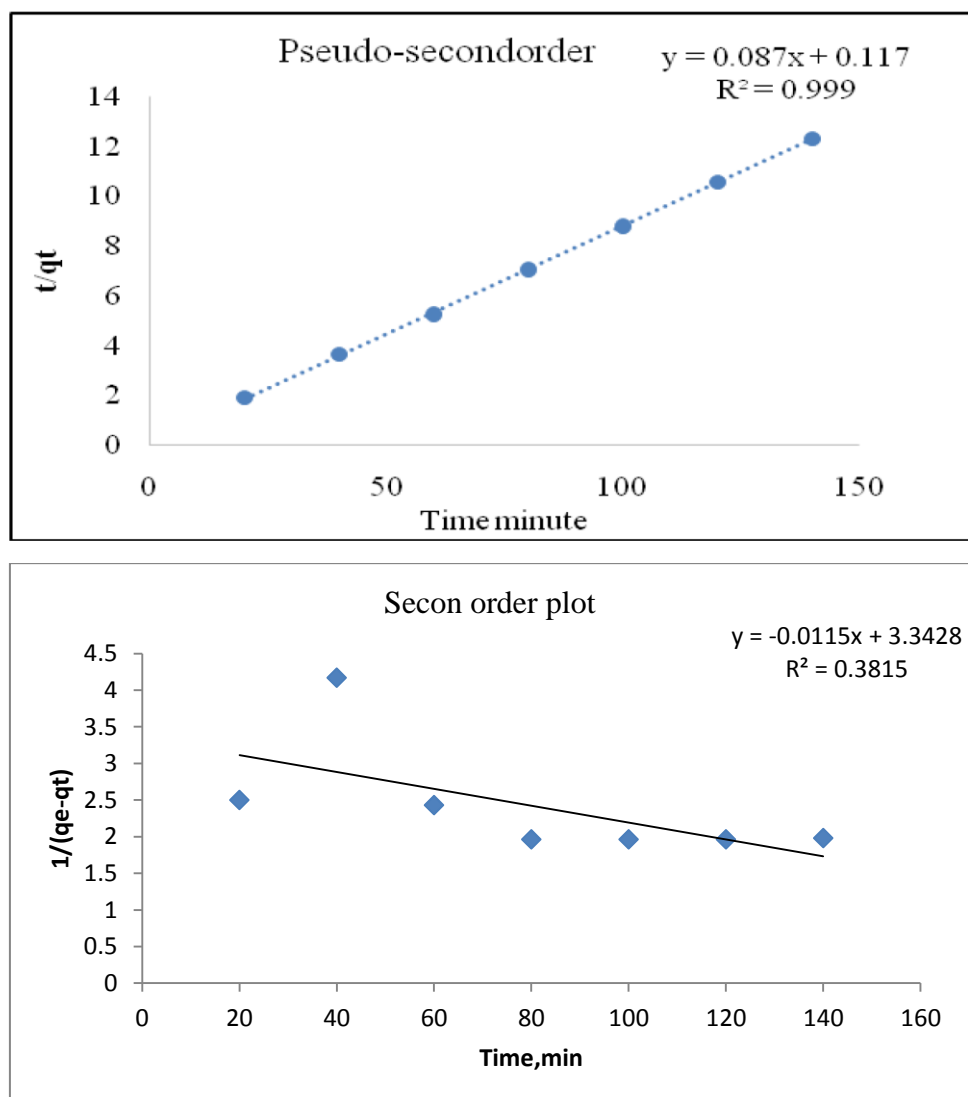


Fig 4.54 Kinetic plots for ammonia nitrogen adsorption onto CH-B-NCF

The kinetic data were further analyzed with two kinetic diffusion models, intraparticle diffusion model, and Dunwald Wagner film diffusion model and are shown in Fig 4.55. In the present study, the intraparticle rate constant is $0.099 \text{ mg/g/min}^{1/2}$, and the slope is 10.34, respectively ($R^2=0.67$). In the Weber-Morris intraparticle diffusion plot, the initial curve represents the boundary layer effect, and the straight line represents intra-particle-diffusion.

The multi-linearity in the plot shows that the intraparticle diffusion is not the sole rate-limiting step. There is the possibility of both particle and pore diffusion in the adsorption process. Dunwald-Wagner diffusion model showed pure fit with $R^2=0.39$.

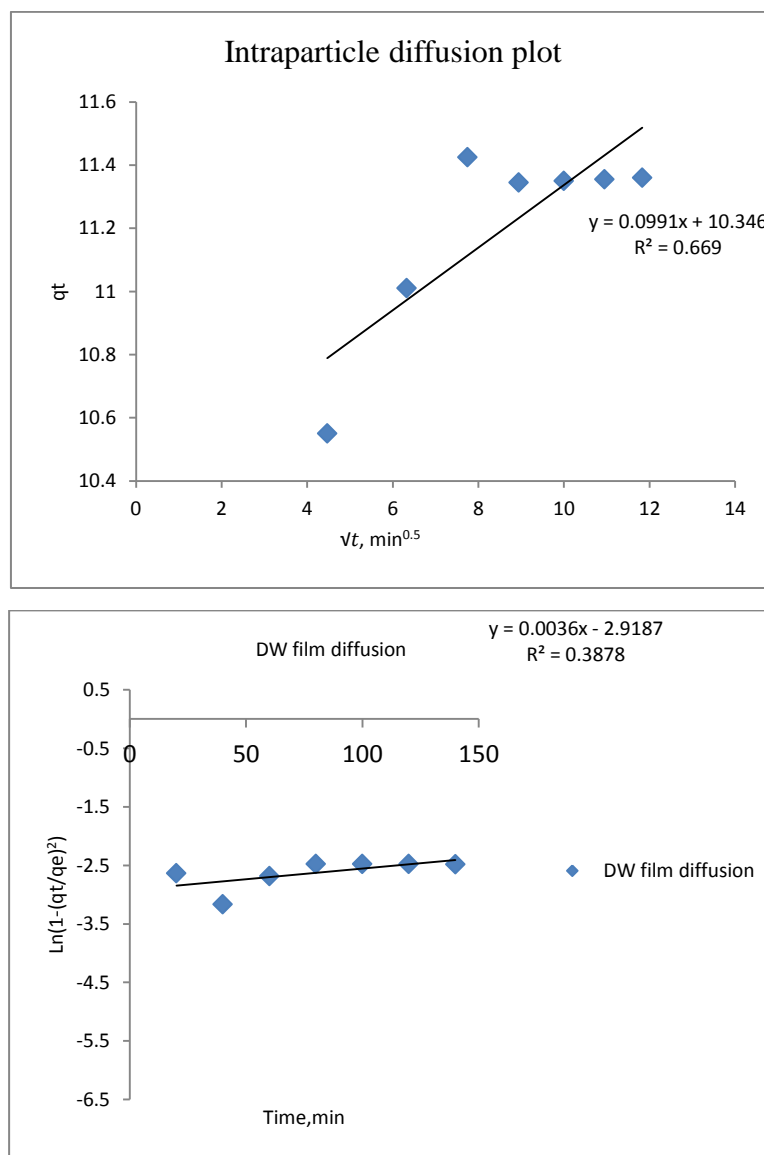


Fig 4.55 Kinetics of adsorption diffusion model of ammonia nitrogen onto chitosan bentonite nanocomposite films.

Table 4.21 The kinetic constants and correlation coefficients for adsorption of ammonia nitrogen on to chitosan bentonitenanocomposite films.

Experimental	Pseudo first order			Second order			Pseudo second order		
	q_{ecal} , mg/g	R^2	k_1 min^{-1}	q_{ecal} , mg/g	R^2	K_2 , $g.mg^{-1}$ min^{-1}	q_{ecal} , mg/g	R^2	k_2 , $g.mg^{-1} min^{-1}$
11.4	0.17	0.45	0.004	0.3	0.38	0.001	11.49	0.99	0.007

4.6.4 Thermodynamics of Adsorption of Ammonia Nitrogen onto CH-B-NCF.

Thermodynamic study in adsorption process helped to find the intensity and driving force. The adsorption of ammonium at different temperatures 30⁰C-70⁰C revealed a decrease in adsorption with increase in temperature. For an initial concentration 50mg/L highest q_e obtained was 21.2 mg/g at a temperature of 40⁰C. A slight increase in adsorption capacity at 40⁰C may be due to the enhancement of retarding forces acting on the adsorbent. The affinity of ammonium molecules to move from solid phase to liquid phase, enhanced solubility of ammonium and the weakening of ion exchange mechanism at higher temperatures lead this adsorption process exothermic (Mehmet and Hamdi, 2011). The results suggest that the adsorption capacity is affected by temperature. The Gibbs function of ammonia nitrogen adsorption has depicted in Fig 4.56. The negative value of Gibb's energy and enthalpy specify that the process is spontaneous and exothermic respectively. As temperature rises, ΔG is increases, means that nanocomposite film adsorption of ammonium ions is better at lower temperatures. The positive value of ΔS clearly indicate that the rise in entropy by the ion exchange process is greater than the entropy reduction by the solute adsorption process (Hanxin *et al.*,

2012). Change of thermodynamic parameters with temperatures have summarized in Table 4.22.

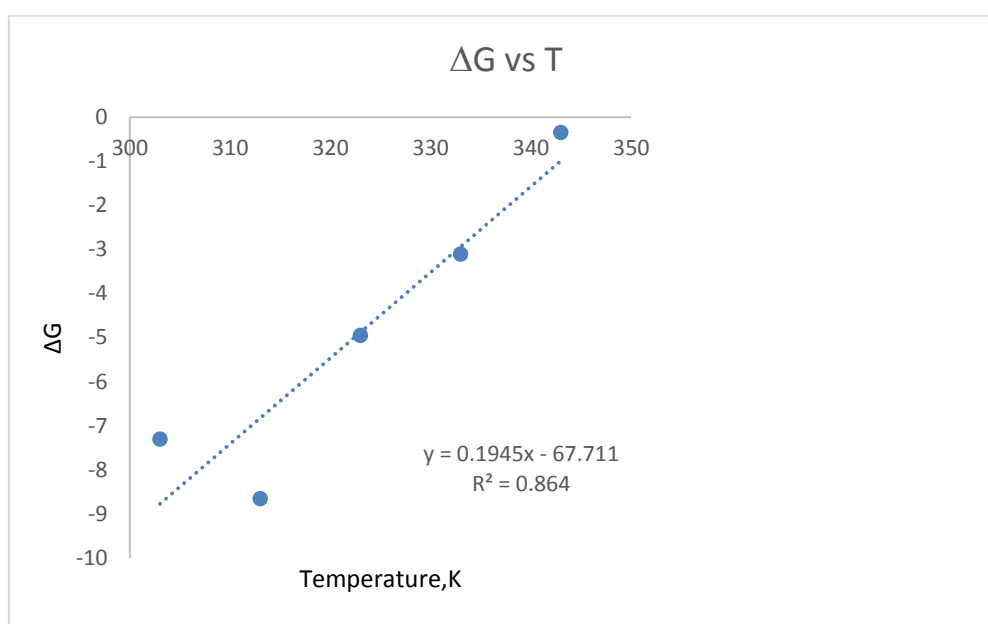


Fig. 4.56. Free energy change of adsorption of ammonium ions using chitosan bentonite nanoclay adsorbent versus temperature

Table 4.22 Distribution coefficients and thermodynamic parameters for ammonia nitrogen adsorption onto CH-B-NCF.

Temperature, K	K_d	ΔG , kJ/mol	ΔH , kJ/mol	ΔS , kJ/mol
303	2.41	-7.30	-67.11	0.194
313	2.83	-8.66		
323	1.81	-4.96		
333	1.45	-3.11		
343	1.04	-0.35		

4.6.5 Characterisation of Nanocomposite Films

The surface morphology and elemental analysis of chitosan-bentonite nanocomposite films before and after ammonia nitrogen adsorption were done with scanning electron microscopy equipped with energy-dispersive X-ray spectroscopy. A description of Scanning electron microscopy and Thermogravimetric analysis of chitosan bentonitenanoclay film composite has been explained in section 4.3.9 and 4.3.11. Fourier transform infrared spectroscopy (FTIR) of the nanocomposite films before and after ammonium adsorption has described in this section.

4.6.6 Scanning Electron Microscopy equipped with Energy Dispersive X-ray Spectroscopy

The surface physical morphology of nanocomposite films before and after adsorption was analyzed by scanning electron microscopy. The SEM images of chitosan bentonite films after ammonia nitrogen has shown in Fig.4.57. The porous and coarse surface of the films decreased after adsorption shows that ammonium ions occupy adsorption sites

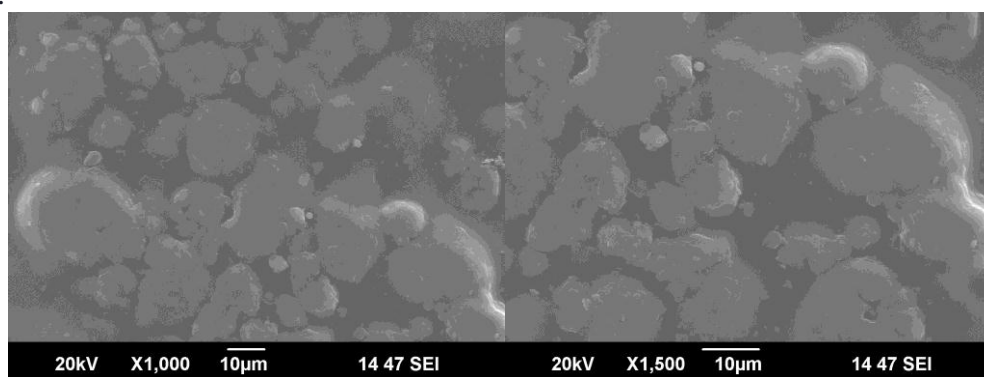


Fig 4.57. SEM Image of nanocomposite film after ammonia nitrogen adsorption at different magnifications

EDX of chitosan bentonite films before and after ammonium adsorption is shown in Fig. 4.58 and Fig 4.59 respectively. The EDAX spectrum analysis indicates that the weight percentage of carbon and oxygen has reduced from 52.38% and 37.22% to 47.66% and 36.88 % after adsorption. Meanwhile, the weight percentage of nitrogen has increased from 1.96% to 2.26%. This result shows that the NH_4^+ -N adsorption capacity of the prepared nanocomposite films. (Gefeniene A *et al.*, 2006). The EDAX analysis is doing at a higher temperature, some ammonia nitrogen may volatilize as gas, and otherwise, a higher weight percentage of the elemental nitrogen may be there on the films after adsorption.

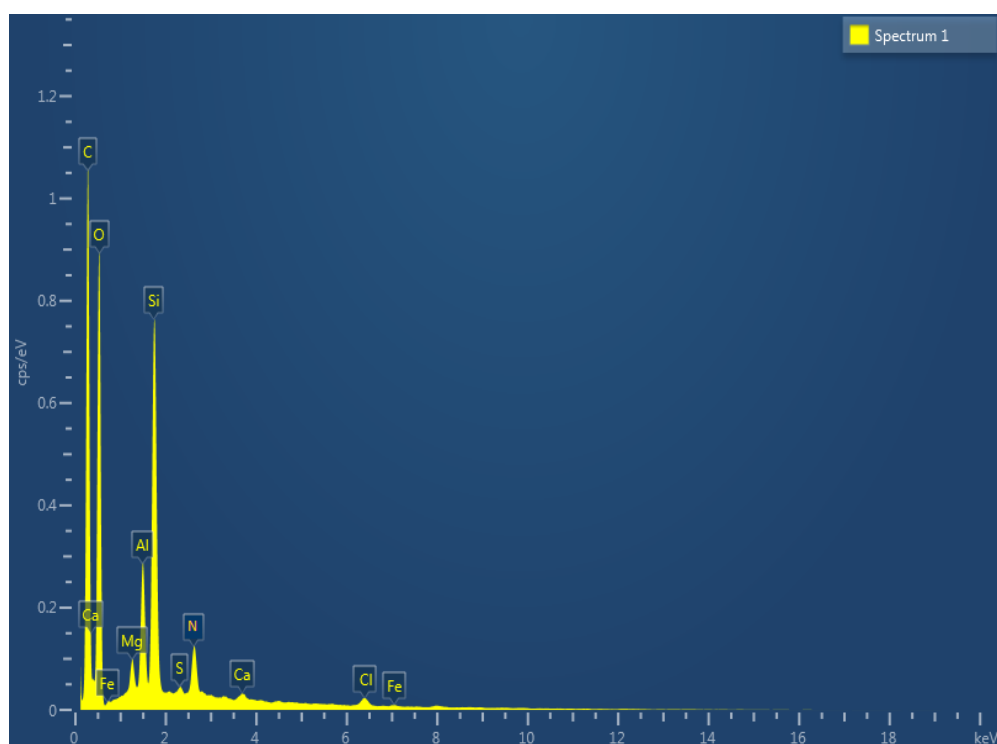


Fig. 4.58 EDX of chitosan bentonite film composite before ammonium adsorption

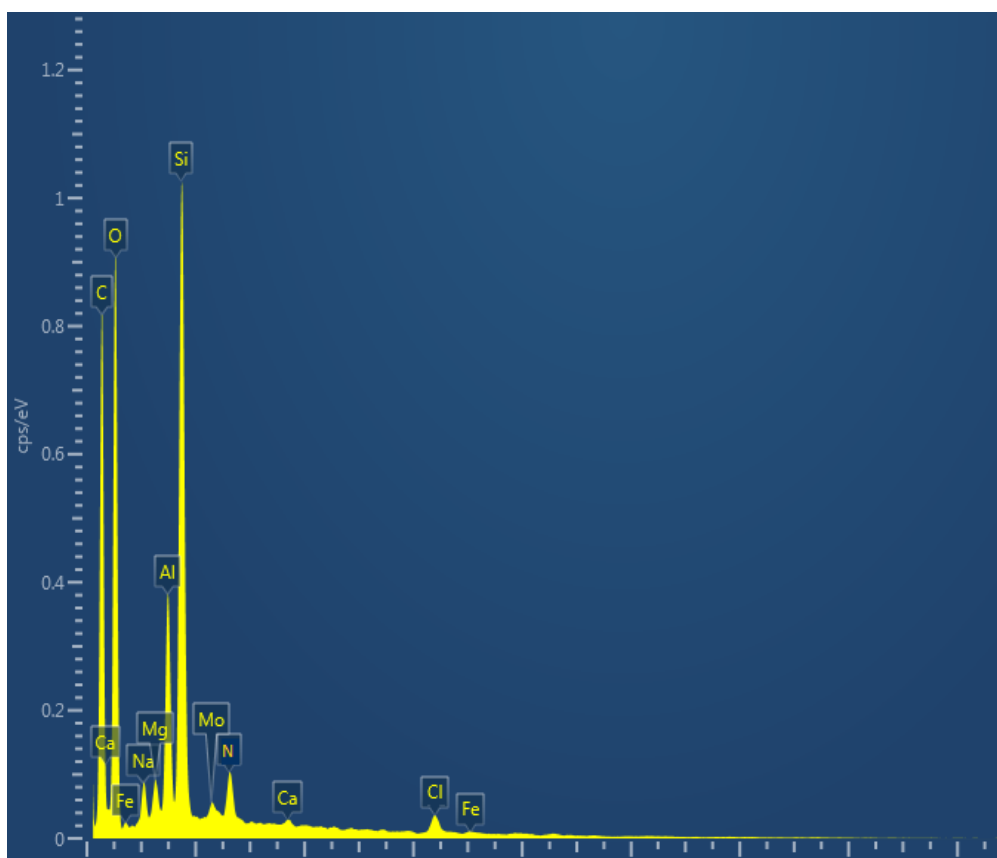


Fig. 4.59 EDX of chitosan bentonite film composite after ammonium adsorption

4.6.7 FT-IR Studies on Ammonia Nitrogen Removal by CH-B-NCF

Fig 4.60 and Fig 4.61 shows the chitosan nanoclay composite film spectral analysis before and after ammonium adsorption. The characteristic bands are seen between the wavelength of 1000cm^{-1} and 1600cm^{-1} . It is observed that considerable change in the frequency of nanocomposite after adsorption is mainly in the series of 3400cm^{-1} and 1600cm^{-1} , where $-\text{OH}$ and $-\text{COO}-$ bonds are present. The significant difference in this wavelength range shows that the adsorption is occurred mainly due to electrostatic attraction of $-\text{OH}$ and $-\text{COO}-$ with NH_4^+ ions (Xinggang *et al.*, 2014). Also, the intensity of

the broad characteristic adsorption peak (1415 cm^{-1}) of NH_4Cl is seen in the film after adsorption.

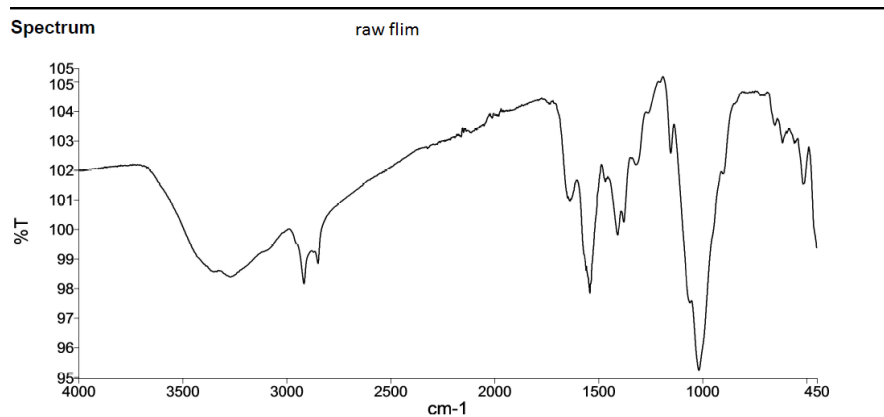


Fig. 4.60 FTIR of Raw Chitosan bentonite nanocomposite film

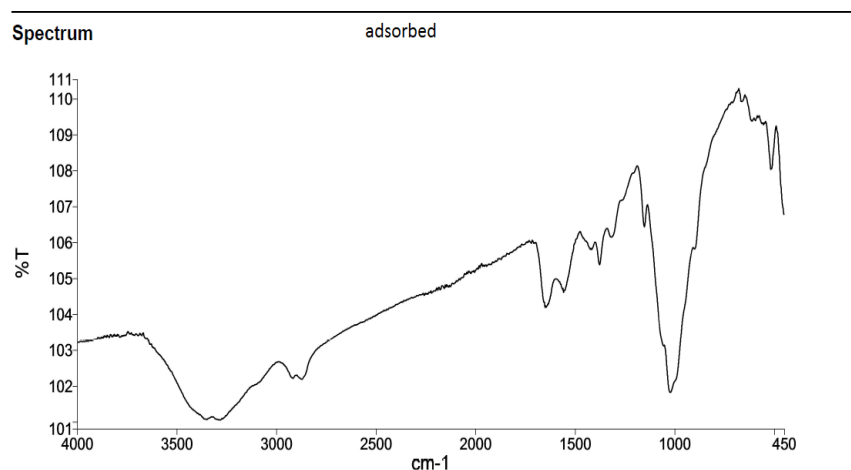


Fig. 4.61 FTIR of Chitosan Bentonite nanocomposite film after ammonium adsorption.

4.6.8 Application of Response Surface Methodology for $\text{NH}_4^+\text{-N}$ Removal Using Nanocomposite Films

RSM is a statistical method that helps to enumerate the significance of the effect of different variables on the response of interest of the particular process (Soumasree *et al.*, 2012). The relationship between several explanatory variables and one or more response variables is explored using response surface methodology. A sequence of designed experiments is being used to obtain an optimal response. A second-order degree polynomial equation is used in RSM to develop the model equation (Yuanhao and Majid 2015). In the present study, Box-Behnken Design was carried out using four factors (initial concentration, pH, time, and temperature) with three centre points and one replication. The parameters prescribed in three levels coded as +1 for high, 0 for intermediate, and -1 for the low value. In this study, the analysis was carried out in coded units to eliminate statistical errors due to the difference in the scale of measurements. The range and level of parameters used in the design of experiments were obtained by conducting batch experiments. The range of variables chosen for the experimental design of the adsorption process is shown in Table 4.23.

Table 4.23 Coded levels of independent variables in Box-Behnken design for $\text{NH}_4^+\text{-N}$ using chitosan bentonitenanocomposite films

Variables	Actually coded levels	
	Low (-1)	High (-1)
pH	4	10
Temperature	30	70
Initial Concentration	10	50
Time of Contact	20	140

Design of experiments using Box Behnken method under response surface methodology gave 27 combinations of four factors viz. pH, temperature, initial concentration and time. The shaking speed was 120 rpm and adsorbent dosage was 0.1g/50mL. The 27 sets are shown in the Table 4.24.

Table 4.24 Experimental design for removal of ammonia nitrogen using chitosan-bentonitenanocomposite films.

Run No	pH	Temperature, °C	Initial concentration, mg/L	Time, minutes	NH ₃ -N removal, %
1	2	50	30	140	85.0
2	2	50	30	21	81.0
3	6	50	30	80	94.0
4	6	50	10	20	84.0
5	2	70	30	80	70.0
6	10	50	30	140	78.0
7	6	50	50	140	62.0
8	6	30	50	80	88.0
9	6	30	30	140	72.0
10	2	50	50	80	66.0
11	10	30	30	80	80.0
12	6	50	30	80	92.0
13	6	70	50	80	85.0
14	2	50	10	80	80.0
15	10	50	10	80	79.0
16	2	30	30	80	75.0

Table Contd..

Run No	pH	Temperature, °C	Initial concentration, mg/L	Time, minutes	NH3-N removal, %
17	10	50	30	20	83.0
18	6	50	30	80	92.0
19	6	50	10	140	70.0
20	6	30	30	20	84.0
21	6	70	10	80	83.0
22	6	70	30	140	65.0
23	6	30	10	80	84.0
24	6	70	30	20	81.0
25	10	70	30	80	65.0
26	10	50	50	80	61.0
27	6	50	50	20	81.0

The equation (4.2) represents the model equation for efficiency in uncoded terms.

Model equation is given by:

$$\begin{aligned} \%EFF = & -0.057 + 1.1011pH + 0.018 Temp + 0.0122 Conc + 0.0036 Time - \\ & 0.0003 pH * Temp - 0.0001 pH * Conc - 0.00009 pH * Time - 0.000001 Temp * \\ & Conc - 0.000008Temp * Time - 0.00001 Conc * Time \end{aligned} \quad (4.2)$$

The estimated regression coefficients in uncoded units are shown in the Table 4.25. The p and t-test were used to analyze the significance of the regression coefficients.

Table 4.25 Coefficients of the model equation and t, p, (1-p) values for ammonia nitrogen removal by nanocomposite films

Factor	Regression Coefficients in uncoded units	t value	p value	significance level (1-p), %
12	-0.057	18.57	0.000	>99
pH	0.1011	78.37	0.020	98
TEMP	0.0180	184.14	0.008	>99
CONC.	0.01223	66.24	0.024	97.6
TIME	0.00369	251.07	0.001	>99
pH*pH	-0.00638	211.73	0.018	98.2
TEMP*TEMP	-0.000165	41.76	0.104	89.6
CONC*CONC	-0.000193	122.06	0.036	96.4
TIME*TIME	-0.000020	70.96	0.041	95.9
pH* TEMP	-0.000313	87.58	0.047	95.3
pH* CONC	-0.000125	21.23	0.021	97.9
pH* TIME	-0.000094	34.52	0.002	>99
TEMP*CONC	-0.000013	76.12	0.010	99
TEMP*TIME	-0.000008	61.23	0.007	>99
CONC*TIME	-0.00001	92.29	0.034	96.6

From the model equation, it is observed that efficiency is mostly influenced by pH and temperature, while initial concentration and time have a lesser influence on adsorption of ammonium ions onto CH-B-NCF. The significance level of temperature was higher than 99%, and that of pH was 98%. The interaction of pH and time has (1-p) > 99%. Also, the interaction of temperature and time has a higher level of significance >99%. This shows that

changes in temperature and pH are mostly influencing the functional groups, which are responsible for adsorption through electrostatic interaction and ion exchange (Suryadi et al.,2015)

Experimental versus predicted efficiency for NH_4^+ -N removal by chitosan bentonitenanoclay films is shown in Fig. 4.62. From statistical verification, it is seen that the model for efficiency given by Box- Behnken design fits well with the experimental data. The R^2 was found to be 0.923 ($R^2_{\text{adj.}}=0.923$), indicating that the empirical model could not describe only less than 7.8% of the total variation.

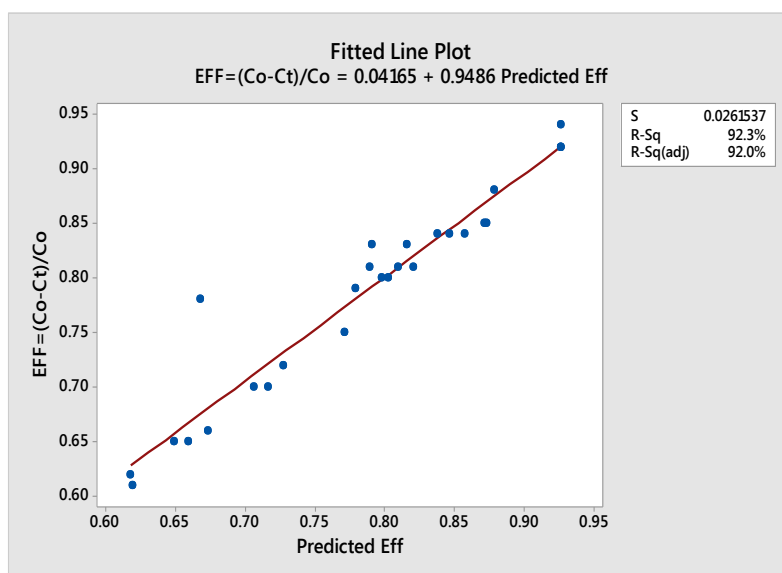


Fig. 4.62 Fitted line plot for ammonia nitrogen removal by CH-B-NCF

The interaction between variables and ANOVA (Analysis of variance) was also studied. (Olmez *et al.*, 2009). Analysis of variance of regression parameters of the predicted response surface quadratic model for percentage efficiency for ammonia nitrogen removal using chitosan-bentonite nanocomposite films is shown in Table 4.26. The model F-value of 228.56

specified the statistical significance for ammonia removal and the probability of F value is less than 0.05. The higher F value for the regression coefficient as 228.5 expresses that the model from BBD can well direct the design space.

Table 4.26 Analysis of variance for adsorption of ammonia nitrogen onto chitosan bentonitenanocomposite films

Source	degrees of freedom	sum of squares	mean Square	F	P	Significance	Remark
Regression	14	0.134	0.0095	228.56	0.039	96.1	Significant
Linear	4	0.054	0.0135	1.81	0.002	99.8	Significant
Square	4	0.0734	0.0183	2.46	0.102	89.8	Insignificant
Interaction	6	0.006	0.0010	0.13	0.089	91.1	Significant
residual error	12	0.090	0.0074				
lack of fit	10	0.089	0.009	2.24	0.102	89.7	Insignificant
pure error	2	0.003	0.0013				
Total	26						

The probability values of more than 0.1 show that the model terms are insubstantial. For square parameters, the P-value was 0.102, which is higher than 0.1, representing that this model term is insignificant and hence could be excluded from the model (Mohammed Bashir *et al.*, 2010).

4.6.9 Optimization of Ammonia Nitrogen Using Response Surface Methodology

An optimization plot provides the deviation of the predicted responses with the variables. The pinnacle point of the surface plot gives the optimum conditions (Solomon *et al.*, 2015). The optimization was carried out using the response optimizer of Minitab 18. The optimization plot of ammonia nitrogen removal using chitosan bentonitenanocomposite films is shown in Fig. 4.63. According to the prediction by the model, the optimum time for experimenting was 60 minutes, with an initial $\text{NH}_4^+\text{-N}$ concentration of 26.56 ppm. The solution pH and temperature were to be maintained at 6 and 46.16, respectively. Then the predicted removal efficiency by the model was 94.03%. Batch experiments were conducted with the conditions predicted by Box-Behnken design, and a removal efficiency 94 % was obtained, which is in par with the expected response value. For the optimum conditions, the desirability function value was 1.0, which was found from the response optimizer plot (Hanxin *et al.*, 2012).

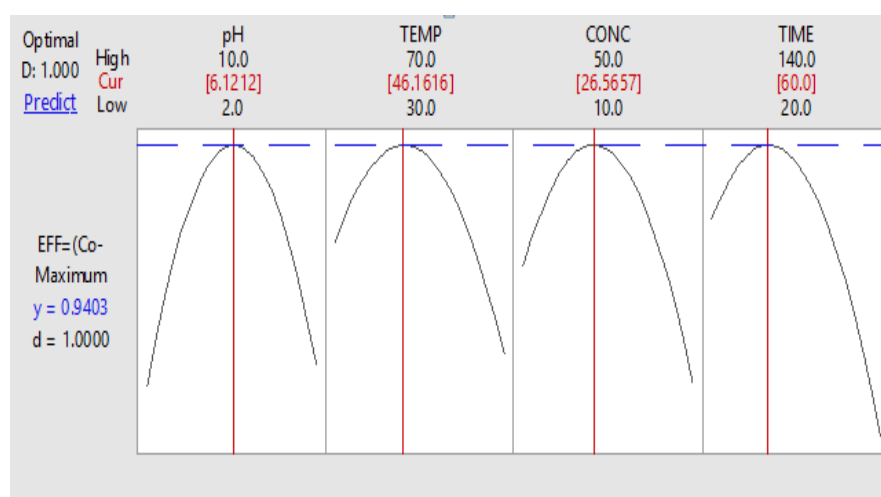


Fig. 4.63. Optimization plot for $\text{NH}_4^+\text{-N}$ removal

4.6.10. Combined Effect of Variables on Adsorption of Ammonia Nitrogen Using CH-B-NCF.

The study of combined effect is significant if a process is influenced by more than one variables. The surface plots of response surface methodology were used to describe the combined effects of the parameters affecting adsorption. The combined consequence of temperature and pH is highly significant in the ANOVA. Response surface methodology was employed to evaluate the interaction among the independent variables. The surface and contour plots of temperature and pH is shown in fig 4.64. The conjugate impact of time and temperature on percentage removal of ammonia is shown in figure 4.65 . From the plot, it is found that percentage recovery decrease rapidly with temperature after 46⁰C, which shows the exothermic nature of the process. The surface of the nanocomposite films attracts ammonia nitrogen in ionic forms during adsorption. So any reaction condition that enhance changed ionic form to non-ionic gaseous form could disturb the removal capacity. The combined effect of temperature and pH decreases the ammonia nitrogen uptake efficiency. The transformation of ammonium ions into ammonia gas at elevated temperature and pH is significant. The adsorption of ammonia at slighter temperature rise from room temperature may be resulting from the enhancement of the adsorption surface and increased chemical attraction of ions onto nanocomposite films. From the 3-D response surface plot of the combined effect of temperature and pH (concentration=30 ppm and time=80 minutes), it is clear that ammonia removal increases with an increase in both temperatures up to 46⁰C and pH 6. The surface and contour plots of the combined effect of time and pH are shown in figure 4.66. Also, the combined effect of concentration and temperature is depicted in Fig 4.67.

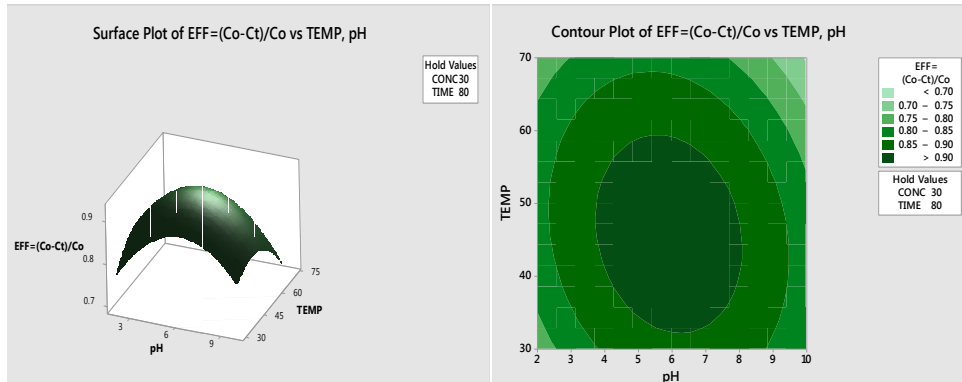


Fig 4. 64. Surface and contour plots of combined effect of temperature and pH

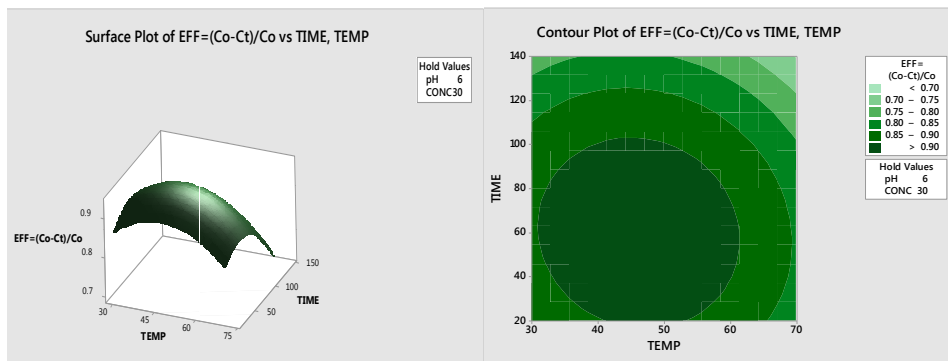


Fig 4.65. Surface and contour plots of combined effect of temperature and time

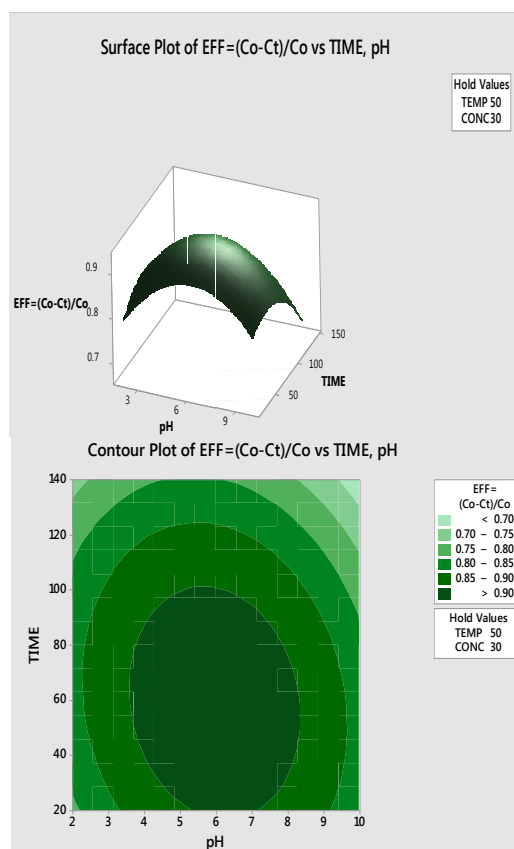


Fig 4.66. Contour and Surface Plots of combined effect of Time and pH

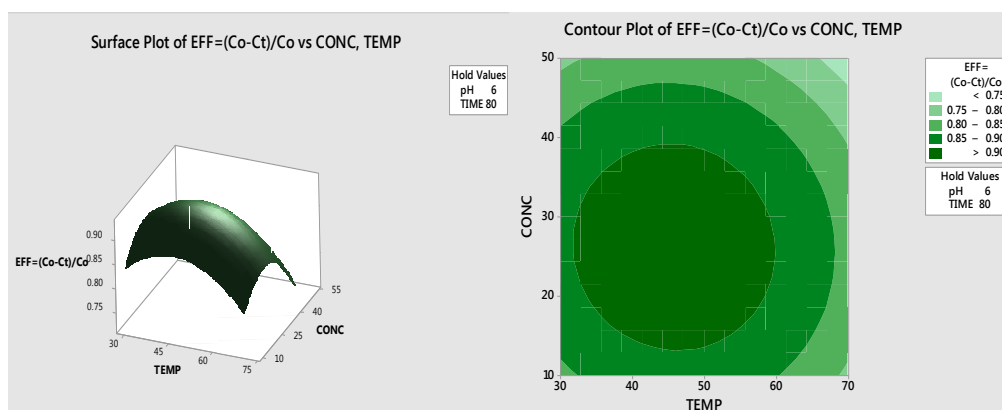


Fig 4.67. Contour and surface plots of combined effect of concentration and temperature

4.6.11 Desorption Studies of Ammonia Nitrogen

The development of methods for reuse of the adsorbent is important to reduce the treatment costs in a water treatment plant. In the present work, 0.5 M NaOH solution has been used for desorption experiments. 50 mL of NaOH solution was mixed with 2 g of ammonia nitrogen saturated chitosan-bentonite nanocomposite films. The mixture was stirred for 60 minutes at an agitation speed of 120 rpm room temperature. The adsorbent residue after shaking was then separated from the solution using Whatman 0.45 filter paper. Then washed with 50 mL distilled water for 10 minutes. The nanocomposite films obtained after washing was dried at 100 °C for one hour. The study on the effect of pH and the effect of temperature was repeated with the regenerated adsorbents. The results obtained with the regenerated nanocomposite films show analogous trends with those of virgin nanocomposite films. The maximum ammonia nitrogen removal with recycled adsorbent was occurred at pH 6. The study of effect of temperature also showed comparable removal as that of original nanocomposite films. Fig 4.68 shows the comparison of uptake capacities of original and regenerated nanocomposite films towards change in pH and temperature. The slight decrease in the ammonium uptake is attributed to the partial structural demolition of the films during regeneration process (Mulan *et al.*, 2011). The active sites available may be not available in the recycled adsorbents.

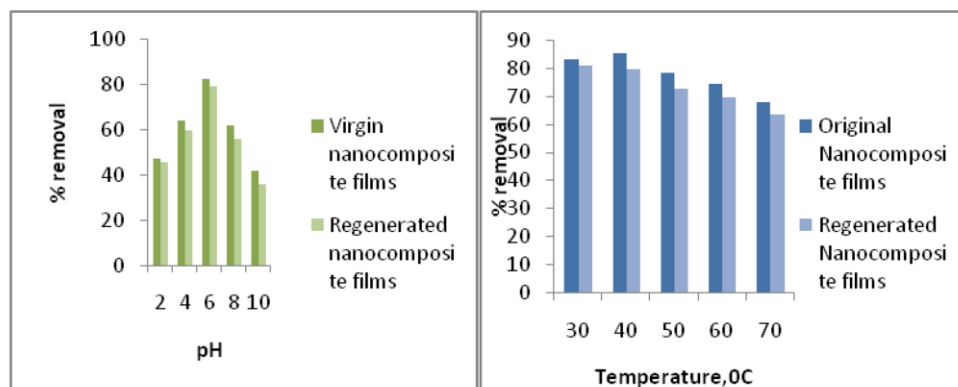


Fig 4.68 Comparison of removal performance of virgin and regenerated nanocomposite films for varying pH and Temperature.

4.7 SUMMARY

In this chapter, the adsorptive removal of nitrate-nitrogen using two adsorbents, Fe loaded chitosan nutmeg shell powder and chitosan-bentonite nanoclay films have been studied. The kinetic, equilibrium, and thermodynamic analysis of the results of the batch studies were conducted. The characterization of the adsorbents was done. Both adsorbents possessed higher adsorption capacities. The adsorption capacity of Fe-CH-NSP was 83.3 mg/g, and chitosan-bentonite nanocomposite films reported an adsorption capacity of 76.9 mg/g nitrate-nitrogen. No harsh chemicals were used in the preparation of nanocomposite films, which is favourable its use in a water treatment system. Also, considering the ease of handling, nanocomposite films were selected for the continuous study. The adsorptive removal of ammonia nitrogen with chitosan-bentonite nanocomposite films has also been studied and found significant removal. Optimization of nitrate nitrogen and ammonia nitrogen adsorption using nanocomposite films was conducted using RSM. The model equation of the second order was developed, and it was validated. Optimization using the response optimizer was carried out, and it was verified. The fixed bed

nitrate column was fabricated with chitosan-bentonite clay nanocomposite film as adsorbent, and the effect of change in bed height and influent velocity in the column were analyzed. The modeling of the column was performed using the Thomas model, Yoon Nelson model, and Adam Bohart model. From the experimental results it can be concluded that chitosan-bentonite nanocomposite films are promising adsorbents for the removal of nitrate-nitrogen and ammonia nitrogen from aqueous solutions.



CHAPTER 5

SUMMARY AND CONCLUSIONS

5.1 SUMMARY

Nitrogen pollution is mainly resulting from nitrogenous fertilizers, livestock farms, septic systems, industrial processes, nitrogen oxide emissions, and municipal solid waste systems. The adverse impacts of overloading of nitrogenous wastes like nitrates, nitrites, and ammonia nitrogen in sensitive ecosystems are becoming increasingly noticeable. The highly soluble nitrates and ammonia nitrogen enters the surface and ground waters by leaching and affects the quality of drinking water. The USEPA and WHO has set a maximum contaminant level of 10 mg/L for nitrate-nitrogen and 1 mg/L for nitrite nitrogen. There are various methods for removing nitrogen compounds from aqueous solutions like denitrification, ion exchange, reverse osmosis, and electrochemical methods. All these methods suffer from certain drawbacks in one form or another.

The adsorption process is commonly considered superior in water treatment because of its convenience, ease of operation, and simplicity of design. The adsorption process has broader applicability in wastewater treatment because it can remove or minimize different types of organic and inorganic pollutants from the water or wastewater.

A variety of adsorbents are available for removing nitrate nitrogen and ammonia nitrogen. The specific surface area and pore size distribution are the essential characteristics that govern the properties of a suitable adsorbent. In the last few decades, nanoparticles have attracted much attention in wastewater treatment. The large surface area and pore size distribution of

nanomaterials are attributed to the higher removal efficiency in adsorption. Different methods have been reported for the synthesis of nanoparticles, but looking from the present circumstance of our environment, suitable methods should be developed with safer, less toxic, and easily degradable chemicals. The use of biomaterials as a precursor for developing nanomaterials is a new research interest nowadays. The concept of green synthesis of nanosorbents from biological systems is environmentally friendly and stable. Present work aimed at developing a suitable nanomaterial-based adsorbent for the removal of low concentration of nitrate-nitrogen and ammonia nitrogen from aqueous solution.

Two biosorbent composite materials were used in the study. (1) Iron loaded chitosan nutmeg shell powder (Fe-CH-NSP) and (2) Chitosan bentonite nanocomposite films (CH-B-NCF). Iron modified nutmeg shell powder was prepared by using chitosan as the bridging reagent. Fe (II) and Fe (III) salts in the presence of NaOH solution is used for the magnetic activation of nutmeg shell powder. One of the drawbacks while using the nanomaterials as adsorbent is the difficulty in separating the material after adsorption. Nanomaterials can be made as a composite with a suitable matrix, and the composite can be used as an adsorbent in contaminant removal. Chitosan is compatible with bentonite nanoclay. In the present study cross linked chitosan-bentonite nanocomposite films (CH-B-NCF) were synthesized by the intercalation of chitosan in bentonite. The nanocomposite film was used for adsorption of both nitrate nitrogen and ammonia nitrogen. The optimization of batch adsorption was carried out with design of experiments using response surface methodology of Minitab.

A fixed bed, continuous packed bed nitrate column, was fabricated using chitosan bentonite nanocomposite films, and experiments were performed. The breakthrough curves were analyzed for varying bed heights and flow rates, and the column was modeled using the Thomas model, Yoon Nelson model, and Adam Bohart model.

5.2 CONCLUSIONS OF BATCH STUDY

- Fe-CH-NSP was used for batch adsorption of nitrate nitrogen ($\text{NO}_3\text{-N}$) from synthetically prepared nitrate solutions. A higher uptake of nitrate nitrogen was observed at pH 8. Initially there was an increase in nitrate removal with initial concentration but beyond 60 mg/L, the removal efficiency showed a decreasing trend. After 90 minutes of shaking time, the adsorption reached an equilibrium state. The results of batch experiments carried out using CH-B-NCF for the removal of $\text{NO}_3\text{-N}$ showed that acidic condition was favourable for adsorption process and the other entire batch studies were carried out at pH 4.0. The equilibrium time for adsorption was 60 minutes.
- The equilibrium adsorption data fitted more to Langmuir isotherm model for adsorption of $\text{NO}_3\text{-N}$ with Fe-CH-NSP and CH-B-NCF. The Fe-CH-NSP offers a maximum equilibrium adsorption capacity of 83.3 mg/g $\text{NO}_3\text{-N}$ (pH=8, mass of adsorbent=0.1g, temperature=30⁰C), and chitosan-bentonite nanocomposite films yield an uptake of 73.3 mg/g nitrate nitrogen (pH=4, mass of adsorbent=0.1g, temperature=30⁰C).
- The experimental batch adsorption data of nitrate removal with Fe-CH-NSP and CH-B-NCF fitted more to pseudo second order kinetic reaction model with $R^2=0.99$. The Weber-Morris intraparticle diffusion analysis showed significant boundary layer effect and intraparticle diffusion is not the sole rate-limiting step.
- Thermodynamic studies on $\text{NO}_3\text{-N}$ removal by Fe-CH-NSP and CH-B-NCF, gave negative values of ΔG , which postulates that process is spontaneous and feasible. The negative values of change in enthalpy

established the exothermic nature of the process. The value of ΔS was found to be positive, which indicates an increase in randomness in the adsorption process.

- The optimization of adsorption of $\text{NO}_3\text{-N}$ by CH-B-NCF by RSM showed that 88.43% removal was obtained at initial concentration of 100 mg/L by providing 120 minutes adsorption time. The adsorbent dosage was 1 g/L. The model was experimentally validated. It has explained in section 4.3.6.
- The desorption study of chitosan bentonite nanocomposite film after nitrate adsorption showed that 1M NaCl could be used as a desorbent and the desorption efficiency decreased with increase in adsorption-desorption cycle.
- Chitosan bentonite nanocomposite films were used for batch adsorption of ammonia nitrogen. The effect of pH study showed that both acidic and alkaline medium is not conducive to ammonia nitrogen adsorption. So pH of 6 was selected for further experiments.
- The experimental batch adsorption data of adsorption of $\text{NH}_4^+\text{-N}$ using chitosan-bentonite nanocomposite films fitted more to pseudo second order kinetics and the equilibrium adsorption data fitted more to Freundlich isotherm model. The maximum equilibrium adsorption capacity of ammonia nitrogen with nanocomposite films was 37.01 mg/g.
- In the statistical evaluation of adsorption of $\text{NH}_4^+\text{-N}$ with chitosan bentonite nanocomposite films using RSM, 94.03% removal of $\text{NH}_4^+\text{-N}$ was obtained at 26.56 mg/L initial $\text{NH}_4^+\text{-N}$ concentration with 0.1g/ 50 mL of adsorbent dosage. The optimum time of adsorption was 60 minutes at pH 6.0. The model was experimentally validated.
- The regeneration of nanocomposite films loaded with ammonia nitrogen was done with 0.5M NaOH. The comparison of removal performance of virgin and regenerated nanocomposite films for varying pH and temperature study showed that recycled adsorbents could be reused.

- Based on the adsorbents regeneration capacity, effortless separation and column behaviour, it is concluded that chitosan-bentonite nano composite films could be used as potential adsorbent for nitrate nitrogen and ammonia nitrogen removal from aqueous solutions.

5.3 CONCLUSIONS OF FIXED BED STUDY

- The analysis of breakthrough curves at bed heights of 10 cm, 15 cm and 20 cm showed that higher the bed height, more volume of water could be treated before breakthrough. The breakthrough time was higher for 20 cm bed than for 10 and 15 cm beds.
- The bed was operated at 6 mL/min, 10 mL/min, and 15 mL/min to study the effect of flow rate on breakthrough curve appearance. From the experimental results the breakthrough curve was found to shift from right to left as the flow rate was increased. Low flow rate was found to be favorable for treating higher volume of feed in the fixed bed packed adsorption column.
- The longer bed delayed the exhaustion time of nanocomposite films. The bed was able to operate for a longer period without changing the adsorbent. The shorter bed height of 10 cm approached faster exhaustion and a declined performance was observed.
- Mathematical modeling of the column was carried out using Thomas model, Yoon Nelson model and Adam Bohart model. The model equations showed that Thomas model and Yoon Nelson model fitted well to the experimental data. Adam Bohart model fitted best to the initial part of the column operation.

5.4 LIMITATIONS OF THE STUDY

- Real wastewater samples could not be used for $\text{NO}_3\text{-N}$ and $\text{NH}_4^+\text{-N}$ removal study under batch as well as continuous mode.
- Effect of co-ions in the aqueous media was not taken up for study.

- Empty Bed Contact Time (EBCT) was not considered in the operation of fixed bed column.
- Hydrodynamic study of fixed bed nitrate column using chitosan-bentonite nanocomposite films was not conducted
- Surface characterization of the adsorbents was not carried out as part of the study

5.5 SCOPE FOR FUTURE RESEARCH

- Surface modification of synthesized adsorbents could be carried out to get higher removal efficiency and adsorption capacity.
- The effects of thickness of chitosan-bentonite nanocomposite films on $\text{NO}_3\text{-N}$ and $\text{NH}_4^+\text{-N}$ adsorption can be taken up for further study.
- The effect of chitosan to bentonite nanoclay weight ratio in the nanocomposite films on adsorption efficiency could be assessed in both batch and fixed bed operation.
- The role of pKa values on pH and point of zero charge for both the adsorbents could be studied to verify the better effect of pH
- The mechanical and thermal stability of the chitosan-bentonite nanocomposite films could be assessed in both batch and fixed bed operation.
- A study on convective mass transfer and film diffusion could be taken up for further study

.....✻.....

REFERENCES

1. **Abdolali, A., W.S. Guo, H.H. Ngo, S.S. Chen, N.C. Nguyen and K.L. Tung** (2014) Typical lignocellulosic wastes and by-products for biosorption process in water and wastewater treatment: A critical review. *Bioresource Technology*, **160**, 57 - 66.
2. **A. Z. Abdullah, B. Salamatinia, A. H. Kamaruddin** (2009) Application of response surface methodology for the optimization of NaOH treatment on oil palm frond towards improvement in the sorption of heavy metals. *Desalination*, **244**, 227-238.
3. **Ahmed Abou-Shady, Changsheng Peng, Jingjing Bi, Huizhen Xu and Juan Almeria** (2012) Recovery of Pb (II) and removal of NO₃ – from aqueous solutions using integrated electrodialysis, electrolysis, and adsorption process. *Desalination*, **286**, 304 - 315.
4. **Ahmed M.E. Khalil, Osama Eljamal, Skander Jribi and Nobuhiro Matsunaga** (2016) Promoting nitrate reduction kinetics by nanoscale zero valent iron in water via copper salt addition. *Chemical Engineering Journal*, **287**, 367 - 380.
5. **Ai Phing Lim and Ahmad Zaharin Aris** (2014) Continuous fixed-bed column study and adsorption modeling: Removal of cadmium (II) and lead (II) ions in aqueous solution by dead calcareous skeletons. *Biochemical Engineering Journal*, **87**, 50 - 61.
6. **Alagumuthu, G. and M. Rajan** (2010) Equilibrium and kinetics of adsorption of fluoride onto zirconium impregnated cashew nut shell carbon. *Chemical Engineering Journal*, **158**, 451 - 457.
7. **Amit Bhatnagar and Mika Sillanpa** (2009) Applications of chitin- and chitosan-derivatives for the detoxification of water and wastewater — A short review. *Advances in Colloid and Interface Science*, **152**, 26 - 38.
8. **Amit Bhatnagar and Mika Sillanpaa** (2010 a) Utilization of agro-industrial and municipal waste materials as potential adsorbents for water treatment-A review. *Chemical Engineering Journal*, **157**, 277 - 296.

9. **Amit Bhatnagar, Eva Kumar and Mika Sillanpaa** (2010 b) Nitrate removal from water by nano-alumina: Characterization and sorption studies. *Chemical Engineering Journal*, **163**, 317 - 323.
10. **Amit Bhatnagar and Mika Sillanpaa** (2011) A review of emerging adsorbents for nitrate removal from water. *Chemical Engineering Journal*, **168**, 493 -564.
11. **Anni Keranen, TiinaLeiviska, Bao-Yu Gao, OsmoHormi and JuhaTanskanen** (2013) Preparation of novel anion exchangers from pine sawdust and bark, spruce bark, birch bark and peat for the removal of nitrate. *Chemical Engineering Science*, **98**, 59 - 68.
12. **Anni Keranen, TiinaLeiviska, Osmo Hormi and JuhaTanskanen** (2015) Removal of nitrate by modified pine sawdust: Effects of temperature and co-existing anions. *Journal of Environmental Management*, **147**, 46 - 54.
13. **Antonio Bodalo, Jose Luis omez, Elsa Gomez, Gerardo Leon, and Maria Tejera** (2005). Ammonium removal from aqueous solutions by reverse osmosis using cellulose acetate membranes *Desalination*, **184**, 149-155.
14. **Antonio E. Palomares, Cristina Franch and AvelinoCorma** (2010) Nitrates removal from polluted aquifers using (Sn or Cu)/Pd catalysts in a continuous reactor. *Catalysis Today*, **149**, 348 - 351.
15. **Appunni Sowmya and Sankaran Meenakshi** (2013). An efficient and regenerable quaternary amine modified chitosan beads for the removal of nitrate and phosphate anions. *Journal of Environmental Chemical Engineering*, **1**, 906 – 915.
16. **Appunni Sowmya and Sankaran Meenakshi** (2014) A novel quaternized chitosan–melamine–glutaraldehyde resin for the removal of nitrate and phosphate anions. *International Journal of Biological Macromolecules*, **64**, 224 - 232.
17. **Arcadio P Sincero and Gregoria A Sincero**(2011). *Environmental Engineering: A Design Approach* 428-430.
18. **Aref Alshameri, Abdullateef Ibrahim, Amer M. Assabri, Xinrong Lei, Hongquan Wang and Chunjie Yan** (2014) The investigation into

- the ammonium removal performance of Yemeni natural zeolite: Modification, ion exchange mechanism, and thermodynamics. *Powder Technology*, **258**, 20 - 31.
19. **Ari Clecius A. de Lima, Ronaldo F. Nascimento, Francisco F. de Sousa, Josue M. Filho and Alcinea C. Oliveira** (2012) Modified coconut shell fibers: A green and economical sorbent for the removal of anions from aqueous solutions. *Chemical Engineering Journal*, **185**, 274 - 284.
 20. **Arshadi, M., M. Soleymanzadeh, J.W.L. Salvacion and F. SalimiVahid** (2014) Nanoscale Zero-Valent Iron (NZVI) supported on seneqelas waste for Pb(II) removal from aqueous solution: Kinetics, thermodynamic and mechanism. *Journal of Colloid and Interface Science*, **426**, 241- 251.
 21. **Arshadi, M., S. Foroughifard, J. EtemadGholtash, A. Abbaspourrad** (2015) Preparation of iron nanoparticles-loaded Spondiaspurpurea seed waste as an excellent adsorbent for removal of phosphate from synthetic and natural waters. *Journal of Colloid and Interface Science*, **452**, 69 - 77.
 22. **Asim Olgun, Necip Atar and Shaobin Wang** (2013) Batch and column studies of phosphate and nitrate adsorption on waste solids containing boron impurity. *Chemical Engineering Journal*, **222**, 108 - 119.
 23. **Auta, M. and B.H. Hameed** (2014) Chitosan–clay composite as highly effective and low-cost adsorbent for batch and fixed-bed adsorption of methylene blue. *Chemical Engineering Journal*, **237**, 352 - 361.
 24. **Azhar Abdul Halim, Hamidi Abdul Aziz, Megat Azmi Megat Johari, Kamar Shah Ariffin and Mohd. NordinAdlan** (2010) Ammoniacal nitrogen and COD removal from semi-aerobic landfill leachate using a composite adsorbent: Fixed bed column adsorption performance. *Journal of Hazardous Materials*, **175**, 960 - 964.
 25. **Batool Shahrooie, LalehRajabi, Ali Ahsraf Derakhshnan and Mohammad Keyhani** (2015) Fabrication, characterization and statistical investigation of a new starch- based hydrogel nanocomposite for ammonium adsorption. *Journal of Taiwan Institute of Chemical Engineers* **51**, 201-215.

26. **Bekhradinassab Ensie and Sabbaghi Samad**(2014) Removal of nitrate from drinking water using nano $\text{SiO}_2\text{-FeOOH-Fe}$ core-shell. *Desalination*, **347**,1-9.
27. **Bing Wang, Johannes Lehmann, Kelly Hanley, Rachel Hestrin and Akio Enders** (2015) Adsorption and desorption of ammonium by maple wood biochar as a function of oxidation and pH. *Chemosphere*, **138**, 120 - 126.
28. **Camargo J A and Alonso A** (2006) Ecological and Toxicological effects of inorganic nitrogen pollution in aquatic ecosystem: A global assessment. *Environmental Introduction*, **32**, 831-849.
29. **Chabani, M., A. Amrane and A. Bensmaili** (2009) Equilibrium sorption isotherms for nitrate on resin Amberlite IRA 400. *Journal of Hazardous Materials*, **165**, 27 - 33.
30. **Chatterjee S, D.S. Lee, M.W. Lee, S.H. Woo** (2009) Nitrate removal from aqueous solutions by cross-linked chitosan beads conditioned with sodium bisulphate, *Journal of Hazardous Materials***166**, 508–513.
31. **Cilai Tang, Zengqiang Zhang and Xining Sun** (2012) Effect of common ions on nitrate removal by zero-valent iron from alkaline soil. *Journal of Hazardous Materials*, **231 - 232**, 114 - 119.
32. **Costas L. Constantinou, Costas N. Costa and Angelos M. Efstathiou** (2010) Catalytic removal of nitrates from waters. *Catalysis Today*, **151**, 190 - 194.
33. **Cristina Onorato, Laura J Banasiak and Andrea I Schafer** (2017) Inorganic trace contaminant removal from real brackish groundwater using electrodialysis. *Separation and Purification Technology*, **187**, 426-435.
34. **David Reyter, Daniel Belanger and Lionel Roue** (2011) Optimization of the cathode material for nitrate removal by a paired electrolysis process. *Journal of Hazardous Materials*,**192**, 507 - 513.
35. **De Silva, R.T., P. Pashakhsh, K.L. Goh, S.P. Chai, and H. Ismail** (2013) Physio-chemical characterisation of chitosan/halloysite composite membranes. *Polymer Testing*, **32**, 265-271.

36. **Deepak Pathania, Shikha Sharma, Pardeep Singh** (2017) Removal of methylene blue by adsorption onto activated carbon developed from Ficus caricifolia *Arabian Journal of Chemistry*, **10**, S1445–S1451
37. **Deepesh Bhardwaj, Monika Sharma, Pankaj Sharma and Radha Tomar** (2012) Synthesis and surfactant modification of clinoptilolite and montmorillonite for the removal of nitrate and preparation of slow release nitrogen fertilizer. *Journal of Hazardous Materials*, **227**, 292 - 300.
38. **Diana Guaya, Cesar Valderrama, Adriana Farran, Chabaco Armijos and Jose Luis Cortina** (2015) Simultaneous phosphate and ammonium removal from aqueous solution by a hydrated aluminum oxide modified natural zeolites. *Chemical Engineering Journal*, **271**, 204 - 213.
39. **Dongjin Wan, Huijuan Liu, Xu Zhao, Jiuhui Qu, Shuhu Xiao and Yining Hou** (2009) Role of the Mg/Al atomic ratio in hydrotalcite-supported Pd/Sn catalysts for nitrate adsorption and hydrogenation reduction. *Journal of Colloid and Interface Science*, **332**, 151 - 157.
40. **Dong-Wan Cho, Chul-Min Chon, Yongje Kim, Byong-Hun Jeon, Frank W. Schwartz, Eung-Seok Lee and Hocheol Song** (2011) Adsorption of nitrate and Cr(VI) by cationic polymer-modified granular activated carbon. *Chemical Engineering Journal*, **175**, 298 - 305.
41. **Emine Malkoca and Yasar Nuhoglu** (2006) Fixed bed studies for the sorption of chromium (VI) onto tea factory waste. *Chemical Engineering Science*, **61**, 4363 - 4372.
42. **Engracia Lacasa, Pablo Canizares, Cristina Saez, Francisco J. Fernandez and Manuel A. Rodrigo** (2011) Removal of nitrates from groundwater by electrocoagulation. *Chemical Engineering Journal*, **171**, 1012 - 1017.
43. **Foo, K.Y. and B.H. Hameed** (2010) Insights into the modeling of adsorption isotherm systems. *Chemical Engineering Journal*, **156**, 2 - 10.
44. **Foo, K.Y., L.K. Lee and B.H. Hameed** (2013) Batch adsorption of semi-aerobic landfill leachate by granular activated carbon prepared by microwave heating. *Chemical Engineering Journal*, **222**, 259 - 264.

45. **Francesca Pagnanelli, Carolina Cruz Viggi and Luigi Toro** (2010) Development of new composite biosorbents from olive pomace wastes. *Applied Surface Science*, **256**, 5492 - 5497.
46. **Gefeniene A, Kauspediene D, Snukiskis J** (2006) Performance of sulphonic acid ion exchangers in the recovery of ammonium from basic and slight acidic conditions, *J. Hazardous Mater.* **135**, 180-187.
47. **Gonzalo Vazquez, M. Sonia Freire, Julia Gonzalez-Alvarez and Gervasio Antorrena** (2009) Equilibrium and kinetic modelling of the adsorption of Cd^{2+} ions onto chestnut shell. *Desalination*, **249**, 855 - 860.
48. **Gruber N. and J.N. Galloway** (2008) An Earth-system perspective of the global nitrogen cycle. *Nature*, **451**, 293 - 296.
49. **Haiming Huang, Xianming Xiao, Bo Yan and Liping Yanga** (2010) Ammonium removal from aqueous solutions by using natural Chinese (Chende) zeolite as adsorbent. *Journal of Hazardous Materials*, **175**, 247 - 252.
50. **Haiwei Liu, Yuanhua Dong, Haiyun Wang and Yun Liu** (2010) Adsorption behavior of ammonium by a bioadsorbent—Boston ivy leaf powder. *Journal of Environmental Sciences*, **22**, 1513 - 1518.
51. **Haiwei Liu, Yuanhua Dong, Haiyun Wang and Yun Liu** (2010) Ammonium adsorption from aqueous solutions by strawberry leaf powder: Equilibrium, kinetics and effects of coexisting ions. *Desalination*, **263**, 70 - 75.
52. **Haiwei Liu, Yuanhua Dong, Yun Liu and Haiyun Wang** (2010) Screening of novel low-cost adsorbents from agricultural residues to remove ammonia nitrogen from aqueous solution. *Journal of Hazardous Materials*, **178**, 1132 - 1136.
53. **Hakan Demiral and Gul Gunduzog** (2010) Removal of nitrate from aqueous solutions by activated carbon prepared from sugar beet bagasse. *Bioresource Technology*, **101**, 1675 - 1680.
54. **Hale S E, V.Alling, V.Martinsen, J.Mulder, G.D.Breedveld, G.Cornelissen** (2013). The sorption and desorption of phosphate-

- P, ammonium-N and nitrate-N in cacao shell and corn cob biochar. *Chemosphere*, **91**, 1612–1619
55. **Hameed, B.H., Daud, F.B.M** (2008). Adsorption studies of basic dye on activated carbon derived from agricultural waste: Heveabrasiliensis seed coat. *Chemical Engineering Journal*, **139**, 48-55.
56. **Hanxin Huo, Hai Lin, Yingbo Dong, Huang Cheng, Han Wang and Lixia Cao** (2012) Ammonia-nitrogen and phosphates sorption from simulated reclaimed waters by modified clinoptilolite. *Journal of Hazardous Materials*, **229**, 292 - 297.
57. **Hazardous Substances Data Bank**: Ammonium chloride. Bethesda, MD, National Library of Medicine, 1990.
58. **Hekmatzadeh A A, Ayoob Karimi-Jashni Naser Talebbeydokhti, Bjorn Kløve** (2013) Adsorption kinetics of nitrate ions on ion exchange resin. *Desalination*, **326**, 125–134.
59. **Hekmatzadeh, A.A., A. Karimi-Jashani, N. Talebbeydokhti and B. Kløve** (2012) Modeling of nitrate removal for ion exchange resin in batch and fixed bed experiments. *Desalination*, **284**, 22 - 31.
60. **Henam Sylvia Devi and Thiyam David Singh** (2016) Iron oxide nanoparticles synthesis through a benign approach and its catalytic application. *Perspectives in Science*, **8**, 287 - 289.
61. **Hernandez-Apaolaza, L. and F. Guerrero** (2008) Comparison between pine bark and coconut husk sorption capacity of metals and nitrate when mixed with sewage sludge *Bioresource Technology*, **99**, 1544 - 1548.
62. **Hualin Jiang, Pinghua Chen, ShenglianLuo, XinmanTu, Qun Cao, Meng Shu** (2013) Synthesis of novel nanocomposite Fe₃O₄/ZrO₂/chitosan and its application for removal of nitrate and phosphate. *Applied Surface Science*, **284**, 942 - 949.
63. **Huang, Y.H and T.C. Zhang** (2004) Effects of low pH on nitrate reduction by iron powder. *Water Resources*, **38**, 2631–2642.
64. **Hui-meiCai, Gui-jie Chen, Chuan-yiPeng, Zheng-zhu Zhang, Yang-yang Dong, Guang-zhi Shang, Xiao-hui Zhu, Hong-jianGao and**

- Xiao-chun Wan** (2015) Removal of fluoride from drinking water using tea waste loaded with Al/Fe oxides: A novel, safe and efficient biosorbent. *Applied Surface Science*, **328**, 34 - 44.
65. **Imen Ghouma, Mejdj Jeguiri, Sophie Dorge, Lionel Limousy, Camelia MateiGhimbeu and Abdelmottaleb Ouederni** (2015) Activated carbon prepared by physical activation of olive stones for the removal of NO₂ at ambient temperature. *C.R. Chimie.*, **18**, 63 - 74.
66. **Imran Ali, Mohd. Asim and Tabrez A. Khan** (2012) Low cost adsorbents for the removal of organic pollutants from wastewater. *Journal of Environmental Management*, **113**, 170 - 183.
67. **Jaafari, K., T. Ruiz, S. Elmaleh, J. Coma and K. Benkhouja** (2004) Simulation of a fixed bed adsorber packed with protonated cross-linked chitosan gel beads to remove nitrate from contaminated water. *Chemical Engineering Journal*, **99**, 153 - 160.
68. **Jia Liu, Yuan Su, Qian Li, Qinyan Yue and BaoyuGao** (2013) Preparation of wheat straw based superabsorbent resins and their applications as adsorbents for ammonium and phosphate removal. *Bioresource Technology*, **143**, 32 - 39.
69. **Jianlong Wang and Can Chen** (2014) Chitosan-based biosorbents: Modification and application for biosorption of heavy metals and radionuclides. *Bioresource Technology*, **160**, 129 - 141.
70. **Jianlong Wang and Libing Chu** (2016) Biological nitrate removal from water and wastewater by solid-phase denitrification process. *Biotechnology Advances*, **6**, 1103-1112.
71. **Jishi Zhang and Qinqing Wang** (2016) Sustainable mechanisms of biochar derived from brewers' spent grain and sewage sludge for ammonia-nitrogen capture. *Journal of Cleaner Production*, **112**, 3927 - 3934.
72. **Kairan Zhu, Hao Fu, Jinghui Zhang, XiaoshuLv, Jie Tang and Xinhua Xu**(2012) Studies on removal of NH₄-N from aqueous solution by using the activated carbons derived from rice husk. *Biomass and bioenergy*, **43**, 18 - 25.

73. **Kassae E. Motamedi, M.Z., A. Mikhak and R. Rahnemai** (2011) Nitrate removal from water using iron nanoparticles produced by arc discharge vs. reduction *Chemical Engineering Journal*, **166**, 490 - 495.
74. **Kumar Suranjit Prasad., Pooja Gandhi and Kaliaperumal Selvaraj** (2014) Synthesis of green nano iron particles (GnIP) and their application in adsorptive removal of As(III) and As(V) from aqueous solution. *Applied Surface Science* **317**, 1052–1059.
75. **Li, W., H. Muhr and E. Plasari**(2012) Use of different rapid mixing devices for controlling the properties of magnetite nanoparticles produced by precipitation. *Journal of Crystal Growth*, **342**, 21-27.
76. **Lim A P and A Z Aris**(2014) Continuous fixed-bed column study and adsorption modeling:Removal of cadmium (II) and lead (II) ions in aqueous solution by dead calcareous skeletons.
77. **Lua, A.C. and Q. Jia** (2009) Adsorption of phenol by oil palm shell activated carbons in a fixed bed. *Chemical Engineering Journal*, **150**, 455-461.
78. **Machado S, S.L. Pinto, J.P. Grosso, H.P.A. Nouws, J.T. Albergaria , C. Delerue-Matos** (2013) Green production of zero-valent iron nanoparticles using tree leaf extracts. *Science of the Total Environment***445–446**, 1–8
79. **Mahatheva Kalaruban, Paripurnanda Loganathan, W.G. Shim, Jaya Kandasamy, GayathriNaidu,TienVinh Nguyen, Sarava namuthu Vignes waran** (2016) Removing nitrate from water using iron-modified Dowex 21K XLT ion exchange resin: Batch and fluidised-bed adsorption studies. *Separation and Purification Technology*, **158**,61-70.
80. **Malkoc, E., and Y. Nuhoglu** (2006), Removal of Ni(II) ions from aqueous solutions using waste of tea factory: Adsorption on a fixed bed column. *Journal of Hazardous Materials*, **135**, 328-336.
81. **Manal F. Abou Taleb, Ghada A. Mahmoud, Samia M. Elsigeny and El-Sayed A. Hegazy** (2008) Adsorption and desorption of phosphate and nitrate ions using quaternary (polypropylene-g-N,N-dimethylaminoethylmethacrylate) graft copolymer. *Journal of Hazardous Materials*, **159**, 372 - 379.

82. **Mehmet Ugurlu and M. Hamdi Karaoglu** (2011). Adsorption of ammonium from an aqueous solution by fly ash and sepiolite: Isotherm, kinetic and thermodynamic analysis. *Microporous and Mesoporous Materials*, **139**,173-178.
83. **Menkouchi Sahli M A, S. Annouar, M. Mountada, A. Soufiane, A. Elmidaoui** (2008) Nitrate removal of brackish underground water by chemical adsorption and by electrodialysis. *Desalination*, **227**, 327-333
84. **Miao Li, ChuanpingFeng, Zhenya Zhang, Rongzhi Chen, QiangXue, Chengjie Gao and Norio Sugiura** (2010) Optimization of process parameters for electrochemical nitrate removal using Box–Behnken design. *Electro chimicaActa*, **56**, 265 - 270.
85. **Miltiadis Zamparas, Marios Drosos, Yiannis Georgiou, Yiannis Deligiannakis and Ierotheos Zacharias** (2013) A novel bentonite-humic acid composite material Bephos™ for removal of phosphate and ammonium from eutrophic waters. *Chemical Engineering Journal*, **225**, 43 - 51.
86. **Moaz K. Seliem, S. Komarneni, T. Byrne, F.S. Cannon, M.G. Shahien, A.A. Khalil and I.M. Abd El-Gaid** (2013) Removal of nitrate by synthetic organosilicas and organoclay: Kinetic and isotherm studies. *Separation and Purification Technology*, **110**, 181 - 187.
87. **Mohamed Ali Wahab , Salah Jellali and Naceur Jedidi** (2010) Effect of temperature and pH on the biosorption of ammonium onto Posidoniaoceanica fibers: Equilibrium, and kinetic modeling studies. *Bioresource Technology*,**101**, 8606 - 8615.
88. **Mohamed Ali Wahab, Hatem Boubakri, Salah Jellali and NaceurJedidi** (2012) Characterization of ammonium retention processes onto Cactus leaves fibers using FTIR, EDX and SEM analysis. *Journal of Hazardous Materials*, **241 - 242**, 101 - 109.
89. **Mohamed Ali Wahab, Salah Jellali and Naceur Jedidi** (2010) Ammonium biosorption onto sawdust: FTIR analysis, kinetics and adsorption isotherms modeling. *Bioresource Technology*, **101**, 5070 - 5075.
90. **Mohamed J .K Bashir, Hamidi Abdul Aziz, Mohd Suffian Yusoff and Mhd.Nordin Adlan** (2010). Application of response surface

- methodology (RSM) for optimization of ammoniacal nitrogen removal from semi-aerobic landfill leachate using ion exchange resin. *Desalination*, **254**, 154-161.
91. **K. Garg and K. Kadirvelu** (2013) Cadmium (II) sorption and desorption in a fixed bed column using sunflower waste carbon calcium–alginate beads. *Bioresource Technology*, **129**, 242 - 248.
 92. **Moumita Kotal and Anil K. Bhowmick**(2015) Polymer nanocomposites from modified clays: Recent advances and challenges. *Progress in Polymer Science*, metals on environmentally friendly *Carpobrotus edulis* plant. *Colloids and Surfaces B: Biointerfaces*, **82**, 267 - 276.
 93. **Mohamed Chiban, Amina Soudani, Fouad Sinan and Michel Persin** (2012) Wastewater treatment by batch adsorption method onto micro-particles of dried *Withania frutescens* plant as a new adsorbent. *Journal of Environmental* **51**, 127 - 187.
 94. **Mulan Zhang, Huayongzhang, Dan xu ,LuHan, Dongxiao Niu,Lui Zhang,Wu and BinghuiTian**(2011)Ammonia removal from aqueous solution by zeolites synthesized from low- calcium and high calcium fly ashes. *Desalination*, **277**, 46-53.
 95. **Nur T, W.G.Shim, P. Loganathan, S. Vigneswaran, J. Kandasamy**(2014). Nitrate removal using Purolite A520E ion exchange resin: Batch and fixed-bed column adsorption modeling. *International Journal of Environmental Science and Technology*, **12**, 1311-1320.
 96. **Pahlavanzadeh, H., R. Katal and H. Mohammadi** (2012) Synthesize of polypyrrolenanocomposite and its application for nitrate removal from aqueous solution. *Journal of Industrial and Engineering Chemistry*, **18**, 948 - 956.
 97. **Parsons, J.G., M.L. Lopez, J.R. Peralta-Videa, and J.L. Gardea-Torresdey** (2009) Determination of arsenic(III) and arsenic(V) binding to microwave assisted hydrothermal synthetically prepared Fe_3O_4 , Mn_3O_4 and MnFe_2O_4 nanoadsorbents. *Microchemical Journal*, **91**, 100-106.

98. **Paunka Vassileva and DimitrinkaVoikova**(2009) Investigation on natural and pretreated Bulgarian clinoptilolite for ammonium ions removal from aqueous solutions. *Journal of Hazardous Materials*, **170**, 948 - 953.
99. **Peijing Kuang, Nan Chen, ChuanpingFeng, Miao Li, Yang Den** (2018)Construction and optimization of an iron particle–zeolite packing electrochemical–adsorption system for the simultaneous removal of nitrate and by-products. *Journal of Taiwan institute of chemical engineers*,**86**, 101-112.
100. **Ponder, S. M., J.G. Darab and T.E. Mallouk** (2000) Remediation of Cr(IV) and Pb (II) aqueous solutions using supported nanoscalezerovalent iron. *Environ. Sci. Technol.*, **34**, 2564-2569.
101. **Pudukadu Munusamy Ayyasamy, Kuppusamy Shanthi, Perumalsamy Lakshmana perumalsamy, Soon-Jae Lee, Dong-Ju**(2007) Two-stage removal of nitrate from groundwater using biological and chemical treatments. *Journal of Bioscience and Bioengineering*, **104**,129-134.
102. **Qili Hu, Nan Chen, ChuanpingFeng and WeiWu Hu** (2015) Nitrate adsorption from aqueous solution using granular chitosan-Fe³⁺ complex. *Applied Surface Science*, **347**, 1 - 9.
103. **Raheleh Malekian, Jahangir Abedi-Koupai, Sayed Saeid Eslamian**(2011) Influences of clinoptilolite and surfactant-modified clinoptilolite zeolite on nitrate leaching and plant growth. *Journal of Hazardous Materials* 185, 970–976.
104. **Rajesh Chintala, Javier Mollinedo, Thomas E. Schumacher, Sharon K. Papiernik, Douglas D. Malo, David E. Clay, Sandeep Kumar, Dylan W. Gulbrandson** (2013). Nitrate sorption and desorption in biochars from fast pyrolysis. *Microporous and Mesoporous Materials* **179**, 250–257.
105. **Ramalingam A., MeeraSheriffa Begum K. M. and Sugashini S** (2015) Removal of Cr(VI) ions using Fe-loaded chitosan carbonized rice husk composite beads (Fe-CCRCB): Experiment and quantum chemical calculations, *J. Molecular Liquids.*,**208**, 380 – 387.

106. **Rangabhashiyam, S., N. Anu, M.S. Giri Nandagopal and N. Selvaraju** (2014) Relevance of isotherm models in biosorption of pollutants by agricultural byproducts. *Journal of Environmental Chemical Engineering*, **2**, 398 - 414.
107. **Ranjan K R. Bharali and Krishna G. Bhattacharyya** (2015) Biosorption of fluoride on Neem (*Azadirachta indica*) leaf powder. *Journal of Environmental Chemical Engineering*, **3**, 662 - 669.
108. **Sachin N. Milmile, Jayshri V. Pande, Shilpi Karmakar, Amit Bansiwala, Tapan Chakrabarti and Rajesh B. Biniwale** (2011) Equilibrium isotherm and kinetic modeling of the adsorption of nitrates by anion exchange Indion NSSR resin. *Desalination*, **276**, 38 - 44.
109. **Salah Jellali, Mohammed Ali Wahab, Makram Anane, Khalifa Riahi and Naceur Jedidi** (2011) Biosorption characteristics of ammonium from aqueous solutions onto *Posidonia oceanica* (L.) fibers. *Desalination*, **270**, 40 - 49.
110. **Sari Kilpimaa, Hanna Runtti, Teija Kangas, Ulla Lassi and Toivo Kuokkanen** (2015) Physical activation of carbon residue from biomass gasification: Novel sorbent for the removal of phosphates and nitrates from aqueous solution. *Journal of Industrial and Engineering Chemistry*, **21**, 1354 - 1364.
111. **Schoeman J J and A. Steyn** (2003) Nitrate removal with reverse osmosis in rural area in South Africa. *Desalination*, **155**, 15-26.
112. **Seyyedalireza Mousavi, Shaliza Ibrahim and Mohamed Kheireddine Aroua** (2012) Sequential nitrification and denitrification in a novel palm shell granular activated carbon twin-chamber upflow bio-electrochemical reactor for treating ammonium-rich wastewater. *Bioresource Technology*, **125**, 256 - 266.
113. **Shahin Ghafari, Masitah Hasan and Mohamed Kheireddine Aroua** (2009) Nitrate remediation in a novel upflow bio-electrochemical reactor (UBER) using palm shell activated carbon as cathode material. *Electrochimica Acta*, **54**, 4164 - 4171.
114. **Shahram Sharifnia, Mohammad Ali Khadivi, Tahereh Shojaei Mehr and Yaser Shavisi** (2013) Characterization, isotherm and kinetic studies

- for ammonium ion adsorption by light expanded clay aggregate (LECA). *Journal of Saudi Chemical Society*, **20**, S342 - S351.
- 115. Siva Kumar, Woo H.S and Min K** (2012) Equilibrium and kinetic studies on biosorption of 2,4,6, trichlorophenol from aqueous solutions by acacia leucocephala bark. *Colloid and Surfaces Bointerfaces*, **94**, 125-132.
- 116. Soleymanzadeh, M., M. Arshadi, J.W.L. Salvacion and F. Salimi Vahid** (2015) A new and effective nanobiocomposite for sequestration of Cd(II) ions: Nanoscale zerovalent iron supported on sineguelas seed waste. *Chemical engineering research and design*, **93**, 696 - 709.
- 117. Soloman, P.A., C. Ahmed Basha, M. Velan, N. Balasubramanian, and P. Marimuthu** (2009) Augmentation of biodegradability of pulp and paper industry wastewater by electrochemical pre-treatment and optimisation by RSM. *Separation and Purification Technology*, **69**, 109-117.
- 118. Soltani, N., A. Bahrami, M.I. Pech-Canul and L.A. Gonzale** (2015) Review on the physicochemical treatments of rice husk for production of advanced materials. *Chemical Engineering Journal*, **264**, 899 - 935.
- 119. Soumasree Chatterjee, Atul Kumara, Srabanti Basu, Susmita Dutta** (2012). Application of Response Surface Methodology for Methylene Blue dye removal from aqueous solution using low cost adsorbent. *Chemical Engineering Journal* **181**, 289-299.
- 120.** Standard Methods for the Examination of Water and Wastewater, 16th Edition, 1985, Method 418A, p.392.
- 121.** Standard X-ray Diffraction Powder Patterns, US Department of Commerce, National Bureau of Standards, Section **18**, 1981.
- 122. Sudipta Chatterjee and Seung Han Woo** (2009a) The removal of nitrate from aqueous solutions by chitosan hydrogel beads. *Journal of Hazardous Materials*, **164**, 1012 - 1018.
- 123. Sudipta Chatterjee, Dae S. Lee, Min W. Lee and Seung H. Woo** (2009) Nitrate removal from aqueous solutions by cross-linked chitosan beads conditioned with sodium bisulfate. *Journal of Hazardous Materials*, **166**, 508 - 513.

124. **Suryadi Ismadji, Dong Shen Tong, Felycia Edi Soetaredjo, Aning Ayucitra, Wei Hua Yu and Chun Hui Zhou** (2015) Reprint of Bentonitehydrochar composite for removal of ammonium from Koi fish tank. *Applied Clay Science*, **114**.
125. **Tchobanoglous, G., F.L. Burton, and H.D. Stensel** *Wastewater Engineering, Treatment and Reuse*. McGraw Hill, 2003.
126. **Ting Wang, Jiajiang Lin, Zuliang Chen, Mallavarapu Megharaj and Ravendra Naidu** (2014) Green synthesized iron nanoparticles by green tea and eucalyptus leaves extracts used for removal of nitrate in aqueous solution. *Journal of Cleaner Production*, **83**, 413 - 419.
127. **USEPA** (2016). National Primary Drinking Water Regulations. *United States Environmental Protection Agency*.
128. **Uttam Kumar Sahu, SibaSankar, Raj Kishore Patel** (2018) Application of Box-Behnken Design in response surface methodology for adsorptive removal of arsenic from aqueous solution using CeO₂/Fe₃O₂/ grapheme nanocomposite. *Materials Chemistry and Physics*, **207**, 233-242.
129. **Vijayaraghavan, K., J. Jegan, K. Palanivelu and M.Velan** (2004) Removal of nickel(II) ions from aqueous solution using crab shell particles in a packed bed upflowcolumn. *Journal of Hazardous Materials*, **113**, 223-230.
130. **Vinodhini, V. and NilanjanaDas** (2010) Packed bed column studies on Cr (VI) removal from tannery wastewater by neem sawdust. *Desalination*, **264**, 9 - 14.
131. **Wan Ngah, W.S., L.C. Teong, R.H. Toh and M.A.K.M. Hanafiah**(2012) Utilization of chitosan–zeolite composite in the removal of Cu(II) from aqueous solution: Adsorption, desorption and fixed bed column studies. *Chemical Engineering Journal*, **209**, 46 - 53.
132. **Ward M.H, Mark S.D, Cantor K.P, Weisenburger D.D, Correa-Villase~nor A, Zahm S.H** (1996). Drinking water nitrate and the risk of non- Hodgkin's lymphoma. *Epidemiology*, **7**, 465-471.

133. **Wen Song, BaoyuGao, Xing Xu, Fang Wang, Nan Xue, Shenglei Sun, Wuchang Song and RuibaoJia** (2016) Adsorption of nitrate from aqueous solution by magnetic amine-crosslinked biopolymer based corn stalk and its chemical regeneration property. *Journal of Hazardous Materials*, **304**, 280 - 290.
134. **Wenjun, J., P. Miguel, D.D. Dionysios, H.E. Mohammad, T. Dimitra and O.S. Kevin**(2013) Chromium (VI) removal by maghemite nanoparticles. *Chemical Engineering Journal*, **222**, 527-533.
135. **Weyer, P.J., Cerhan, J.R., Kross, B.C., Hallberg, G.R., Kantamneni, J., Breuer, G., Jones, M.P., Zhen, W., Lynch, C.F** (2001). Municipal drinking water nitrate level and cancer risk in older women: the Iowa women's health study. *Epidemiology*, **12** , 327–338.
136. **Xiaolin Wang, Xu Zhang, Yaoming Wang, Yuxiang Du, TongwenXu** (2015) Simultaneous recovery of ammonium and phosphorus via the integration of electrodialysis with struvite reactor. *Journal of Membrane Science*, **490**, 65-71.
137. **Xing Xu, Bao-Yu Gao, Qin-Yan Yue and Qian-Qian Zhong** (2010) Preparation of agricultural by-product based anion exchanger and its utilization for nitrate and phosphate removal. *Bioresource Technology*, **101**, 8558 - 8564.
138. **Xing Xu, BaoyuGao , Xin Tan, Xiaoxiao Zhang, QinyanYue, Yan Wang and Qian Li** (2013 *a*) Nitrate adsorption by stratified wheat straw resin in lab-scale columns. *Chemical Engineering Journal*, **226**, 1 - 6.
139. **Xing Xu, Baoyu Gao, QinyanYue, Qian Li and Yan Wang** (2013 *b*) Nitrate adsorption by multiple biomaterial based resins: Application of pilot-scale and lab-scale products. *Chemical Engineering Journal*, **234**, 397 - 405.
140. **Xing Xu, BaoyuGao, Yaqing Zhao, Suhong Chen, Xin Tan, QinyanYue, Jianya Lin, Yan Wang** (2012) Nitrate removal from aqueous solution by Arundodonax L. reed based anion exchange resin. *Journal of Hazardous Materials*, 203 - 204, 86 - 92.
141. **Xinggang Wang, Shaoyu Lu, ChunmeiGao, XiubingXu, Xinjie Zhang, Xiao Bai, Mingzhu Liu and Lan Wu** (2014) Highly efficient adsorption of ammonium onto palygorskite nanocomposite and

- evaluation of its recovery as a multifunctional slow-release fertilizer. *Chemical Engineering Journal*, **252**, 404 - 414.
- 142. Xu Xing, Bao-Yu Gao, Qian-QianZhong, Qin-Yan Yue and Qian Li** (2011) Sorption of nitrate onto amine-crosslinked wheat straw: Characteristics, column sorption and desorption properties. *Journal of Hazardous Materials*, **186**, 206 - 211.
- 143. Yan Li, Li Gan, Zuliang Chen, Mallavarapu Megharaj and Ravi Naidu** (2012) Removal of nitrate using Paracoccus sp. YF1 immobilized on bamboo carbon. *Journal of Hazardous Materials*, **229 - 230**, 419 - 425.
- 144. Yanhui Zhan, Jianwei Lin and Zhiliang Zhu** (2011) Removal of nitrate from aqueous solution using cetylpyridinium bromide (CPB) modified zeolite as adsorbent. *Journal of Hazardous Materials*, **186**, 1972 - 1978.
- 145. Yanmei Zhou, Bin Gao, Andrew R. Zimmerman, June Fang, Yining Sun and Xinde Cao** (2013) Sorption of heavy metals on chitosan-modified biochars and its biological effects. *Chemical Engineering Journal*, **231**, 512 - 518.
- 146. Yian Zheng and Aiqin Wang** (2009) Evaluation of ammonium removal using a chitosan-g-poly (acrylic acid)/rectorite hydrogel composite. *Journal of Hazardous Materials*, **171**, 671 - 677.
- 147. Yian Zheng, Junping Zhang and Aiqin Wang** (2009) Fast removal of ammonium nitrogen from aqueous solution using chitosan-g-poly(acrylic acid)/attapulgitite composite. *Chemical Engineering Journal*, **155**, 215 - 222.
- 148. Yian Zheng , Yi Liu and Aiqin Wang** (2011) Fast removal of ammonium ion using a hydrogel optimized with response surface methodology. *Chemical Engineering Journal*, **171**, 1201-1208.
- 149. Yian Zheng, YuntaoXie and Aiqin Wang** (2012) Rapid and wide pH-independent ammonium-nitrogen removal using a composite hydrogel with three-dimensional networks. *Chemical Engineering Journal*, **155**, 215 - 222.

150. **Ying Wang, JiuhuiQu, Huijuan Liu, ChengZhi Hu** (2007) Adsorption and reduction of nitrate in water on hydrotalcite-supported Pd-Cu catalyst. *Catalysis Today*, **126**, 476 - 482.
151. **Yinghua Li, Haibo Li, Tieheng Sun and Xin Wang** (2011) Study on nitrogen removal enhanced by shunt distributing wastewater in a constructed subsurface infiltration system under intermittent operation mode. *Journal of Hazardous Materials*, **189**, 336 - 341.
152. **Yuanhao Ding and Majid Sartaj** (2015) Statistical analysis and optimization of ammonia removal from aqueous solution by zeolite using factorial design and response surface methodology. *Journal of Environmental Chemical Engineering*, **3**, 807 - 814.
153. **Yuansheng Pei, Zhifeng Yang and BinghuiTian** (2010) Nitrate removal by microbial enhancement in a riparian wetland. *Bioresource Technology*, **101**, 5712 - 5718.
154. **Yu-Hoon Hwang, Do-Gun Kim and Hang-Sik Shin** (2011) Mechanism study of nitrate reduction by nano zero valent iron. *Journal of Hazardous Materials*, **185**, 1513 – 1521
155. **Yu Wang, Bao-Yu Gao, Wen-Wen Yue, Qin-Yan Yue** (2007) Adsorption kinetics of nitrate from aqueous solutions onto modified wheat residue. *Colloids and Surfaces A: Physicochem. Eng. Aspects*, **308**, 1–5
156. **Zhenya Zhang, Zhongfang Lei, Xiaoyan He, ZhiyinZhang ,Yingnan Yang, Norio Sugiur** (2009) Nitrate removal by *Thiobacillusdenitrificans* immobilized on poly(vinyl alcohol) carriers. *Journal of Hazardous Materials*, **163**, 1090 - 1095.
157. **Zhongfei Ren, Xing Xu, Xi Wang, BaoyuGao, QinyanYue, Wen Song, Li Zhang and Hantao Wang** (2016) FTIR, Raman, and XPS analysis during phosphate, nitrate and Cr(VI) removal by amine cross-linking biosorbent. *Journal of Colloid and Interface Science*, **468**, 313 - 323.
158. **Zhongmin Feng and Ting Sun** (2015) A novel selective hybrid cation exchanger for low-concentration ammonia nitrogen removal from natural water and secondary wastewater. *Chemical Engineering Journal* ,**281** 295–302.

-
159. **Zhu Wen-Ling, CUI Li-Hua, O Ying, Cui-Fen and Tang Xiao-Dan** (2011) Kinetic Adsorption of Ammonium Nitrogen by Substrate Materials for Constructed Wetlands. *Pedosphere*, **21(4)**, 454 - 463.
160. **Zhou, Y.T., H.L. Nie, C. Branford-White, Z.Y. He and L.M. Zhu** (2009) Removal of Cu^{2+} from aqueous solution by chitosan coated magnetic nanoparticles modified with α -ketoglutaric acid. *Journal of Colloid and Interface Science*, **330**, 29-37.
161. **Zihong Cheng, Zhanxian Gao, Wei Maa, Qi Sun, Baodong Wang, Xiaoguang Wang** (2012) Preparation of magnetic Fe_3O_4 particles modified sawdust as the adsorbent to remove strontium ions. *Chemical Engineering Journal*, **209**, 451 - 457.
162. **Zukhra. Kadirova, Mirabbos Hojamberdiev, Longli Bo, Rustam Hojiyeva and Kiyoshi Okada** (2015) Simultaneous removal of NH_4^+ , H_2PO_4^- and Ni^{2+} from aqueous solution by thermally activated combinations of steel converter slag and spent alumina catalyst. *Journal of Water Process Engineering*, **8**, 151 - 159.
163. **Zuohao Ma, Qian Li, Qinyan Yue, Baoyu Gao, Wenhong Li, Xing Xu and Qianqian Zhong** (2011) Adsorption removal of ammonium and phosphate from water by fertilizer controlled release agent prepared from wheat straw. *Chemical Engineering Journal*, **171**, 1209 - 1217.

.....❁*❁.....

ANNEXURES

Annexure I (Section 3.4)

Calibration of UV-vis Spectrophotometer

Equipment used- Hitachi U-2900

Method- Calibration curve was plotted by taking 0, 1, 2, 3, 4, 5, 6, 7, ppm nitrate solution and noting the absorbance for each concentration at 220 nm and 275 nm. From the corrected sample absorbance calibration curve (Fig. A1) the concentration of nitrate nitrogen can be measured.

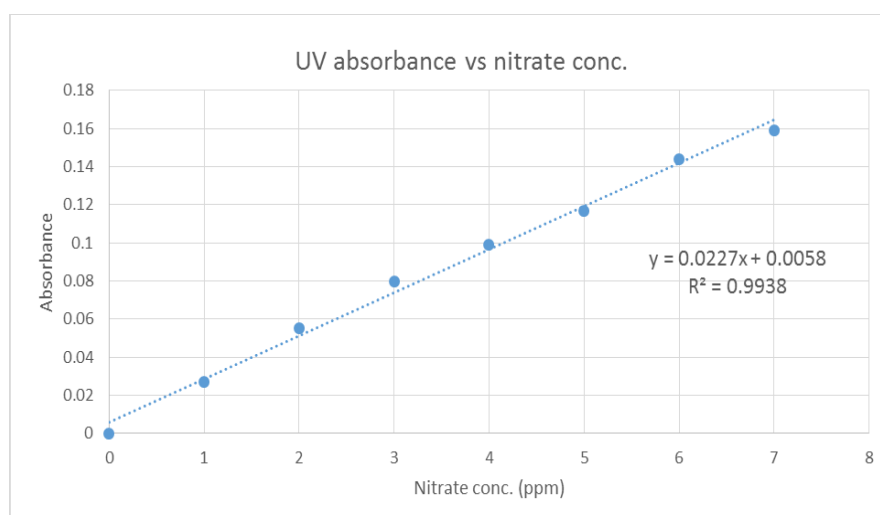


Fig. A1 Standard calibration curve of UV vis spectrophotometer (Nitrate)

The ammonium ions are detected by Nesslerization method. Calibration curve was plotted by taking 1, 2, 3, 4, 5, 6, 7, 8, 10, 15 ppm ammonium chloride solution and noting the absorbance for each concentration at 430 nm. From the standard calibration (Fig. A2) the concentration of NH_4^+ -N solution can be measured

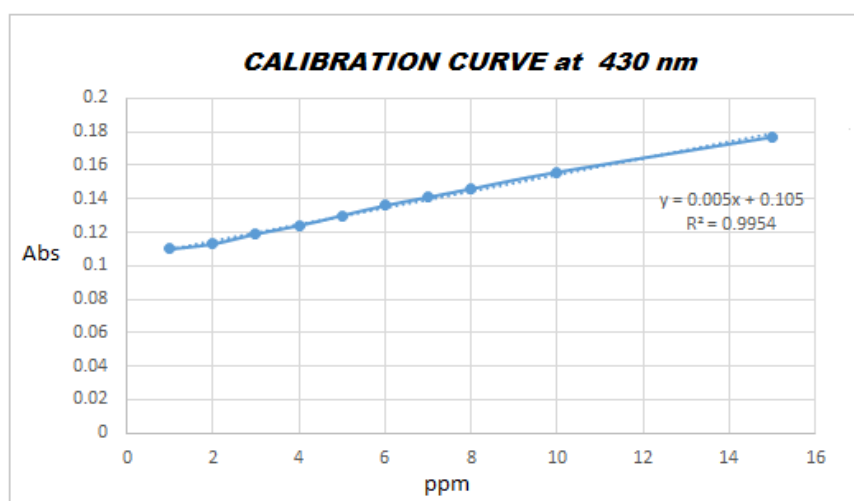


Fig. A2 Standard calibration curve of NH_4^+ -N in U Vis spectrophotometer

Annexure II (Section 3.5)

Determination of average grain size of nanoadsorbents

The average grain size of nanocomposite films used for adsorption was calculated using Debye Scherrer equation using the data obtained from XRD spectrum. Table A.1 represents the determination of average crystallite size of chitosan bentonite nanocomposite films.

Debye Scherrer equation is given by $D = \frac{K\lambda}{\beta \cos \theta}$

- D = mean diameter of nanoparticles
- β = The full width at half maximum value of XRD diffraction lines in radians (FWHM)
- λ = the wavelength of X-ray radiation source = 1.5406 Å
- θ = angle of incidence in radians
- K = the Scherrer constant with value from 0.9 to 1.

Table A.1 Determination of average crystallite size of chitosan-bentonite nanocomposite films

Peak position $2\theta^\circ$	FWHM $^\circ$	D_p , (nm)	D_p average, (nm)
5.365	1.315	6.05	9.86
19.438	0.686	11.65	
61.438	0.784	11.79	

For $2\theta=5.365$, FWHM ($^\circ$) = 1.315

$$D_p = \frac{0.9 \times 1.5406}{\text{radians}(1.315) \times \cos(\text{radians}(\frac{5.365}{2}))} = 6.05 \text{ nm}$$

Annexure III (section: 3.7)**Calibration Details of Peristaltic Pump**

Peristaltic Pump used: Ravel (Make); RHP 100L-200 (Model)

The calibration of peristaltic pump was performed by setting various rpm and measuring the flow rate using a stop watch. Table A.2 represents the calibration data of peristaltic pump used in the operation of packed bed adsorption column for nitrate nitrogen removal. Calibration curve was plotted between rpm and flow rate (Fig. A2).

Table A.2 Calibration data of peristaltic pump

rpm	Flow rate, mL/min
0.5	6
0.8	10
1	12
1.2	14
1.5	17
1.8	21
2	22
2.3	25
2.5	27
3	31
5	50

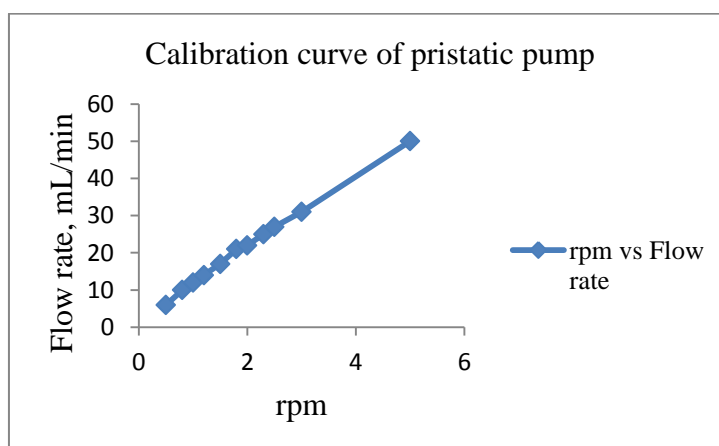


Fig. A2 Calibration curve of peristaltic pump used in the fixed bed nitrate column

Annexure IV : Experimental Data
Table A.3 Sorption kinetics (section 4.3.2)

Time, minutes	Initial concentration, ppm	Final concentration, ppm
20	70	20.5
40	70	14.1
60	70	5.7
80	70	5.7
100	70	5.7
120	70	5.7

Table A.4 Adsorption isotherm (section 4.3.3)

Initial concentration, ppm	Equilibrium concentration, ppm
20	1.6
40	3.16
60	4.1
80	10.4
100	31

Table A.5 Thermodynamic experimental data, $C_0=70$ mg N/L (section 4.3.4)

Temperature, °C	Final concentration, ppm
30	5.7
40	4.6
50	12.8
60	19.6
70	24.4

Table A.6 Desorption data (section 4.3.5)

Cycle	Initial solution concentration, ppm	Final solution concentration, ppm	Initial adsorbent concentration, ppm	Final eluent concentration, ppm
1	60	4.1	55	2
2	48	6.8	40	7.5
3	32	7.0	22	5.5
4	14	3.6	10	3.1
5	6	1.6	3	1.0

Table A.7 Effect of bed height on the working of fixed bed column (section 4.4.1)

Bed Height, cm	C _f , ppm	Time, hour	Bed Height, cm	C _f , ppm	Time, hour	Bed Height, cm	C _f , ppm	Time, hour
10	0.5	1	15	0.1	1	20	0.01	1
10	0.6	2	15	0.2	2	20	0.02	2
10	0.8	3	15	0.3	3	20	0.03	3
10	1.2	4	15	0.4	4	20	0.05	4
10	2.6	5	15	0.5	5	20	0.06	5
10	3.5	6	15	1.8	6	20	0.09	6
10	9.2	7	15	3	7	20	0.1	7
10	19.3	8	15	4.7	8	20	0.3	8
10	23.6	9	15	7.6	9	20	0.5	9
10	36.4	10	15	8.9	10	20	0.6	10
10	42.6	11	15	12.6	11	20	0.8	11
10	48.2	12	15	15.6	12	20	1.1	12
10	53.6	13	15	17.6	13	20	2.4	13
10	57.2	14	15	22.3	14	20	3.6	14
10	61.8	15	15	28.8	15	20	6.5	15
10	64	16	15	32.6	16	20	9.8	16
10	65	17	15	38.2	17	20	13.5	17
10	65	18	15	41.5	18	20	18.7	18
10	66	19	15	45.8	19	20	23.5	19
10	66	20	15	48.4	20	20	28.9	20
10	66	21	15	51.6	21	20	33.7	21
			15	54.3	22	20	40.7	22
			15	58.4	23	20	45.6	23
			15	61.2	24	20	49.9	24
			15	63	25	20	53.1	25
			15	64	26	20	55.5	26
			15	65	27	20	57.7	27
			15	66	28	20	60.3	28
			15	67	29	20	62.4	29
			15	67	30	20	64.3	30
			15	67	31	20	65.6	31
			15	67	32	20	66.2	32
						20	66.9	33
						20	67.8	34
						20	68.6	35
						20	68.7	36
						20	69.8	37
						20	69.8	38
						20	69.8	39
						20	69.8	40

Table A.8 Effect of flow rate on the working of fixed bed column (section 4.4.2)

Flow rate, mL/min	C _t , ppm	Time, hour	Flow rate, mL/min	C _t , ppm	Time, hour	Flow rate, mL/min	C _t , ppm	Time, hour
6	0.1	1	10	0.1	1	15	10.8	1
6	0.2	2	10	0.2	2	15	12.2	2
6	0.3	3	10	0.3	3	15	14.3	3
6	0.4	4	10	0.5	4	15	15.6	4
6	0.5	5	10	0.7	5	15	18.3	5
6	1.8	6	10	2.2	6	15	21.2	6
6	3	7	10	3.9	7	15	24.4	7
6	4.7	8	10	5.3	8	15	28.2	8
6	7.6	9	10	8.5	9	15	31.3	9
6	8.9	10	10	14.8	10	15	35.2	10
6	12.6	11	10	22.4	11	15	40.3	11
6	15.6	12	10	32.6	12	15	42.3	12
6	17.6	13	10	44.6	13	15	46.4	13
6	22.3	14	10	50.3	14	15	54.3	14
6	28.8	15	10	53.6	15	15	58.8	15
6	32.6	16	10	57.6	16	15	60	16
6	38.2	17	10	59.4	17	15	60	17
6	41.5	18	10	60.2	18	15	60	18
6	45.8	19	10	61.8	19			
6	48.4	20	10	63	20			
6	51.6	21	10	64	21			
6	54.3	22	10	65	22			
6	58.4	23	10	66	23			
6	61.2	24	10	67	24			
6	63	25	10	67	25			
6	64	26	10	67	26			
6	65	27						
6	66	28						
6	67	29						
6	67	30						
6	67	31						
6	67	32						

Experimental data of Ammonia Nitrogen

Table A.9 Adsorption isotherm (section 4.6.2)

Initial concentration, ppm	Equilibrium concentration, ppm
10	2.28
20	4.44
30	6.33
40	10
50	16

Table A.10 Sorption kinetics (section 4.6.3)

Time, minutes	Initial concentration, ppm	Final concentration, ppm
20	28	8.9
40	28	7.98
60	28	7.15
80	28	7.31
100	28	7.33
120	28	7.29
140	28	7.28

Table A.11 Thermodynamic experimental data, $C_0=50$ mg /L (section 4.6.4)

Temperature, °C	Final concentration, ppm
30	8.6
40	7.5
50	10.8
60	12.8
70	16.2

.....*.....

LIST OF PAPERS SUBMITTED ON THE BASIS OF THIS THESIS

REFEREED JOURNALS

- **Pothiyil Veeravu Haseena, Chandran M Akash, Gopal Madhu, and Sahoo Dipak Kumar** Adsorption of nitrate anions by Fe-loaded chitosan nutmeg shell powder: Equilibrium, kinetics, and thermodynamics. *Research Journal of Chemistry and Environment*, Vol 24 (2019).
- **Haseena Pothiyil Veeravu, Krishnapriya S, G. Madhu and Dipak Kumar Sahoo.** A statistical investigation into ammoniacal nitrogen adsorption on chitosan/bentonitenanocomposite films by response surface methodology. *Indian Journal of environmental protection* Vol 40 (2019).

PRESENTATIONS IN CONFERENCES

- **P.V. Haseena, K.S. Padmavathy, P.Rohit Krishnan, G.Madhu** (2016) , Adsorption of ammonium nitrogen from aqueous systems using Chitosan- Bentonite film composite. Elsevier Procedia, 24, 733 -740.
- **P. V. Haseena, K.S. Padmavathy, G.Madhu** (2016). A review on emerging adsorbents for removal of ammonia nitrogen from aqueous solutions. International Conference on advances in applied mathematics, materials science and nanotechnology for engineering and industrial applications (IC-AMMN-2K16), Federal Institute of Science and Technology, Hormis Nagar, Angamaly, Kerala, 7 - 9 January, 2016.
- **P.V. Haseena, S. Krishnapriya, G. Madhu** (2018) Adsorption of ammonia nitrogen using nutmeg shell as biosorbent. National conference on Energy, Ecology and Environment (NCEEE-2018). Bannari Amman Institute of Technology, Erode,Tamilnadu, August 2-3,2018.
- **P.V. Haseena, A.S. Sajitha, R. Renjana** (2019). A review on nitrogenous waste removal from aqueous solutions by adsorption process. TECHFEST by Kerala Technological University, Govt Engineering College Thrissur, February 17-19,2019.

.....∞*∞.....

CURRICULUM VITAE

Name : **HASEENA P. V.**
Date of Birth : 39 years, 17-05-1980

EDUCATIONAL QUALIFICATIONS

- November 1998- June 2002
B.Tech in Chemical Engineering
Government Engineering College, Thrissur, Kerala, India
- January 2003- December 2007
M.Tech in Process Control (Chemical)
Government Engineering College, Thrissur, Kerala, India
- November 2011- Present
Doctor of Philosophy
Faculty of Engineering, SOE
Cochin University of Science and Technology
Reg. Date : 23-11-2011

EXPERIENCE

- June 2007- May 2013 & March 2014- June 2019
Assistant Professor in Chemical Engineering,
Government Engineering College, Thrissur, Kerala, India
- June 2013- February 2014 & July 2019- Till date
Assistant Professor in Chemical Engineering,
Government Engineering College, Kozhikode, Kerala, India

.....*.....

